IEc

Estimating the Economic Damages of Climate Change in the Dominican Republic

September 11, 2023

Prepared for:
Katharina Siegmann

World Bank

Prepared by:

Brent Boehlert, Kenneth Strzepek, and Diego Castillo
Industrial Economics, Incorporated
2067 Massachusetts Avenue
Cambridge, MA 02140 USA
+1 617 354 0074

TABLE OF CONTENTS

ACRONYM LIST

CCDR	Country Climate Development Report
CMIP6	Coupled Model Intercomparison Project 6
GCM	General Circulation Models
GDP	Gross domestic product
RCP	Representative Concentration Pathway
SSP	Shared Socioeconomic Pathway
USD	United States Dollar
WEAP	Water Evaluation And Planning

1. INTRODUCTION

This report outlines the process of estimating the economic damages of climate change for the Dominican Republic, with these damage estimates subsequently informing a *Climate Change Development Report* (CCDR) for the Dominican Republic. The development of a CCDR provides an opportunity to better understand the benefits and costs of climate action and cross-sectoral policy priorities to manage climate risks effectively.

Within the activity documented in this report, climate projections are run through biophysical and economic models to assess the country's vulnerability to climate change under a no-action scenario, and how adaptation investments can enhance resilience. This is done by first selecting a representative set of climate scenarios, used to assess the macroeconomic effects of climate change. Macroeconomic shocks arising from relevant "channels of impact" under climate change are then explored, with these shocks serving as input for a country-specific macroeconomic model as well as additional modeling to estimate the poverty impacts of climate change. Finally, the potential benefits of different adaptation options to reduce the impacts of climate change are assessed.

With this section having provided an introduction to the project, Section 2 goes on to provide country-specific geographic, climatological and socio-economic background. Section 3 provides an overview of the analytical approach used to estimate economic damages from climate change. Section 4 presents results for each impact channel assessed and Section 5 presents a summary of the key findings as well as conclusions. Appendices A and B present details on the methodologies used for the development of climate scenarios and impact channels, respectively. Appendix C documents the data sources used to conduct the analysis.

2. COUNTRY OVERVIEW

This section provides a description of the geography and historical climatology of the Dominican Republic, as well as an overview of the country's socioeconomic context. This background information was used to inform the development of both the analytical approach and key assumptions for estimating climate change damages in the country.

2.1 GEOGRAPHY AND CLIMATE

The Dominican Republic, located in the Caribbean Region, occupies the eastern two-thirds of Hispaniola. Its administrative capital is Santo Domingo, located on the southeast coast of the country (Figure 1). It is bounded by the Atlantic Ocean to the north, the Caribbean Sea to the south, and Haiti to the west.

FIGURE 1. COUNTRY MAP

Source: WorldAtlas (2021)

The country consists of five natural regions: (1-3) tropical moist broadleaf forests, tropical dry broadleaf forests, and tropical coniferous forests among the peaks of the country's mountains; (4) flooded grasslands to the southwest and nestled within the valleys of the mountains; and (5)

mangrove swamps lining the coastal areas. The main rivers are the Yaque del Norte, which flows northwestward, and the Camu-Yuna, which flows eastward (Wiarda and González 2023).

Figure 2 shows the country's Köppen-Geiger climate classification, which consists primarily of tropical monsoon (Am), rainforest (Af), and savanna climates (Aw). These three regions are characterized by high temperatures. While the tropical rainforest climate presents high precipitation year-round, tropical monsoon and tropical savanna climates have distinct wet and dry seasons. In the center of the country is a temperate oceanic climate (Cfb), which has mild, wet winters, and cool, moist summers.

FIGURE 2. KÖPPEN-GEIGER CLIMATE CLASSIFICATION MAP, 1991-2020

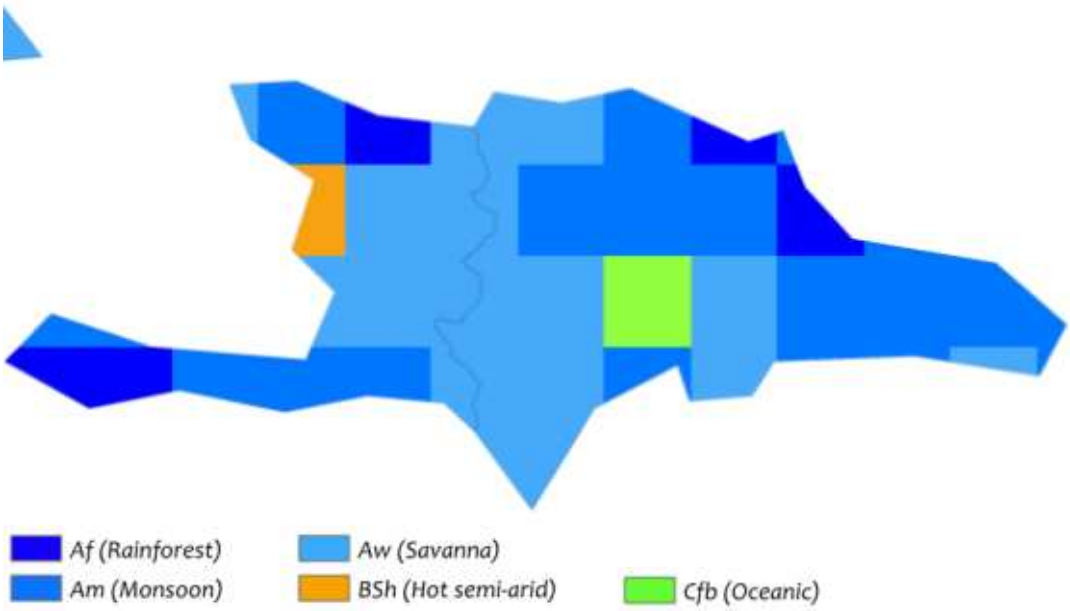

Source: World Bank Climate Change Knowledge Portal

The Dominican Republic has two seasons: the wet season (May to November) and the dry (December to April). Monthly average temperatures between 1991 and 2020 ranged between 22.5˚C in January and 26.1˚C in August. Overall, temperature varies little spatially, with the center of the country around 5˚C cooler than the warmest portion of the country. Precipitation is more variable, with areas in the northwest receiving over 700 mm less precipitation annually than the middle of the country. Mean monthly rainfall in the Dominican Republic ranges between 63 mm in March and 196 mm in May (World Bank 2021a). Figure 3 shows the spatial variability of mean annual temperature and precipitation in the country, and Figure 4 shows the monthly variability of the same variables. Figure 3 shows the spatial variability of mean annual temperature and precipitation across the country, and Figure 4 shows the monthly variability of the same variables.

FIGURE 3. MEAN TEMPERATURE AND PRECIPITATION BY 1/2 DEGREE GRID CELL, 1995-2020

Precipitation:

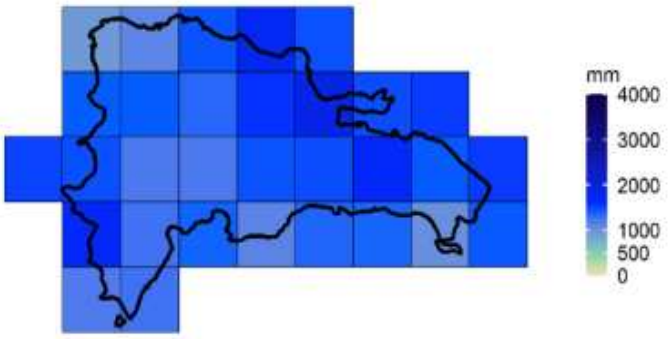

Temperature:

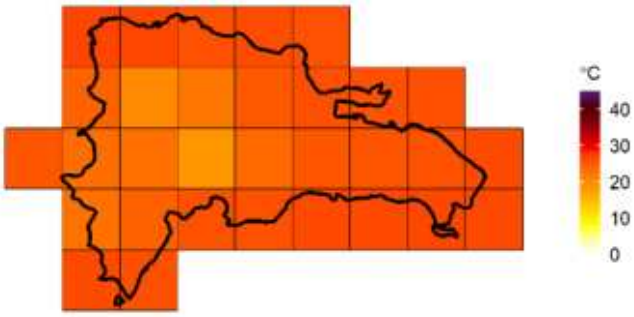

Source: World Bank Climate Change Knowledge Portal

FIGURE 4. MONTHLY MEAN TEMPERATURE AND PRECIPITATION, 1991-2020

Source: World Bank Climate Change Knowledge Portal

2.2 SOCIOECONOMIC CONTEXT

The Dominican Republic had a population of 11 million people in 2020. The country's population grew by 14 percent during the last 10 years and is expected to continue growing at a slower rate going forward, potentially reaching about 13.2 million people by 2050 (United Nations 2022). The population is mainly concentrated in urban areas (see Figure 5). The population is currently over 80 percent urban, and urbanization is projected to continue. Santo Domingo has 3.5 million people in the metropolitan area or 31.8 percent of the total country population.

FIGURE 5. POPULATION DISTRIBUTION BY ½ DEGREE GRID CELL, 2020

Source: United Nations Population Prospects

The Dominican Republic's gross domestic product (GDP) in 2021 was 94.2 billion USD. The country is classified as an upper-middle income country, with a per capita income of about $18,600 in 2021 (in purchasing power parity terms, in constant 2017 international dollars). As seen in Figure 6, GDP per capita has grown steadily, overcoming the average for Latin America and Caribbean countries in 2016 (World Bank 2021b).

In 2021, 5.4 percent of the country's GDP came from services, while the industry and agriculture sectors contributed 32.7 and 5.7 percent respectively. Now, tourism has become one of the Dominican Republic's more important sources of foreign exchange and the country is one of the most popular tourist destinations in the Caribbean. In 2021, 0.3 percent of the population was below the international poverty line (United Nations 2021). This is a decrease from 21 percent in 2019.

FIGURE 6. GDP PER CAPITA (PURCHASING POWER PARITY, IN CONSTANT 2017 THOUSAND INTERNATIONAL DOLLARS)

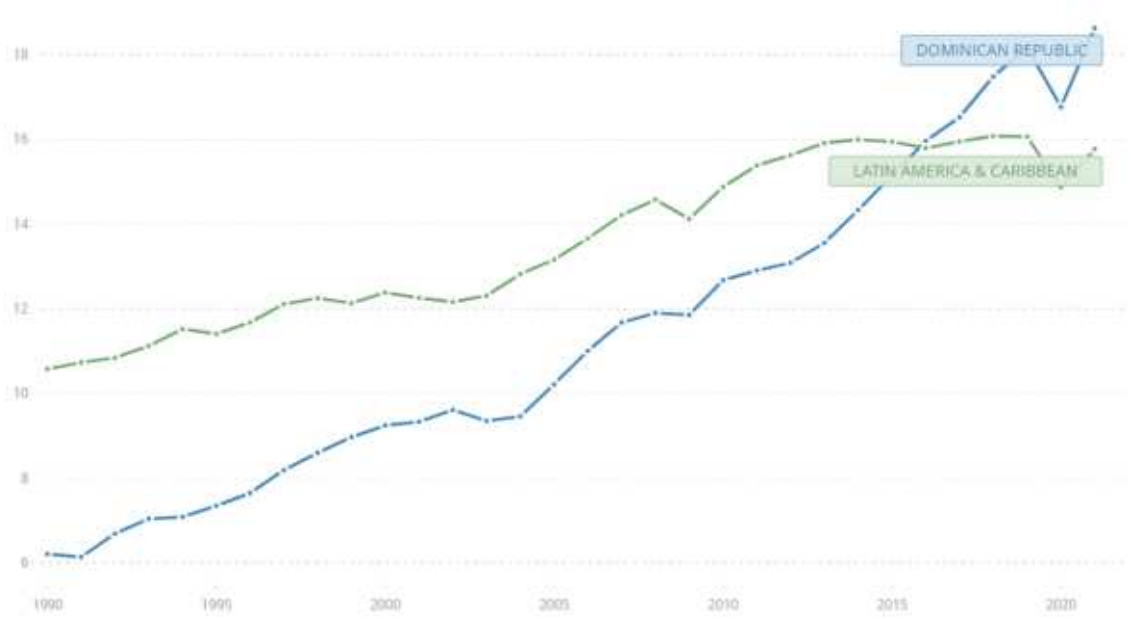

Source: World Bank DataBank

3. METHODOLOGICAL OVERVIEW

As introduced above, this study aims to estimate economic damages from climate change to the Dominican Republic's economy, with these estimates to be used in the development of the CCDR. The analysis is built around different "impact channels" through which climate change will result in shocks to the country's macroeconomy. This study considers the following different types of shocks, namely

(1) shocks to **human capital**, including from *heat stress on labor*, impacts to *human health*, and *water, sanitation, and hygiene*

(2) shocks to **water and agriculture**, including changes in *water supply and demand*, *crop production*, *erosion,* and *hydropower*

(3) shocks to **infrastructure and services**, including *inland flooding*, *tropical cyclones, sea-level rise and storm surge*, and *tourism*

This section presents the overarching analytical framework used to model impact channels and their linkages to the macroeconomic and poverty model(s), the climate scenarios considered, and the development policy and adaptation scenarios evaluated. Appendix A presents further detail on the methods used to process climate data and select scenarios, while Appendix B presents detailed methodological information for each impact channel. Appendix C documents the various sources of data used in the analysis.

3.1 ANALYTICAL APPROACH

Within this study's analytical framework, developing impact channels involves four stages (see Figure 7):

(1) obtaining gridded historical and projected climate data for a set of climate scenarios;

(2) selecting, tailoring, and/or developing biophysical models that convert changes in climate data into biophysical shocks for each of the impact channels evaluated for the country;

(3) aggregating grid-level biophysical shocks to national and/or sectoral scales using high-resolution geospatial data; and

(4) producing shocks to be fed into the country's macroeconomic and poverty model(s).

Results are aggregated either to national scale inputs (e.g., capital or labor) or to economic sectors (e.g., agriculture) to match the macroeconomic model's resolution, or are provided at higher resolution for use in a poverty model.

FIGURE 7. IMPACT CHANNEL MODELING APPROACH

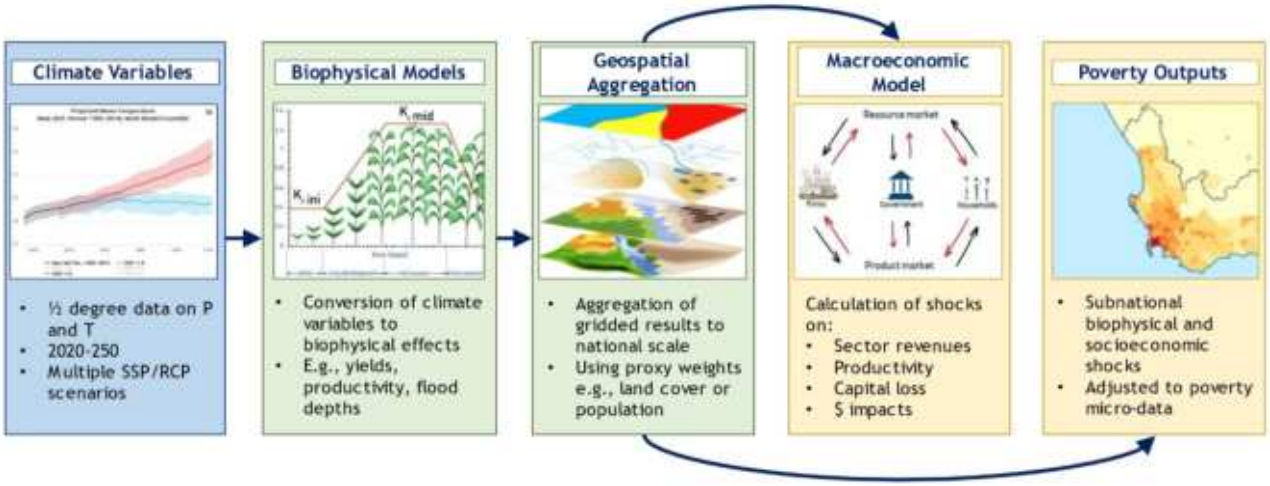

For this particular analysis, we consider eleven channels of impact. Table 1 provides a high-level description of each channel broken down by the categories introduced above (i.e., human capital, water and agriculture, and infrastructure and services). The shocks caused by climate change through each impact channel are calculated based on changes in climate variables (e.g., monthly precipitation or daily maximum temperature) for the 30-year period from 2021 to 2050 (i.e., the period covered in the CCDR), relative to a climate baseline from 1995 to 2020. These shocks are then used as input to the existing country's macroeconomic and poverty model(s).

TABLE 1. OVERVIEW OF IMPACT CHANNELS EVALUATED

CHANNEL OF IMPACT		DESCRIPTION OF HOW CLIMATE CHANGE TRANSLATES TO DAMAGES
HUMAN CAPITAL		
1	**Labor heat stress**	Shock to labor productivity from daily heat stress to both indoor and outdoor workers. Considers occupation-specific work ability curves from the International Labor Organization.
2	**Human health**	Shock to labor supply from changes in the incidence and mortality of vector-borne (malaria and dengue), water-borne (i.e., diarrheal), and temperature-related diseases.
3	**Water, sanitation, and hygiene**	Shock to labor supply from changes in diarrheal incidence and mortality due to investments in improved water supply and sanitation coverage.
4	**Water supply and demand**	Shock to water-dependent sector's productivity. Uses a water-agriculture nexus model to evaluate unmet demand s and replacement costs of water supply.
5	**Crop production**	Shock to crop revenues through changes in yields. Based on the Food and Agriculture Organization's crop-specific yield response functions to water availability and heat stress.
6	**Erosion**	Shock to crops from topsoil erosion and flooding due to vegetation conditions. Impacts on erosivity from changes in rainfall are based on the Revised Universal Soil Loss Equation model.

CHANNEL OF IMPACT		DESCRIPTION OF HOW CLIMATE CHANGE TRANSLATES TO DAMAGES
7	**Hydropower**	Shock to energy generation resulting from changes in river runoff. Utilizes a water systems model.
INFRASTRUCTURE AND SERVICES		
8	**Inland flooding**	Shock to capital from changes in the recurrence of peak precipitation events that result in fluvial (riverine) flooding. Models streamflows and floodplains, with damages estimated using depth-damage curves.
9	**Tropical cyclones**	Shock to capital from changes in tropical storm recurrence intervals, evaluated by assessing the impact of thousands of synthetically generated tropical storm tracks.
10	**Sea-level rise and storm surge**	Shock to coastal capital from changes in mean sea level and storm surge, using a bathtub approach.
11	**Tourism**	Shock to tourism sector revenues due to changes in climate variables, which produce changes in tourism potential.

As summarized in Table 1, each individual impact channel relies on stylized biophysical models that are capable of accepting climate information and projections, and simulating changes in biophysical (e.g., streamflow or infrastructure conditions) and/or socioeconomic (e.g., labor supply hours) variables under these altered climatic conditions. The biophysical models are customized to the country context by using country-specific inputs, obtaining key assumptions from country experts and available literature, and calibrating outputs using local data. Where locally collected data are not available, we rely on global sources. Alternative scenarios that consider different possible policy decisions and investments (for the purpose of climate change adaptation or general development of the country) can also be included in the modeling by modifying inputs and assumptions. Detailed descriptions of the impact channel methodologies, including the models used, resolution of the analysis, and key assumptions and limitations are presented in Appendix B, while Appendix C documents the specific data sources utilized in the impact channel analysis.

The output variables of these biophysical models are then translated into inputs to a Computable General Equilibrium model. These models are used to simulate the effects of policy changes and external shocks on the economy as a whole. Computable General Equilibrium models incorporate data on the interactions between different sectors and agents in the economy, and can be used to analyze the distributional impacts of policy changes on different groups. The economy is then divided into different sectors, such as agriculture, manufacturing, and services. These sectors are further divided into sub-sectors, depending on the level of detail required for the analysis. The Social Accounting Matrix is an important component of the model, used to represent the structure of the economy being studied and containing information on the flows of goods and services between different sectors, households, and the government. Typically, the Social Accounting Matrix would consider multiple sectors (e.g., agriculture, industry, services) as well as labor and capital as factors of production. These variables are shocked by results from the biophysical models.

In addition to macroeconomic metrics, these models can also generate poverty-related outputs by estimating changes in household income, consumption, employment, and welfare measures. These measures can then be used to assess the impact of climate change on poverty indicators as well as on different policies seeking to address poverty and inequality. The calculation of poverty shocks follows the same approach as the macroeconomic shock, i.e., the same biophysical models, inputs, and assumptions, except that results are provided at subnational resolutions to match available poverty microdata. IEc is working with the Poverty team to use available household survey data to improve the accuracy and resolution of the parameters in the biophysical models, and to calculate household-level shocks derived from the impact channels. Inputs for poverty analyses currently include the following impact channels: labor heat stress, human health, crop production, and livestock.

3.2 POLICY AND ADAPTATION SCENARIOS

The biophysical modeling conducted for each impact channel considers policy scenarios defined for the country. In general, these scenarios consider (1) **a business-as-usual trajectory**, in which the country continues its current growth and/or development trends and (2) **an aspirational development trajectory** in which more ambitious development is pursued as compared to the recent past. For example, a business-as-usual trajectory may consider a median projection of population or a constant coverage of clean water supply, while an aspirational growth trajectory may consider a reduced fertility scenario or a constant increase in clean water access. These scenarios are then incorporated into each impact channel by modifying assumptions on socioeconomic- and development-related variables.

Modeling of the relevant impact channels also considers **proactive adaptation interventions that seek to reduce the negative effects of climate change experienced through a particular channel**. Generally, greater levels of adaptation can achieve larger reductions in the cost of climate change, but with decreasing marginal benefits for incremental expenses in adaptation (see the left panel in Figure 8 below, taken from the Intergovernmental Panel on Climate Change's *Economics of Adaptation*). In practice, full adaptation to the impacts of climate change is not possible due to technological limitations and other implementation barriers, leaving unavoidable residual costs (as seen in the right panel of Figure 8). The adaptation scenarios considered in this study aim to strike a realistic balance between adaptation costs and residual impacts, where the marginal benefits of adaptation meet the marginal residual costs and overall benefit-cost ratios of the interventions are positive.

FIGURE 8. REPRESENTATION OF ADAPTATION COSTS AND RESIDUAL COSTS OF CLIMATE CHANGE

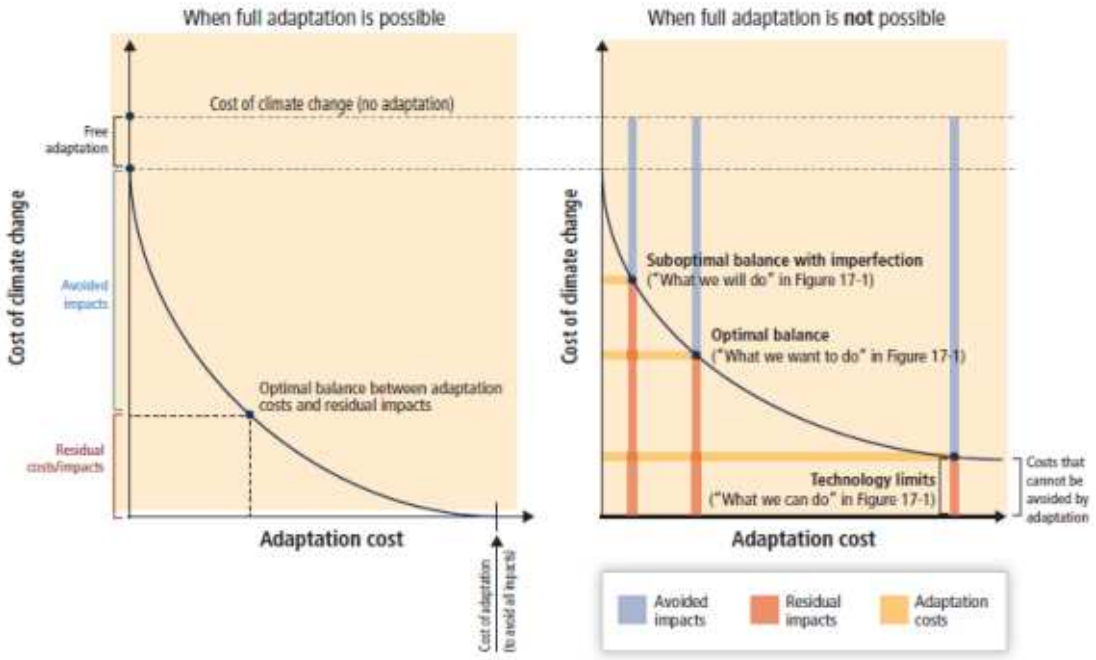

Source: The Intergovernmental Panel on Climate Change (Chambwera et al. 2014)

The modeled adaptation interventions for each impact channel were selected based on modeling feasibility, applicability to the specific country context, and the degree of climate change impacts. Adaptation costs are based on unit cost estimates obtained from international and, where available, local sources. Furthermore, the timing and magnitude of adaptation interventions were determined in coordination with the World Bank team and, if available, informed by existing sectoral and/or government plans in order to ensure fiscal realism of the investments (i.e., investment amounts and timings are realistic considering the country's investment capacity). Shocks were then generated for all policy scenarios, for both **a no-action baseline** as well as for **a proactive adaptation case**. The selected adaptation measures and modeling assumptions are detailed in the corresponding impact channel sections provided in Chapter 4.

3.3 CLIMATE SCENARIOS

To address climate uncertainty in the analysis, a total of ten climate scenarios were selected from among a larger set of available scenarios. The inclusion of multiple, carefully selected climate scenarios is critical to account for uncertainty in both future greenhouse gas emissions trajectories as well as uncertainty across different climate model projections.

Available climate scenarios were first obtained from the World Bank's Climate Change Knowledge Portal for 29 General Circulation Models (GCMs) from the Coupled Model Intercomparison Project 6 (CMIP6) suite of model outputs. Each GCM has up to five combinations of Shared Socioeconomic Pathway (SSP) and Representative Concentration Pathway (RCP) emissions scenario runs available. For each GCM-SSP combination, a modeled history from 1995 to 2014 and projections from 2015 to 2100 were available, for monthly mean

temperature and precipitation at a 1x1 degree grid resolution. Given that GCM outputs are biased relative to observed climate conditions, bias-correction and spatial disaggregation were conducted, before then interpolating monthly variables to a daily timestep. Appendix A provides further details on the climate inputs utilized as well as the bias-correction, spatial disaggregation and daily interpolation processes.

Figure 9 shows the projected mean temperature (left panel) and precipitation (right panel) in the country through 2100 across a range of SSP-RCP combinations. The bold lines are averages across GCM projections for each SSP, and the shaded zones surrounding those lines are the full range of GCM projections within an SSP. As can be seen, while GCM ensemble averages for precipitation (the bold lines in the right panel) do not change significantly relative to baseline precipitation, the precipitation projected across the full range of GCMs (the shaded zones in the right panel) varies widely. This emphasizes the importance of selecting a set of climate scenarios that captures a wide range of possible future conditions.

FIGURE 9. PROJECTED CLIMATE VARIABLES ACROSS A RANGE OF SSP-RCPs

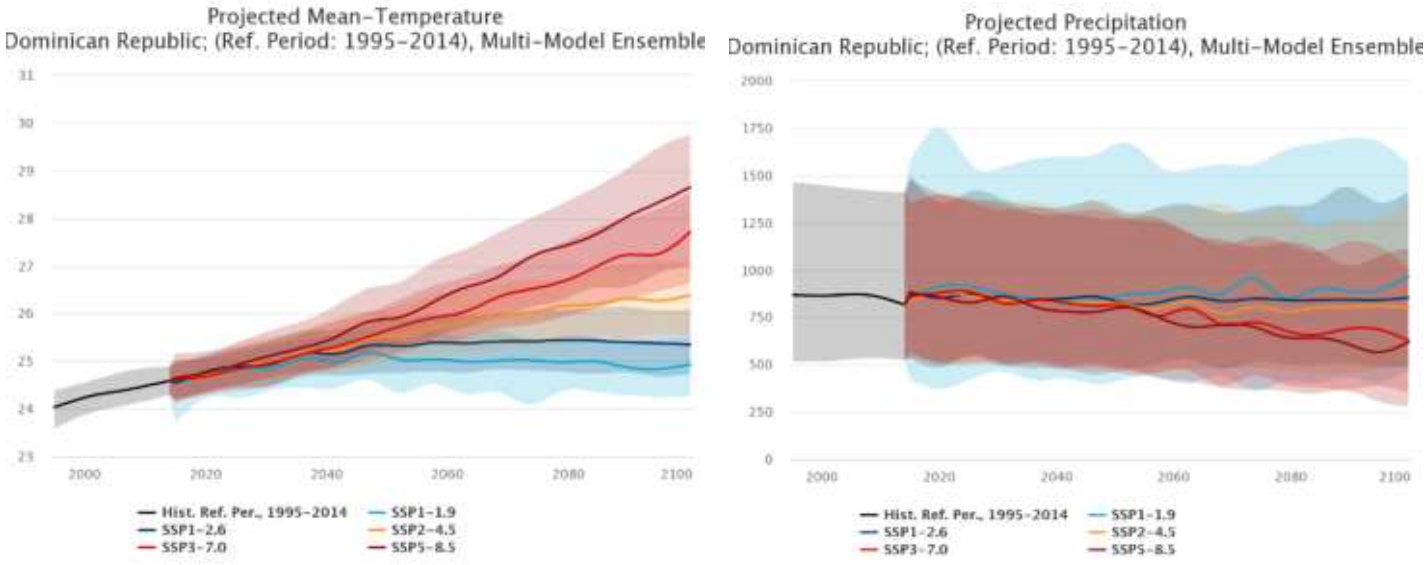

Source: World Bank Climate Change Knowledge Portal

Following World Bank guidance titled *Global scenarios for CCDR analyses* (February 3, 2022), two of the ten scenarios included in this project were selected to allow for comparisons across emissions scenarios - these are referred to as mitigation scenarios. The guidance specifies the following two mitigation scenarios:

- **Ensemble average of SSP3-7.0 GCMs**: Pessimistic Case. Scenario in which warming reaches 4°C by 2100, due to lax climate policies or a reduction in ecosystems and oceans' ability to capture carbon.
- **Ensemble average of SSP1-1.9 GCMs**: Optimistic Case. Represents reductions in greenhouse gas emissions in line with limited 1.5°C of warming by 2100.

In addition to enabling comparison across emissions scenarios, climate scenarios should also be selected in such a way as to capture the broadest range of climate change effects across GCMs.

In doing so, the vulnerability of the economy and the performance of adaptation options under possible wet vs. dry and hot vs. warm GCM outcomes can be assessed. We selected the following set of eight scenarios, based on changes from the baseline climate as compared to the period between 2051 and 2060:

- **Dry/hot scenarios:** Three scenarios around the 10th percentile of mean precipitation changes (i.e., dry) and the 90th percentile in mean temperature changes (i.e. hot), across SSP2-4.5 and SSP3-7.0 GCMs, as well as a mean across those three scenarios.
- **Wet/warm scenarios:** Three scenarios around the 90th percentile of mean precipitation changes (i.e., wet) and the 10th percentile in mean temperature changes (i.e. warm), across SSP2-4.5 and SSP3-7.0 GCMs, as well as a mean across those three scenarios.

The selected scenarios are summarized in Table 2, with further detail provided in Appendix A.

TABLE 2. SELECTED CLIMATE SCENARIOS

TYPE	SCENARIO
Mitigation	SSP1-1.9 MEAN
	SSP3-7.0 mean
Dry / hot future	SSP2-4.5 TAIESM1
	SSP3-7.0 KACE-1-0-G
	SSP3-7.0 IPSL-CM6A-IR
	Dry/hot mean
Wet / warm future	SSP2-4.5 CMCC-CM2-SR5
	SSP2-4.5 NORESM2-LM
	SSP3-7.0 CMCC-CM2-SR5
	Wet/warm mean

These same climate scenarios are utilized across all impact channels with the exception of the channels looking at *inland flooding, tropical cyclones* and *sea-level rise and storm surge*. The *inland flooding* analysis relies on data for the peak 1-day precipitation magnitude and frequency, rather than mean precipitation volumes. Since these data are only available for SSP ensemble aggregates in the Climate Change Knowledge Portal, we do not consider dry/hot or wet/warm futures and instead perform the analysis for SSP1-1.9 and 3-7.0 median (50th percentile) results.

In addition, for the impact channels that examine *tropical cyclones* and, *sea-level rise and storm surge,* our analysis does not utilize raw climate data from the Climate Change Knowledge Portal. Rather, we rely on processed variables resulting from changes in global temperatures and other effects on atmospheric and oceanic phenomena (i.e., changes in global and regional mean sea levels and cyclone tracks, frequency, magnitude, and duration). While these estimates are based on the same underlying data from the CMIP6 suite of model outputs, projections are not available for each individual GCM, hence we utilize median (50th percentile) results for SSP1-1.9 and 3-7.0.

4. IMPACT CHANNEL RESULTS

This section presents the results of the impact channel assessment by which climate change damages are estimated. For each impact channel considered, we first provide a brief overview table that summarizes key findings for this channel. This is followed by a description of how the channel was modeled, with further methodological detail available in Appendix B and data sources described in Appendix C. Finally, the results are presented, looking first at climate change effects and then at the resilience offered by different possible adaptation actions.

4.1 HUMAN CAPITAL

Climate change can negatively impact human capital in a variety of ways. Increased heat stress to workers can reduce labor productivity, while the increased incidence of infectious diseases can reduce labor supply. In addition, a lack of investments in activities like clean cooking services or water, sanitation, and hygiene can further exacerbate these climate-driven impacts on human capital. We use a labor supply model to calculate the total labor hours in the country under different future conditions, with the estimated impacts to the Dominican Republic's human capital due to climate change presented below.

4.1.1 LABOR HEAT STRESS

SUMMARY	
SUMMARY	Our analysis estimates the impact of climate change on labor productivity across the agriculture, industry, and services sectors. We estimate that by 2050 increasing temperatures may result in a labor supply shock ranging from around -3.5 to -9 percent.
ESTIMATED CLIMATE CHANGE IMPACTS BY 2041-2050	From 2041-2050, labor productivity shocks are expected to be highest for the agriculture sector, followed by the industry and services sectors. The Wet/Warm mean scenario is estimated to result in a -7 percent, -5 percent, and -4 percent impact to the agriculture, industry, and services sectors respectively. Overall, shocks from the Dry/Hot mean scenario are higher, with impacts estimated at around -13 percent, -9 percent, and -8 percent for the agriculture, industry, and service sectors, respectively.

Overview of Impact Channel

Climate change can impact labor supply by increasing workday temperatures and decreasing the number of hours an individual can perform work. To estimate labor heat stress impacts due to climate change, we calculate workday wet bulb globe temperatures as a measure of heat stress to derive labor productivity loss curves across three levels of physical activity. Our quantification of wet bulb globe temperatures assumes that relative humidity remains constant into the future

and that all occupations are performed evenly throughout the year. A detailed description of this method and its limitations are presented in Appendix B.

For each sector, the labor productivity shocks are based on the relative labor hours by occupation within each industry, and the extent to which these occupations are exposed to outdoor work. Within the agriculture sector, most labor hours are completed by skilled agricultural, forestry, and fishery workers, while a small portion of labor hours are conducted by elementary occupations (see Figure 10). Approximately 75 to 90 percent of labor hours in the agriculture sector occur in outdoor conditions (see Figure 11). Within the industry sector, labor hours are mainly divided among craft and trade workers, elementary occupations, services and sale workers, and technical professionals (see Figure 10). Exposure to outdoor work ranges from 10 to 90 percent of working hours (see Figure 11). Labor hours within the services sector are the most diverse of the sectors considered, with a range of occupations performed. The majority of labor hours in the services sector include service and sales workers elementary occupations (see Figure 10), who conduct around 25 and 90 percent of working hours outside, respectively (see Figure 11).

FIGURE 10. LABOR HOURS BY OCCUPATION

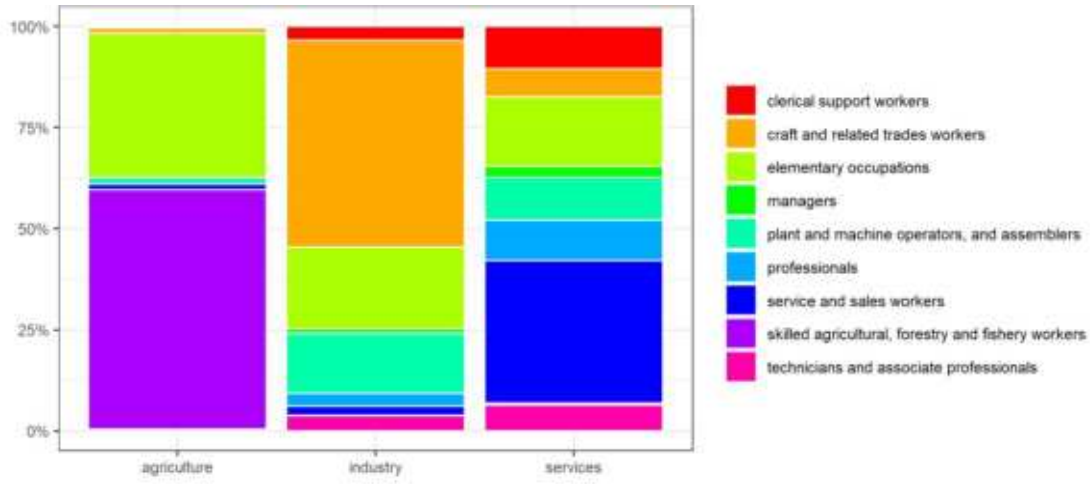

FIGURE 11. SHARE OF INDOOR OUTDOOR LABOR

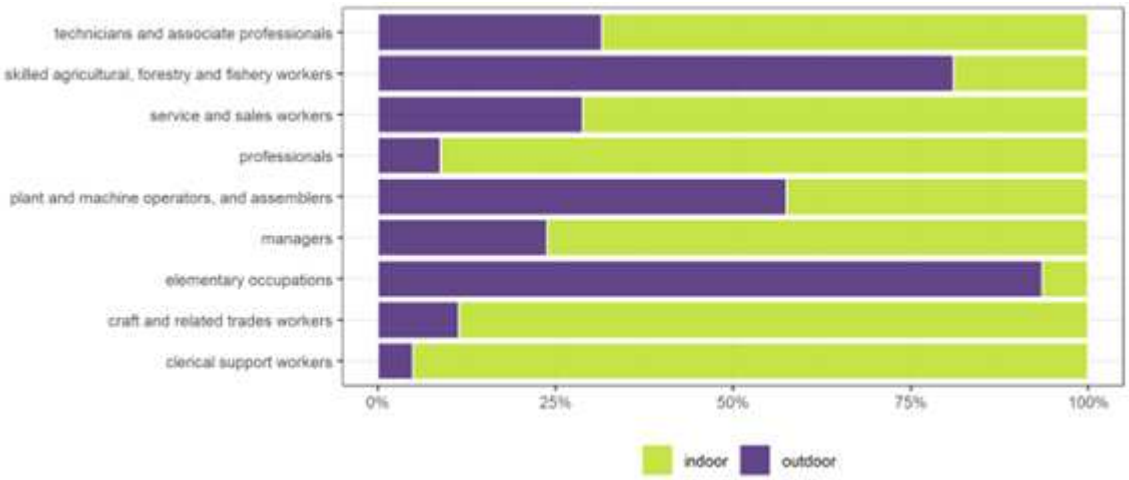

While both indoor and outdoor workers can be impacted by heat stress, outdoor workers are generally exposed to higher wet bulb globe temperatures at full sun exposure. In contrast, a portion of indoor workers are assumed to perform work in air-conditioned environments. Overall, the effect of heat stress intensifies for labor types that are outdoors and conducting more intense physical work.

The total impacts to labor supply are estimated for agriculture, service, and industry workers using available data on labor supply, relative heat and air-conditioning exposure, and labor force distribution, with the specific data sources detailed in Appendix C.

Results: Climate Change Effects

Results presented here describe labor productivity shocks relative to a baseline period (1995-2020) by sector until 2050 (Figure 12 and Figure 14).

In the baseline period, we observe a mean maximum workday wet bulb globe temperature that ranges from about 27°C to 36°C. This corresponds to a heat stress factor of 0.90, 0.88, and 0.80 for indoor workers performing low, medium, and high physical activity occupations respectively, on average. The heat stress factor is a multiplier that captures the percentage of an hour that laborers can perform work at a certain temperature. Low-activity occupations are generally linked to the services sector, medium to manufacturing (industry), and high to agriculture and construction (industry). For outdoor workers, mean maximum workday wet bulb globe temperature corresponds to a heat stress factor of 0.87, 0.75, for low, medium, and high physical occupations respectively, on average.

Based on the changes in labor productivity relative to the baseline, the overall labor productivity (i.e., the three sectors aggregated based on their share of labor supply) decreases over time (Figure 12). Shocks across different climate scenarios are projected to range from around -2 percent to -4 percent in 2030. When considering individual GCMs (i.e., the grey-shaded range shown in Figure 12), labor productivity shocks range from about 1 percent to -5.5 percent by 2030. Following 2035, the spread between the different scenarios increases, with shocks most severe under the Dry/Hot mean, followed by SSP3-7.0, the Wet/Warm mean, and SSP1-1.9

scenarios. Across GCMs, labor productivity shocks range from around -6 percent to -9 percent by 2050.

FIGURE 12. LABOR PRODUCTIVITY SHOCKS, 3-YEAR MOVING AVERAGE

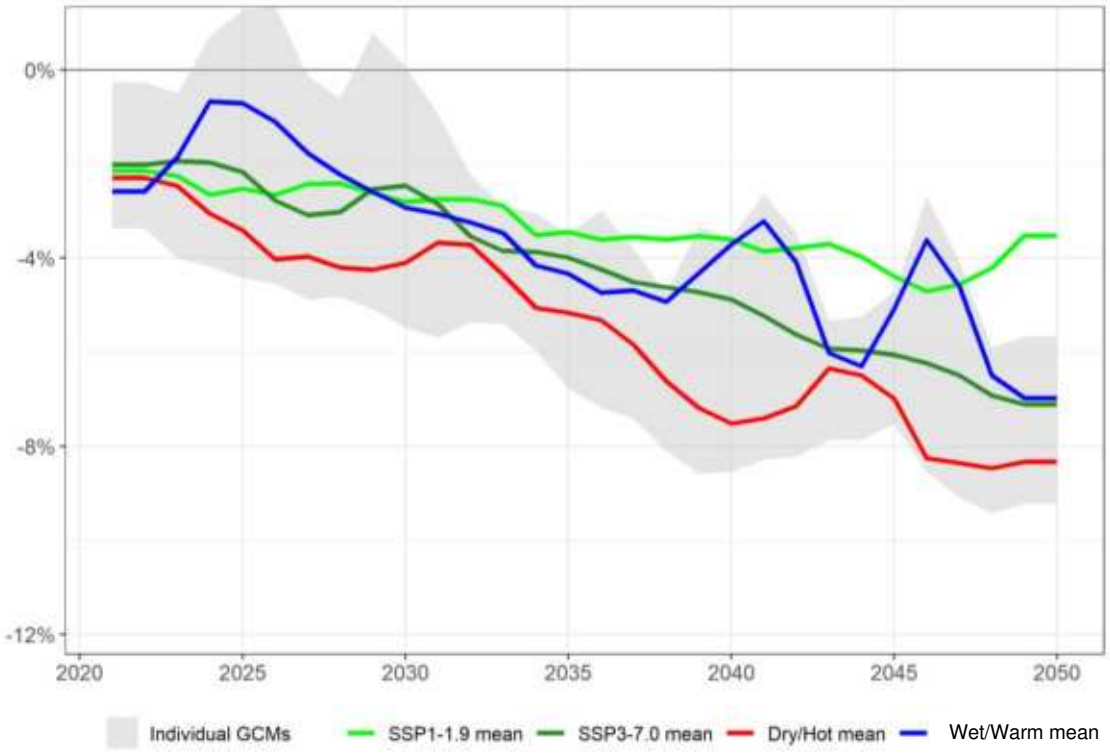

Figure 13 illustrates agriculture labor productivity impacts by region under the Dry/Hot and Wet/Warm mean scenarios from 2041 through 2050. Overall, we anticipate the Dry/Hot mean scenario will have harsher impacts by mid-century, with productivity shocks as great as -17 percent in some provinces. Under both scenarios, effects are most severe in north and southeast provinces.

FIGURE 13. AGRICULTURE LABOR PRODUCTIVITY IMPACT (%) BY PROVINCE, 2041-2050

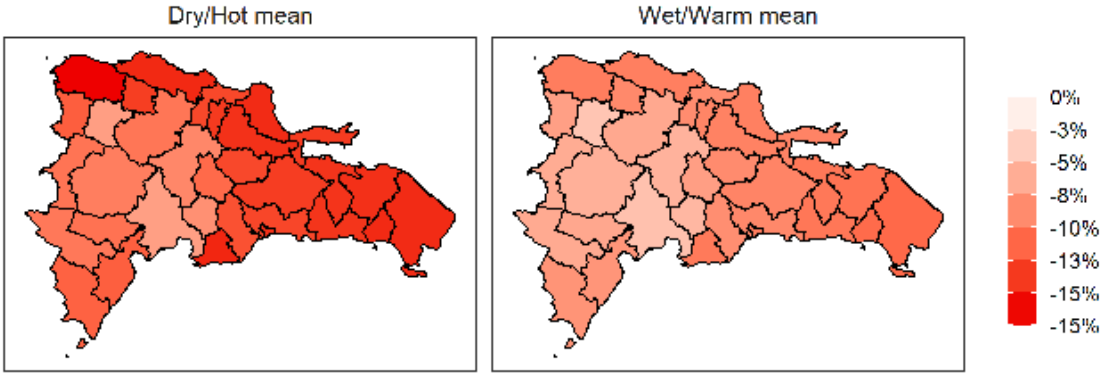

Across macroeconomic sectors, agriculture is expected to experience the highest labor productivity shock by 2041-2050, followed by industry and services sectors respectively (Figure 14).

FIGURE 14. LABOR PRODUCTIVITY SHOCK 2041-2050

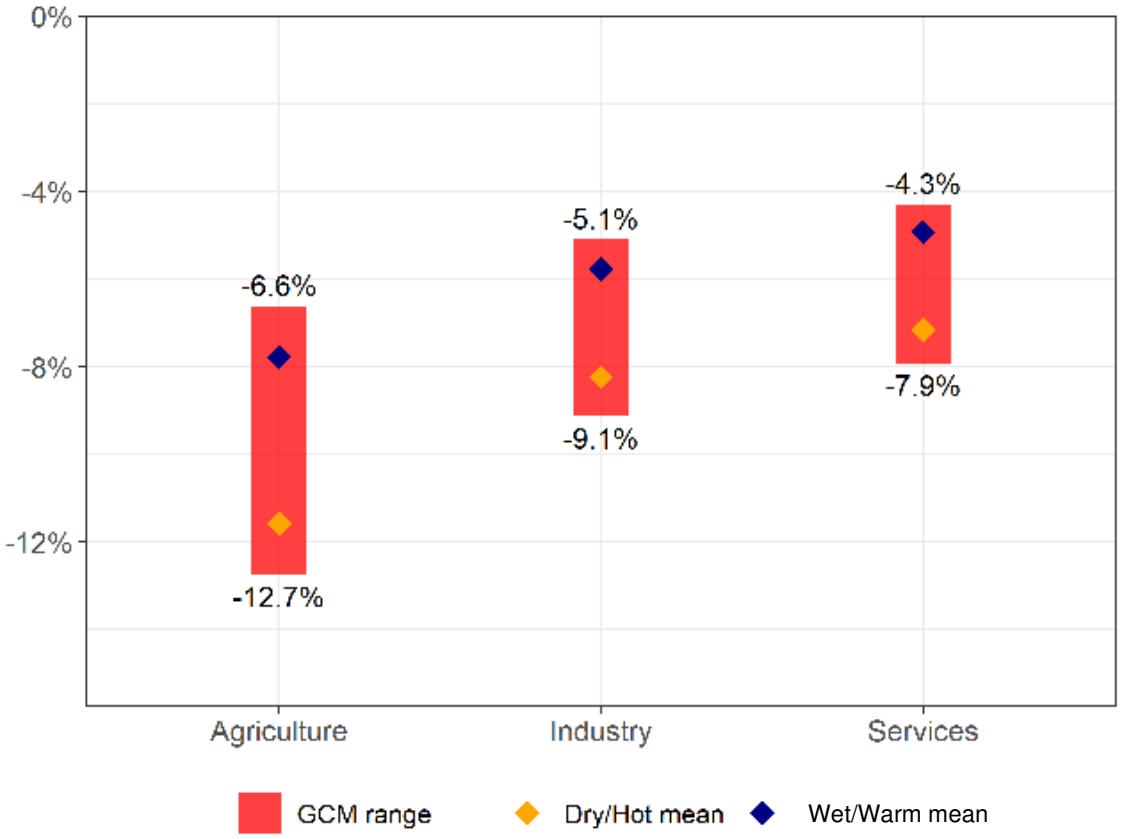

Adaptation

With the modeled effects of climate change on labor productivity documented above, this section now looks at the effect of investing in adaptation measures. As introduced in Section 3.2, we consider a **proactive adaptation scenario** and compare it to a **no-action baseline**. This no-action baseline is a fairly pessimistic scenario in that it does not take into account the fact that the country is growing and developing, and that some adaptation may take place as part of this growth.

When it comes to reducing the labor productivity shocks of climate change, there are a variety of possible adaptation interventions that could be pursued. These include changing the time of day that outdoor physical labor is conducted (e.g., more work during the early morning and evening), investing in active or passive cooling technologies (e.g., improved ventilation, fans, or air-conditioning), or minimizing the urban heat island effect (e.g., through green roofs, tree-planting etc.). For this channel, the specific adaptation intervention evaluated is **an increase in air-conditioning**. Table 3 shows details of the adaptation intervention for three different adaptation scenarios considered.

TABLE 3. ADAPTATION SCENARIOS AND INTERVENTIONS EVALUATED

ADAPTATION INTERVENTION	SCENARIO		
	NO-ACTION BASELINE	LOW ADAPTATION	HIGH ADAPTATION
Increase in air-conditioning for indoor workers	No change in air-conditioning coverage by 2050 (30% coverage)	Increasing air conditioning coverage by +20% by 2050 (reaching 50% coverage)	Increasing air conditioning coverage by +30% by 2050 (reaching 60% coverage)

Figure 15 shows the estimated labor productivity shocks due to climate change for the period between 2041 to 2050 relative to a baseline period of 1995 to 2020. The panel on the left shows the results for the no-action baseline case, assuming air-conditioning coverage is 30 percent at the outset; the panel in the middle shows results for the low adaptation scenario which assumes air-conditioning coverage increases to 50 percent by 2050; and the panel on the right shows results for the high adaptation scenario which assumes air-conditioning coverage increases to 60 percent by 2050.

Across macroeconomic sectors, agriculture is consistently expected to experience the highest labor productivity shocks in the period between 2041 and 2050, across all adaptation scenarios considered. Adaptation investments in air-conditioning have the greatest impact on the industrial sector, followed closely by the services sector. Labor productivity in industry is expected to experience shocks of between 0.5 and -2.8 percent under the high adaptation case compared to between -5.1 and -9.1 percent under the no-action baseline. While increased air-conditioning does reduce the shock experienced by the agriculture sector, the magnitude of this positive effect is much smaller than for industry and services, likely because most agricultural activities are conducted outdoors where air-conditioning is not possible and thus offers limited benefit.

FIGURE 15. LABOR PRODUCTIVITY SHOCK UNDER DIFFERENT ADAPTATION SCENARIOS, 2041-2050

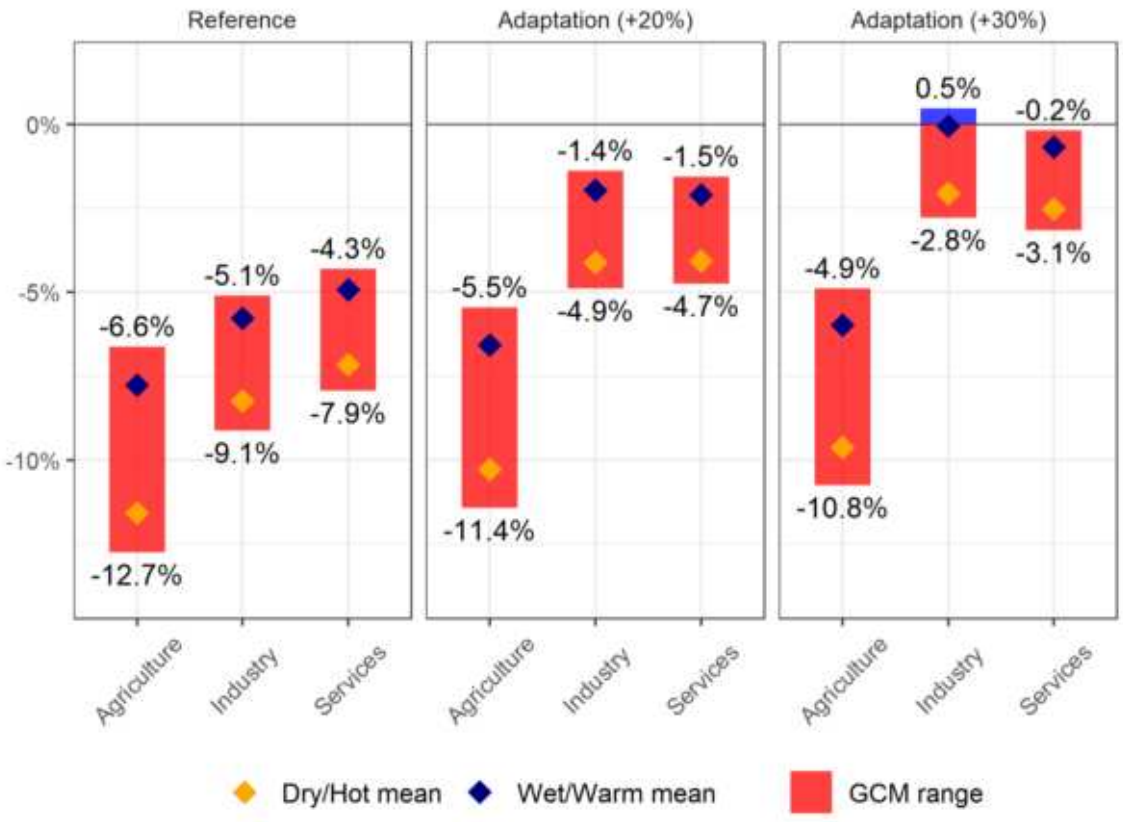

Figure 16 shows the labor productivity shock between 2020 and 2050 under current air-conditioning coverage (left panel), an increase of 20 percent coverage (center panel), and an increase of 30 percent coverage (right panel). In all three scenarios, shocks improve until around 2025 under the Wet/Warm mean scenario, after which shocks grow through mid-century under the no-action baseline and low adaptation scenario. Under the high adaptation scenario, shocks improve slightly during the 2040s before declining again by mid-century. Under the Dry/Hot mean scenario, shocks in the no-action baseline and low adaptation scenarios grow across the study period and stay at a similar level in the high adaptation scenario. While shocks under the Wet/Warm and Dry/Hot mean scenarios are negative for the no-action baseline and low adaptation scenario, under the high adaptation scenario, we expect small positive shocks in the 2040s. Overall, under the Wet/Warm and Dry/Hot mean scenarios, a 30 percent increase in air-conditioning coverage results in -1 and -2 percent shock in 2050, as compared to a -7.5 and -8.5 percent under the no-action baseline.

FIGURE 16. LABOR PRODUCTIVITY SHOCK UNDER DIFFERENT ADAPTATION SCENARIOS, 3-YEAR MOVING AVERAGE

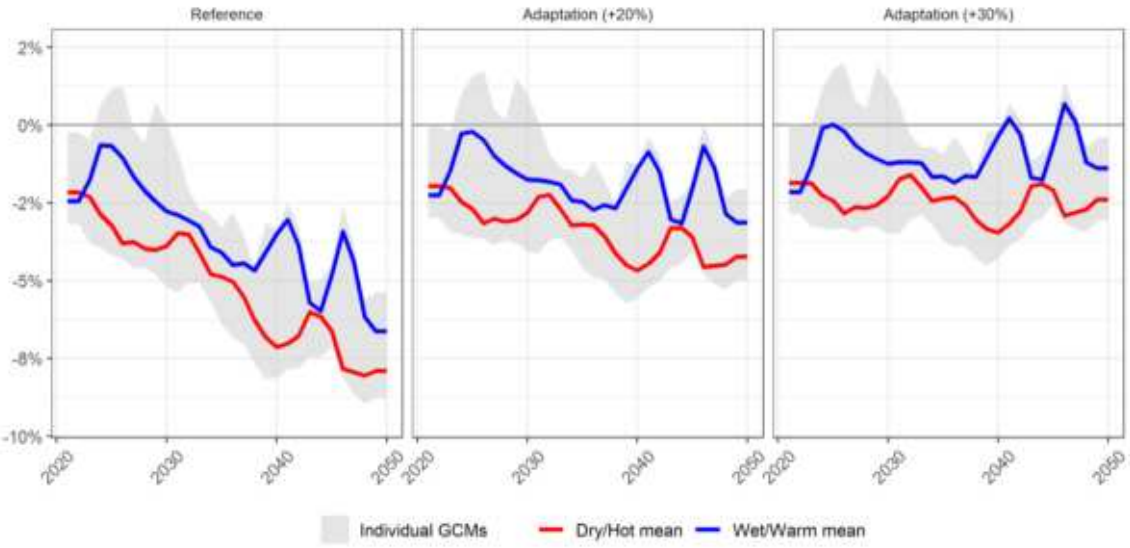

Summary and discussion

Overall, the analysis suggests that climate change will result in losses in labor productivity in the Dominican Republic due to increases in daytime temperatures, particularly daily maximums. Impacts are expected across all sectors of the economy and for both indoor and outdoor workers. However, the effects on agricultural labor are higher because the sector has a higher proportion of outdoor workers and requires higher levels of physical labor. This sector is followed by industry, and then by services. Between 2041-2050, mean annual impacts can range between -7 and -13 percent for agriculture, -5 and -9 percent for industry, and -4 and -8 percent for services. While the negative impacts are ubiquitous across the country, eastern and northern areas of the country are likely to experience higher impacts due to both higher current and projected temperatures. In contrast, western, higher-altitude regions will be less impacted.

While air conditioning can effectively reduce the impact of climate change, the benefits of this measure are limited to the indoor workforce only. That said, increasing the share of indoor workers with access to air conditioning to about 60 percent would virtually eliminate the effect of climate change under a Wet/Warm future for industry and service workers, which have a higher proportion of indoor labor. However, for both agriculture and the remainder of the outdoor workforce, additional adaptation measures would need to be considered in order to reduce the negative impact of climate change.

4.1.2 HUMAN HEALTH

SUMMARY	
SUMMARY	Our analysis estimates the impact of climate change on labor supply as a result of the changing incidence of illnesses and deaths from vector-borne diseases, heat-related diseases, and waterborne infectious diseases. We estimate that by 2050, increasing temperatures may result in a labor supply shock ranging from around -0.028 to -0.055 percent.
ESTIMATED CLIMATE CHANGE IMPACTS BY 2041-2050	From 2041-2050, labor supply shocks are expected to be highest from heat-related diseases, followed by water-borne and vector-borne diseases. The Wet/Warm mean scenario is estimated to result in a -0.038 percent labor supply impact. Shocks from the Dry/Hot mean scenario are higher, with impacts estimated at around -0.048 percent in total.

Overview of Impact Channel

Climate change may impact human health through increased incidence of and deaths from **vector-borne diseases** such as malaria and dengue, **heat-related diseases**, and **waterborne infectious diseases** that cause acute diarrhea, which all influence the total labor supply. We apply different biophysical and statistical relationships between climate variables and the incidence of or transmissibility for each disease, with changes in disease incidence and death rates then used to estimate the number of hours of labor supply lost. A summary of the methodology used is presented below, with a more detailed description available in Appendix B.

When considering **vector-borne diseases,** the same general methodology is applied to both malaria and dengue. These are both mosquito-borne diseases whose spread depends on the right environmental conditions occurring for the mosquitoes to live, breed and increase in number. These conditions are approximated from three climate variables, namely mean monthly temperatures, cumulative annual precipitation, and minimum annual winter temperature, and are used to calculate a suitability index ranging 0 (unsuitable) to 1 (suitable). The exposed population is then estimated, as a probability of the occurrence of the disease in the area, with the resulting deaths due to and cases of the disease calibrated using reported deaths and prevalence rates from official sources.

Heat-related illnesses are modeled based on calculating excess mortality from daily maximum temperatures. The temperature–mortality relationship is assumed to be V-shaped (see Figure 17), and the temperature value at which mortality is lowest is defined as the optimum temperature (OT). For temperatures above the optimum threshold for a given location, excess heat-mortality is defined daily as a fraction of the average total non-injury-related deaths occurring that day, with the excess mortality calibrated to nationally reported statistics of non-injury heat-related mortality.

FIGURE 17. V-SHAPED FUNCTION OF EXCESS MORTALITY DUE TO HIGH TEMPERATURES

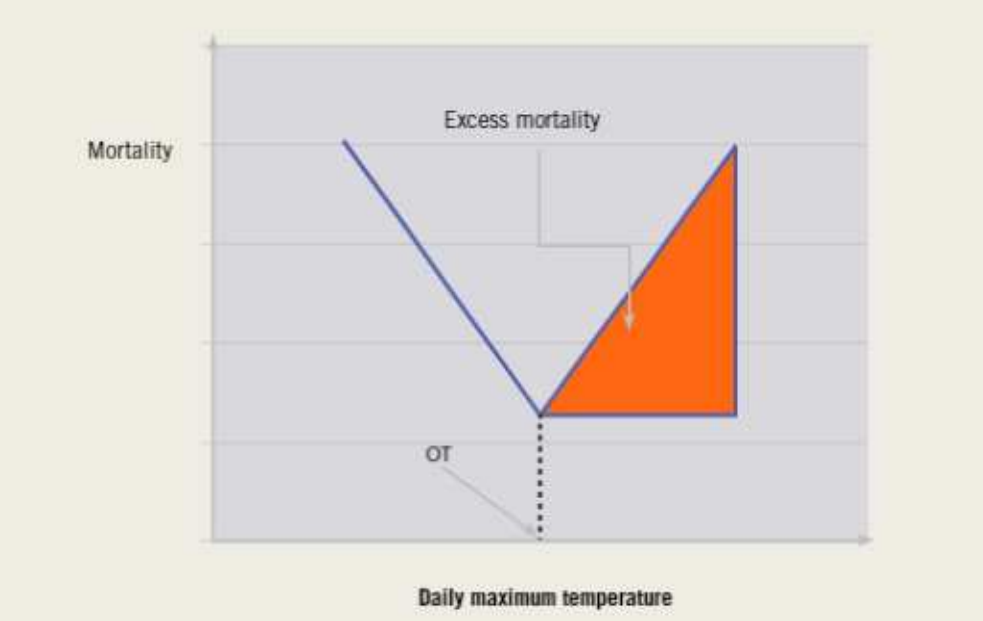

Source: World Health Organization 2014

For **waterborne diseases,** we follow the modeling approach described by the World Health Organization (2014), which applies gridded estimates of average annual temperature anomalies to a statistical temperature–mortality risk relationship. The approach calculates the total estimated diarrheal deaths and cases in the future without climate change, and then estimates the climate change-attributable percent change.

Finally, the changes in the incidence and death rates of the different types of diseases described above are then used to model the number of hours of labor supply lost. Additional deaths relative to the baseline and absenteeism from work due to people falling sick directly reduce the total labor available. Additionally, there is also an indirect effect from children getting sick and needing parental care for the duration of the disease. The total hours of labor lost for each disease are then calculated for the country for both historical periods as well as future projections. The specific data sources used to complete the analysis are detailed in Appendix C.

Results: Climate Change Effects

Results presented here describe labor supply shocks relative to a baseline period (1995-2020) as projected until 2050.

Figure 18 shows the breakdown of the mortality and morbidity for the different diseases considered from 2015 to 2019. Of the four disease categories, only water-borne diseases and heat-related diseases contribute to non-injury-related deaths in the country. Their respective share of deaths is low, with 0.9 percent of the total non-injury deaths recorded in the Dominican Republic caused by water-borne diseases and 0.1 percent caused by heat-related diseases. The incidence of water-borne diseases and heat-related diseases are both low at 0.3 percent and 0.1 percent respectively.

FIGURE 18. BREAKDOWN OF DISEASE MORTALITY AND MORBIDITY FOR 2015-2019

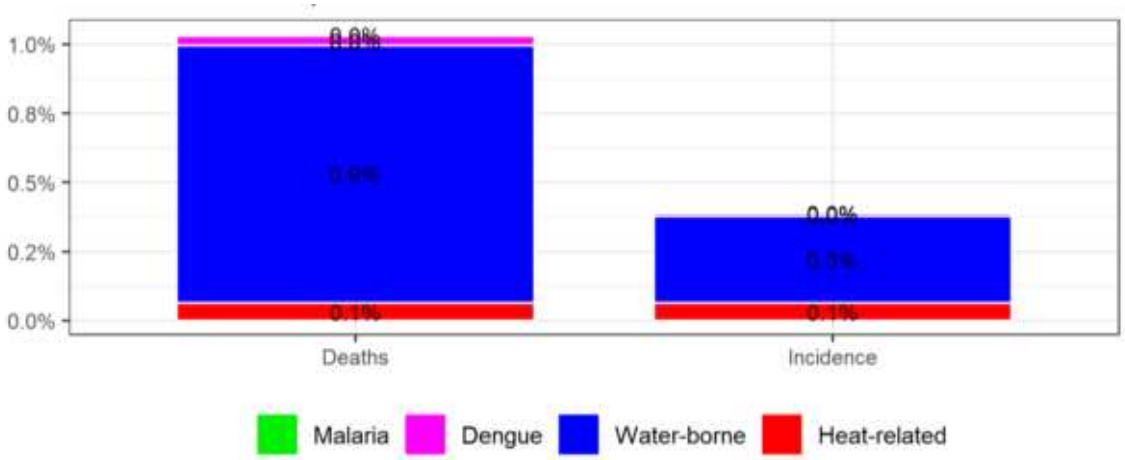

Figure 16 shows how the mortality and morbidity of the different diseases are expected to change relative to the historic breakdown shown above when considering the impacts of climate change. Heat-related diseases are expected to be impacted the most, with increases in mortality and morbidity of more than 2,000 percent by 2050, as compared to 41 percent for waterborne diseases, 22 percent for dengue and 11 percent for malaria. Impacts from dengue, heat-related diseases, and water-borne diseases are all expected to grow as mid-century approaches. Impacts from malaria show a decreasing trend across the Dry/Hot mean scenario and specific GCMs. Malaria impacts relative to the baseline are greater under the Wet/Warm mean scenario than the Dry/Hot mean scenario. This occurs as temperatures in the Dry/Hot mean scenario exceed identified thresholds, thereby reducing malaria transmissibility. However, the Dry/Hot mean scenario is expected to result in greater impacts for heat-related illnesses, water-borne illnesses, and dengue, when compared to the Wet/Warm mean scenario.

FIGURE 19. CHANGES IN DISEASE MORTALITY AND MORBIDITY DUE TO CLIMATE CHANGE COMPARED TO BASELINE

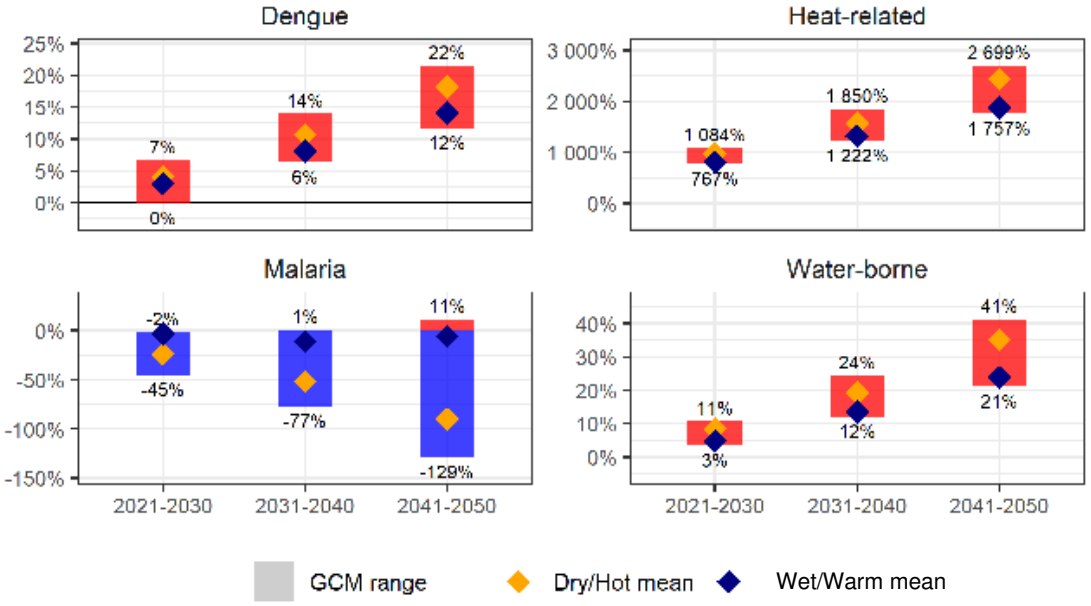

Figure 20 shows the annual number of heat-related deaths in the country during the baseline period and under the Dry/Hot and Wet/Warm mean scenarios for the period from 2041 to 2050. During the baseline period, heat-related deaths are concentrated in central areas of the country, with heat-related mortality peaking at approximately 5 deaths annually. Overall, the prevalence of heat-related deaths is greatest under the Dry/Hot mean scenario, with most deaths occurring near Santo Domingo and in the north. In these areas, mortality ranges from approximately 2.5 to 17.5 deaths annually. Under the Wet/Warm mean scenario, similar areas are expected to be affected, though estimated impacts are less severe.

FIGURE 20. PROJECTED ANNUAL HEAT RELATED DEATHS

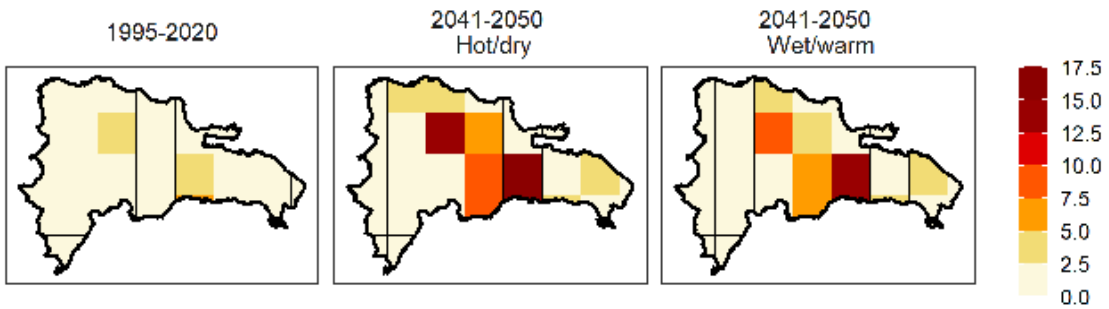

Based on the changes in labor supply due to disease mortality and morbidity relative to the baseline, the overall labor supply decreases over time, with the magnitude of the decrease being fairly small (Figure 21). By 2030, the Dry/Hot mean scenario is expected to result in the most severe shock, with a magnitude of -0.02 percent. Shocks from the Wet/Warm mean scenario are slightly less negative at -0.015 percent. When considering individual GCMs (i.e., the grey

shaded range in Figure 21), labor supply shocks range from around -0.01 percent to -0.025 percent in 2030. By mid-century, divergence between the four scenarios increases, with SSP1-1.9 scenario resulting in the smallest shock followed by the Wet/Warm mean, SSP3-7.0 and the Dry/Hot mean scenarios. Across GCMs, labor supply shocks range from around -0.035 percent to -0.055 percent by 2050.

FIGURE 21. LABOR SUPPLY SHOCKS, 3-YEAR MOVING AVERAGE

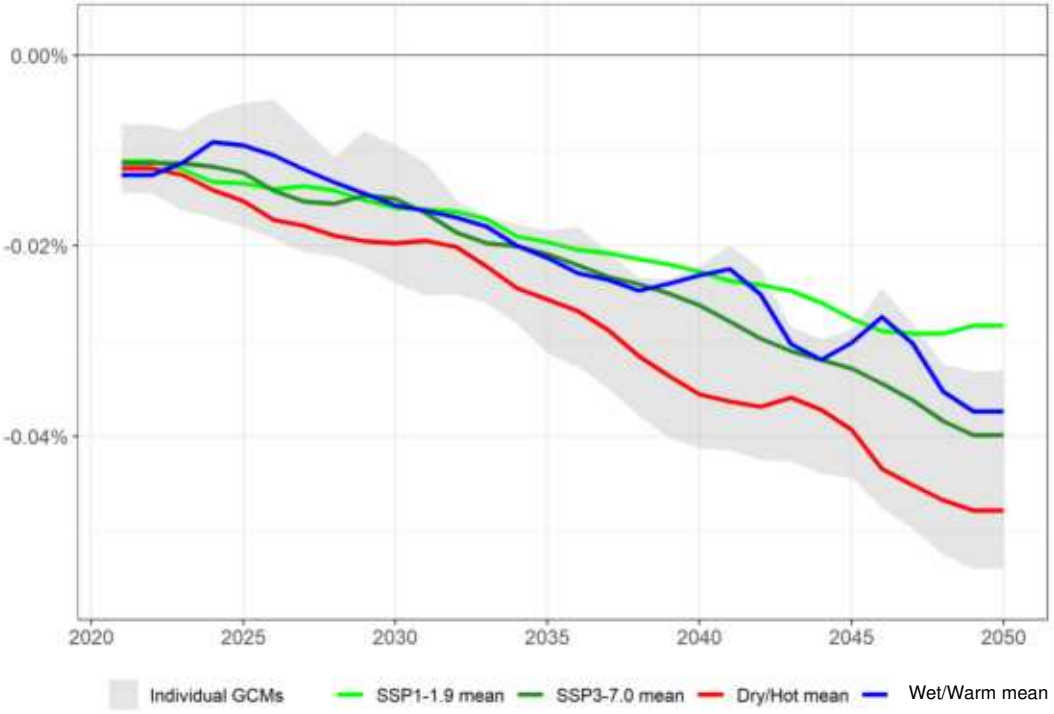

Summary and discussion

Climate change is likely to produce significant changes in the mortality and morbidity of vector-borne, heat-related, and waterborne diseases in the Dominican Republic. The transmissibility of dengue and waterborne pathogens is expected to increase up to 22 and 41 percent by 2041-2050 under the worst-case scenario, primarily from increases in mean temperatures. Dengue transmissibility is likely to expand to higher elevation areas as temperatures increase, where current mean temperatures cause sub-optimal levels of mosquito reproductive rates. For waterborne diseases, ubiquitous increases in mean temperature will result in overall higher incidence rates everywhere in the country. Heat-related diseases will experience the highest percent increase in incidence and death rates, caused by a combination of a current low baseline rates and a steep increase in daily peak temperatures. However, all things equal, the share of mortality and morbidity from these diseases will still remain a small fraction of the total country rates. Lastly, in contrast to the other three diseases modeled, malaria transmissibility is expected to reduce under most scenarios, as a result of temperatures surpassing the optimal level for mosquito reproduction. As such, a Dry/Hot mean scenario would result in the highest decrease in malaria incidence, compensating for part of the effects from the other diseases modeled.

Overall, the resulting effect on labor supply is negative, and more significant under a Dry/Hot future by mid-century. However, while the changes in each specific disease are significant, the resulting macroeconomic shock to labor supply is small because of two reasons. First, these four diseases combined represent only about 1 percent of the total number of deaths in the Dominican Republic today and less than half a percent of the total incidence rate. Second, while death or illness can cause grave consequences at the individual or household levels, the proportion of adults that die or fall sick during a year is still a relatively low proportion of the total workforce. Hence, increases in mortality and morbidity rates are expected to result in limited impacts on labor supply.

4.1.3 WATER, SANITATION, AND HYGIENE

SUMMARY	
SUMMARY	Our analysis estimates the impact of water, sanitation, and hygiene investment on the incidence of water-borne diseases and related mortality. We estimate that by 2050, water, sanitation, and hygiene investments under a business-as-usual and an aspirational scenario would result in a positive labor supply shock of approximately 0.05 percent and 0.09 percent across all four climate scenarios, as compared to a reference scenario that sees water, sanitation, and hygiene coverage levels remain unchanged.
ESTIMATED CLIMATE CHANGE IMPACTS BY 2041-2050	From 2041-2050, the effects of water-borne illness on mean labor hours vary across the different investment scenarios, with impacts most severe from the no action reference scenario. Overall, the Dry/Hot mean scenario is expected to result in the most negative impacts to labor supply, with shocks of -1.2 percent, -0.3 percent, and 0.4 percent for the reference, business-as-usual, and aspirational scenarios, respectively. The Wet/Warm mean scenario is expected to result in slightly less negative impacts with shocks of -1.1 percent, -0.2 percent, and 0.5 percent for the reference, business-as-usual, and aspirational scenarios, respectively

Overview of Impact Channel

Development policy initiatives related to water, sanitation, and hygiene can indirectly influence the severity of potential climate change impacts on human capital, as the quality of infrastructure can help to reduce disease incidence and related mortality. This impact channel evaluates the benefits of enhanced investments in water, sanitation, and hygiene, by comparing a no action reference scenario, a baseline scenario where current trends of coverage and quality of infrastructure continue over time, and an aspirational scenario where additional investments in water, sanitation, and hygiene services reduce the incidence of water-borne diseases. A summary

of the modeling methodology used is presented below, with a more detailed description available in Appendix B.

We follow the methodology applied by Wolf et al. (2019), which is based on a statistical relationship between a fecal contamination composite index and the relative risk of diarrheal diseases. The fecal contamination composite index utilizes a rubric to assign a 0, 1, or 2 value to eight indicators related to water, sanitation and hygiene access (see Figure 22). The index corresponds to the sum of these indicators (ranging from 0 to 16 in total), with higher index values generally corresponding with higher relative risk of diarrheal disease. The resulting relative risks are then calibrated for the country using reported data on mortality and morbidity linked to inadequate water, sanitation, and hygiene infrastructure, with the specific data sources used to complete the analysis detailed in Appendix C.

FIGURE 22. FAECAL CONTAMINATION COMPOSITE INDEX INDICATORS

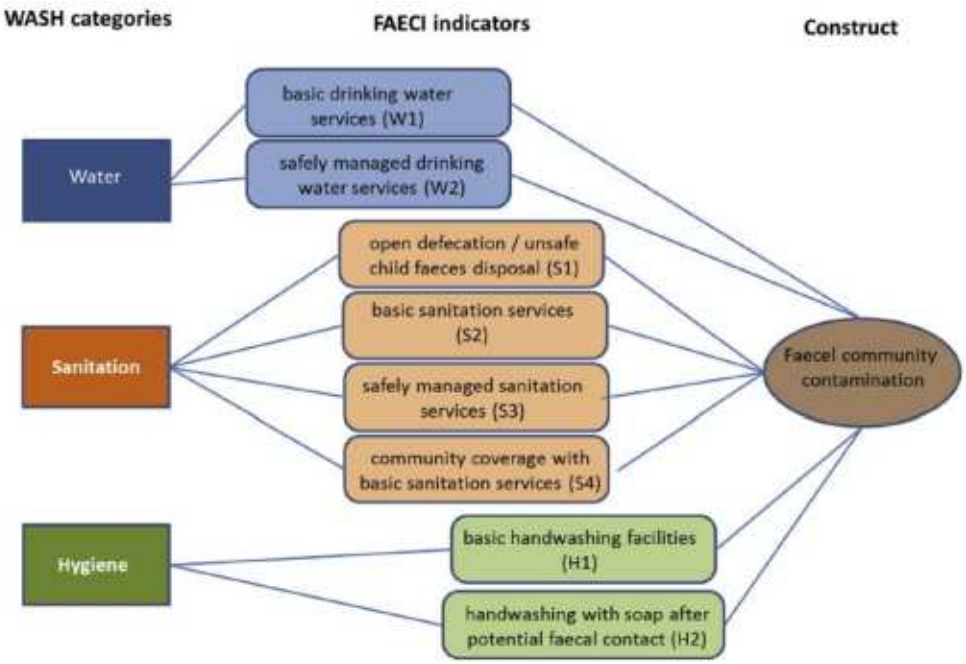

Source: Wolf et al. 2019

Table 4 shows the business-as-usual and aspirational scenarios for 2030 and 2050 of water, sanitation, and hygiene coverage as compared to the base year coverage in 2020 (i.e., the reference scenario). For instance, 87.2 percent of Dominicans had basic sanitation services in 2020, which grows to 91 percent and 98.6 percent under the business-as-usual and aspirational scenarios by 2030 respectively. By mid-century, the business-as-usual scenario reaches the same coverage rates of the aspirational scenario in 2030, while under the aspirational scenario, the entire Dominican population is served by basic or safely managed sanitation services as well as basic drinking water services. (Note that for the indicator S1/Open defecation, a decrease from 2.3 percent in 2020 to 0 percent by 2050 under the business-as-uusual and aspirational scenarios is a positive outcome where none of the population is exposed to open defection. This decrease works in tandem with the increase in the provision of basic sanitation services).

TABLE 4. COVERAGE OF WASH SERVICES (% OF POPULATION)

Indicator/Description	Base (i.e., reference case) (2020)	Business-As-Usual scenario (2030)	Aspirational scenario (2030)	Business-As-Usual scenario (2050)	Aspirational scenario (2050)
S1/Open defecation	2.3	1.5	0	0	0
S2/Basic sanitation services	87.2	91	98.6	98.6	100
S3/Safely managed sanitation services	69	88.8	100	100	100
S4/Community coverage with basic sanitation services	87.2	91	98.6	98.6	100
W1/Basic drinking water services	96.7	97.3	98.5	98.5	100
W2/Safely managed drinking water services	80.9	81.9	83.9	83.9	89.9
H1/Basic handwashing facilities	60.7	61.9	64.3	64.3	71.5
H2/Handwashing with soap after potential contact	46.9	47.9	49.9	49.9	55.9
FAECI/Fecal contamination composite index	5	5	3	3	2
RR/Relative risk (i.e., share of diarrheal diseases from water, sanitation, and hygiene)	90%	90%	58%	58%	40%

Results: Climate Change Effects

Figure 23 shows the combined effect of increased water-borne illness due to climate change (derived from the human health impact channel) and investments in water, sanitation, and hygiene infrastructure for the case of the Dominican Republic. Results are represented for 3 scenarios: (1) a reference scenario in which water, sanitation, and hygiene coverage is kept at 2020 levels, (2) a business-as-usual scenario that assumes the percent coverage in each metric follows the trends observed in the last five years, and (3) an aspirational scenario in which water, sanitation, and hygiene coverage increases over time according to stated policy goals.

Under the reference scenario, shocks hover around -1 percent by 2030 and gradually become more negative by mid-century. This occurs as water, sanitation, and hygiene coverage rates remain constant while both population and climate change impacts increase. The business-as-usual scenario results in a shock of around -1 percent in 2030 and gradually becomes less negative, reaching a value of around -0.25 percent by 2050. Similarly, under the aspirational scenario, shocks are negative in 2030, becoming less negative over time, and reaching a positive value of around +0.45 percent by mid-century.

FIGURE 23. EFFECT OF WATER-BORNE ILLNESS ON MEAN LABOR HOURS IN THE DOMINICAN REPUBLIC, PER WORKER PER YEAR

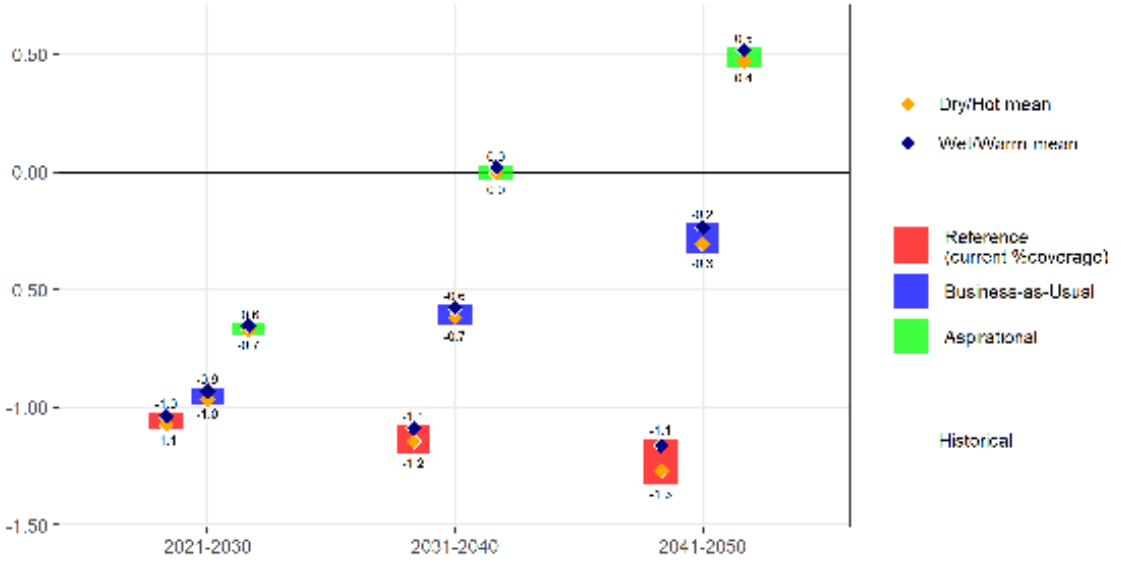

Figure 24 shows the gross labor supply effect of water, sanitation, and hygiene investments (i.e., not considering climate change impacts on waterborne diseases) for the Dominican Republic. In this case, both business-as-usual and aspirational scenarios would result in benefits (i.e., positive labor supply shocks). By mid-century, the aspirational scenario, which sees greater investments in water, sanitation, and hygiene coverage, would have a greater positive impact on labor supply across all climate scenarios than the business-as-usual scenario (Figure 24). Under the aspirational scenario, labor supply shocks of approximately +0.09 percent are projected for all four climate scenarios considered, while under the business-as-usual scenario, the four climate scenarios converge at shocks of approximately +0.05 percent by 2050.

FIGURE 24. LABOR SUPPLY SHOCK FROM WATER-BORNE DISEASES AND WASH INVESTMENTS, 3-YEAR MOVING AVERAGE

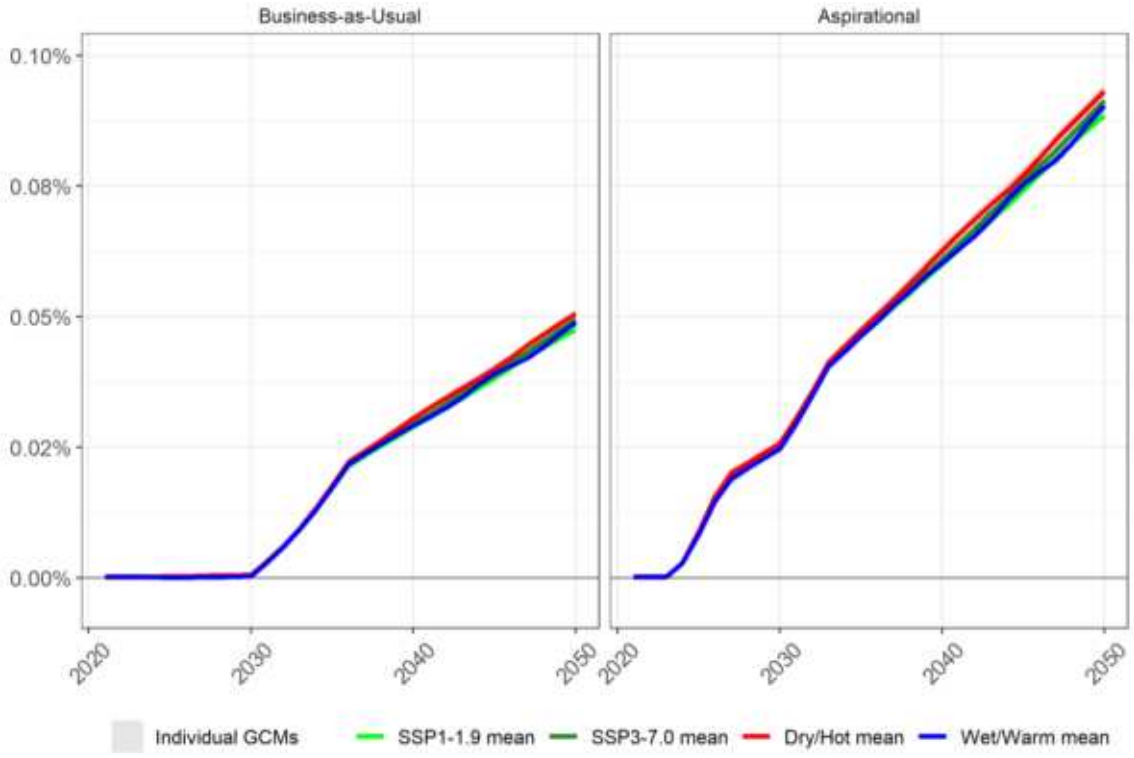

Summary and discussion

Overall, enhancing access to water, sanitation, and hygiene services in the country will result in positive impacts on labor supply due to a reduced number of deaths and absenteeism from work of people in the workforce. A business-as-usual scenario in which recent sanitation and clean water growth trends are continued over the course of the coming decades out to 2050, would result in a gain in labor supply of about +0.05 percent. A more ambitious aspirational scenario that sees the achievement of stated policy goals in terms of water, sanitation, and hygiene coverage could result in an almost a twofold gain (i.e., a labor supply shock of about +0.09 percent) as compared business-as-usual conditions.

Without any advances in water, sanitation, and hygiene (i.e., keeping current coverage, as quantified under the reference scenario) labor supply is expected to be negatively impacted over time. Under business-as-usual, water, sanitation, and hygiene investments will offset the negative impacts of climate change on waterborne diseases (i.e., the effects analyzed in the Human Health impact channel), regardless of the climate scenario. As in the Human Health channel, the overall impacts on labor supply are small due to the small share of waterborne illnesses in mortality and morbidity, and the limited impact of disease incidence on the labor force.

4.2 WATER AND AGRICULTURE

Natural resources are expected to experience a variety of impacts from climate change. Temperature increases are likely to reduce the suitability and productivity of crops, pastures, and livestock, and changes in precipitation patterns can result in reduced water resources available for users including agriculture and hydropower generation, as well as impacting erosion levels that can result in additional downstream effects. The estimated impacts to the Dominican Republic's agriculture and natural resources sectors due to climate change are presented below.

4.2.1 WATER SUPPLY AND DEMAND

SUMMARY	
SUMMARY	Our analysis estimates the impact of climate change on water supply by modeling changes in water availability due to variations in precipitation. Relative to baseline conditions, we estimate that by the 2040s, unmet demand will increase by 40 percent under the Wet/Warm mean scenario to 21 million cubic meters. Under the Dry/Hot mean scenario, impacts are expected to be more severe with unmet demand more than doubling to 35 million cubic meters.
ESTIMATED CLIMATE CHANGE IMPACTS BY 2041-2050	From 2041-2050, negative impacts to the municipal and industrial water sectors are expected to be highest under the Dry/Hot mean scenario, resulting in a +1.9 percent increase in unmet water demand on average, relative to the baseline. The Wet/Warm mean scenario is anticipated to lead to a smaller negative shock, resulting in +1.1 percent increase in unmet demand on average by mid-century.

Overview of Impact Channel

Insufficient water supply can affect manufacturing and other water-dependent industries in a country, as well as domestic use by the general population. We use a Water Evaluation And Planning (WEAP) water systems model to evaluate shortfalls to municipal and industrial demand, given competing uses, climate change effects, and available storage infrastructure. Figure 25 illustrates the basin delineation used for the WEAP model. The macroeconomic shock from water availability is quantified as either the impact of shortages or the cost of a replacement water supply (e.g., desalinization), for the scenarios being considered. A summary of the modeling methodology used is presented below, with a more detailed description available in Appendix B.

FIGURE 25. BASIN DELINEATION FOR WATER SYSTEMS MODEL

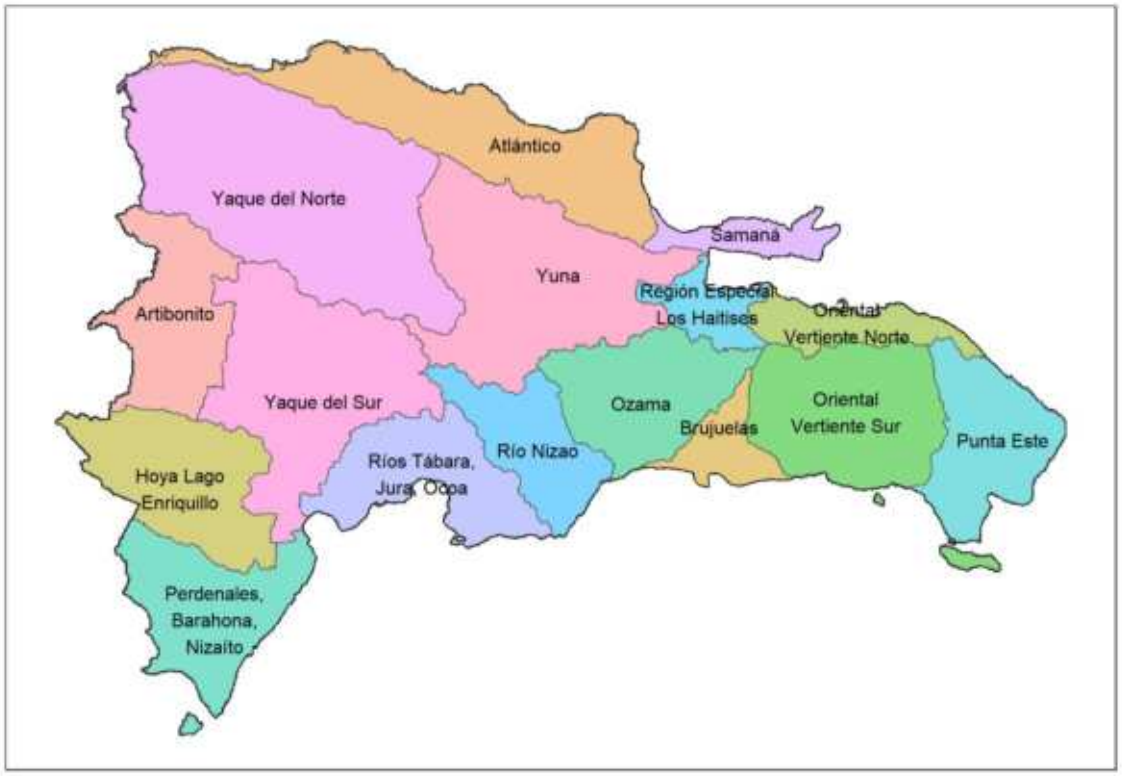

Figure 26 summarizes the modeling approach of the water system for the country. First, local data sources are collected and used as inputs together with the projected CMIP6 temperature, precipitation, and potential evapotranspiration, to run and calibrate the rainfall-runoff model (Turc-Pike) and the crop water demand model (FAO66). The results of these two models are respectively the river runoff and the irrigation needs of each basin that feed into the WEAP model. Next, the historical and projected water demands (or socio-economic factors determining a trend in such demands) in the municipal and industrial sectors are estimated. The WEAP model uses all of these inputs to have complete information on the various demands for water resources. A river (blue line), a node (red dot) for each demand sector, one or more reservoirs (green triangle) and the environmental flow requirement for the river (purple crossed circle) are then attributed to each of the 16 basins as shown in Figure 27. Most of the local sources used derive information from the Plan Hidrológico Nacional República Dominicana (INDRHI, 2012), with this plan providing information on irrigated areas, current and future industrial and municipal demands at different resolutions, as well as the gaged mean, minimum, and maximum historical average monthly flows of the main rivers. Available information on reservoirs and hydropower facilities is used alongside data obtained from AQUASTAT. Additionally, historical runoff data, collected from the Global Runoff Data Centre and from local sources, is used to calibrate the rainfall-runoff model.

FIGURE 26. WATER RESOURCES MODELING APPROACH

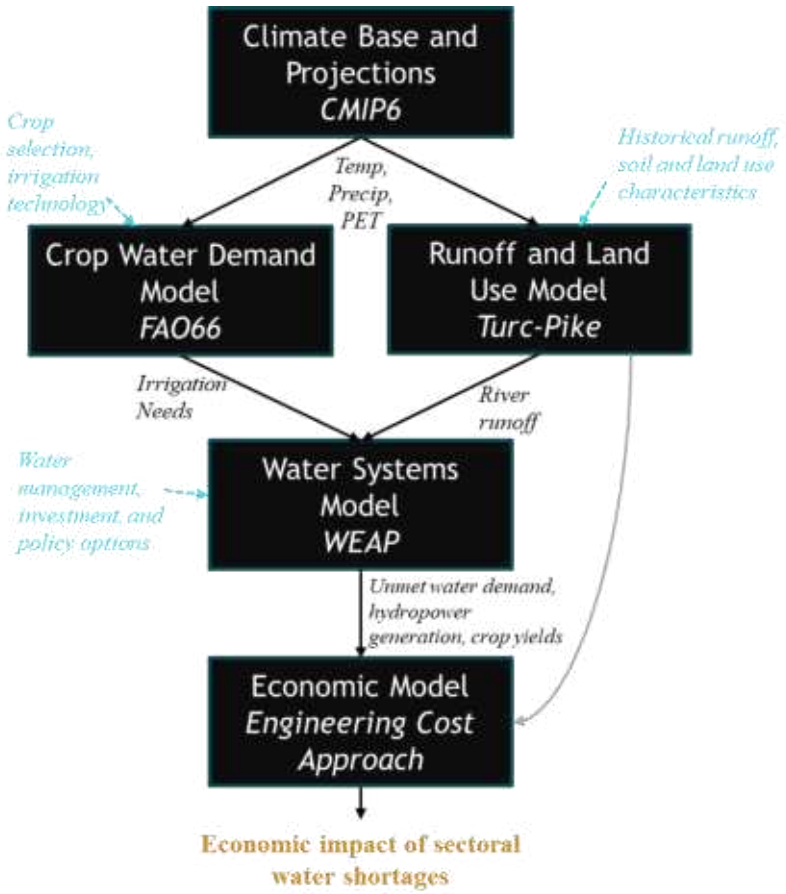

The WEAP water systems model converts the availability of water resources for municipal and industrial users into estimates of unmet demand, broken down by sector of the economy (e.g., manufacturing) and population (urban, rural). Unmet demands are driven by changes in water resources due to climate change, changes in demand from other water-intensive sectors due to capital or technological changes, environmental flow requirements, and the priority of uses in the country. For municipal and industrial users, the latest water demand volumes were sourced from reported statistics, recent master plans, or previously completed studies. Projected demands were estimated using historical population growth factors.

FIGURE 27. ILLUSTRATION OF A CATCHMENT MODEL IN WEAP (LEFT) AND OF THE DOMINICAN REPUBLIC SPECIFIC WEAP MODEL (RIGHT)

Our analysis also estimates the reduced investment dollars available to identified sectors due to spending on water supply infrastructure (e.g., pumping). For example, without sufficient water supply, manufacturing industries will need to make capital investments to continue operation (e.g., investments to increase water efficiency, investments in infrastructure for inter-basin water transfers, investments in desalination technology, etc.). This is implemented in the model as a decrease in the capital endowments of manufacturing industries (i.e., since a portion of capital will be diverted to ensure sufficient water supply).

Pumping capacity is constructed to meet any industrial and municipal demands that are not met on average, with this capital spending reflected annually in the model. This analysis uses the capital costs of pumping groundwater as a proxy for all supply costs, including conveyance and delivery infrastructure (EPA 2013).

The yearly unmet water demand in cubic meters for the industrial and municipal sectors for each climate scenario is extrapolated from the WEAP outputs for the period 2021-2050 and then the total value is multiplied by the average energy requirement per pumped cubic meter and consequently, by the average cost per unit of energy. To determine the average cost of energy per unit, we tried to give priority to local energy sources whenever possible. In cases where local sources weren't available, international sources were considered as a viable option. An average total value of 0.6 kWh/m^3 that comprises extraction (hypothesizing 30 m depth of wells), treatment, and conveyance for an average transfer was selected (see Table 5 and Figure 28).

TABLE 5. ENERGY REQUIREMENT FOR EXTRACTION, TREATMENT, AND CONVEYANCE OF GROUNDWATER

ENERGY REQUIREMENT (KWH/M^3)		
EXTRACTION	Groundwater	0.25
TREATMENT		0.0606
CONVEYANCE	Average Transfer (EPA 2013)	0.3
TOTAL		0.6106

Source: (Shannak 2018)

FIGURE 28. AVERAGE ENERGY INTENSITY OF EXTRACTING WATER FROM GROUNDWATER AQUIFERS AT DIFFERENT DEPTHS

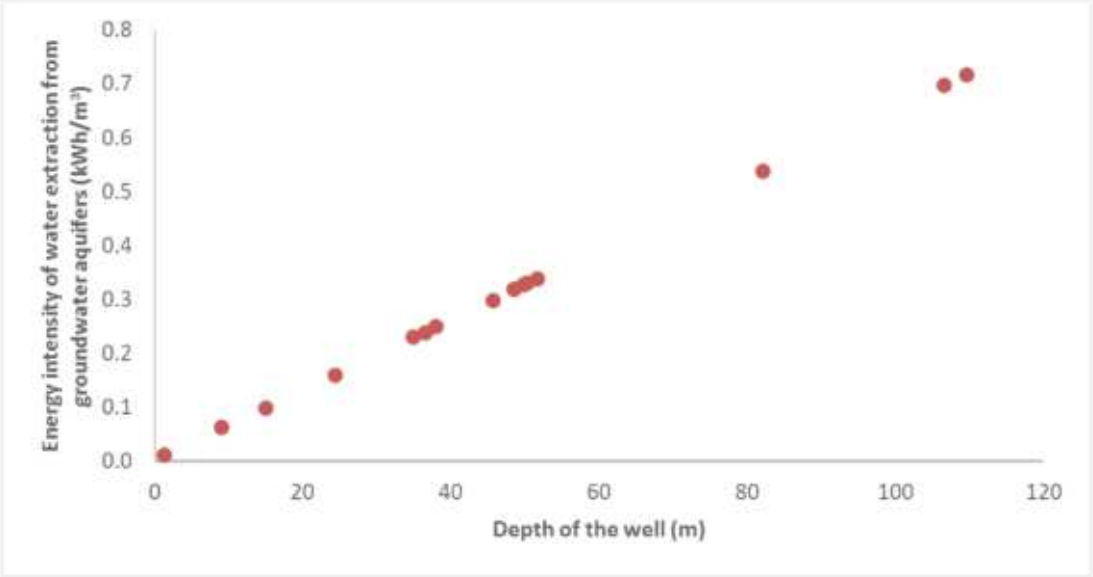

Source: (Burt and Soto 2008)

The annual pumping costs are accompanied by the fixed capital costs of the wells themselves. First, we assume an average lifespan of approximately 20 years for each well, with the funding starting from 2021 and the construction of new wells taking place in 2031. Then, the average number of needed wells is calculated assuming each well can pump 75,700 l/h for 8 h/day for 7 and 5 days per week for municipal and industrial use respectively (WHO and Wagner 1959). These figures result in a value of 1,547,308 m^3/y and 1,105,220 m^3/y of pumping capacity for the two sectors. Finally, the final number of wells to cover the unmet supply is multiplied by the average cost of each well, assumed to be $4,342/well (USAID 2004). This fixed cost is distributed across the period between 2021-2050, with an interest rate of 5 percent. We then estimate shocks assuming 90 and 100 percent coverage.

Further details on the data sources used to complete the analysis are provided in Appendix C.

Results: Climate Change Effects

Water availability is calculated through Turc-Pike and calibrated with local gauged data taken from local sources and the National Hydrological Plan. The regions with larger water availability are Yaque del Norte and Yuna, followed by Yaque del Sur, as shown in Table 6.

TABLE 6. HISTORICAL MAXIMUM, MINIMUM, AND MEAN AVERAGE MONTHLY FLOWS IN THE SIX HYDROLOGICAL REGIONS OF THE DOMINICAN REPUBLIC

HISTORICAL AVERAGE MONTHLY FLOW [M3/SEC]			
HYDROLOGICAL REGIONS	MAX	MIN	MEAN
YUNA	1533.52	37.85	354.11

OZAMA-NIZAO	311.35	9.94	59.41
ESTE	193.27	1.61	29.61
ATLANTICA	646.32	4.14	58.27
YAQUE DEL SUR	687.34	15.02	111.76
YAQUE DEL NORTE	2921.87	71.93	415.64

FIGURE 29. AVAILABLE GAUGED HYDROLOGICAL DATA FOR THE DOMINICAN REPUBLIC

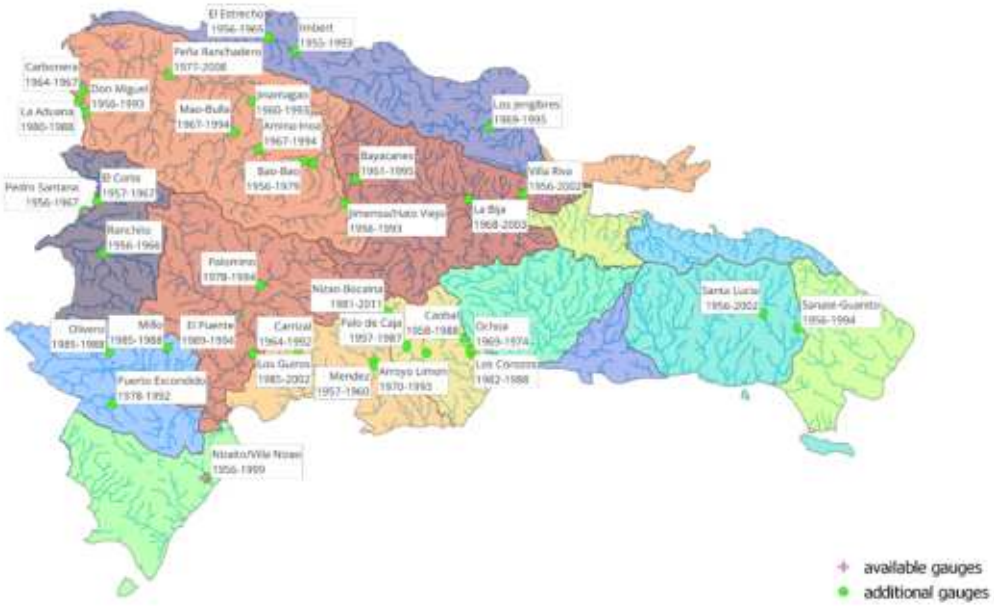

The country's municipal and industrial water demand is mostly proportional to the population density, with demand concentrated in the northern and central parts of the country. Figure 30 and Figure 31 show the distribution of industrial and municipal water demand respectively for the baseline scenario, consistent with the period from 1995-2020. Demand is expected to increase in the future as driven by the further development of the country. Projections of future demand used in the WEAP model are taken from the country's national plan for water resource management (INDRHI, 2012).

FIGURE 30. BASELINE INDUSTRIAL WATER DEMAND DISTRIBUTION, 1995-2020

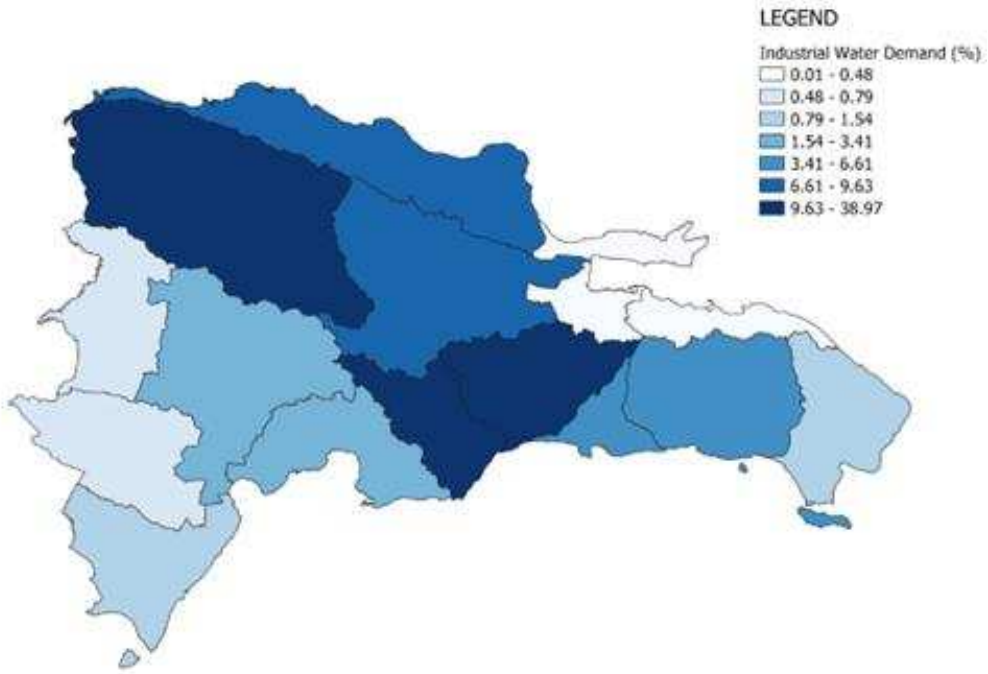

FIGURE 31. BASELINE MUNICIPAL WATER DEMAND DISTRIBUTION, 1995-2020

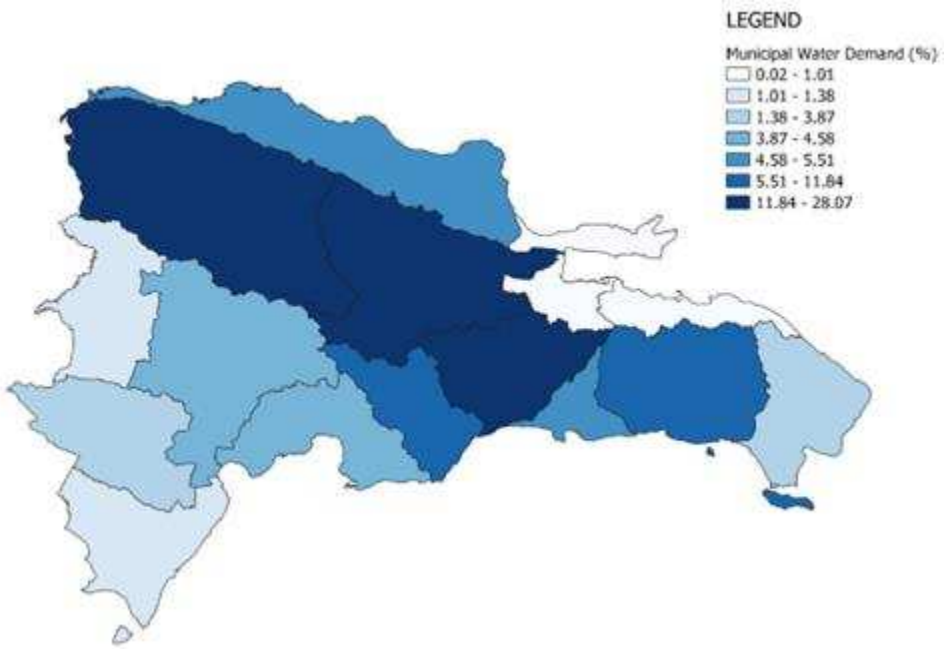

Figure 32 illustrates the distribution of water demand for irrigation under the baseline scenario, with the central and north-western regions accounting for the highest share of the country's total irrigation demand.

FIGURE 32. BASELINE IRRIGATION WATER DEMAND DISTRIBUTION, 1995-2020

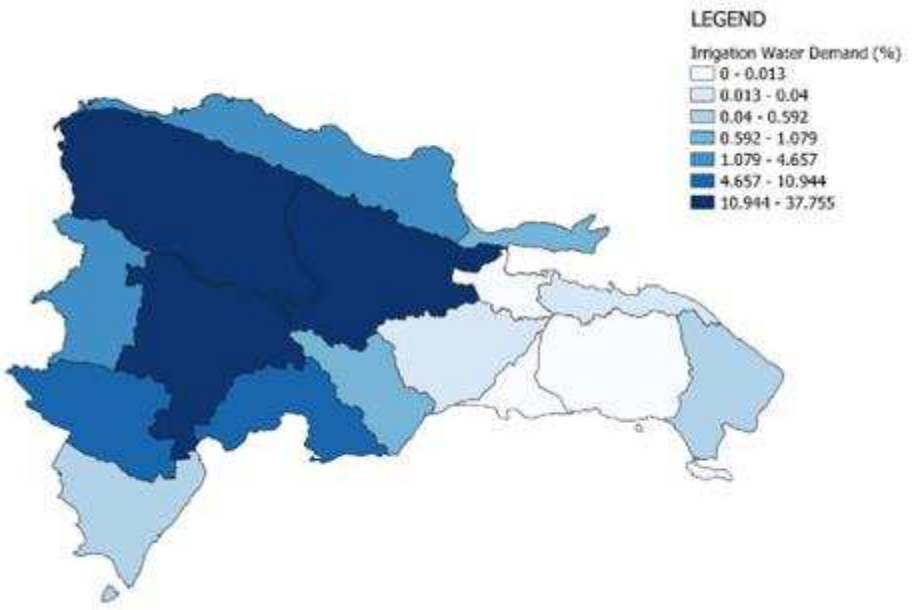

Figure 33 shows the distribution of irrigated areas in the country. Overall, the Yaque del Norte, Yaque del Sur, and Yuna account for the highest share of the country's total irrigation demand.

FIGURE 33. DISTRIBUTION OF IRRIGATION AREAS

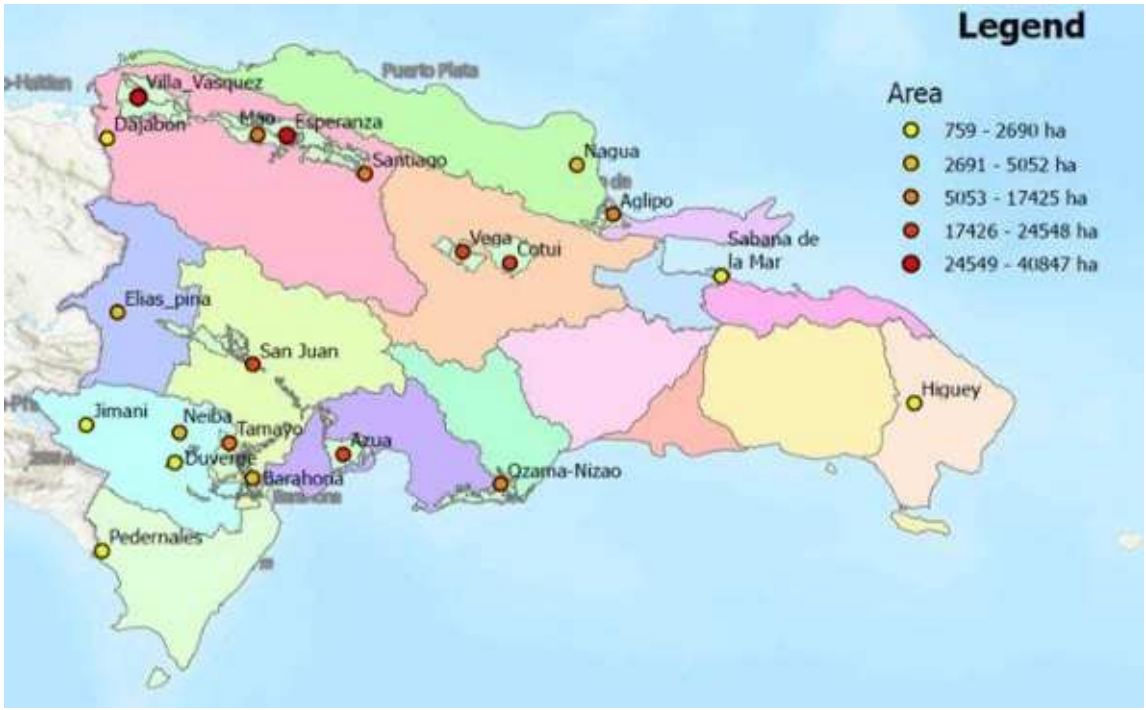

The average unmet irrigation demand for the baseline period (1995-2020) is mostly concentrated in Yaque del Norte, and despite the high runoff of the region, it presents an annual water deficit

between 40 and 50 percent (see Figure 34). Atlantica and the regions in the South surrounding the capital present between 10 and 20 percent of annual unmet irrigation demand due to their lower runoff and the priority given to the municipal and industrial sectors, which are predominant in those regions. As a result of this allocation of priorities, in general, the unmet demand for the municipal and industrial sectors tends to be lower (between 1 and 5 percent) than the unmet irrigation demand, and is concentrated in the most populous areas (see Figure 35).

FIGURE 34. AVERAGE UNMET IRRIGATION DEMAND, 1995-2020

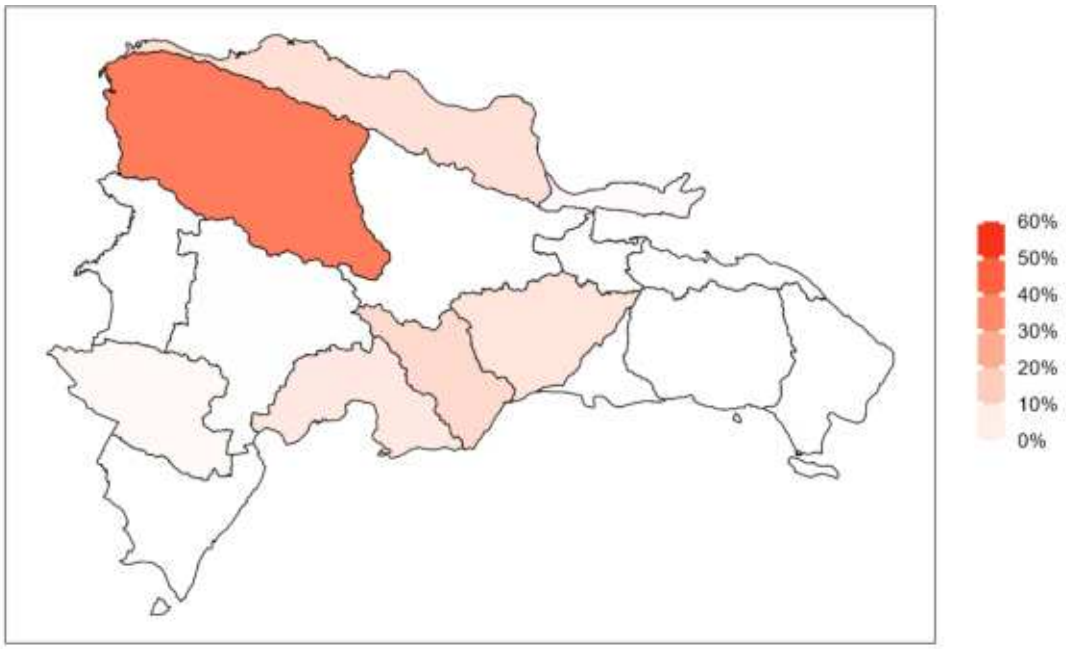

FIGURE 35. AVERAGE MUNICIPAL AND INDUSTRIAL UNMET DEMAND, 1995-2020

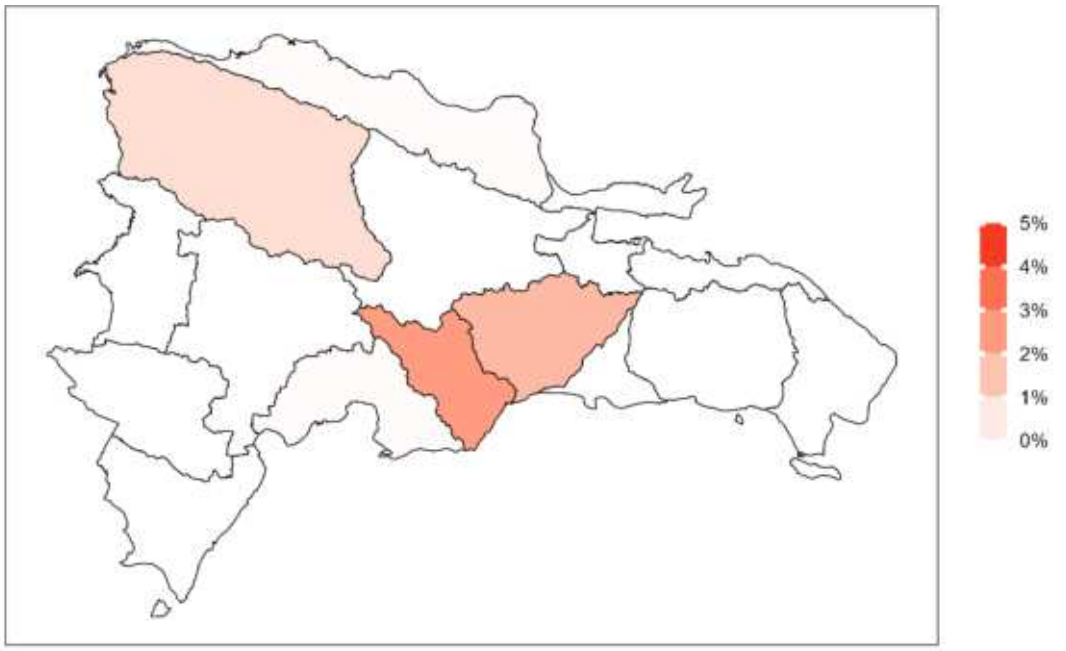

Our modeling results suggest there may be significant variation in unmet irrigation demand by mid-century. Across scenarios, the Dry/Hot mean scenario is expected to result in a substantial increase in unmet demand, while the Wet/Warm mean scenario is expected to lead to a smaller increase in unmet demand. Under the Dry/Hot mean scenario, changes in unmet demand range from +6 to +16 percent, relative to the baseline for the period 2041 to 2050 (see Figure 36). These high values of unmet demand for the irrigation channel are driven to some extent by the priority sequence of water allocations to different water users within the water systems model. The municipal and industrial sectors experience relatively low unmet demand as they are first in the water allocation sequence, while irrigated agriculture experiences much higher unmet demand under certain future scenarios as it is deprioritized in the water allocation sequence. That said, the Wet/Warm mean scenario is associated with a smaller negative effect (i.e., reductions in unmet irrigation demand), with the change in unmet irrigation demand ranging from +3 percent to +11 percent between 2041 to 2050, relative to the baseline (see Figure 36).

FIGURE 36. CHANGE IN UNMET IRRIGATION DEMAND, 3-YEAR MOVING AVERAGE

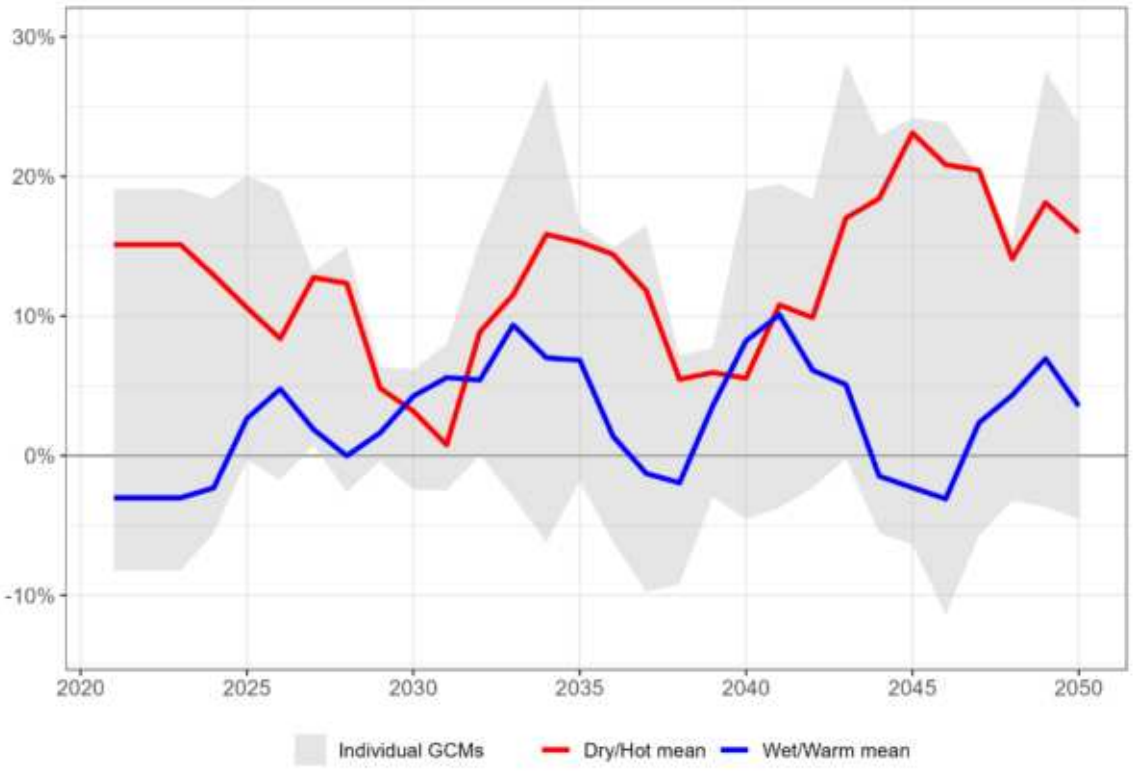

The output of the WEAP model shows a mean unmet water demand of 4 percent of total demand for the municipal and industrial sectors during the baseline period. By the 2040s, unmet demand increases. Relative to the baseline period, unmet demand is projected to increase by +1.9 percent on average under the Dry/Hot mean scenario from 2041-2050. Changes under the Wet/Warm mean scenario are expected to be less pronounced for the period 2041-2050, resulting in a +1.1 percent increase in unmet water demand on average, relative to the baseline (see Figure

37). It is worth noting that these estimates of unmet demand are likely low compared to the unmet demand experienced across other water-using sectors (such as irrigation) given that the municipal and industrial sectors (as well as water for environmental flows) are given the highest priority when it comes to allocating limited available water resources within the water systems model used. In terms of the total unmet demand by 2041-2050, these values correspond to an increase in the volume of unmet demand from 15 million m^3 under the baseline to 35 million m^3 (+133 percent) under the Dry/Hot mean scenario. Under the Wet/Warm mean scenario, unmet demand increases by approximately 40 percent to 21 million m^3, relative to the baseline.

FIGURE 37. CHANGE IN THE UNMET MUNICIPAL AND INDUSTRIAL WATER DEMAND, 3-YEAR MOVING AVERAGE

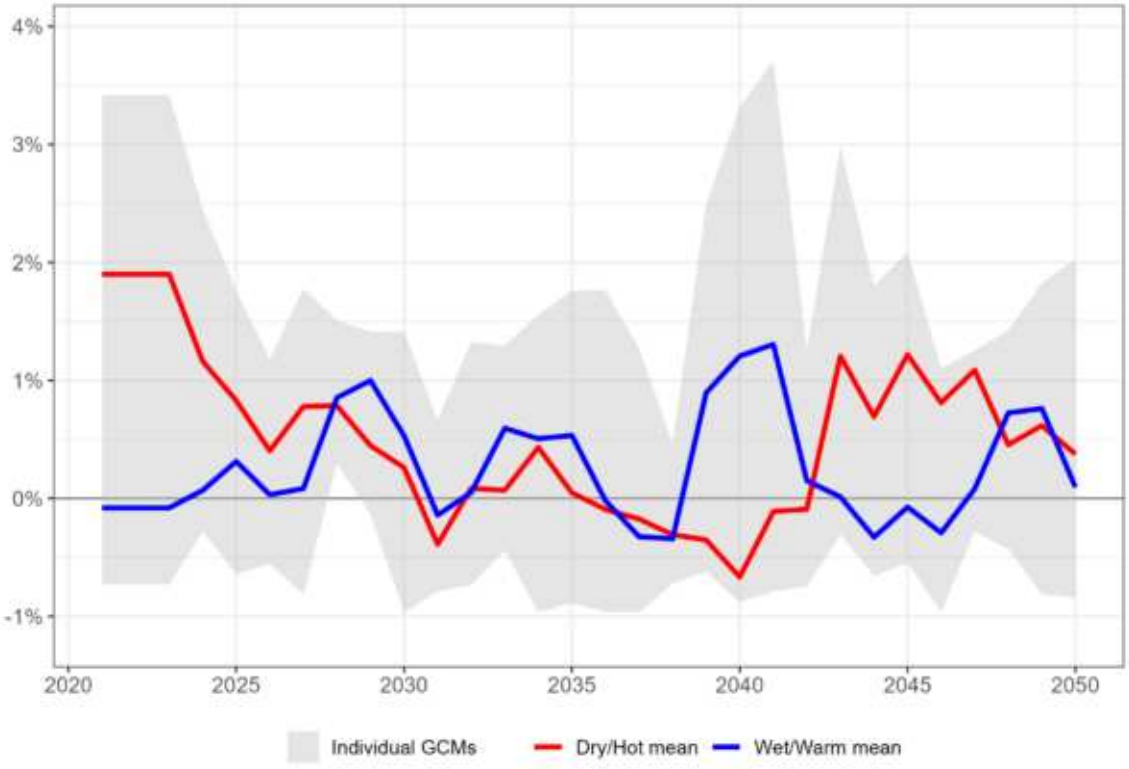

The municipal and industrial water supply shock in the Dominican Republic is calculated annually in dollars as reported above. The country-specific energy costs in this case are equal to 0.16 $/kWh for industry and 0.125 $/kWh for households (DOE 2020) and, multiplied by the necessary pumping energy and by the supply to be delivered. This results in an average of $2.29 million and $3.37 million respectively for the Wet/Warm and Dry/Hot mean scenarios, assuming the total unmet water demand is covered all the time. If instead a 90 percent coverage is assumed, these values decrease to $1.44 and $1.69 million for the same scenarios in the period 2031-2050.

Regarding the fixed capital costs, a total of 21 wells will be needed for the Wet/Warm mean scenario, rising to 22 in the Dry/Hot mean scenario, for a total annual cost of $ 5,984.25 and $6,078.83, respectively, if we assume a 5 percent interest rate. With 90 percent coverage, we

expect annual costs will decrease to $3962.47 and to $3978.17 for the Wet/Warm and Dry/Hot mean scenarios, respectively.

TABLE 7. AVERAGE ANNUAL COSTS FOR PUMPING UNMET WATER SUPPLY IN THE DOMINICAN REPUBLIC

	100% COVERAGE		90% COVERAGE	
	WET/WARM	DRY/HOT	WET/WARM	DRY/HOT
FIXED CAPITAL COST ($)	5,984	6,078	3,962	3,979
ENERGY COST ($)	2,309,094	2,355,500	1,443,340	1,690,258
TOTAL	2,315,078	2,361,579	1,447,303	1,694,237

Results: Adaptation

The proposed adaptation strategies involve improving the irrigation efficiency from a baseline of 20 percent to a target of 40 percent and increasing the volume of reservoirs specifically designated for irrigation purposes by 20 percent. Figure 38 illustrates the projected impacts of implementing these measures on unmet demand by the year 2050, in relation to the respective baselines for the Hot/Dry and Wet/Warm mean scenarios. For the Hot/Dry mean scenario, the implementation of the proposed adaptation measures is estimated to result in a change in unmet demand from +15 to –10 percent in the year 2050, with respect to the baseline. Conversely, for the Wet/Warm mean scenario, these adaptation measures result in a change from +5 to –12 percent in the year 2050, with respect to the baseline.

FIGURE 38. CHANGE IN UNMET IRRIGATION DEMAND, 3-YEAR MOVING AVERAGE

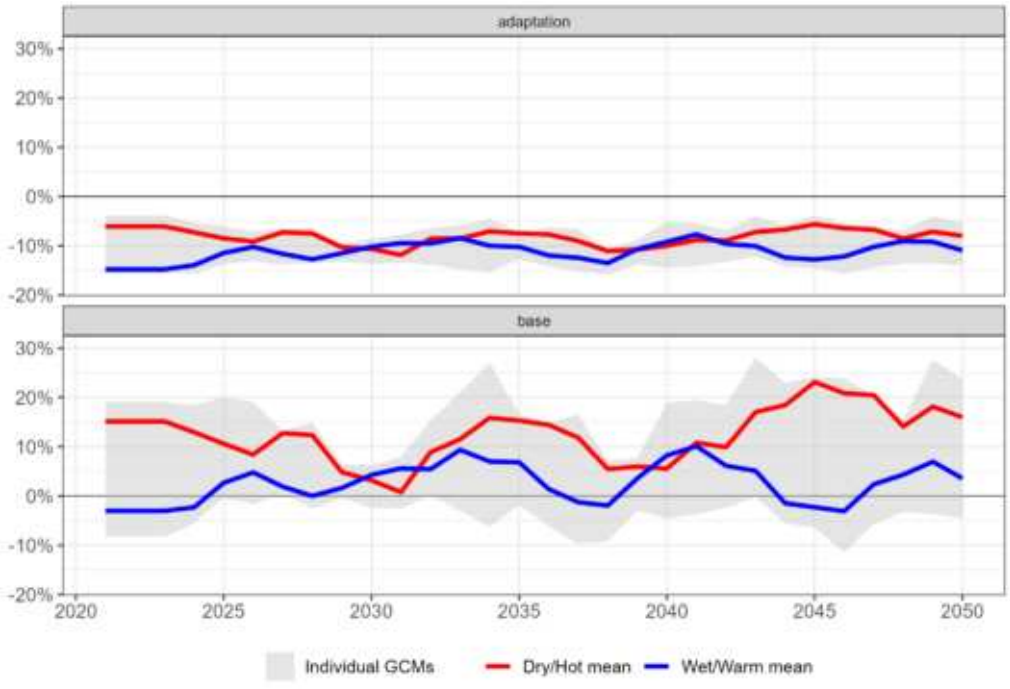

Figure 39 shows the average unmet irrigation demand by basin and highlights the positive changes under both in the Dry/Hot and Wet/Warm mean scenarios due to the irrigation adaptation measures. In the Dry/Hot mean scenario, we can observe a change with respect to the no adaptation case of around +30 percent.

FIGURE 39. AVERAGE UNMET IRRIGATION DEMAND BY BASIN, 2041-2050

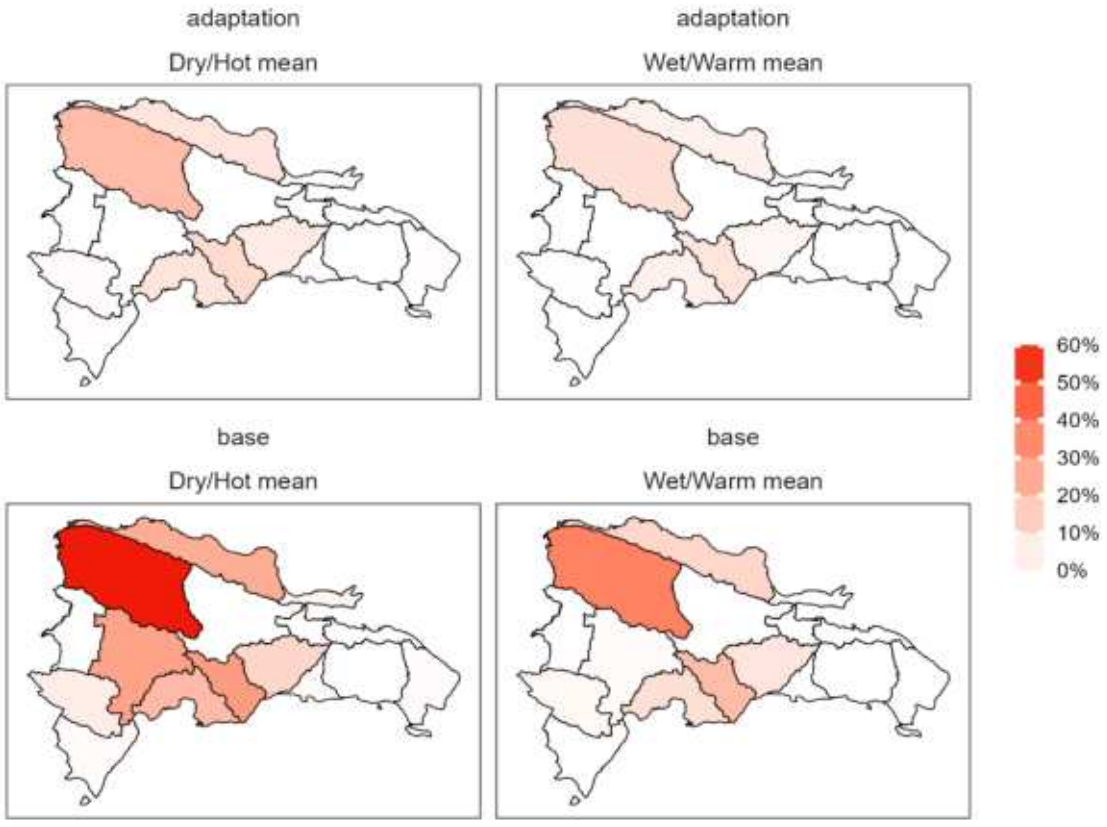

Figure 40 shows the change in unmet irrigation demand for each water basin in the 2040s compared to the historical baseline with and without adaptation. Implementing the adaptation measures is projected to reduce unmet demands for most basins under the Dry/Hot and Wet/Warm mean scenarios. Without adaptation, the most negatively impacted basin is projected to have around 30 percent higher unmet irrigation demand compared to the baseline under the Dry/Hot mean scenario (bottom left panel). With adaptation, unmet irrigation demand is expected to decrease in that basin by around 20 percent compared to the baseline under the Dry/Hot mean scenario (top right panel).

FIGURE 40. CHANGE IN UNMET IRRIGATION DEMAND BY BASIN, 2041-2050

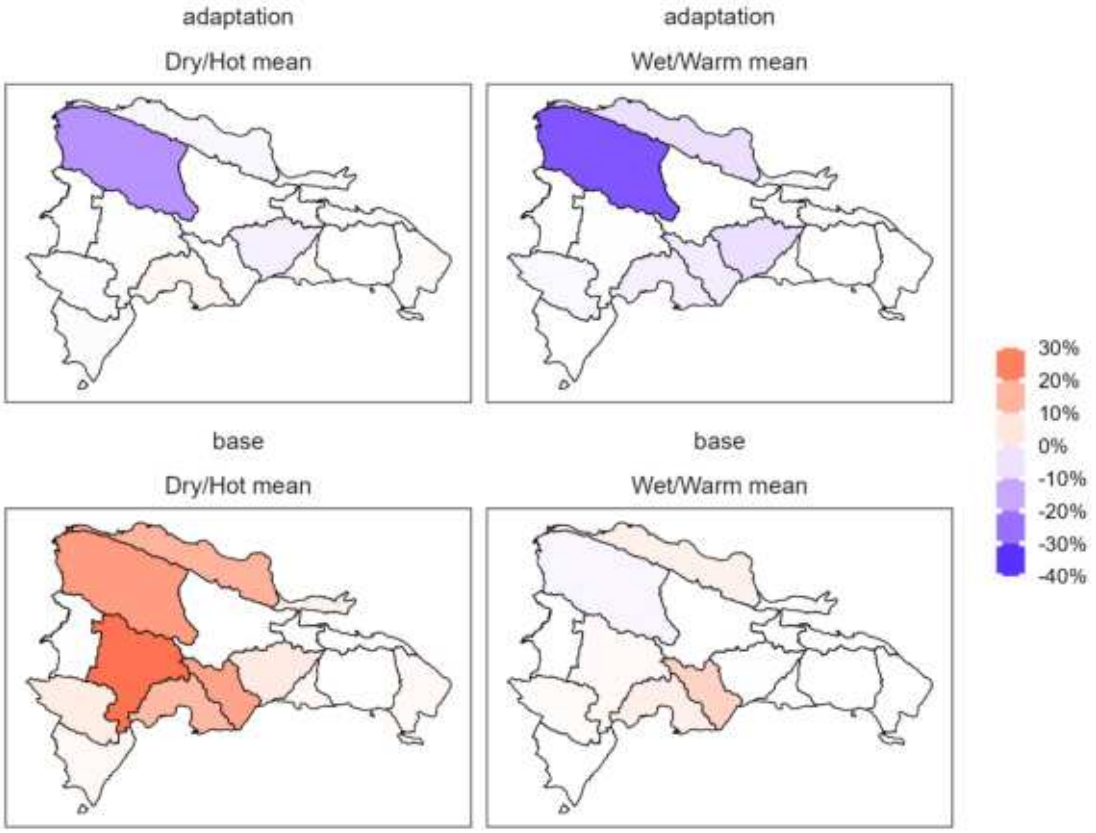

The adaptation interventions evaluated for the irrigation channel also lead to a slight improvement (i.e., reduction of unmet water demand) for the municipal and industrial sectors. Figure 41 shows a reduction in unmet municipal and industrial water demand of 0.3 percent on average for both Dry/Hot and Wet/Warm mean scenarios, between the years 2045 and 2050 compared to the baseline.

FIGURE 41. CHANGE IN UNMET MUNICIPAL AND INDUSTRIAL WATER DEMAND, 3-YEAR MOVING AVERAGE

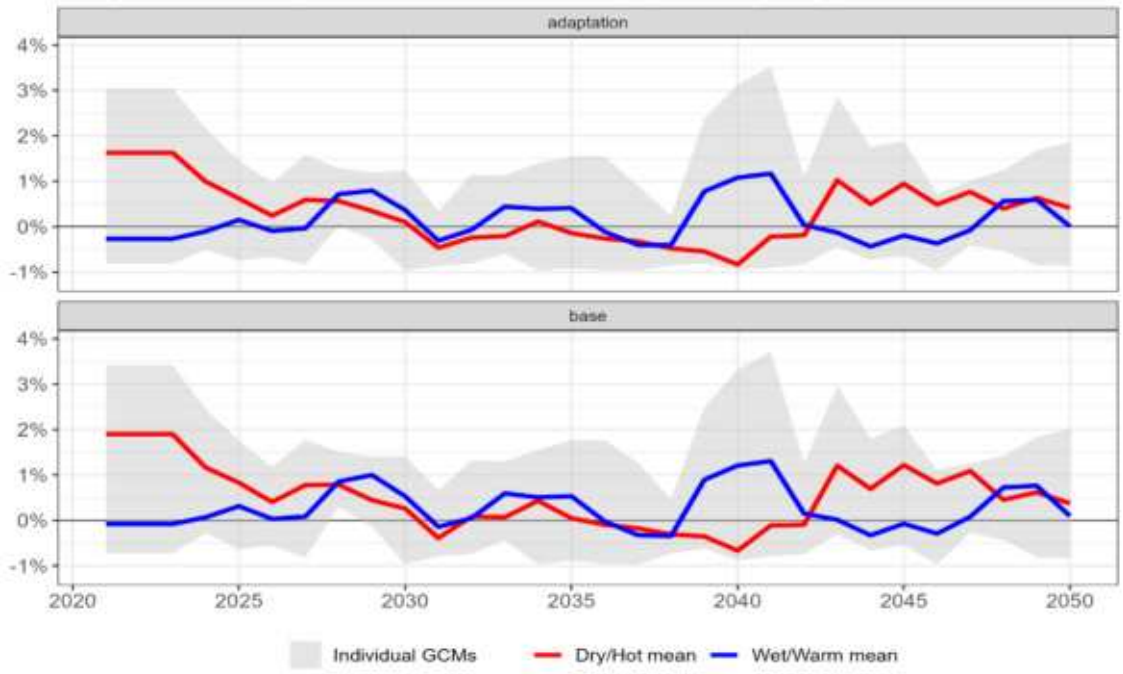

Figure 42 shows the average unmet municipal and industrial demand by basin and highlights the relatively limited changes for both the Dry/Hot and Wet/Warm mean scenarios resulting from the irrigation adaptation measures. The limited effect of irrigation adaptation measures on reducing unmet municipal and industrial demand is due to the fact that municipal and industrial demand already have higher priority in the water allocation sequence. Figure 43 shows the change in unmet municipal and industrial water demand for each basin in the 2040s compared to the historical baseline with and without adaptation. These results similarly show relatively limited changes between the no adaptation base case and the adaptation case.

FIGURE 42. AVERAGE UNMET MUNICIPAL AND INDUSTRIAL WATER DEMAND BY BASIN, 2041-2050

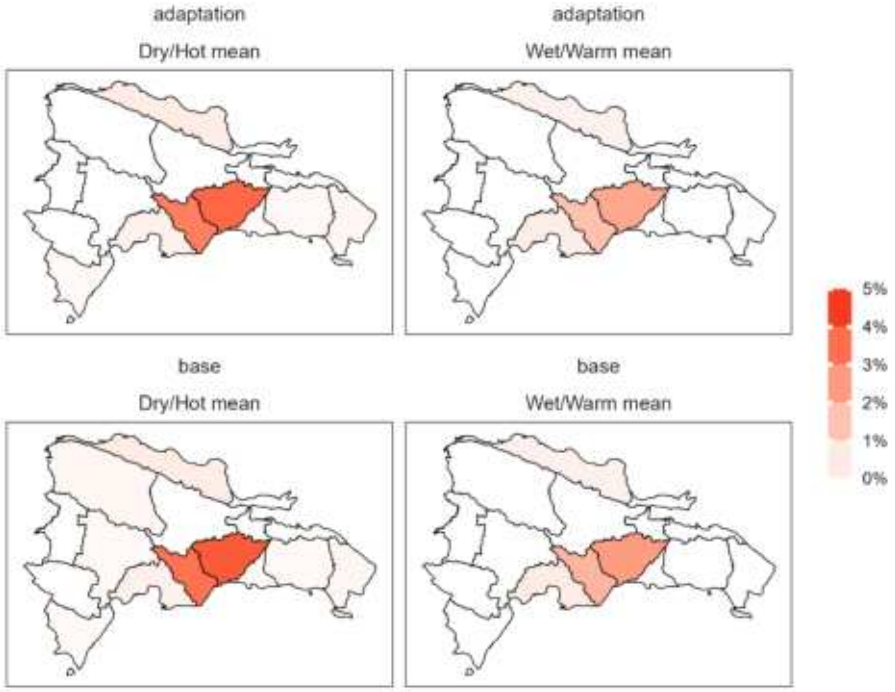

FIGURE 43. CHANGE IN UNMET MUNICIPAL AND INDUSTRIAL WATER DEMAND BY BASIN, 2041-2050

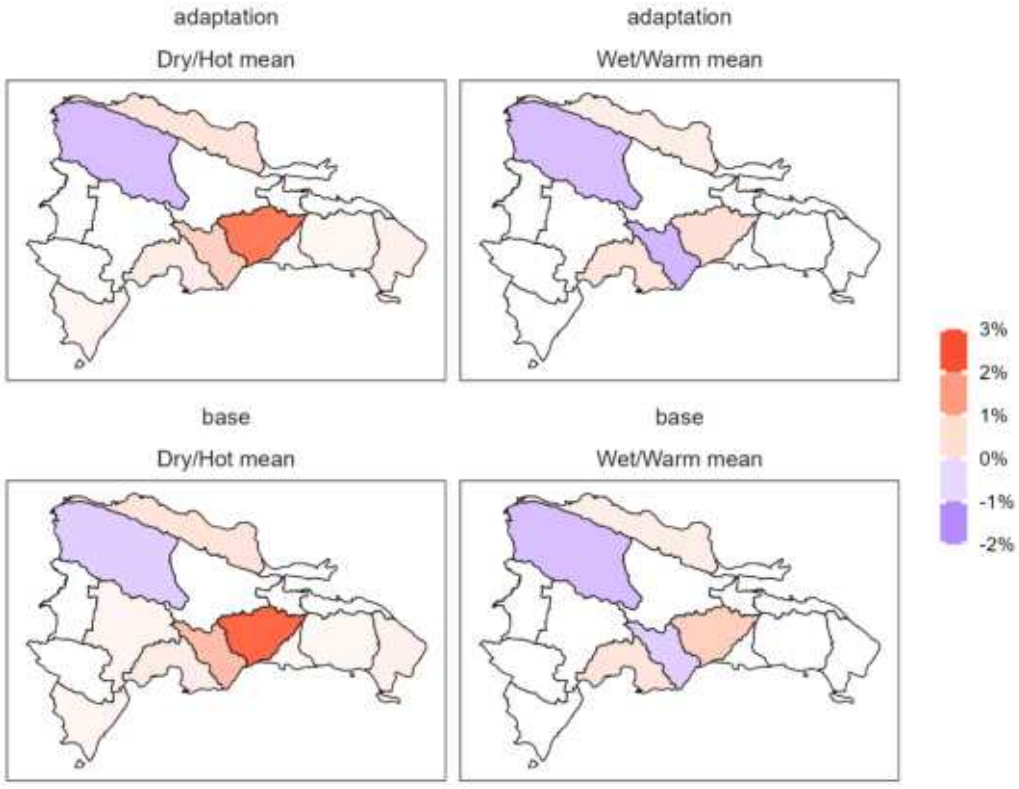

Summary and discussion

Overall, the regions with the highest water availability in the country are Yaque del Norte and Yuna, followed by Yaque del Sur. Municipal and industrial water demands are primarily influenced by population density, with higher demand concentrated in the Central-south regions of the country. Projections for future demands, calculated with the WEAP model, show that the regions featuring larger irrigated areas are Yaque del Norte, Yaque del Sur, and Yuna, accounting for a substantial portion of the country's total irrigation demand. However, Yaque del Norte experiences a considerable deficit in irrigation supply, ranging between 40 and 50 percent annually. The regions of Atlantica and the areas surrounding the capital exhibit unmet irrigation demand ranging from 10 to 20 percent due to lower runoff and the prioritization of the municipal and industrial sectors in these regions. The unmet demand for the municipal and industrial sectors is generally lower (between 1 and 5 percent) and concentrated in the more densely populated areas.

Modeling outcomes indicate the potential for significant variations in unmet irrigation demand by the middle of the century. The Dry/Hot mean scenario is anticipated to result in a substantial increase in unmet demand, ranging from +6 to +16 percent relative to the baseline period (1995-2020). In contrast, the Wet/Warm mean scenario exhibits a smaller increase in unmet demand, ranging from +3 to +11 percent over the same period. For the municipal and industrial sector, the unmet demand is expected to rise by an average of 1.9 percent from 2041 to 2050 for the Hot/dry mean scenario, while the Wet/Warm mean scenario predicts a smaller increase of 1.1 percent compared to the baseline.

The implementation of adaptation strategies aimed at enhancing irrigation efficiency (increasing efficiency from 20 percent to a target of 40 percent), as well as expanding the capacity of reservoirs dedicated to irrigation by 20 percent. In the Dry/Hot mean scenario, the implementation of these measures is projected to result in a change in unmet irrigation demand from +15 to -10 percent in 2050 compared to the scenario without adaptation. On the other hand, in the Wet/Warm mean scenario, the change ranges from +5 to -12 percent in 2050 compared to the scenario without adaptation. The adaptation strategies implemented for the irrigation sector also have an effect on the municipal and industrial sector, slightly decreasing unmet demand in these sectors.

4.2.2 CROP PRODUCTION

SUMMARY	
SUMMARY	Our analysis estimates the impact of climate change on irrigated and rainfed crop production by modeling changes in water availability and extreme heat. We estimate that by 2050, climate change may result in total production shocks ranging from +4 percent to -22 percent.

ESTIMATED CLIMATE CHANGE IMPACTS BY 2041-2050	From 2041-2050, negative impacts to rainfed and irrigated crop production are highest from the Dry/Hot mean scenario. For the rainfed crops considered, the Dry/Hot mean scenario is anticipated to result in a -19 percent shock by mid-century. For the irrigated crops considered, the Dry/Hot mean is expected to result in a -16 percent production shock by mid-century.

Overview of Impact Channel

Under climate change, crop yields have the potential to be affected by changes in rainfall patterns/irrigation water availability, increasing evaporative demands, and extreme heat as temperatures rise. A summary of the modeling methodology used to estimate the impacts of climate change on crop production is presented below, with a more detailed description available in Appendix B.

First, representative crops were identified for the country, with the chosen crops representing at least 80 percent of the total production revenues as well as harvested area in the country. Data on harvested area, production, yield, revenue statistics, as well as irrigation statistics, were collected for each crop from available sources. When it comes to **water availability**, we apply the methods documented in the Food and Agriculture Organization's Irrigation and Drainage Paper 66, in which rainfed crop yields are estimated by applying crop-specific water sensitivity coefficients to the ratio of effective precipitation to potential crop evapotranspiration. For irrigated crops, the water availability analysis additionally utilized a water system model, namely WEAP. The unmet water demands at a basin scale estimated by the water system model were then used to quantify reductions in crop yields, similar to rainfed crops. For **heat stress**, the impacts to crop yields from extreme heat were modeled using AquaCrop's approach, which considers a negative relationship between supra-optimal temperatures during the flowering stage of crop development.

Finally, water availability and temperature shocks were then combined into a single shock by crop, with these effects aggregated nationally based on the spatial distribution of crop production. Crop-specific shocks were also aggregated into a total production shock using crop revenues as weights. Details on the data sources used to complete the analysis are provided in Appendix C.

Results: Climate Change Effects

The majority of crop production area in the country is reserved for cocoa bean and sugarcane production, which utilize around 15 percent and 17 percent of agricultural land, respectively (Figure 44). However, when considering production yields, cocoa beans accounted for around 1 percent of total production from 2016 – 2020, while sugarcane accounted for around 38 percent of the country's production. The share of revenues by crops is roughly split between tropical fruits, avocados, vegetables, and bananas, with these four crops accounting for roughly 60 percent of revenues.

FIGURE 44. SHARE OF CROPS BY AREA, PRODUCTION, AND REVENUE, 2016 - 2020

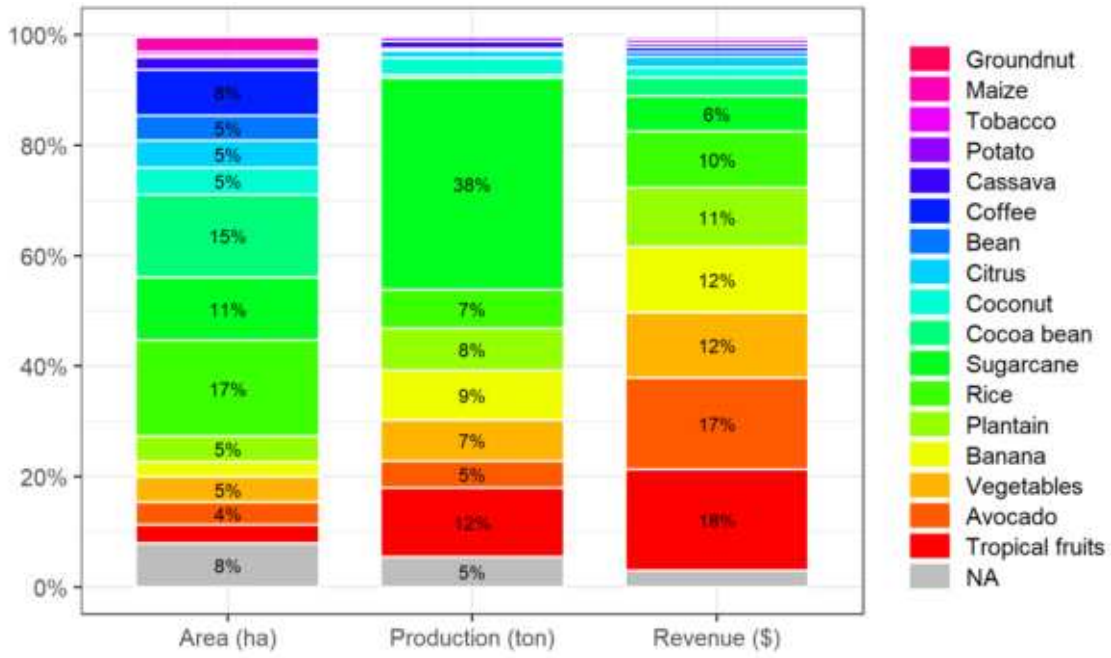

By 2050, climate change is anticipated to result in varied production shocks on rainfed crops (Figure 45). Among high-yielding crops such as sugarcane, the Wet/Warm mean and Dry/Hot mean scenarios are expected to result in a +2 percent and -26 percent shock, respectively. Across GCMs, production shocks for sugarcane range from around +6 percent to -31 percent. High-revenue crops such as avocadoes and bananas are expected to experience a 0 percent shock under the Wet/Warm mean scenario, and a -25 and -28 percent shock from the Dry/Hot mean scenario, respectively. Generally, most crops are expected to experience a positive production shock under at least some GCMs, with the magnitude of the shock ranging from +1 percent to +8 percent for different crops. However, vegetables are expected to exclusively experience negative production shocks across the Dry/Hot mean scenario, Wet/Warm mean scenario, and selected GCMs.

FIGURE 45. RAINFED CROP PRODUCTION SHOCK, 2041 - 2050

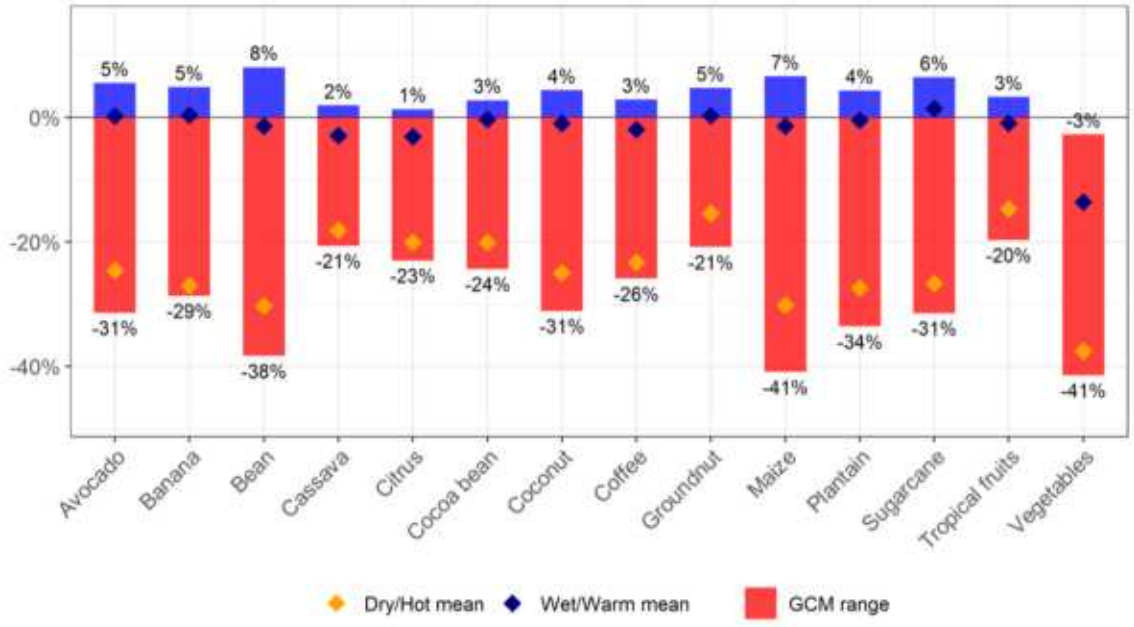

Based on the projected production shocks during the period out to 2050 as compared to the baseline, the overall impact of climate change on rainfed crops results in both positive and negative shocks (Figure 46). Overall, the Dry/Hot mean scenario is anticipated to result in only negative production shocks, while the Wet/Warm mean scenario is expected to result in small positive production shocks through the early century which grow more negative by mid-century. When considering individual GCMs (i.e. the grey-shaded range shown in Figure 46), production shocks range from around 0 percent to -10 percent by 2030. Here, the Wet/Warm and Dry/Hot mean scenarios result in a production shock of around -6 and -4 percent, respectively. By 2050, the Wet/Warm and Dry/Hot mean scenarios are expected to result in a -1 percent and -20 percent shock. Across GCMs, production shocks range from +6 percent to -26 percent.

FIGURE 46. RAINFED CROP PRODUCTION SHOCK, 3-YEAR MOVING AVERAGE

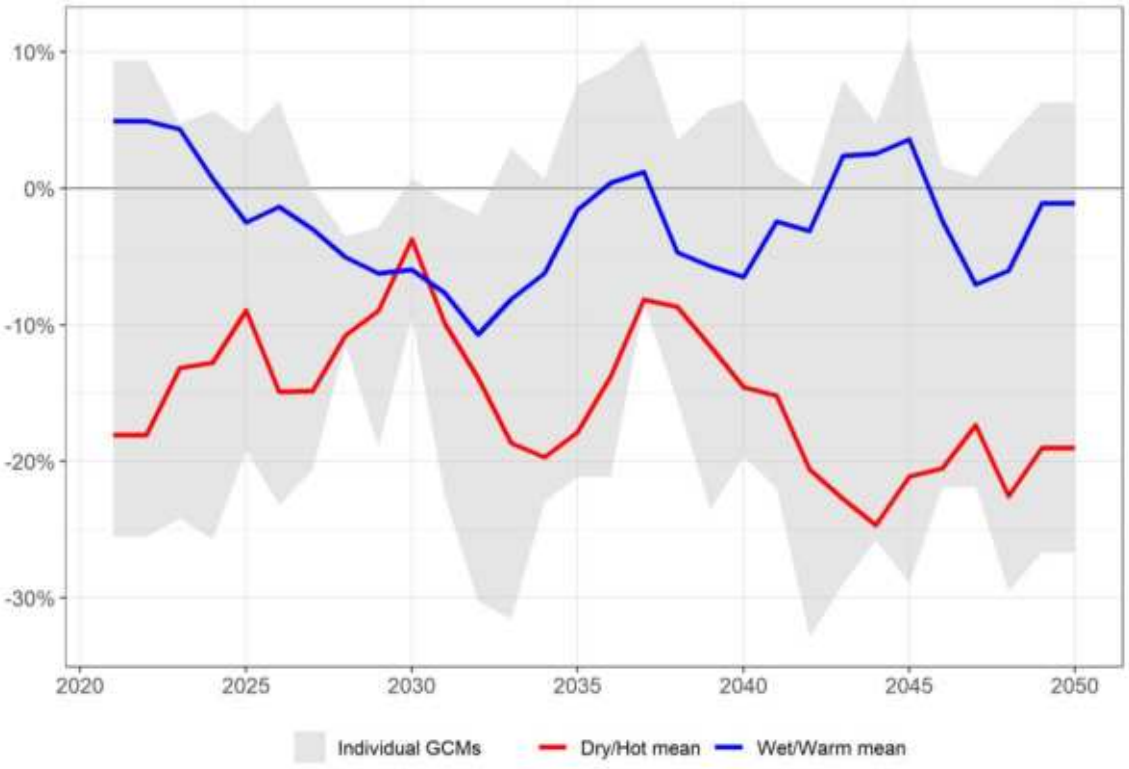

By 2050, climate change is anticipated to have varied shocks on a majority of irrigated crops (Figure 47). Among high-yielding crops such as sugarcane, the Wet/Warm mean and Dry/Hot mean scenarios are expected to result in a -1 percent and -12 percent shock, respectively. Across GCMs, production shocks for sugarcane range from around 1 percent to -16 percent. High-revenue crops such as avocadoes are expected to experience a 0 percent shock under the Wet/Warm mean scenario, and a -3 from the Dry/Hot mean. Generally, across GCMs, most crops are expected to experience a positive production shock that ranges from 1 percent to 4 percent. However, citrus, tobacco, potatoes, and vegetables are expected to exclusively experience negative production shocks across the Dry/Hot mean, Wet/Warm mean, and selected GCMs.

FIGURE 47. IRRIGATED CROP PRODUCTION SHOCK, 2041 - 2050

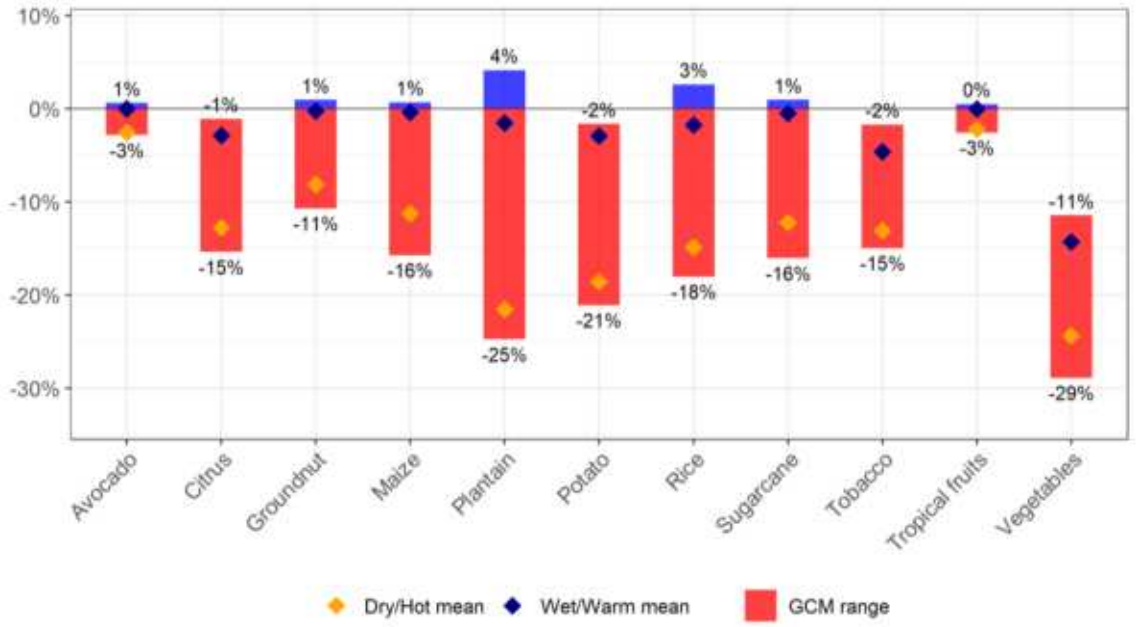

Based on the projected production shocks relative to the baseline, the overall impact of climate change on irrigated crops results in predominantly negative shocks (Figure 48). Overall, the Dry/Hot mean scenario is anticipated to result in only negative production shocks out to 2050, while the Wet/Warm mean scenario is expected to result in small positive production shocks through the early century which begin to become more negative by mid-century. When considering individual GCMs (i.e. the grey shaded range shown in Figure 48), production shocks range from around -2 percent to -9 percent by 2030. Here, the Wet/Warm and Dry/Hot mean scenarios result in a production shock of around -5 and -3 percent, respectively. By 2050, the Wet/Warm and Dry/Hot mean scenarios are expected to result in a -3 percent and -13 percent shock, respectively. Across GCMs, production shocks range from 0 percent to -18 percent.

FIGURE 48. IRRIGATED CROP PRODUCTION SHOCK, 3-YEAR MOVING AVERAGE

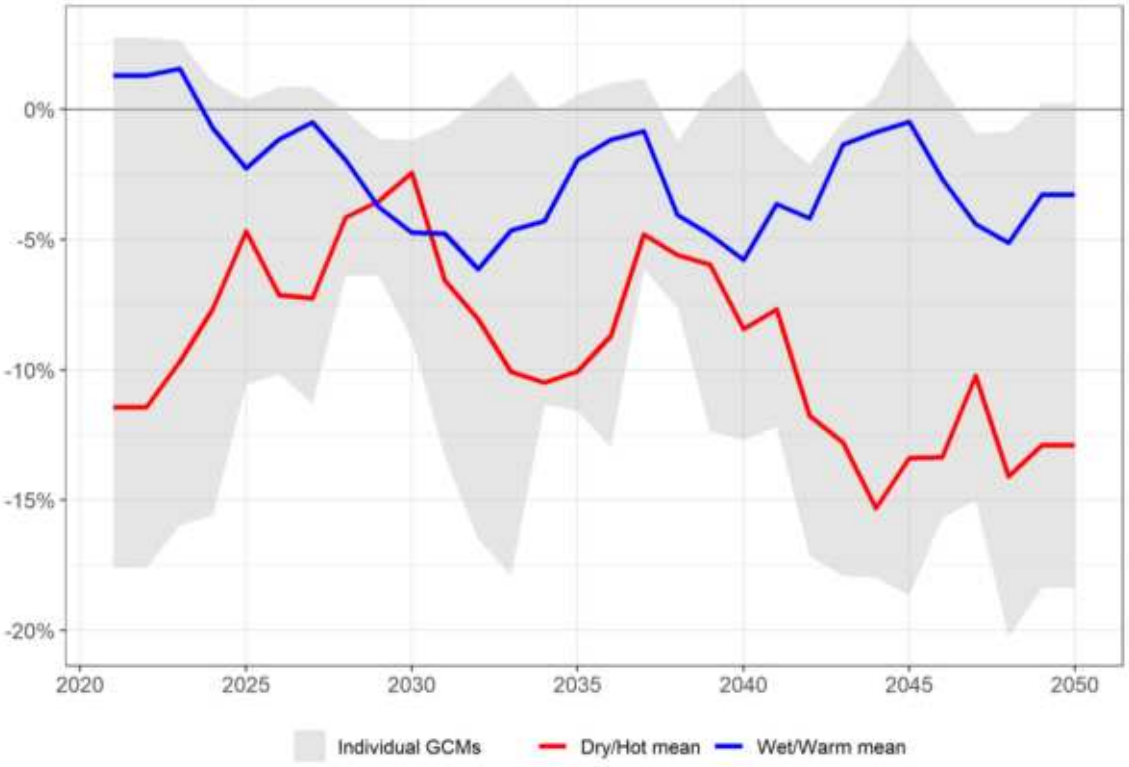

Adaptation

With the modeled effects of climate change on rainfed and irrigated crop production documented above, this section now looks at the effect of investing in adaptation measures. As introduced in Section 3.2, we consider a **proactive adaptation scenario** and compare it to a **no-action baseline** that assumes no change in crop management practices.

When it comes to reducing the impacts of climate change on crop production, there are a variety of possible adaptation interventions that could be pursued. These include growing more heat and drought-tolerant and resistant crop species and individual varieties, as well as management practices such as increasing the use of mulching, cover crops, and fertilizers. Table 8 shows the different adaptation interventions evaluated for this channel.

TABLE 8. ADAPTATION SCENARIOS AND INTERVENTIONS EVALUATED

ADAPTATION INTERVENTION	SCENARIO	
	NO-ACTION BASELINE	PROACTIVE ADAPTATION
Development of new irrigation infrastructure to address water stress	No change	Add new irrigated areas up to 100% of the estimated irrigation potential in the country (i.e., an additional 403,500 hectares) by 2050.

Reduction in unmet demand for irrigated crops		20% increase in the volume of reservoirs designated for irrigation, as well as improvements in irrigation efficiency from 20% to 40%.
Crop switching to more climate-resilient crops (e.g., citrus, avocado, tropical fruits, maize, groundnuts, potato, and cassava)		Increase relative size of selected crops by 2 (i.e., a 100% increase in the production of these crops).
Increase share of heat-tolerant crop varieties (e.g., cassava, vegetables, potatoes, citrus, coffee, rice, and cocoa) to reduce heat stress on vulnerable crops		Substitute 50% of current production of the selected crops for a heat-tolerant variety by 2050.
All interventions		All of the above.

Figure 49 shows the impact of the different individual adaptation interventions on overall crop production in the country. Under the no-action baseline scenario, we estimate crop production shocks by 2050 of approximately -3 and -15 percent under the Wet/Warm and Dry/Hot mean scenarios respectively. When considering adaptation interventions that increase the use of heat-tolerant varieties and utilize crop-switching techniques, these strategies do little to lessen climate change related impacts and result in shocks comparable to the no-action baseline. In contrast, investments aimed at increasing irrigation, reducing unmet irrigation demand, and employing a combination of all interventions appear to be most effective in reducing shocks relative to the no-action baseline. For all of these investment options, the Wet/Warm mean scenario is expected to result in a positive production shock by mid-century, ranging from 1 to 5 percent, as compared to -3 percent under the no-action baseline. Under the Dry/Hot mean scenario, these interventions are expected to result in a production shock ranging from -10 to -3 percent, as compared to -15 percent under the no-action baseline.

FIGURE 49. CROP PRODUCTION SHOCKS, 3-YEAR MOVING AVERAGE, ASSUMING INVESTMENT IN IRRIGATION INFRASTRUCTURE, REDUCED IRRIGATION DEMAND, CROP-SWITCHING, AND HEAT-TOLERANT VARIETIES

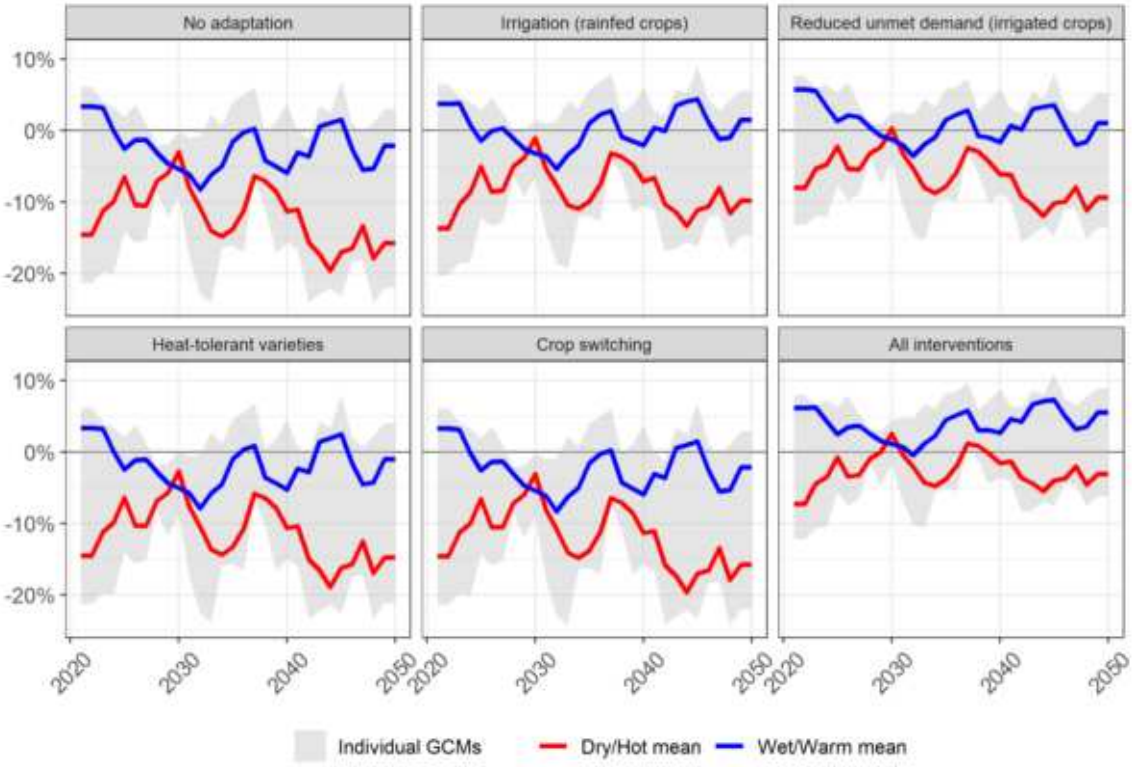

Figure 50 shows the effects on crop production when utilizing all adaptation interventions. Overall, this intervention is expected to have positive impacts on a majority of selected crops by lessening the production shock relative to the no-action baseline. For some crops, specifically, plantains, sugarcane, tropical fruits, and rice, this adaptation strategy results in only a positive range of production shocks, as compared to the no-action baseline. Yet, some crops such as beans, coconut, and bananas are expected to experience no change in shocks relative to the no-action baseline.

FIGURE 50. CROP PRODUCTION SHOCK WITH ALL ADAPTATION INTERVENTIONS, 2041-2050

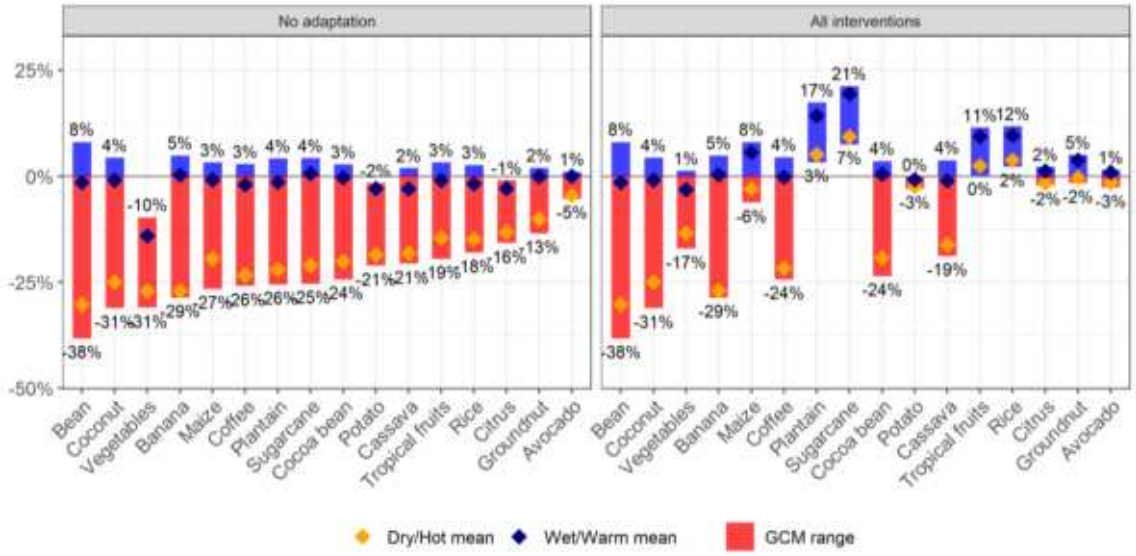

Summary and discussion

In general, climate change is expected to result in yield losses for both rainfed and irrigated crops in the country. That said, the effect on rainfed productivity is expected to drop by -19 percent by mid-century under a Dry/Hot future, while irrigated productivity by -16 percent. Assuming harvested areas remain constant, yield losses will translate directly into production and revenue losses.

The variability of impacts by mid-century, however, is high. For all rainfed crops but vegetables, the best-case scenario could result in positive yield gains that range between 1 and 8 percent, while the worst-case estimate ranges between -20 and -41 percent. Mean Wet/Warm projections estimate impacts around zero for most crops. The three most vulnerable rainfed crops (i.e., the ones with the lowest worst-case) are beans, maize, and vegetables. The most resilient crops include primarily cash crops: citrus fruits, cocoa beans, groundnuts, and tropical fruits, as well as cassava. Shock variability for irrigated crops is also large, but less homogeneous across crops. While plantains, vegetables, and potatoes impacts range widely and could even see positive gains, avocados, and tropical fruits show high resilience to climate change. These two crops are also the two most important for revenue generation in the country.

Overall, both the magnitude and variability of impacts on crop production of most crops come from changes in water resources. In this regard, avocados, citrus, vegetables, and potatoes are the least impacted by changes in the water supply (both irrigation and precipitation). Heat stress on crop productivity has limited effects in the Dominican Republic. In general, the shock does not surpass a -5 percent negative shock, except for vegetables that can see yield declines up to -20 percent by mid-century. Avocado, beans, coconut, maize, groundnuts, and sugarcane are not impacted due to lack of exposure (i.e., location of harvested areas) or vulnerability (i.e., high tolerance to heat by the crop).

In terms of adaptation, expanding irrigation and increasing its efficiency could result in the highest gains, roughly offsetting the climate change impacts under a Wet/Warm mean scenario by mid-century, with other measures having smaller and more localized benefits.

4.2.3 EROSION

SUMMARY	
SUMMARY	Our analysis estimates the impact of climate change on soil loss risk by modeling changes in runoff, climatic and land factors, and farm management practices. We estimate that by 2040, erosion risk will be highest in the southern and western regions of the country, with impacts more pronounced under the Wet/Warm mean. Additionally, we expect the Dry/Hot mean scenario to result in a decrease in erosion and an increase in production for selected crops, with shocks ranging from -1 percent to -8 percent by 2040.
ESTIMATED CLIMATE CHANGE IMPACTS BY 2041-2050	Under the Wet/Warm mean scenario, the impact of erosion on crop production intensifies in the early part of this period, with impacts peaking in 2045 at -0.67 percent, and becoming less severe by 2050. Under the Dry/Hot mean, production shocks are positive, peaking at 0.38 percent by 2050.

Overview of Impact Channel

Erosion can be detrimental to landscapes, impacting plant and animal life, reducing the efficacy of reservoir storage and hydropower production through sedimentation, and causing declines in agricultural production by removing valuable nutrients from the topsoil, all of which can be made worse if climate change intensifies future rainfall intensity. A summary of the modeling methodology used to estimate the impacts of climate change on erosion is presented below, with a more detailed description available in Appendix B.

To determine erosion rates, we use the Revised Universal Soil Loss Equation, which requires five key inputs, namely rainfall-runoff erosivity, climate and land factors, as well as activity and farm-level management factors. Generally, areas that are impermeable (e.g., rocky surfaces or waterbodies) and areas with mean slopes that exceed 20 percent are excluded from the analysis because erosion on these surfaces tends to be low or highly uncertain with the Revised Universal Soil Loss Equation approach.

Soil loss can reduce the nutrients available to crops, if not replenished by fertilizers, by eroding the topsoil. Although topsoil is generated naturally, natural generation is slow. To approximate the impact erosion has on the major crops grown in the country, we use a method developed by the Food and Agriculture Organization (Kassam et al. 1991). The approach is based on a tolerable loss rate over time and varies by levels of fertilizer inputs as well as the susceptibility of soils to productivity loss. We use raster data of fertilizer use (nitrogen and phosphorus) to

determine the level of input in a country. Further details on the data sources used to complete the analysis are provided in Appendix C.

Results: Climate Change Effects

During the baseline period, soil erosion risk is concentrated in the southern and western regions of the country, specifically surrounding urban areas (Figure 51). In the south and southwest, soil erosion risk is high in the areas surrounding San Cristóbal and Barahona. Here, soil erosion risk ranges from around 154 - 6851 tons/ha/year. Similarly, in the west, erosion risk is high outside of San Juan, which experiences similar soil erosion risks as San Cristobal and Barahona.

FIGURE 51. EROSION DURING BASELINE PERIOD

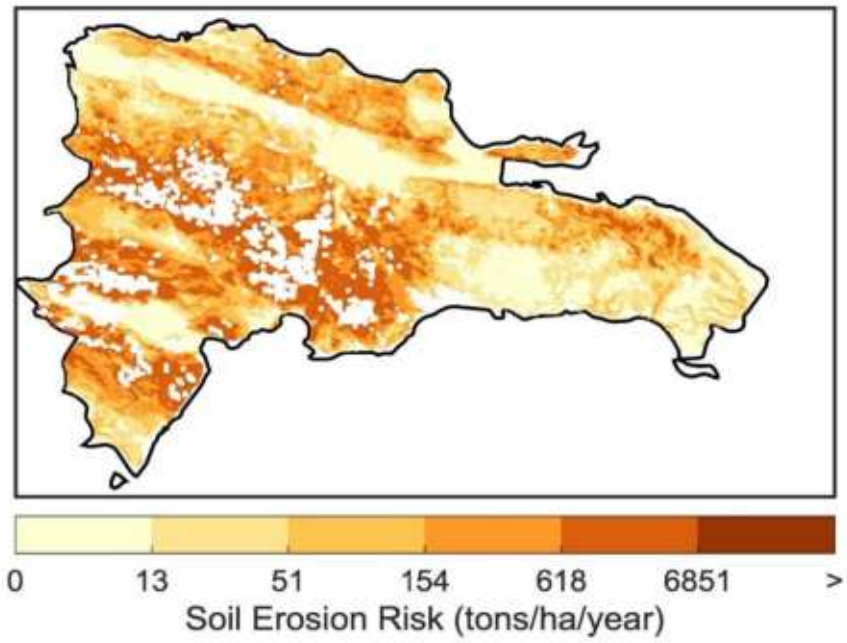

Relative to baseline conditions, the Wet/Warm mean scenario is expected to result in an increase of erosion while the Dry/Hot mean scenario is expected to result in a decrease in erosion by 2040 (Figure 52 and Figure 53). From the Wet/Warm mean scenario, changes in erosion risk range from 0 to -50 tons/ha/year throughout the country. Areas surrounding San Cristobal and Barahona are expected to experience high relative changes in risk at around -50 ton/ha/year. Areas in the eastern part of the country surrounding El Seibo are also expected to experience a similar magnitude of erosion risk by 2040.

Compared to the Wet/Warm mean scenario, erosion from the Dry/Hot mean scenario declines from baseline conditions. Overall, erosion declines throughout the country with areas in the southern and southwest portions of the country seeing a larger decrease in risk.

FIGURE 52. EROSION RISK BY 2040 UNDER WET/WARM MEAN SCENARIO

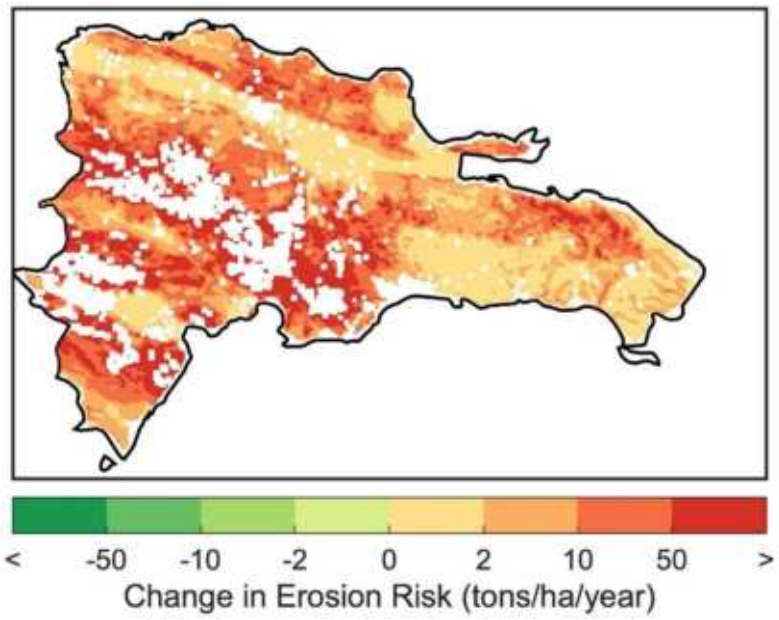

FIGURE 53. EROSION RISK BY 2040 UNDER DRY/HOT MEAN SCENARIO

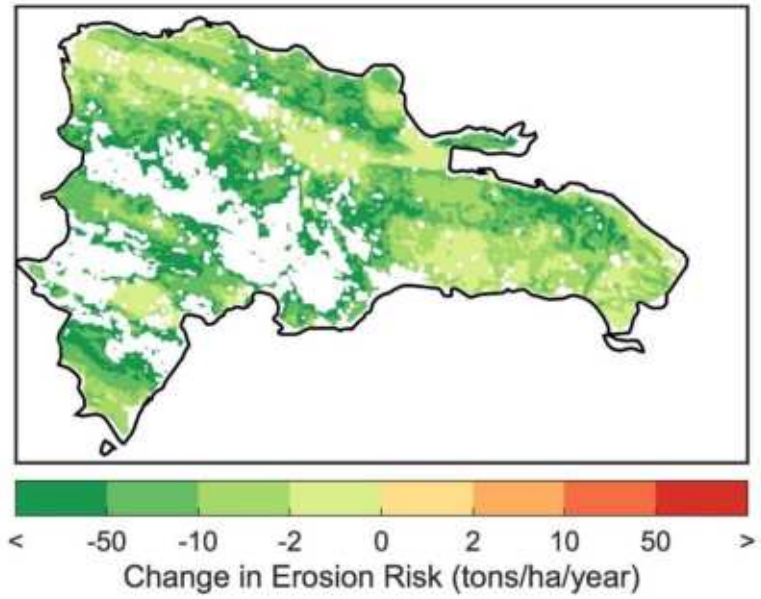

Erosion is also expected to have important implications for crop production within the country. Specifically, the Dry/Hot mean scenario is expected to result in production gains for all crops considered (Figure 54). Shocks from the Dry/Hot mean scenario are highest for potatoes and vegetables which are expected to experience production gains (i.e., negative production losses) of around -8 percent and -6 percent, respectively. For high-yielding crops such as sugarcane, the Dry/Hot mean scenario is expected to result in productivity gains of around -4 percent by mid-century. The Wet/Warm mean scenario results in negative impacts to most crops considered.

Under this scenario, crops generally experience a negative production shock ranging from 0 percent to 2 percent.

FIGURE 54. CROP PRODUCTION LOSS DUE TO EROSION BY 2040

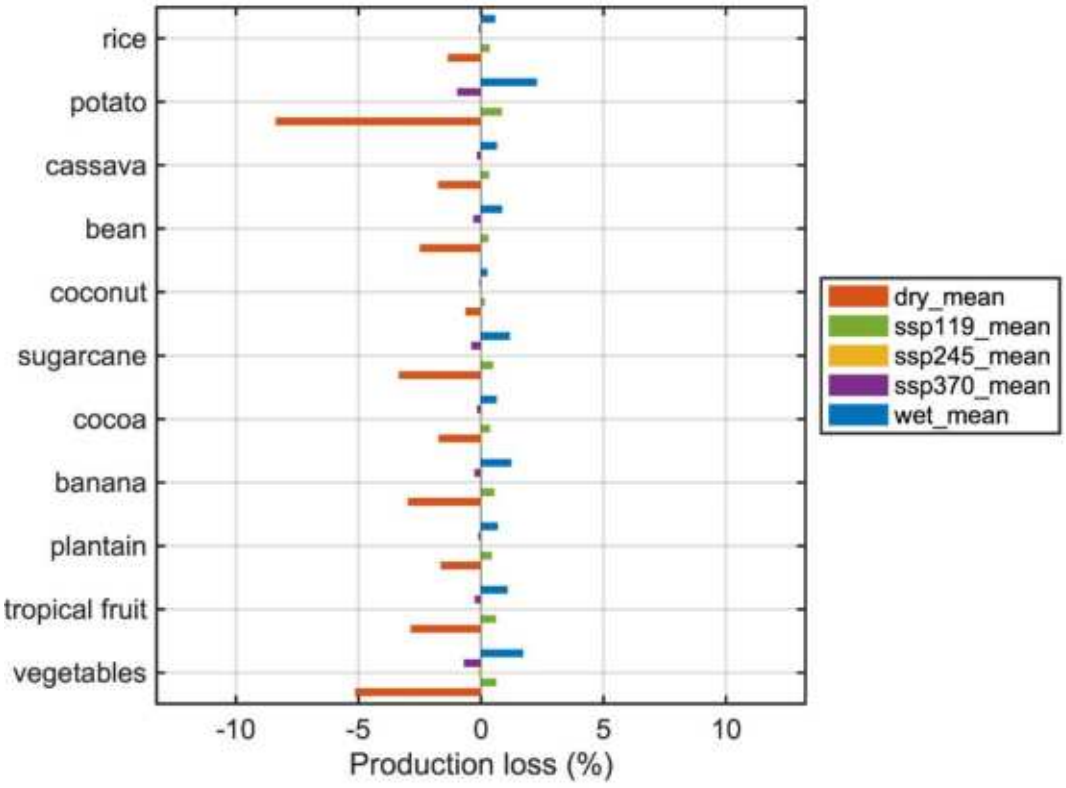

Adaptation

With the modeled effects of climate change on erosion and subsequently on crop production documented above, this section now looks at the effect of investing in adaptation measures. As introduced in Section 3.2, we consider a **proactive adaptation scenario** and compare it to a **no-action baseline** that assumes no change in soil management practices. When it comes to reducing the impacts of climate change on erosion, there are a variety of possible adaptation interventions that could be pursued, with most focused on improving soil conservation practices such as reduced or zero tillage, mulching, leaving of crop residue on the field post-harvest, or the planting of cover crops. Table 9 shows the different adaptation interventions evaluated for this channel, with these actions assumed to be implemented in 2025.

TABLE 9. ADAPTATION SCENARIOS AND INTERVENTIONS EVALUATED

ADAPTATION INTERVENTION	SCENARIO		
	NO-ACTION BASELINE	PROACTIVE ADAPTATION	
		LOW	HIGH
Practice conservation tillage	No change	Increase conservation tillage to achieve an adoption rate of 10% by 2050	Increase conservation tillage to achieve an adoption rate of 20% by 2050
Leave crop residue on fields		Increase the practice of leaving crop residue on fields to 10% by 2050	Increase the practice of leaving crop residue on fields to 20% by 2050
Combination of conservation tillage and crop residues being left on fields		10% conservation tillage + 10% crop residues by 2050	20% conservation tillage + 20% crop residues by 2050

Results: Adaptation

Figure 55 shows the estimated crop production shocks for the various adaptation interventions by 2041-2050, relative to a baseline period of 1995-2020. The top "no adaptation" row of Figure 55 represents the shocks that would be experienced if no adaptation actions were taken and serves as the baseline for comparing the effect of different adaptation actions. Across both the no-action baseline as well as most of the adaptation interventions considered, the production shocks are generally worse (i.e., production losses, or smaller production gains) under the Wet/Warm mean scenario (wetter scenarios typically result in more soil erosion, which drives greater losses in crop production) as compared to the Dry/Hot mean scenario (drier scenarios typically have less soil erosion, retaining more of the topsoil, resulting in smaller negative impacts to crops).

Under the Wet/Warm mean scenario we expect low conservation tillage and low use of crop residues to result in less severe crop production shocks as compared to the no-action baseline. Under the no-action baseline, the Wet/Warm mean scenario is anticipated to result in a crop production shock of -0.75 percent. However, low crop residue use and low conservation tillage practices are expected to result in production shocks of approximately -0.5 and -0.4 percent, respectively. Under the Dry/Hot mean scenario, the adaptation strategies evaluated are expected to result in positive production shocks, however, these shocks are smaller than those projected for the no-action baseline case under the Dry/Hot mean scenario (+1.75 percent). Under this scenario, a low combined adaptation approach and low conservation tillage practices are expected to be the most beneficial adaptation strategies analyzed, resulting in shocks of +1.6 and +1.55 percent respectively. Further, with both adaptation interventions we expect lower levels of each adaptation intervention to produce greater improvements than higher levels (i.e., 10 percent versus 20 percent conservation tillage or crop residues).

FIGURE 55. CROP PRODUCTION SHOCK BY THE 2040S, WITH AND WITHOUT ADAPTATION

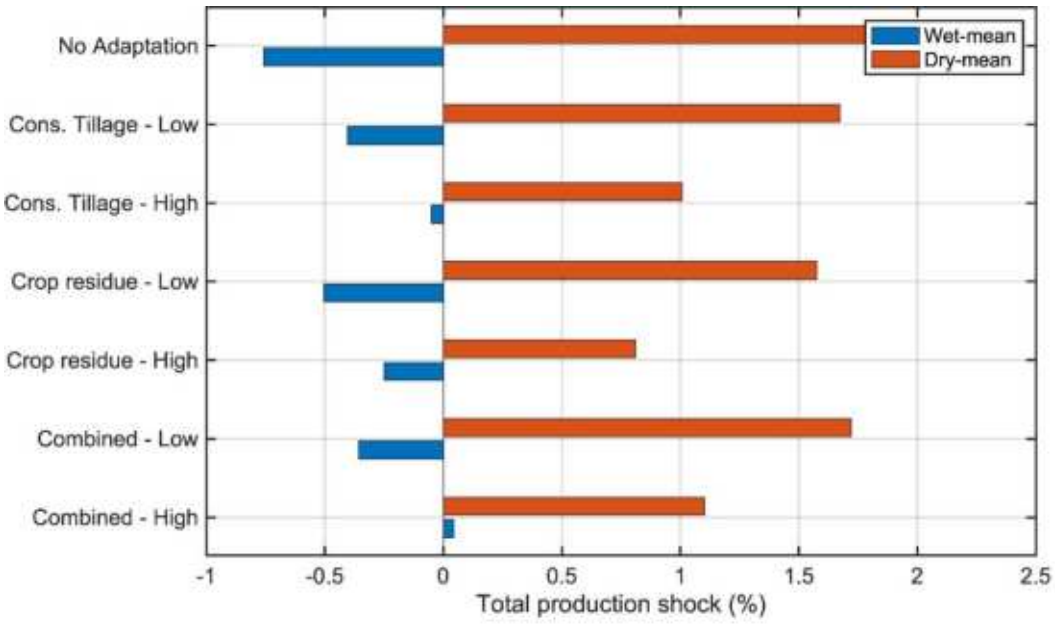

4.2.4 HYDROPOWER

SUMMARY	
SUMMARY	Our analysis estimates the impact of climate change on hydropower production by modeling changes in water availability and extreme heat. We estimate that by 2050, climate change may result in hydropower production shocks ranging from +4 percent to +17 percent.
ESTIMATED CLIMATE CHANGE IMPACTS BY 2041-2050	From 2041-2050, negative impacts to hydropower production are highest from the Dry/Hot mean scenario which is expected to result in a -22 percent shock by 2045. We expect the Wet/Warm mean scenario to result in a significant positive production shock of +17 percent by 2045.

Overview of Impact Channel

Climate change may impact hydropower generation directly through a reduction in river runoff and reservoir levels, and indirectly through changes in the water demands for competing uses (e.g., irrigation). We model these nexus effects using a WEAP water systems model. To estimate the effect of climate change on hydropower production, we apply a reservoir balance approach to each catchment, with the change in reservoir storage driven by inflows, reservoir releases, and evaporative losses. A summary of the modeling methodology used is presented below, with a more detailed description available in Appendix B.

Hydropower generation is a function of flow through the turbines and potentiometric water head each month. To convert reservoir storage to hydropower generation (including for run-of-river facilities) requires a volume-elevation curve to relate volume to head, as well as turbine elevations, maximum turbine flows, turbine efficiencies, minimum turbine flows, and capacity factors. Modeled runoff data from the water systems model, as well as data on reservoir storage, demand, and outflows, served as inputs into the reservoir balance model. Monthly hydropower generation was produced as model output and an evaluation of climate change impacts was carried out by comparing the baseline production across the different scenarios being considered. Details on the data sources used to complete the analysis are provided in Appendix C.

Results: Climate Change Effects

Hydropower production in the country varies based on the total runoff of each basin. We consider 35 reservoirs within the model, with a total production of approximately 1.16 TWh/y. They are mainly distributed in the Yaque del Norte (Tavera and Moncion complex), Nizao (Aguacate and Jiguey) and Yuna region (see Figure 56 and Figure 57).

FIGURE 56. MAJOR HYDROPOWER FACILITIES

FIGURE 57. BASELINE HYDROPOWER PRODUCTION

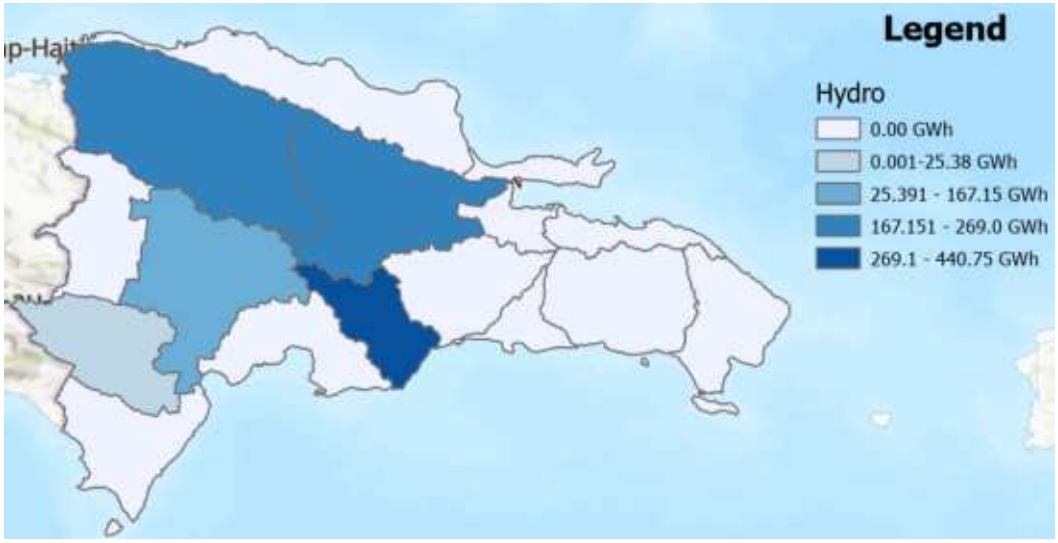

The final output of the model shows an increase in the production under the Warm/Wet mean scenario in the 2040s, ranging from -1 percent to +17 percent. The impacts of the Dry/Hot mean scenario are instead always negative, with a range of -8 percent to -22 percent in the 2040s (Figure 58). Under the Dry/Hot mean scenario, Aguacate, Jiguey, Moncion and Tavera are expected to experience a decrease in production of -7, -9.35, -7.8, and -10.6 percent, respectively. This reflects the need to explore and implement concrete adaptation options in order to meet the future energy demand of the country. The change in production by basin under the Wet/Warm and Dry/Hot mean scenarios with respect to the baseline are shown in Figure 58.

FIGURE 58. HYDROPOWER GENERATION SHOCK, 3-YEAR MOVING AVERAGE

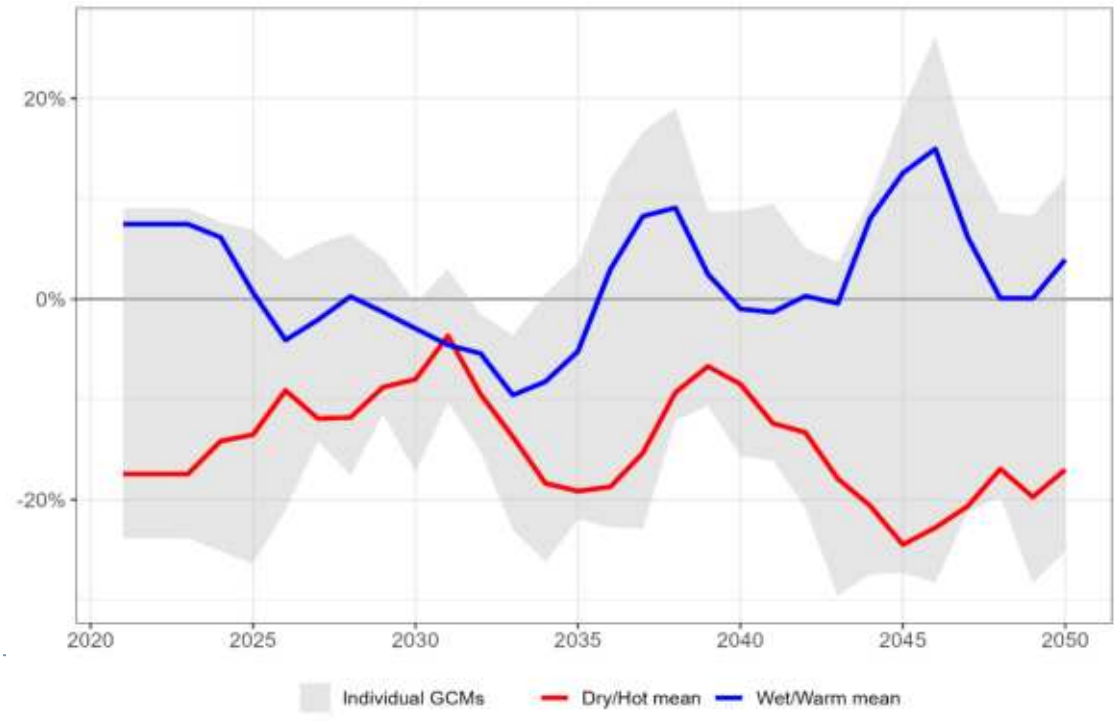

FIGURE 59. CHANGE IN HYDROPOWER GENERATION SHOCK, 3-YEAR MOVING AVERAGE, RELATIVE TO THE BASELINE

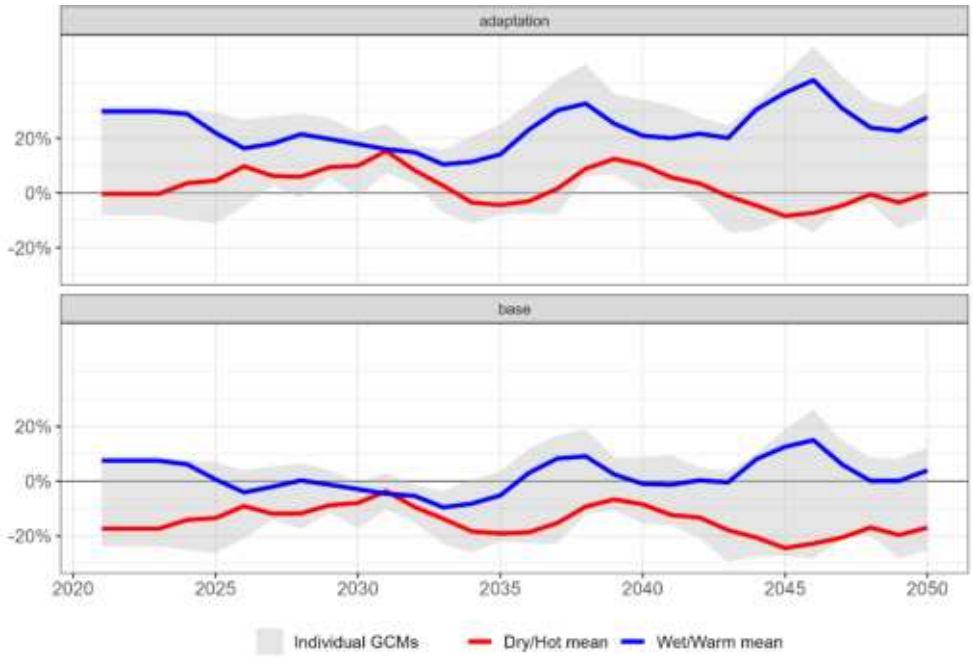

Results: Adaptation

Being prepared for the climate change effects on water availability and consequently on hydropower generation will require careful planning and water management in the future. A key component of this will be an increase in water storage, that will contribute to minimizing shortfalls in dry months of the year. We model an increase of 10 percent in the country's reservoir capacity, as well as a 20 percent increase in the maximum turbine capacity for hydropower facilities. It is assumed these changes will be achieved by shifting to more efficient turbines and increasing the capacity of reservoirs.

As seen in Figure 59, this adaptation intervention will result in a significant hydropower generation increase (+20 percent) under both the Wet/Warm mean and the Dry/Hot mean scenarios. This corresponds to an increase in energy production from 900 to 1125 GWh and from 750 to 875 GWh respectively, by 2050 (see Figure 60). These results highlight that informed investments in adaptation could bring important positive impacts on the country's hydropower production.

FIGURE 60. CHANGE IN HYDROPOWER GENERATION (GWH), 3-YEAR MOVING AVERAGE, RELATIVE TO THE BASELINE

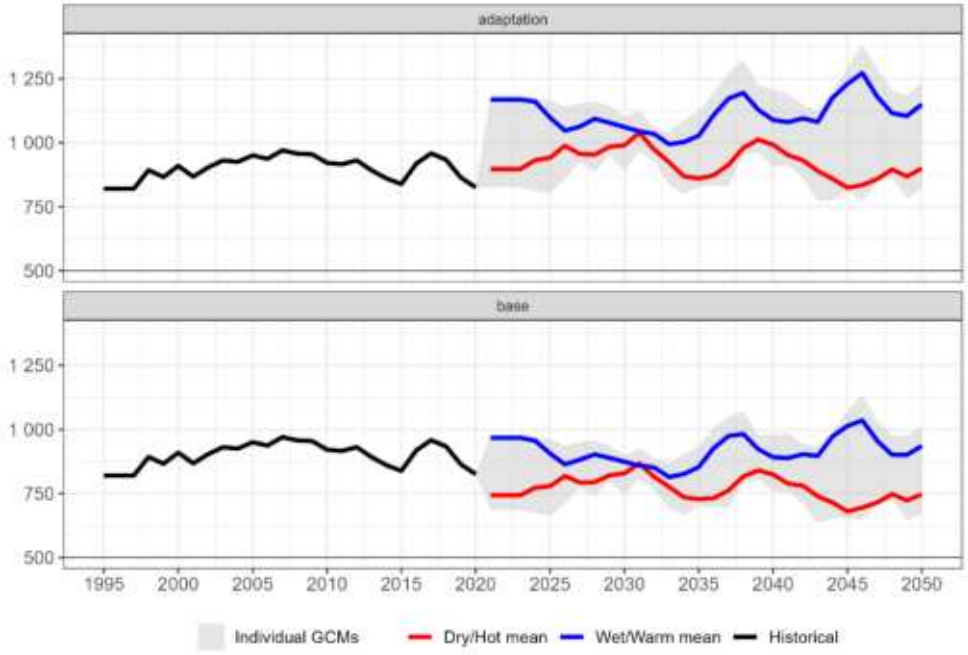

Figure 61 shows projected hydropower production under different climate scenarios. These results show how both with and without an increase in the turbine capacity, the Wet/Warm scenarios (blue lines) tend to be above the Hot/Dry ones (red lines). Total generation will be higher in the adaptation case, ranging from 750 to more than 1350 GWh. With adaptation, the Hot/Dry scenarios will result in production ranging between 740 to 1125 GWh, which is, as expected, still below the production levels achieved under the Wet/Warm scenarios.

FIGURE 61. HYDROPOWER GENERATION (GWH) FOR EACH SCENARIO, 3-YEAR MOVING AVERAGE

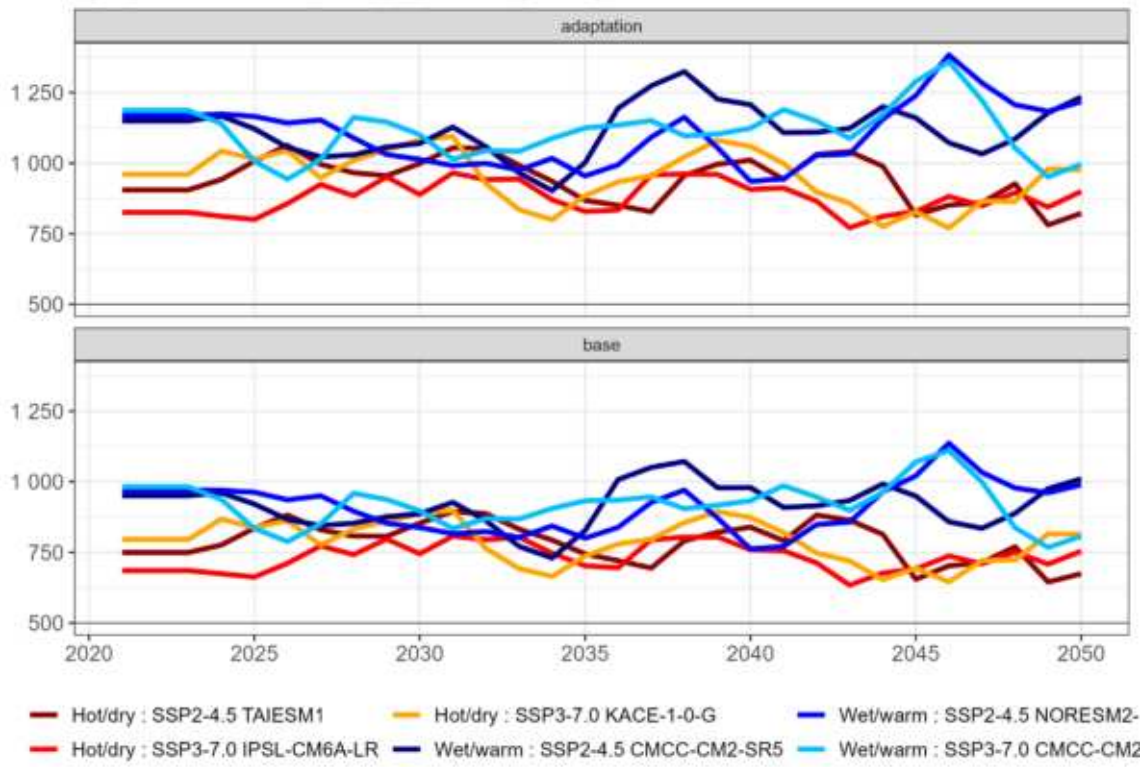

4.3 INFRASTRUCTURE AND SERVICES

Climate change is likely to impact infrastructure, and the services provided by it in a variety of ways including by increasing the frequency and magnitude of extreme events that result in damages to assets, as well as by increasing deterioration caused by heat and precipitation levels. The estimated impacts to the Dominican Republic's infrastructure and services due to climate change are presented below.

4.3.1 INLAND FLOODING

SUMMARY	
SUMMARY	This analysis estimates the impact of climate change on inland flooding events and quantifies impacts to capital relative to baseline conditions. Our results suggest that both SSP1-1.9 and SSP3-7.0 will result in an increase in expected annual capital losses relative to baseline conditions, with impacts being most severe under SSP1-1.9. Overall, we expect climate change to impact low-frequency events the most, resulting in, for example, increases in the magnitude of the 20-year flooding event of up to 130 percent.

ESTIMATED CLIMATE CHANGE IMPACTS BY 2041-2050	From 2041 to 2050, we expect additional annual capital losses for SSP1-1.9 and SSP3-7.0 of 0.09 and 0.06 percent, respectively. When considering impacts from 50-year flooding events, we estimate capital shocks will increase from a -8.4 percent of capital loss by 2050, to a -9.1 and -8.8 percent loss under SSP-1.9 and SSP3-7.0, respectively.

Overview of Impact Channel

Climate change may exacerbate flooding by increasing the frequency, intensity and duration of storm events. This analysis relies on projected changes in the return interval of precipitation events from the World Bank's Climate Knowledge Portal. Flood hazard maps are developed to determine areas with a certain probability of flooding for a given baseline and climate change projected return period. The outputs of the flood hazard mapping include the extent and depth of flood inundation, which are then used to estimate damages to infrastructure. The analysis is done for the 2030s and 2050s eras, SSP1-1.9 and 3-7.0, and 5, 10, 20, 25, 50, and 100-year recurrence interval, at a spatial resolution determined by the available hydrology and infrastructure asset distribution data. The resulting outputs are aggregated to a national scale, and correspond to the expected share of capital damaged relative to a historic baseline (1995 to 2020).

A more detailed description of the modeling methodology used is available in Appendix B, with Appendix C offering details on the data sources utilized in the analysis.

Results: Climate Change Effects

Figure 62 shows the historical riverine floodplain of the country during the baseline period and highlights major waterways including the Yaque del Norte River in the north, the Yaque del Sur in the south, and the Cuma River in the east.

FIGURE 62. HISTORICAL RIVERINE FLOODPLAIN, 1981-2010

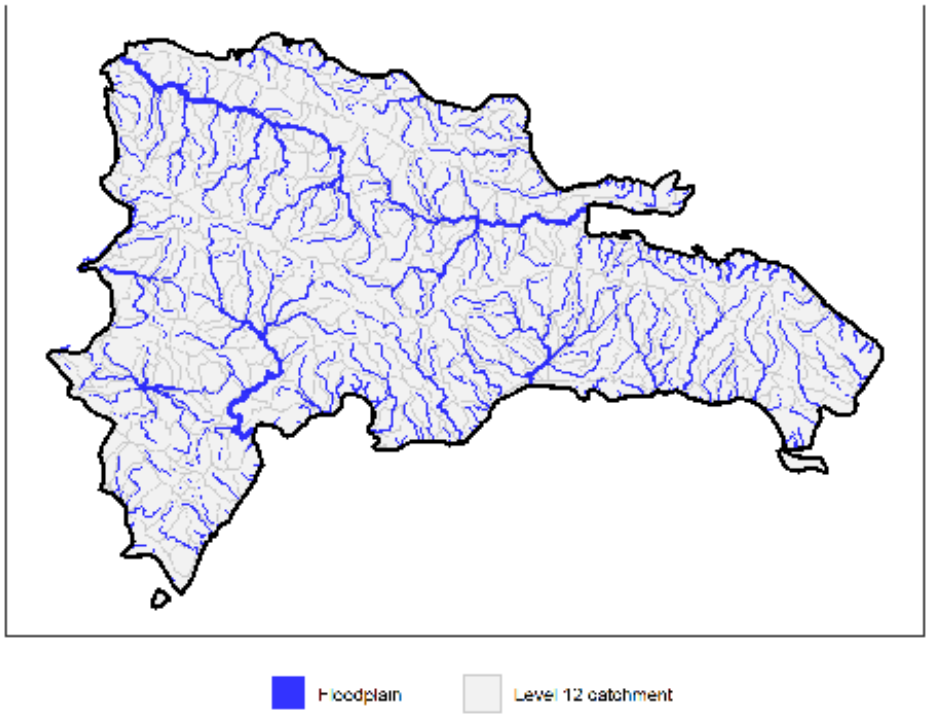

Relative to baseline conditions, the SSP1-1.9 and SSP3-7.0 scenarios are projected to result in an increase in capital infrastructure damage by 2050, with SSP1-1.9 resulting in greater impacts. That said, when considering shocks from different flooding events, both the SSP3-7.0 and SSP1-1.9 scenarios result in generally similar impacts to capital relative to the baseline period (Table 10). While capital shocks for 10-year flooding events are relatively low at -0.6 percent and -0.9 percent for SSP3-7.0 and SSP1-1.9 respectively, shocks are greater for the 100-year flood event, increasing from -10.1 percent under the baseline to to -10.4 percent and 10.6 percent for SSP3-7.0 and SSP1-1.9 respectively.

TABLE 10. INLAND FLOODING SHOCK FOR THE 2050 ERA

SSP	ERA	10 YR RETURN PERIOD	20 YR RETURN PERIOD	25 YR RETURN PERIOD	50 YR RETURN PERIOD	100 YR RETURN PERIOD
HISTORIC	BASELINE	0.0%	-4.6%	-5.8%	-8.4%	-10.1%
SSP1-1.9	2050	-0.9%	-5.5%	-6.6%	-9.1%	-10.6%
SSP3-7.0	2050	-0.6%	-5.1%	-6.2%	-8.8%	-10.4%

In the baseline period, flood risk is highest in southern areas of the country, specifically in the areas surrounding Santo Domingo (Figure 63). During this period, impacts to capital from inland flooding also extend further north and east, though are less pronounced. Overall, impacts to capital become more severe with more severe flooding events, with impacts from 100-year

flooding events in a single catchment resulting in capital losses of up to 3 percent of the total capital stock of the country.

FIGURE 63. HISTORICAL INLAND FLOODING DAMAGES (% OF TOTAL CAPITAL), 1981-2010

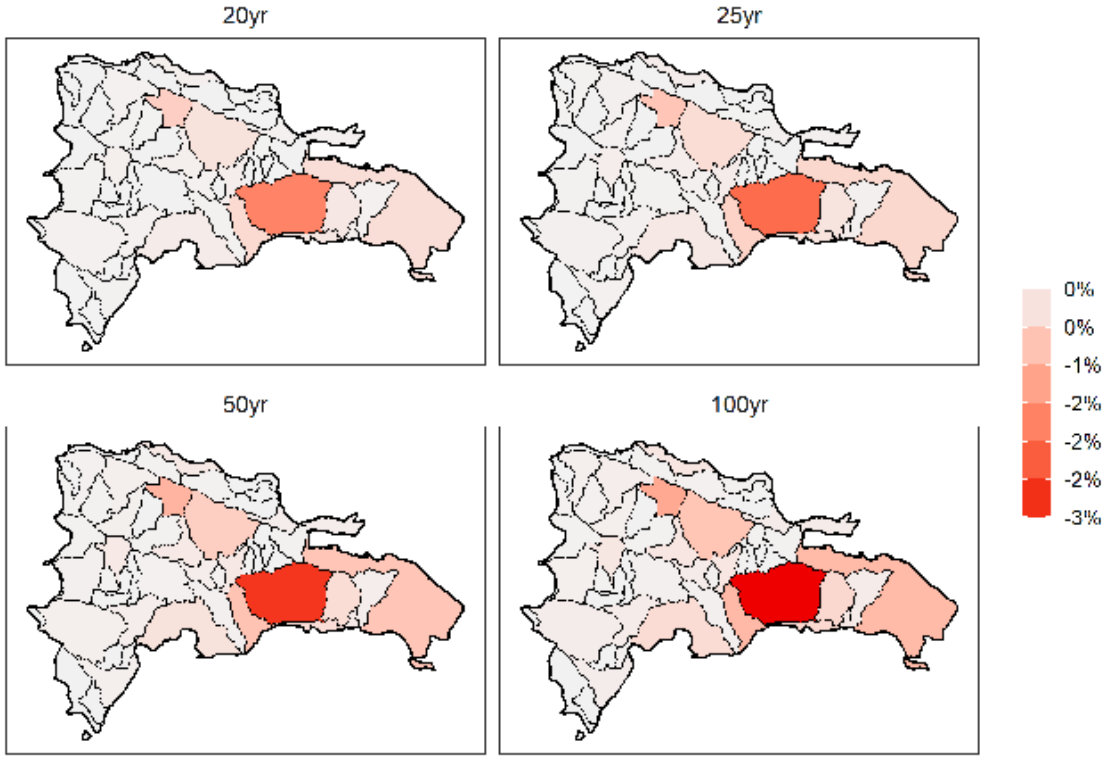

Generally, for 2035 to 2064, changes in the magnitude of flooding events due to climate change are highest in catchments located in the center of the country, specifically in the areas surrounding San Juan, Santiago, and La Vega. Changes tend to become less severe when moving further south and east (Figure 64). Impacts to capital relative to the baseline period are expected to be highest for more frequent events such as the 20- and 25-year flooding, with shocks increasing up to 27 percent in the center of the country. Increases in the magnitude of country-wide impacts to capital are expected to decline when considering less frequent events (i.e., 50- and 100-year events).

FIGURE 64. CHANGE IN CAPITAL LOSSES (% CHANGE RELATIVE TO BASELINE), SSP3-7.0. 2035-2064

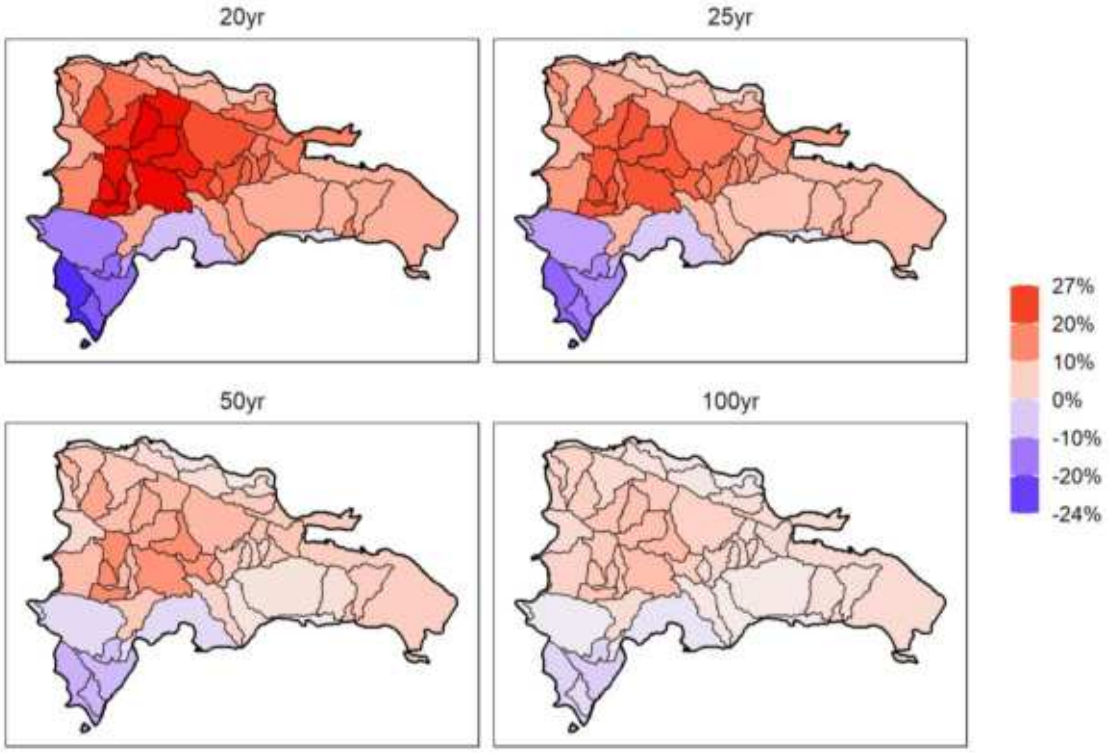

Considering all events, the expected damages (i.e., the sum of the probability of each event times its magnitude) from inland flooding will worsen by -0.1 percent additional capital losses by 2050 under SSP1-1.9. As mentioned, SSP3-7.0 is expected to result in lower incremental damages than SSP1-1.9, seeing about -0.07 percent additional capital losses by 2050 (see Figure 65).

FIGURE 65. INLAND FLOODING SHOCK

Results: Adaptation

With the modeled effects of climate change on inland flooding in the country documented above, this section now looks at the effect of investing in adaptation measures. As introduced in Section 3.2, we consider a **proactive adaptation scenario** and compare it to a **no-action baseline**.

When it comes to reducing the impacts of future inland flooding damages, there is a range of possible adaptation interventions that could be pursued, from zoning to prevent new developments in flood-prone areas, floodproofing infrastructure, or diverting floodwater away from at-risk areas. Our analysis considers an adaption intervention in which infrastructure is hardened to withstand the 20-year flood, instead of the assumed design of current infrastructure for the 10-year flood.

Table 11 shows the impact of the adaptation investment on inland flooding damages compared to the no-action baseline by decade under SSP3-7.0. Overall, the proactive adaptation intervention described above is expected to reduce capital damages in each decade. The adaptation intervention proves to be most beneficial in the last decade from 2041 – 2050 where inland flooding damages under the proactive adaptation scenario are expected to decrease by 0.025 percent relative to the no-action baseline.

TABLE 11. CHANGE IN INLAND FLOODING DAMAGES UNDER THE NO-ACTION BASELINE AND ADAPTION INTERVENTION, SSP3-7.0

ADAPTATION SCENARIO	CLIMATE SCENARIO		
	2021- 2030	2031 - 2040	2041- 2050
NO-ACTION BASELINE	-0.014%	-0.039%	-0.064%
PROACTIVE ADAPTATION	-0.013%	-0.034%	-0.039%

Summary and discussion

Climate change will likely increase the severity of flooding events in the country by mid-century. Generally, basins in the north coast, central mountains, and eastern areas of the country will experience increases in flooding magnitudes i.e., higher peak precipitation events that result in increased reverine flood depths. Only some basins in the south-west of the country are likely to see reduced flood peaks. However, at a national scale, the aggregate negative impacts on capital due to inland flooding are expected to increase.

Higher impacts from all design storms are likely to be experienced, but while the overall magnitude of a future low-frequency event such as a 100-year storm may be larger, more frequent events (e.g., 10-year storms) would see the biggest percent increase. And while single events can cause devastating economic impacts by destroying capital and disrupting economic activity, the marginal effect of climate change on inland flooding is limited when measured in expected value terms, nationally. Without proactive adaptation, an additional 0.06 percent of the country's capital stock is expected to get damaged every year due to flooding. For the 100-year event by mid-century, incremental damages could reach up to about 0.4 percent of the capital stock relative to the historical baseline.

4.3.2 TROPICAL CYCLONES

SUMMARY	
SUMMARY	Our work estimates the impact of climate change on hurricane occurrence and associated wind-related damage. Our results suggest that the occurrence of all hurricane types considered will increase relative to the baseline. By 2050, we estimate that approximately 1 and 1.1 category 1, 2, and 3 hurricanes will occur each year under SSP2-4.5 and SSP3-7.0, respectively (as compared to 0.7 such storms per year under the baseline). We also estimate that approximately 0.2 and 0.3 category 4 and 5 hurricanes will occur by 2050, under SSP2-4.5 and SSP3-7.0, respectively (as compared to 0.1 such storms per year under the baseline).

ESTIMATED CLIMATE CHANGE IMPACTS BY 2030-2050	Overall, we expect annual damages to increase relative to the baseline, with damages highest from SSP3-7.0 in the 2050s, with capital shocks of approximately 2.2 percent.

Overview of Impact Channel

Tropical cyclones and hurricanes can have substantial economic consequences to the country's infrastructure and population. We model the impacts of cyclones by first generating a large number of synthetic hurricane tracks. This is done by randomly seeding a given ocean basin with weak tropical cyclone-like disturbances, and using an intensity model to determine which one of these develops to tropical storm strength or greater. Figure 66 shows an example of hindcast wind speeds and paths produced by this method. For each of these tracks, we then simulate the storm intensity (i.e., a maximum wind speed and a radius of maximum winds) and estimate the incremental damages to capital value relative to the baseline period. Shocks are calculated for specific infrastructure types based on available data on the value and location of infrastructure assets.

FIGURE 66. HINDCAST WIND SPEEDS AND PATHS

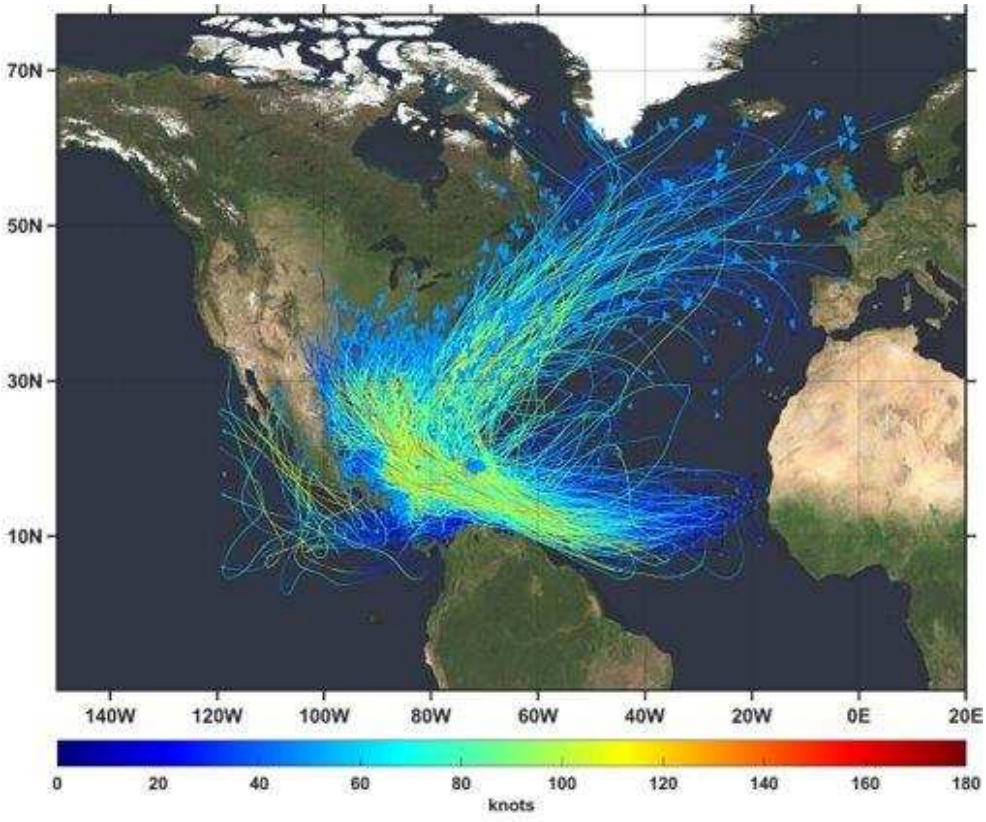

A more detailed description of the modeling methodology used is available in Appendix B, with Appendix C offering details on the data sources utilized in the analysis.

Results: Climate Change Effects

Figure 67 illustrates peak wind speed under SSP3-7.0 for the period 2041 to 2060. Overall, most of the country experiences peak wind speed of around 70 knots, while areas near the coast are expected to experience higher peak wind speeds, ranging from 85 to 95 knots.

FIGURE 67. PEAK WIND SPEEDS UNDER SSP3-7.0, 2041 - 2060

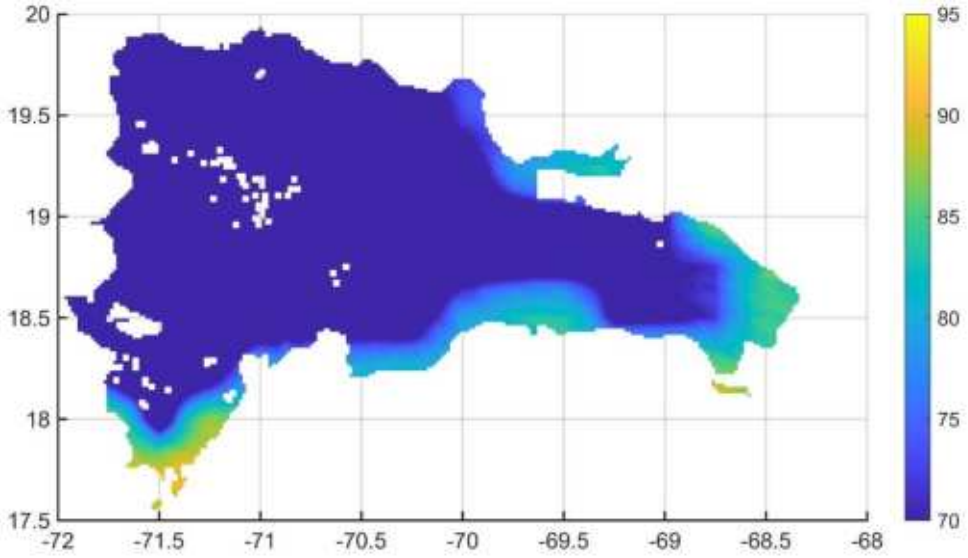

Figure 68 and Figure 69 present the change in the annual occurrence of category 1-3 and 4 and 5 hurricanes in the Dominican Republic, respectively. Overall, through 2090, both climate scenarios suggest that the occurrence of category 1-3 and category 4 and 5 events will increase relative to hindcast estimates. Among category 1-3 hurricanes, SSP3-7.0 is expected to result in a higher annual occurrence in the 2030s and 2050s. When considering category 4 and 5 events, we expect SSP3-7.0 to result in a higher annual occurrence by the 2050s. This trend is reversed by the 2090s.

FIGURE 68. CHANGE IN ANNUAL OCCURRENCE OF HURRICANES OF CATEGORIES 1-3

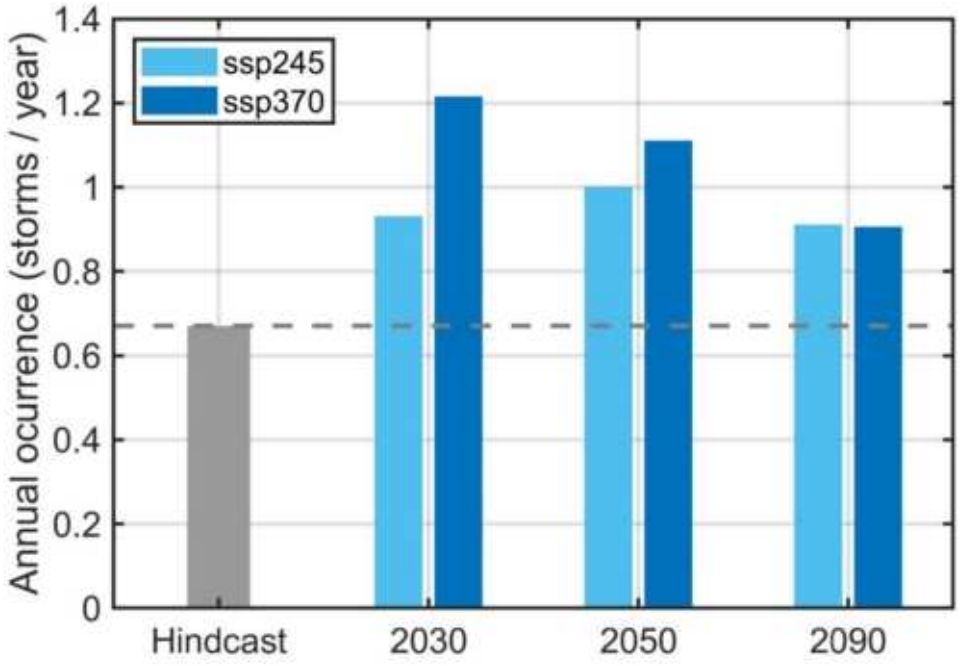

FIGURE 69. CHANGE IN ANNUAL OCCURRENCE OF HURRICANES OF CATEGORIES 4 AND 5

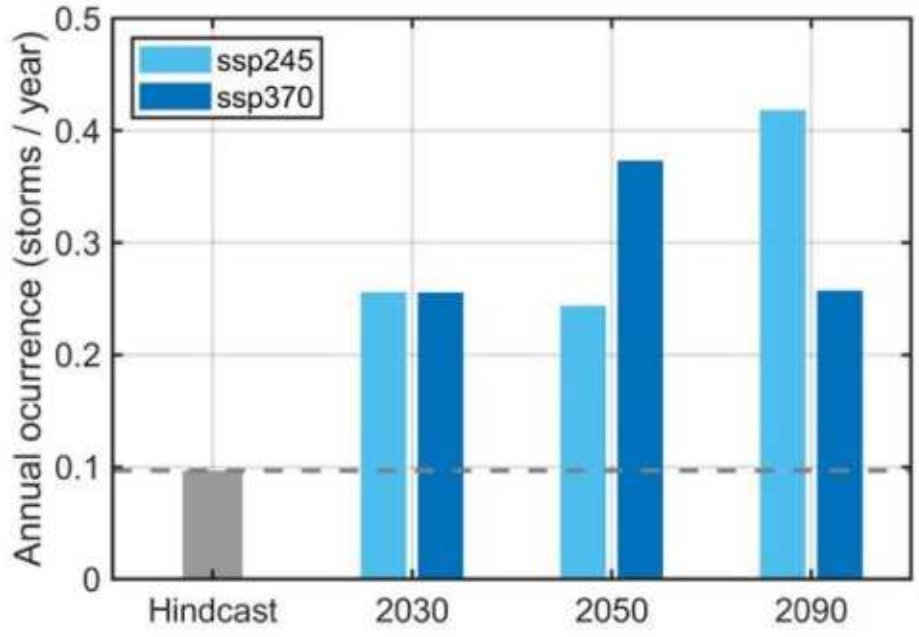

Figure 70 shows the expected annual damages from all hurricane types considered through 2100. Overall, we expect annual damages to increase relative to the baseline, with damages highest from SSP3-7.0 in the 2030s and 2050s. Here, we expect capital shocks of approximately 3.5 percent and 2.2 percent in the 2030s and 2050s, respectively.

FIGURE 70. EXPECTED ANNUAL DAMAGES (% CAPITAL SHOCK)

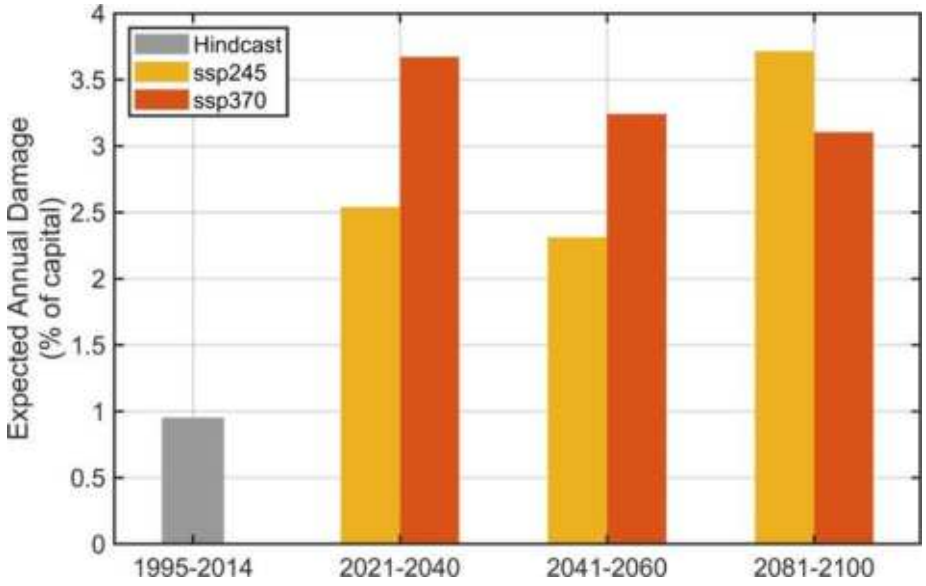

Figure 71 presents a map of expected annual damages as a percentage of asset value under SSP3-7.0 for the period 2041 to 2060. Overall, damages are highest along the southwest and southeast coast, peaking at around 5 percent.

FIGURE 71. EXPECTED ANNUAL DAMAGE RATIO (% OF ASSET VALUE) UNDER SSP3-7.0, 2041-2060

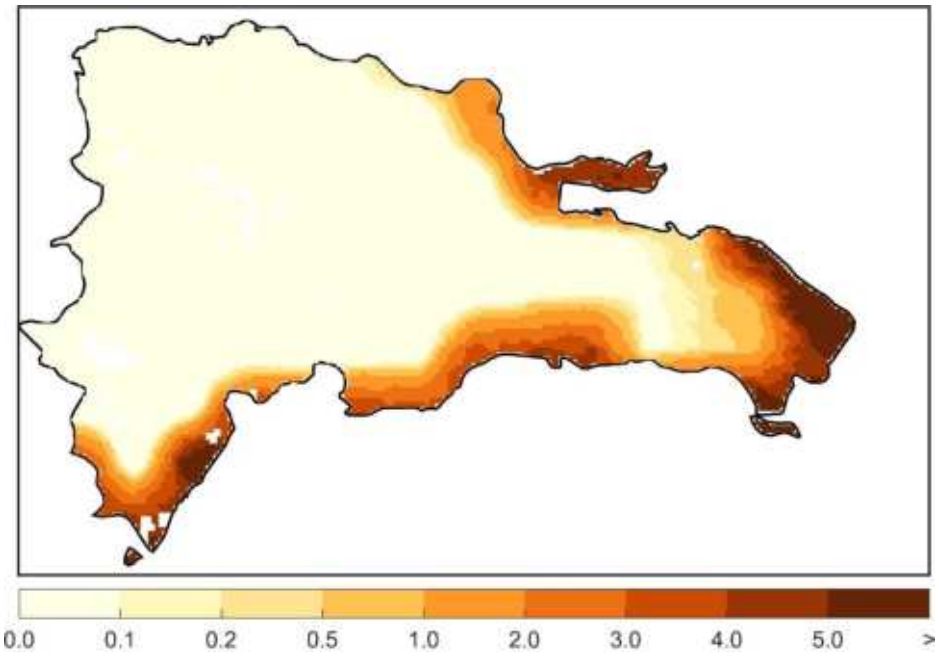

Results: Adaptation

With the modeled effects of climate change on tropical cyclones in the country documented above, this section now looks at the effect of investing in adaptation measures. As introduced in Section 3.2, we consider a **proactive adaptation scenario** and compare it to a **no-action baseline**.

When it comes to reducing the impacts of future tropical cyclone damage, there is a range of possible adaptation interventions that could be pursued. Our analysis considers an adaptation intervention in which (1) roof connection anchors are improved and (2) connection anchor bolts and stiffeners are added. Overall, we assumed that these interventions cost 10 percent of the building value with both interventions reducing vulnerability by 50 percent. These interventions are applied using a benefit-cost test on a 1 km grid. We assume that two levels of adaptation can be implemented: (1) high adaptation, in which the benefit-cost ratio exceeds 1, and (2) medium adaptation, in which the benefit-cost ratio exceeds 4.

Figure 72 shows the expected annual damages from tropical cyclones in the country (expressed as a percentage of the whole capital stock that is damaged in any given year over the baseline) for the SSP3-7.0 climate scenario. It compares the damages without adaptation, with medium protection, and with high protection. Without adaptation, the proportion of additional capital damages are expected to decline throughout the period from around 3.6 percent by 2030 to 3.1 percent by 2090. Under medium protection, expected annual damages are estimated at 1.9, 1.8 and 1.7 percent by 2030, 2050, and 2090 respectively. High protection is anticipated to be most beneficial, with capital damages projected at around 1, 0.8, and 0.7 percent by 2030, 2050, and 2090 respectively.

FIGURE 72. EXPECTED ANNUAL DAMAGES FROM HURRICANES UNDER SSP3-7.0 WITH AND WITHOUT ADAPTATION

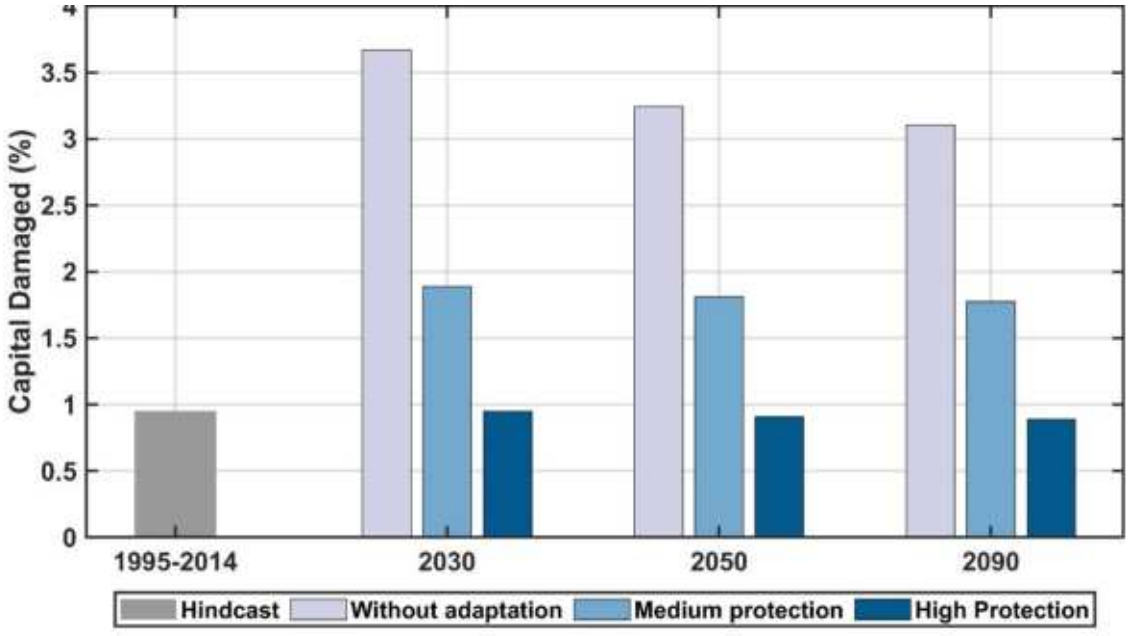

4.3.3 SEA-LEVEL RISE AND STORM SURGE

SUMMARY	
SUMMARY	Our work estimates the impact of sea level rise and storm surge on capital infrastructure using GIS analysis to intersect areas of coastal inundation with areas that contain infrastructure assets. We estimate that by 2050, sea level rise and storm surge will result in an additional -0.5 percent and -0.03 percent capital shock, respectively.
ESTIMATED CLIMATE CHANGE IMPACTS BY 2041-2050	The change in mean sea level relative to baseline conditions is expected to increase as 2050 approaches. The spread between climate scenarios will continue to increase towards mid-century, with the highest change in mean sea level resulting from SSP5-8.5. Overall, by mid-century we expect the SSP3-7.0 scenario to result in a shock of -0.5 percent incremental capital losses.

Overview of Impact Channel

Rising mean sea levels and temporary flooding from storm surge events threaten coastal infrastructure and land. This analysis used a Geographic Information System to estimate the share of assets (i.e., capital and land) inundated under various sea-level rise scenarios. We use a "bathtub" approach to estimate the impacts of **rising sea levels**, whereby land grid cells become inundated as the total water level increases based on the projected sea level rise. We then intersected the inundated areas resulting from discrete sea level rise increments with the infrastructure asset classes of interest to estimate the share that gets inundated. **Storm surge** impacts were estimated similarly to the impacts from sea level rise, except for the application of a historical storm surge height above mean tidal levels. While the inundation associated with sea level rise is treated as permanent, storm surge impacts are both temporary and repairable, even though the cost for repair can be substantial and potentially unaffordable for property owners. In this way, it is akin to inland flooding and we apply depth-damage functions to estimate the repair costs of impacts on capital stock.

A more detailed description of the modeling methodology used is available in Appendix B, with Appendix C offering details on the data sources utilized in the analysis.

Results: Climate Change Effects

By early-century, mean sea level is expected to increase by approximately 0.1 meters (Figure 73), with the scenarios evaluated resulting in a -0.1 percent shock to capital stock. By mid-century, the variance between the different climate scenarios increases, with SSP3-7.0 resulting in the second largest relative change in mean sea-level, at around 0.2 meters. This is associated with a -0.5 percent shock to coastal capital. While the change in sea level is relatively small by 2050, by the end of the century, sea level rise is expected to increase by a magnitude of 3. By 2100, the spread between scenarios continues to increase, with SSP3-7.0 resulting in a 0.7 meter increase in mean sea level.

FIGURE 73. MEDIAN SEA-LEVEL RISE BY 2100

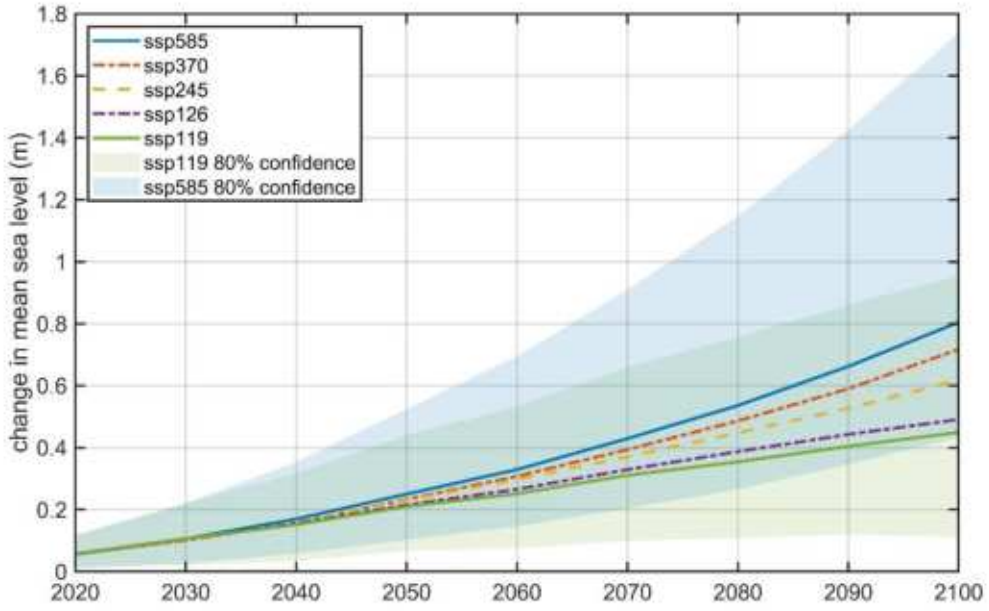

Overall, impacts to capital from sea-level rise and storm surge increase consistently through mid-century relative to baseline conditions, with impacts from sea-level rise (versus those from storm surge) accounting for the majority of impacts to capital (Figure 74). However, while relatively smaller in magnitude compared to sea level rise, annual damage from storm surge events also increases in the decades leading to 2050. By 2050, impacts from sea-level rise result in a -0.5 percent shock to capital (i.e., an additional incremental loss of 0.5 percent of capital relative to the baseline), while impacts from storm surge result in an approximately -0.03 percent incremental shock to capital. Note that the values on the y-axis in Figure 74 correspond to an increase in damages, hence a negative shock.

FIGURE 74. CAPITAL SHOCK FROM SEA LEVEL RISE AND STORM SURGE, RELATIVE TO 2020

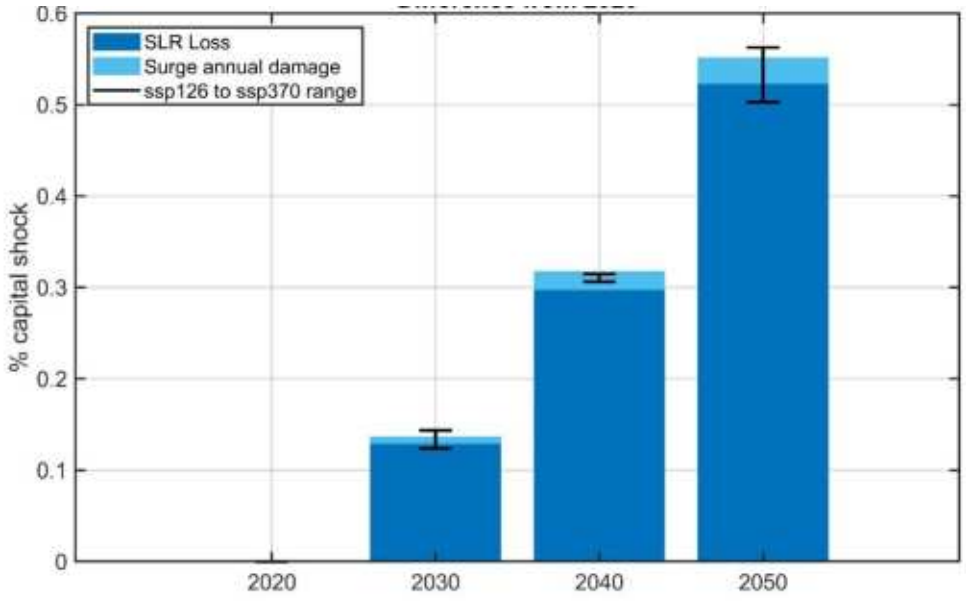

Results: Adaptation

With the modeled effects of climate change on sea-level rise and coastal tidal levels documented above, this section now looks at the effect of investing in adaptation measures. As introduced in Section 3.2, we consider a **proactive adaptation scenario** and compare it to a **no-action baseline**. When it comes to reducing the impacts of future sea-level rise and coastal tidal levels, a variety of possible adaptation interventions could be pursued, from planned retreat, to zoning to prevent new developments in at-risk coastal areas, to elevated buildings, floodwalls, or pumping and drainage systems.

In this study, we consider an adaptation strategy where any new infrastructure built in the future is located at an elevation that is above the projected sea level by 2050 under the SSP3-7.0 climate scenario. This not only protects new structures from anticipated changes in sea level by 2050, but by building at higher elevations, damages from coastal tidal levels to new buildings will also be reduced. We assume this adaptation strategy commences in 2025. The rate of new infrastructure constructed is modeled to mirror the population growth rate of Santo Domingo, as reported by the United Nations World Urbanization Prospects (2018).

We also consider an adaptation strategy where sea walls are built to protect the structures with the highest annual expected damage under SSP3-7.0 by 2050. This strategy is assumed to cost 15 percent of a structure's value and reduces vulnerability by 80 percent. Adaptation is applied using a benefit-cost test, where benefits equal mean expected avoided damages over a 20-year planning horizon and costs equal the value of a structure as a share of national capital stock. Two adaptation levels are considered: high adaptation wherein adaptation is applied when the benefit-cost ratio exceeds 1 and medium adaptation wherein adaptation is applied only when the benefit-cost ratio exceeds 4.

Table 12 shows the different adaptation interventions evaluated for this channel, focusing on ensuring new infrastructure is built away from the most hazardous areas as well as protecting existing infrastructure.

TABLE 12. ADAPTATION SCENARIOS AND INTERVENTIONS EVALUATED

ADAPTATION INTERVENTION	SCENARIO		
	NO-ACTION BASELINE	PROACTIVE ADAPTATION	
Building new infrastructure above the projected sea level change by 2050	No change	Build all new structures above the projected sea level change by 2050 for SSP3-70, starting in 2025	
Building sea walls to protect the highest-risk structures		Medium: apply adaptation when benefit-cost ratio exceeds 4	High: apply adaptation when benefit-cost ratio exceeds 1

Figure 75 shows the expected annual damages from coastal flooding in the country (expressed as a percentage of the whole capital stock that is damaged in any given year over the baseline) for the SSP3-7.0 climate scenario. It compares the damages without adaptation, with medium protection, and with high protection. Without adaptation, the proportion of additional capital damages from coastal flooding are projected to quadruple, from around 0.0008 percent above baseline in the 2030s to around 0.003 percent above baseline in the 2050s. Medium protection (i.e., applying adaptation when the benefit-cost ratio exceeds 4) does not alter the projected damages as compared to the without adaptation case. High protection (i.e., applying adaptation when the benefit-cost ratio exceeds 1) has a significant and immediate impact, with capital damages projected at around 0.015 percent below baseline in the 2030s, 2040s, and 2050s.

FIGURE 75. EXPECTED ANNUAL DAMAGE FROM COASTAL FLOODING UNDER SSP3-7.0 WITH AND WITHOUT ADAPTATION

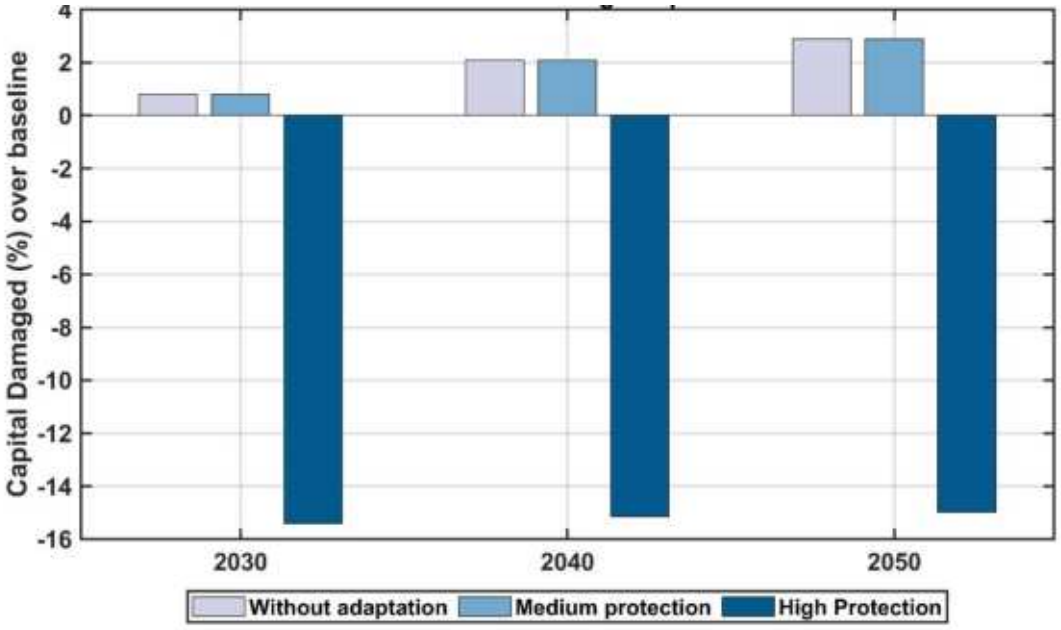

Summary and discussion

An increase in sea level due to climate change will result in negative shocks to capital in the Dominican Republic, as coastal infrastructure is permanently flooded and a larger share gets exposed to surge events. Overall, the annual expected impact of permanent inundation is much higher than surge events, accounting for more than 90 percent of the total effect.

By 2050, variability in the expected shocks is limited due to a small range of potential changes in sea level, with median projections around 0.2 meters across all SSPs. However, by 2100, sea-level rise could reach around 0.7 meters under SSP3-7.0, ranging between 0.4 and 0.8 meters across SSPs for the median projection. As such, the greatest impacts from sea-level rise and surge events that result in coastal flooding should be expected by late-century.

4.3.4 TOURISM

SUMMARY	
SUMMARY	Our work estimates the effect of climate change on tourism revenues by considering how changes in average climatic conditions will impact arrivals from domestic and international travelers. Across four climate scenarios, we estimate that tourism revenues will experience shocks ranging from -7 percent to -16 percent by mid-century. When considering the impact of hurricanes on tourism we estimate that by 2050, tourism arrivals may decline up to 6 percent.

ESTIMATED CLIMATE CHANGE IMPACTS BY 2041-2050	Generally, the Dry/Hot mean scenario is expected to result in the harshest impacts to tourism revenues throughout the period to 2050. Impacts from the Wet/Warm mean scenario oscillate, with shocks from the two means converging by mid-century: the Wet/Warm mean results in a -15 percent shock and the Dry/Hot mean results in a -16 percent shock.

Overview of Impact Channel

Climate change may affect tourism through disruptions caused by increased frequency and magnitude of extreme events (e.g., flooding or tropical cyclones), as well as from changes in the suitability or attractiveness of a particular location for travelers. Our analysis relies on estimates of total tourism revenues generated from domestic and international travelers, as well as from business and leisure travelers. We utilize data on the total number of travelers and revenue per traveler to distribute tourism revenues to grid cells covering the whole country using the location of tourist points of interest.

Impacts on leisure revenues due to changes in **average climatic conditions** are estimated following the approach developed by Hamilton, Maddison, and Tol (2005), which was also applied by Roson and Sartori (2016). Work by Hamilton et al. identified a functional relationship between mean annual temperature and total visitor arrivals and departures. This work suggests that arrivals peak around 14°C and decline as temperature increases, which indicates that international travelers prefer more pleasant (i.e., less hot) destinations. Departures reach a minimum at 19°C and increase with higher temperatures following the same logic as international travelers.

We consider the percent change in total arrivals as a proxy for the percent change in revenues from international leisure travelers. If available, we utilize seasonal or monthly visitation statistics to weigh monthly temperature and estimate a relevant mean annual temperate (i.e., a temperature value that weighs higher in the months with higher demand) to quantify the change in arrivals. For changes in domestic leisure travelers, we consider the percent change in total departures, which results in a decrease in revenues from an increase in departures (i.e., as a region gets hotter, residents will prefer more pleasant locations elsewhere).

A more detailed description of the modeling methodology used is available in Appendix B, with Appendix C offering details on the data sources utilized in the analysis.

Results: Climate Change Effects

Figure 76 describes the proportion of tourism revenues generated by traveler type and purpose. The majority of tourism revenue in the country is generated from international travelers participating in leisure travel in Punta Cana or in other parts of the country.

FIGURE 76. SHARE OF TOURISM REVENUE, 2019

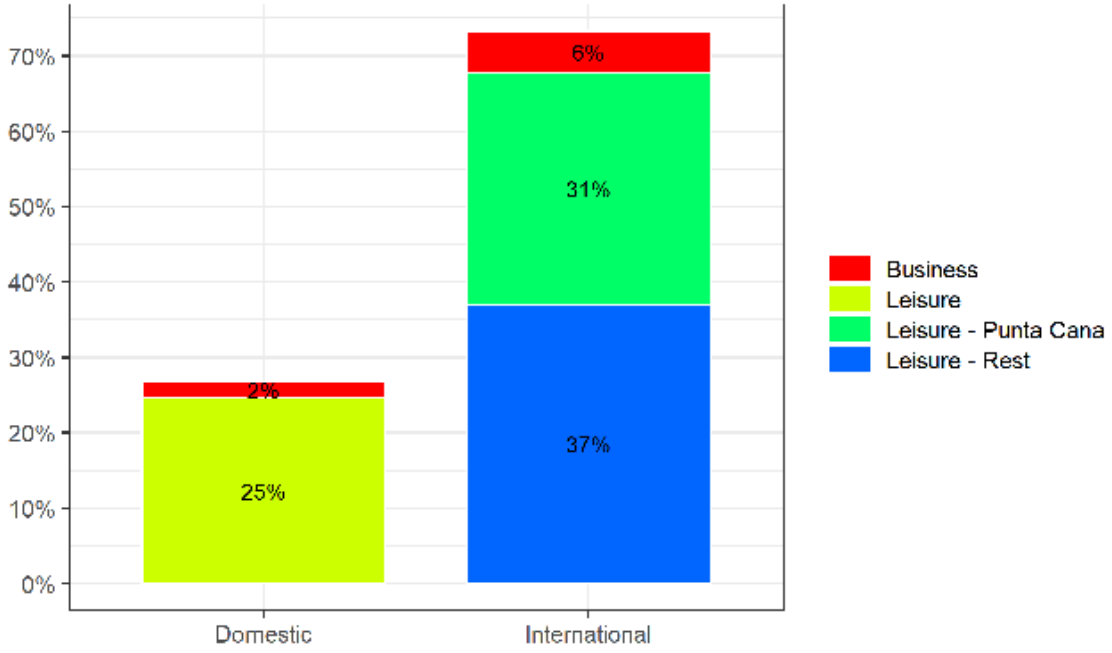

Relative to baseline conditions, climate change is expected to reduce tourism revenues generated from both domestic and international leisure travelers (Figure 77). For domestic travelers and international travelers, the Dry/Hot mean scenario results in more severe impacts compared to the Wet/Warm mean scenario through 2050. For domestic travelers, the Wet/Warm and Dry/Hot mean scenarios are expected to result in a -4.5 percent and -5.5 percent shock by mid-century, respectively. We estimate that revenue impacts from international travelers are more pronounced throughout the period to 2050 when compared to impacts from domestic travelers. Here, the Wet/Warm mean scenario is expected to result in a tourism revenue shock of -15 percent, while the Dry/Hot mean scenario results in a shock of -20 percent by 2050.

FIGURE 77. CHANGE IN REVENUE FROM LEISURE TRAVELERS

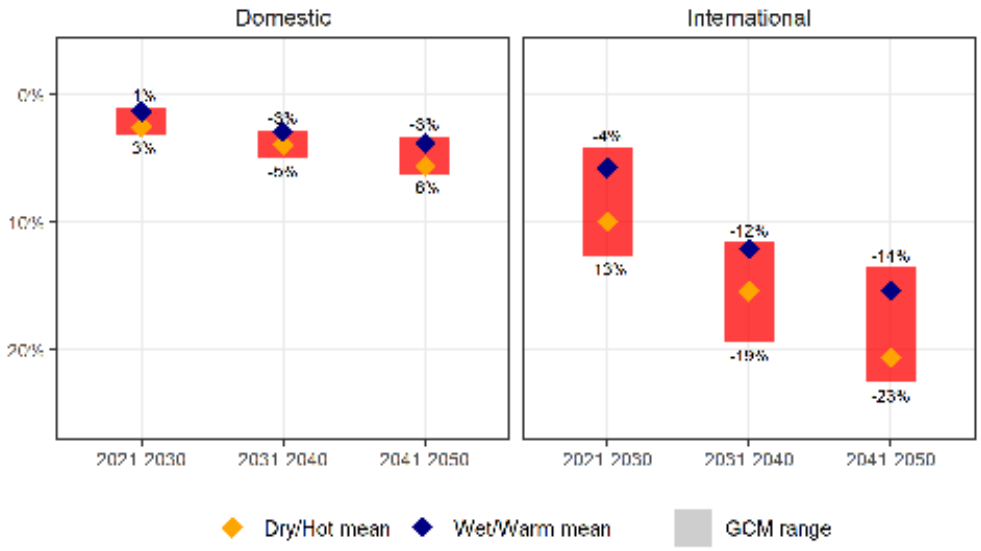

Overall, as shown on Figure 78, the Dry/Hot mean scenario represents a worst-case scenario, projected to result in the most severe impacts to tourism revenues throughout the period to 2050. By 2030, the Wet/Warm mean, SSP1-1.9 mean, and SSP3-7.0 mean scenarios result in similar shocks of around -6 percent. When considering individual GCMs (i.e., the grey-shaded range in Figure 78), tourism shocks range from around 1 percent to -12 percent by 2030. By mid-century, the spread between the four scenarios increases, with shocks ranging from about -7 percent to -16 percent. Across GCMs, revenue shocks range from -13 percent to -18 percent by 2050.

FIGURE 78. TOURISM REVENUE SHOCK, 3-YEAR MOVING AVERAGE

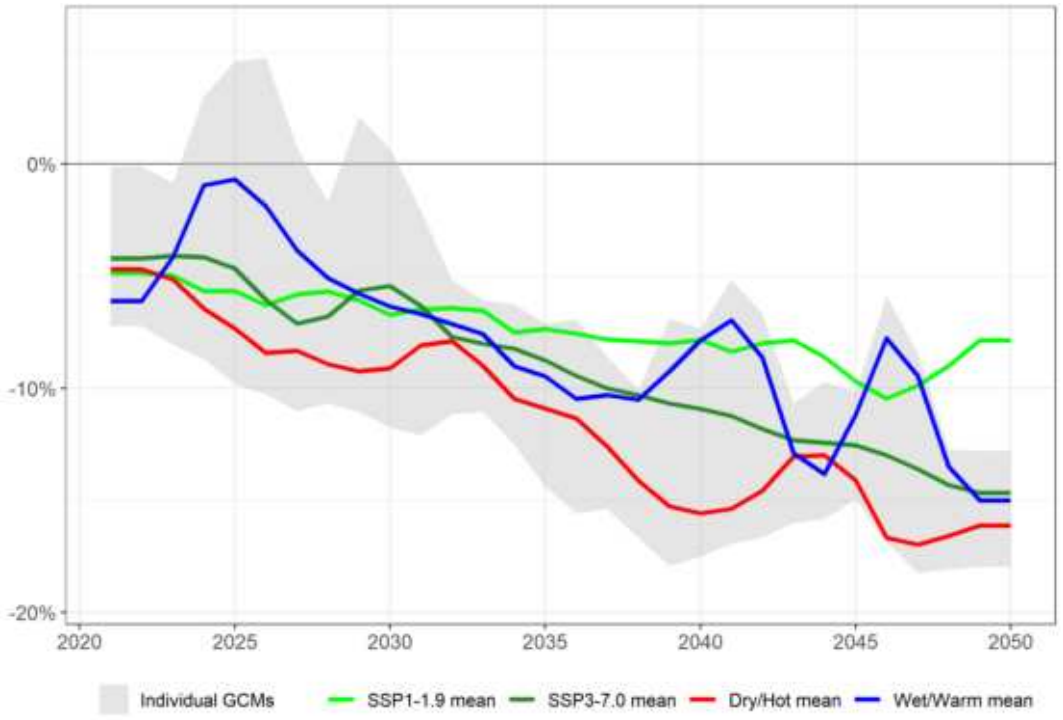

Our analysis also considers the impact of increased wind speeds and hurricane occurrence on tourism arrivals to the country. Currently, the majority of inbound tourists arrive to the country by plane, with around 85 percent arriving on aircrafts and 15 percent arriving by water (UNWTO 2021). Yet, potential increases in wind speeds might impact airplane arrivals by delaying or cancelling air travel. Specifically, when crosswinds exceed an identified threshold, flights are unable to safely depart and land. Maximum crosswind thresholds can vary by aircraft type and airport, however, these values generally range from around 10 to 35 knots (Arnot 2019). Further, in the United States, METerological Aedrome Reports are used to communicate information on potentially adverse meteorological conditions, including high wind speeds to pilots and aircraft operators. When maximum wind speeds exceed 25 knots, this phenomenon is flagged in associated METerological Aedrome reports (FAA 2017). In our analysis, we consider the number of days per month when wind speeds are expected to reach or exceed this threshold. Additionally, tourism arrivals can be negatively impacted by hurricane events which may prevent departures and damage critical transportation infrastructure in a country. Therefore, our analysis also considers the expected change in annual hurricane occurrence to estimate potential impacts to tourism through the end of the century.

Table 13 shows the average number of days per month and the maximum days per month when winds are estimated to reach 25 knots in the baseline from 1995-2014. When considering the average number of days per month when wind speeds exceed 25 knots in the 95th percentile, only a small subset of months, namely August and September, are impacted (with these months

having 0.16 and 0.60 such days respectively). When considering the maximum number of days across the country by month, we anticipate around 1.5 days in August, 2 days in September, and 0.5 days in October.

TABLE 13. DAYS PER MONTH WITH WIND SPEEDS GREATER THAN 25 KNOTS IN THE 95TH PERCENTILE, 1995-2014

MONTH	1	2	3	4	5	6	7	8	9	10	11	12
AVERAGE NUMBER OF DAYS/MONTH	0.00	0.00	0.00	0.00	0.00	0.00	0.00	0.16	0.60	0.00	0.00	0.00
MAX NUMBER OF DAYS/MONTH	0.00	0.00	0.00	0.00	0.00	0.00	0.00	1.56	2.10	0.52	0.00	0.00

Moving from baseline conditions, we next examine projected future wind conditions, under SSP2-4.5 and SSP3-7.0. When considering the maximum number of days per month in the 95th percentile under SSP2-4.5, impacted months span from August through October in the period from 2021- 2040 (see Table 14). During this period, parts of the country will experience an additional day above 25 knots in August, nearly two additional days in September, and an additional 1.23 days in October. Under SSP3-7.0, impacts are relatively similar for this same time period, with impacted months spanning from August through October, with August and September experiencing an additional 1.40 days above 25 knots and October experiencing an additional 0.83 days. While the number of additional impacted days is relatively small, this change represents a doubling in the annual number of days during which wind speeds exceed 25 knots relative to the baseline and subsequently, this may have important consequences on air travel to the country and associated tourism expenditure.

TABLE 14. CHANGE IN THE NUMBER OF DAYS PER MONTH WITH WIND SPEEDS GREATER THAN 25 KNOTS IN THE 95TH PERCENTILE UNDER SSP2-4.5 AND SSP3-7.0 IN 2021-2040 RELATIVE TO THE BASELINE

SSP	MONTH	1	2	3	4	5	6	7	8	9	10	11	12
SSP2-4.5	AVERAGE NUMBER OF DAYS/MONTH	0.00	0.00	0.00	0.00	0.00	0.00	0.00	0.31	0.43	0.05	0.00	0.00
	MAX NUMBER OF DAYS/MONTH	0.00	0.00	0.00	0.00	0.00	0.00	0.00	1.02	1.80	1.23	0.00	0.00
SSP3-7.0	AVERAGE NUMBER OF DAYS/MONTH	0.00	0.00	0.00	0.00	0.00	0.00	0.00	0.77	0.09	0.03	0.00	0.00
	MAX NUMBER OF DAYS/MONTH	0.00	0.00	0.00	0.00	0.00	0.00	0.00	1.40	1.41	0.83	0.00	0.00

Further, impacts from hurricanes can also lead to immediate impacts on tourism arrivals. Research from 2013 suggests that an average hurricane strike can cause a 2 percent decline in tourism arrivals (Granvorka 2013). Consistently with the assumptions used in impact channel analysis above, a 1 percent decline in arrivals would translate to a 0.73 percent decline in total tourism revenues (see Figure 76), assuming domestic travel is not disrupted. In the baseline period, if all projected category 0 through 5 hurricanes do in fact occur, this would result in approximately 1.89 hurricane events (see Table 15). Thus, this may be associated with a decline of 3.78 percent in tourism arrivals or roughly 270,000 passengers assuming 2019 levels of tourism arrivals to the country (Central Bank of the Dominican Republic 2019). Following this same logic, immediate impacts to tourism arrivals would peak in the 2030s under SSP3-7.0 with approximately 2.98 hurricane events per year, translating to a nearly 6 percent decline in tourism arrivals or a decrease of 425,000 passenger trips. However, other research also suggests that hurricane events may be accompanied by a recovery in tourism through an increase in airplane arrivals that may result in a net positive effect on tourism (Carballo Chanfon et al. 2021). Thus, the net impact of hurricanes on tourism may vary depending on hurricane type and associated damage.

TABLE 15. ANNUAL EXPECTED HURRICAN EVENTS BY PERIOD AND IMPACT ON TOURISM ARRIVALS

		2030		2050		2090	
CATEGORY	BASELINE	SSP2-45	SSP3-70	SSP2-45	SSP3-70	SSP2-45	SSP3-70
CAT 0 (TROPICAL STORMS)	1.12	1.49	1.51	1.43	1.40	1.34	1.28
CAT 1	0.44	0.55	0.63	0.68	0.69	0.51	0.56
CAT 2	0.16	0.25	0.40	0.16	0.24	0.24	0.16
CAT 3	0.07	0.14	0.19	0.16	0.18	0.16	0.19
CAT 4	0.06	0.17	0.19	0.14	0.25	0.28	0.14
CAT 5	0.04	0.08	0.06	0.11	0.12	0.13	0.12
POTENTIAL DECLINE IN ARRIVALS	3.78%	5.36%	5.97%	5.35%	5.77%	5.34%	4.88%

In addition to immediate impacts, hurricanes may also result in prolonged effects to tourism arrivals that extend outside of the days following the initial hurricane landfall. For cruise ship arrivals to the Caribbean, Carballo Chanfon et al. (2017) find hurricanes are associated with a 1.21 percent decline in arrivals in the month following the hurricane landfall. Further, for more intense events, research suggests that the cleanup period following category 4 and 5 hurricanes may extend up to 5 months following the initial landfall, and also result in a recovery period of up to 20 months (BuildFax 2017). In the Dominican Republic, we estimate an annual occurrence of 0.10 for category 4 and 5 events in the baseline. Yet, by 2050, under SSP2-4.5 and SSP3-7.0, the expected annual occurrence of these types of events more than doubles to approximately 0.25 and 0.37 events respectively. This increase relative to the baseline may be associated with prolonged clean-up periods and recovery times. In turn, this may discourage tourism arrivals as vital mechanical, electrical, and plumbing infrastructure is still being restored.

Summary and discussion

Overall, our results suggest that climate change related effects, specifically, changes in temperature, wind speed, and hurricane occurrence may negatively impact tourism arrivals by making locations less desirable and potentially reducing tourism arrivals to the country. Previous work has also aimed to estimate the impacts of climate change in the Caribbean and generally finds negative impacts to tourism in the region. Specifically, research by Sookram (2009) considers how tourism demand and revenues in the Caribbean will change under different emissions scenarios through a tourism demand model. They estimate that tourism losses for the nine Caribbean countries considered could range from $111.3 to $116.3 million by 2050 due to changes in temperature and precipitation (Sookram 2009). When also considering extreme events (e.g., increases in the frequency of hurricanes, windstorms, floods, and landslides), impacts increase to anywhere between $15,503 and $14,950 million by 2050 (Sookram 2009).

While our analysis does not explicitly explore any adaptation measures to help minimize these impacts on the country's tourism industry, future work could evaluate such interventions. As presented in the textbox below, nature-based solutions are an important group of actions that can help reduce the impacts of a changing climate on the Dominican Republic's valuable natural resources such as coral reefs and wildlife habitat, and thus on its tourism industry.

Textbox: Nature-Based Solutions

Given the estimated impacts of climate change on tropical cyclone occurrence and subsequent damage to the tourism sector, it is important to consider the role of nature-based solutions in helping to mitigate estimated impacts. Overall, several strategies might be useful when seeking to limit climate change related impacts to coastline environments. Yet, in the Caribbean, strategies aimed at increasing mangrove and coral reef ecosystems are most discussed in relevant literature. By preventing impacts from waves and storm surges from reaching the coastline, these environments can provide important ecosystem services. Specifically, research from 2016 estimates that coral reefs may reduce wave heights by 70 percent while mangroves may reduce heights by 31 percent (Siddharth et al., 2016). Further, a global analysis by Beck et al. 2018 found that without coral reef ecosystems, global expected damages from flooding may double while damages from storm surges may triple. In the Dominican Republic, it is estimated that $96 million in damages are averted annually due to the presence of coral reefs or approximately 0.11 percent of GDP (Beck et al. 2018). Generally, these benefits are concentrated in the eastern regions of the country where avoided damages peak at around $50 million (see Figure 69).

Figure 69. Value of Coral Reefs for Flood Protection

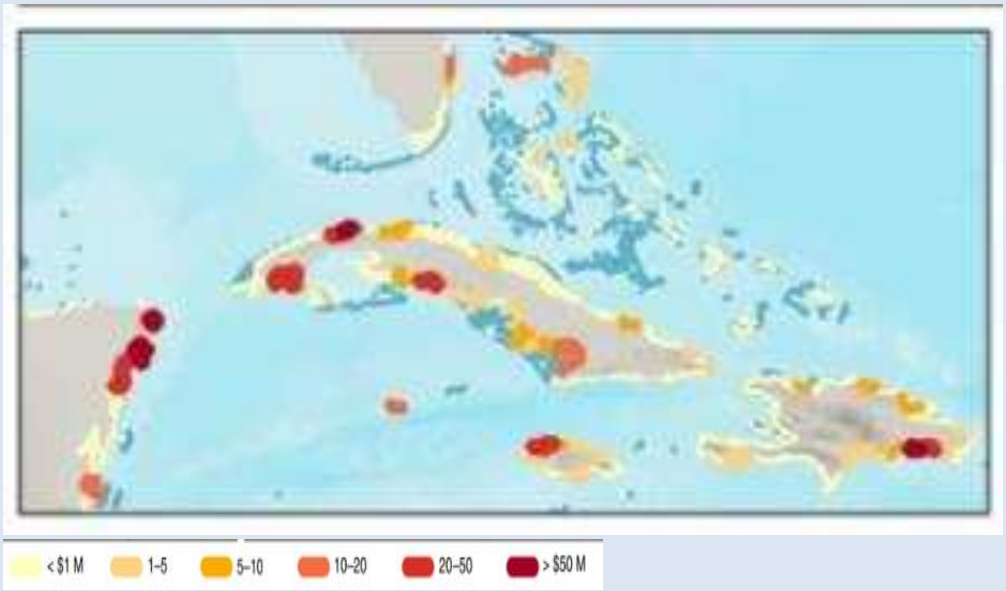

Source: Beck et al., 2018

Further, work from Rozenberg et al. 2021 found that mangrove ecosystems may be useful in limiting economic impacts associated with hurricane events in the Caribbean, with hurricane impacts declining with increased mangrove width. Investment in restoration efforts of these ecosystems may prove to be efficient as research from Beck et al. 2022 suggests that coral reef and mangrove restoration efforts could be cost effective and result in a benefit cost ratio greater than 15:1 in some parts of the country (Beck et al. 2022).

5. SUMMARY AND CONCLUSIONS

5.1 SUMMARY

The objective of this report is to outline the process and present the results of estimating the economic damages of climate change for the Dominican Republic. This analysis helps provide a better understanding of the benefits and costs of climate action and cross-sectoral policy priorities to manage climate risks effectively.

Across the channels considered, the Dry/Hot and Wet/Warm mean scenarios are anticipated to result in varying degrees of impact by mid-century. When looking at impacts to labor productivity, as evaluated through the labor heat stress, human health, and water supply and sanitation channels, the Dry/Hot mean scenario is generally expected to have harsher impacts on labor productivity compared to the Wet/Warm mean scenario, though relative differences are small. The Dry/Hot mean scenario is anticipated to result in a larger shock as compared to the Wet/Warm mean scenario for the labor heat stress and human health channels. Differences between the mean scenarios is also expected to be small for the water supply and sanitation channel, with both scenarios resulting in similar shocks to labor supply under the business-as-usual and aspirational policy scenarios. Additionally, for the tourism channel, differences between the Dry/Hot and Wet/Warm mean scenario are relatively small by mid-century with the Dry/Hot mean scenario resulting in a 2 percent larger shock.

Differences between the two scenarios is more pronounced for the water supply, crop production, and hydropower channels. For the water supply channel we anticipate unmet irrigation demand will be 15 percent larger under the Dry/Hot mean scenario as compared to the Wet/Warm mean scenario. When considering crop production, the Dry/Hot mean scenario results in a 20 and 13 percent larger shock for rainfed and irrigated crops respectively, as compared to the Wet/Warm mean scenario. In contrast, for the erosion channel, the Wet/Warm mean is anticipated to result in more severe impacts to erosion and crop production as compared to the Dry/Hot mean scenario. For the inland flooding channel, differences in climate change-related impacts across the different climate scenarios is also expected to be varied. For example, by the 2050s, we estimate inland flooding shocks ranging from 0.08 to 0.12 percent. Similarly, for the sea-level rise channel, selected climate scenarios are expected to result in similar levels of sea-level rise by mid-century.

When it comes to adaptation interventions, the analysis explored the effect of several adaptation strategies that might help mitigate climate change related impacts. For the labor heat stress channel, we explored the impact of increasing air-conditioning coverage by 20 percent and 30 percent on labor productivity. Within this channel, investment in air-conditioning is expected to have the greatest impact on the industrial sector, followed closely by the services sector. While increased air-conditioning does reduce the shock experienced by the agriculture sector, the magnitude of this positive effect is much smaller than for industry and services.

For the crop production channel, we explored the effect of developing new irrigation infrastructure, reducing unmet irrigation demand, crop switching to more climate-resilient crops, increasing the share of heat-tolerant crop varieties, and a combination of these individual strategies. Overall, the majority of strategies resulted in crop production shocks similar to the no-action baseline. However, investments aimed at increasing irrigation, reducing unmet irrigation demand, and employing a combination of all interventions appear to be most effective in reducing shocks relative to the no-action baseline, with positive shocks (i.e., production gains) highest under the Wet/Warm mean scenario.

For the water supply channel we explored the affect of increasing irrigation efficiency from a baseline of 20 percent to 40 percent and an increase in reservoir volume by 30 percent. With adaptation, our results suggest unmet irrigation demand is expected to decrease up to 20 percent in selected basins. For the erosion channel, we considered the impact of conservation tillage, increased use of crop residues, and a combination of conservation tillage and crop residue use. Overall, under the Dry/Hot mean scenario, all three strategies proved to be effective when used at the "low" adaptation rate. For the inland flooding channel, our analysis considers an adaption intervention in which infrastructure is hardened to withstand the 20-year flood, instead of the assumed design of current infrastructure at the 10-year flood. Overall, the strategy proved to be effective, with impacts under the proactive adaption scenario declining relative to the no-action baseline by mid-century.

For the tropical cyclone channel, we explored the impact of roof connection anchors being improved and connection anchor bolts and stiffeners being added. Overall, relative to the no-action baseline, we expect medium adaptation to result in the largest reduction in damages by 2090. Finally, for the sea-level rise channel, adaptation interventions targeted at building new infrastructure away from hazardous areas and protecting existing infrastructure were evaluated. Overall, we found the high adaptation scenario to be most effective at reducing impacts by mid-century.

5.2 CONCLUSIONS

Our analysis helps to quantify the effect climate change may have on human capital, agriculture and natural resources, and infrastructure and services in the Dominican Republic by mid-century. While our analysis works to fill a gap in climate change research, further work to quantify climate change related impacts across additional channels will help provide further guidance to stakeholders on how to manage climate risks effectively moving forward.

REFERENCES

Arnot, Mike. 2019. "How Windy Does It Have to Be Before Planes Can't Take Off?" The Points Guy. https://thepointsguy.com/news/how-windy-does-it-have-to-be-before-planes-cant-take-off/.

Beck, Michael, Nadine Heck, Siddharth Narayan, and Pelayo Menéndez. 2022. "Return on Investment for Mangrove and Reef Flood Protection." *Ecosystem Services* 56: 101440. https://doi.org/10.1016/j.ecoser.2022.101440.

Beck, Michael, Inigo Losada, Pelayo Menéndez, and Borja Reguero. 2018. "The Global Flood Protection Savings Provided by Coral Reefs." *Nature Communications* 9 (1). https://doi.org/10.1038/s41467-018-04568-z.

BuildFax. 2017. "Post-Hurricane Recovery: How Long Does It Take?Implications for Disaster Recovery a Fter Hurricanes Harvey and Irma." BuildFax Property History. https://webassets.inman.com/wp-content/uploads/2017/10/BuildFax-Hurricane-Recovery-Study.pdf.

Burt, Charles, and Monte Soto. 2008. "Conversion to Groundwater Pumping with Drip/Micro Irrigation Systems." California Polytechnic State University. https://digitalcommons.calpoly.edu/cgi/viewcontent.cgi?article=1183&context=bae_fac.

Carballo Chanfon, Pablo, Preeya Mohan, Eric Strobl, and Thomas Tveit. 2021. "The Impact of Hurricane Strikes on Cruise Ship and Airplane Tourist Arrivals in the Caribbean." *Tourism Economics*, no. 2021. https://doi.org/10.1177/13548166211037406.

Central Bank of the Dominican Republic. 2019. "Monthly Arrivals of Passengers by Residence and Airport Used, 2019." Department of National Accounts and Economic Statistics.

Chambwera, Muyeye, Geoffrey Heal, Carolina Dubeux, Stéphane Hallegatte, Liza Leclerc, Anil Markandya, Bruce A. McCarl, Reinhard Mechler, and James E. Neumann. 2014. "Economics of Adaptation." In *Climate Change 2014: Impacts, Adaptation, and Vulnerability. Part A: Global and Sectoral Aspects. Contribution of Working Group II to the Fifth Assessment Report of the Intergovernmental Panel on Climate Change*, edited by C.B. Field, V.R. Barros, D.J. Dokken, K.J. Mach, M.D. Mastrandrea, T.E. Bilir, M. Chatterjee, et al., 945–77. Cambridge, UK and New York, USA: Cambridge University Press.

DOE. 2020. "Dominican Repunlic Energy Snapshot." U.S. Department of Energy. https://www.energy.gov/eere/articles/dominican-republic-island-energy-snapshot-2020.

EPA. 2013. "Strategies for Saving Energy at Public Water Systems." Environmental Protection Agency. https://www.epa.gov/sites/default/files/2015-04/documents/epa816f13004.pdf.

FAA. 2017. "Aeronautical Information Manual." U.S. Department of Transportation; Federal Aviation Administration. https://www.faa.gov/air_traffic/publications/media/aim.pdf.

Granvorka, Charley. 2013. "The Impact of Hurricane Strikes on Tourist Arrivals in the Caribbean." *Tourism Economics* 19 (6): 1401–9. https://doi.org/10.5367/te.2013.0238.

Kassam, A. H., H. T. van Velthuizen, P. H. Sloane, G. W Fischer, and M. M. Shah. 1991. "Agro-Ecological Land Resources Assessment for Agricultural Development Planning: A Case Study of Kenya." Resources Data Base and Land Productivity. Rome: Food and Agriculture Organization of the United Nations (FAO) and International Institute for Applied Systems Analysis (IIASA).

Narayan, Siddharth, Michael Beck, Borja Reguero, Inigo Losada, Bregje van Wesenbeeck, and Nigel Pontee. 2016. "The Effectiveness, Costs and Coastal Protection Benefits of Natural and Nature Based Defence." *PLoS One* 11 (5). https://doi.org/10.1371/journal.pone.0154735.

Rozenberg, Julie, Nyanya Browne, Sophie De Vries Robbe, Melanie Kappes, Woori Lee, and Abhad Prasas. n.d. "Publication: 360° Resilience: A Guide to Prepare the Caribbean for a New Generation of Shocks." World Bank. https://www.worldbank.org/en/events/2021/11/05/360-resilience-a-guide-to-prepare-the-caribbean-for-a-new-generation-of-shocks.

Shannak, Sa'd. 2018. "Energy and Economic Implications of Water Transfer." *Open Water Journal* 5 (2). https://scholarsarchive.byu.edu/openwater/vol5/iss2/4.

Sookram, Sandra. 2009. "The Impact of Climate Change on the Tourism Sector in Selected Caribbean Countries." *Caribbean Development Report* 2 (30): 204–25.

United Nations. 2021. "SDG Country Profile." Department of Economic and Social Affairs, Statistics. 2021. https://unstats.un.org/sdgs/dataportal.

———. 2022. "World Population Prospects 2022." Department of Economic and Social Affairs, Population Division. 2022. http://population.un.org/wpp/.

UNWTO. 2021. "Tourism Data Dashboard." UN World Tourism Organization. 2021. https://www.unwto.org/unwto-tourism-dashboard.

USAID. 2004. "USAID Investments in Drinking Water Supply Projects and Related Activities in 2004, A Report to the U.S. House and Senate Appropriations Committees." https://www.ircwash.org/sites/default/files/USAID2004-USAID.pdf.

WHO. 2014. "Quantitative Risk Assessment of the Effects of Climate Change on Selected Causes of Death, 2030s and 2050s." World Health Organization. https://apps.who.int/iris/handle/10665/134014.

WHO, and E.G. Wagner. 1959. "Water Supply for Rural Areas and Small Communities." World Health Organization.

Wiarda, Howard J., and Nancie L. González. 2023. "Dominican Republic." Encyclopedia Britannica. 2023. https://www.britannica.com/place/Dominican-Republic.

Wolf, Jennyfer, Richard Johnston, Paul R. Hunter, Bruce Gordon, Kate Medlicott, and Annette Prüss-Ustün. 2019. "A Faecal Contamination Index for Interpreting Heterogeneous Diarrhoea Impacts of Water, Sanitation and Hygiene Interventions and Overall, Regional

and Country Estimates of Community Sanitation Coverage with a Focus on Low- and Middle-Income Countries." *International Journal of Hygiene and Environmental Health* 222 (2): 270–82. https://doi.org/10.1016/j.ijheh.2018.11.005.

World Bank. 2021a. "Climate Change Knowledge Portal." 2021. https://climateknowledgeportal.worldbank.org/.

———. 2021b. "World Bank National Accounts Data." Available at World Bank Open Data. https://data.worldbank.org/.

APPENDIX A. CLIMATE DATA AND SCENARIO SELECTION

The evaluation of climate change impacts conducted in this study required climate information as an input to the modelling process. This appendix details the process of generating and processing the necessary climate scenarios.

A1. GLOSSARY OF KEY TERMS

Climate projections: Simulated response of the climate system to a scenario of future emissions or concentrations of greenhouse gases (GHGs) and aerosols, and changes in land use.

Global Climate Model (GCM), also General Circulation Models: A modeled representation of the physical relationships of the global climate system that are used to generate climate projections. These capture atmospheric and ocean dynamics, and other water and biogeochemical cycles. Typical outputs include variables such as precipitation and temperature.

Emission scenarios: A plausible representation of the future development of emissions of substances that are radiatively active (e.g., GHGs, aerosols). These are used in the form of illustrative Representative Concentration Pathways (RCPs).

Representative Concentration Pathways (RCPs): Scenarios of emissions and concentrations of GHGs, aerosols, and land use/land cover. They represent different intensities in the additional radiative forcing caused by human activities.

Shared Socioeconomic Pathways (SSPs): Different possible evolutions of the world in terms of demography, technology, economy, etc., with these socioeconomic conditions in turn achieving certain RCPs.

A2. CLIMATE DATA AND PROJECTIONS USED

To develop climate scenarios and future projections, historical and future projected datasets were obtained, with precipitation and temperature the main variables of interest for this study.

Historical monthly climate data was obtained for 1950 to 2020 from the Climatic Research Unit (CRU) gridded Time Series of the University of East Anglia (CRU TS 4.05) (Harris et al. 2020). These data are available from 1959 to 2020 at a spatial resolution of 0.5 x 0.5 degree grids and monthly temporal resolution for various variables including mean, maximum and minimum temperature, and total precipitation.

Future climate projections were obtained from the World Bank's Climate Change Knowledge Portal for 29 GCMs from the Coupled Model Intercomparison Project 6 (CMIP6) suite of Intergovernmental Panel on Climate Change (IPCC) model outputs (World Bank 2021). This large suite of GCMs was run for a set of emissions scenarios, as shown in Figure A79.

FIGURE A79. CMIP6 SSPs (SHADED AREA SHOWS RANGE OF NO-POLICY BASELINE SCENARIOS)

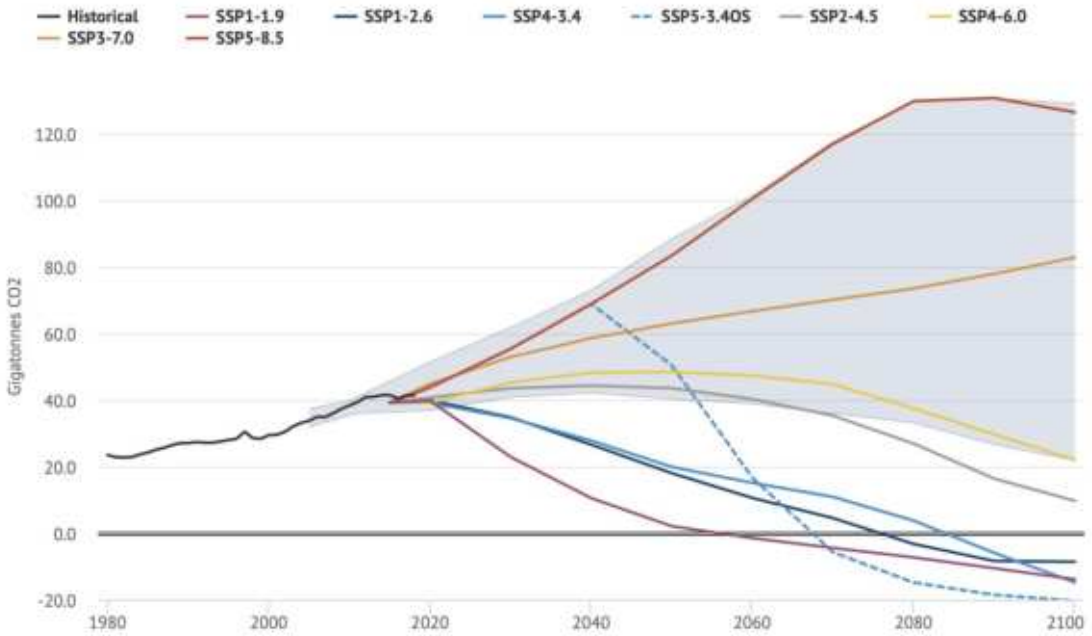

Notes: Interactive version with more data available at Carbon Brief: *https://www.carbonbrief.org/cmip6-the-next-generation-of-climate-models-explained*

Table A1 shows a comprehensive list of the available data utilized for this project organized by GCM and Historical data/SSP. Each GCM has up to five combinations of SSP and RCP emissions scenario runs, including SSP 1-RCP 1.9 (1-1.9), 1-2.6, 2-4.5, 3-7.0, and 5-8.5. For each GCM-SSP combination, the Climate Change Knowledge Portal provides a modeled history from 1995 to 2014 and projections from 2015 to 2100. For the selection of climate scenarios, we employed 31 GCMs, originally provided at a spatial resolution of 1 x 1 degree grids for the globe and monthly temporal resolution for years 1995 to 2100 and monthly mean daily temperature and monthly total precipitation.

TABLE A1. LIST OF GCMs AND THE ASSOCIATED SSPs AVAILABLE FOR THIS STUDY

Model	Hist	SSP1-1.9	SSP1-2.6	SSP2-4.5	SSP3-7.0	SSP5-8.5
access-cm2	✓		✓	✓	✓	✓
access-esm1-5	✓		✓	✓	✓	✓
awi-cm-1-1-mr			✓	✓	✓	✓
bcc-csm2-mr	✓		✓	✓	✓	✓
cams-csm1-0	✓	✓	✓	✓	✓	✓
canesm5	✓	✓	✓	✓	✓	✓
cesm2	✓					
cmcc-cm2-sr5	✓		✓	✓	✓	✓
cmcc-esm2	✓		✓	✓	✓	✓
cnrm-cm6-1	✓		✓	✓	✓	✓
cnrm-esm2-1	✓	✓	✓	✓	✓	✓
ec-earth3	✓	✓	✓	✓	✓	✓
ec-earth3-veg	✓	✓	✓	✓	✓	✓
fgoals-g3	✓	✓	✓	✓	✓	✓
gfdl-esm4	✓	✓	✓	✓	✓	✓
hadgem3-gc31-ll	✓		✓	✓		✓
inm-cm4-8	✓		✓	✓	✓	✓
inm-cm5-0	✓		✓	✓	✓	✓
ipsl-cm6a-lr	✓	✓	✓	✓	✓	✓
kace-1-0-g	✓		✓	✓	✓	✓
kiost-esm	✓		✓	✓		✓
miroc-es2l	✓	✓	✓	✓	✓	✓
miroc6	✓	✓	✓	✓	✓	✓
mpi-esm1-2-hr	✓		✓	✓	✓	✓
mpi-esm1-2-lr	✓		✓	✓	✓	✓
mri-esm2-0	✓	✓	✓	✓	✓	✓
nesm3	✓		✓	✓		✓
noresm2-lm	✓		✓	✓	✓	✓
noresm2-mm	✓		✓	✓	✓	✓
taiesm1	✓		✓	✓	✓	✓
ukesm1-0-ll	✓	✓	✓	✓	✓	✓
Count	***30***	***12***	***30***	***30***	***27***	***30***

A3. PROCESSING OF CLIMATE INFORMATION

Given that GCMs are biased relative to observed climate conditions, we applied the bias-correction and spatial disaggregation technique to disaggregate the projections to 0.5 x 0.5 degree grid cells, and to then bias correct these projections using the observed historical dataset from 1995 to 2000 from the CRU TS 4.05 dataset. For each grid cell, the bias correction procedure sets up "quantile maps" for each month to statistically compare the GCM hindcast to the CRU observations, and then uses those maps to bias correct all projections. This approach

was previously applied in the World Bank's *Enhancing the Climate Resilience of Africa's Infrastructure* study (Cervigni et al. 2015), using the CMIP5 ensemble.

We use standard spatial downscaling practice to reduce the spatial resolution from 1 x 1 degree grids to 0.5 x 0.5 degree grids and properly line the data up with the historical data, both reduced to the 67,420 CRUs of the CRU TS 4.05 data covering the land area of the globe. This includes the following steps for each file:

1. Obtain the raw data (resulting spatial dimensions are 181 latitude x 360 longitude).[1]
2. Perform Inverse Distance Weighting with a multiplier of 2, power of 2, and radius of 2 to increase the resolution to 0.5 x 0.5 degree (resulting spatial dimensions are 362 latitude x 720 longitude).
3. Remove the 1st and 362nd latitude rows, because centroids of the original 181 one-degree latitude bands range from -90 to +90, which means that latitude bands at -90 and +90 are each only 0.5-degree rather than 1-degree. As a result, removing the 1st and 362nd reduces the size of these bands to 0.5 degree (resulting spatial dimensions are 360 latitude x 720 longitude).
4. Reduce and vectorize the data to the 67,420 CRUs covering the land areas of the glove (resulting spatial dimensions are 67,420 CRUs).

Figure A80 presents a visual representation of a few of these steps for a (randomly selected) scenario, namely access-cm2 SSP2-4.5.

FIGURE A80. SPATIAL DOWNSCALING METHODOLOGY FOR ACCESS-CM2 SPP2-4.5

Panel A. Result of Step 1

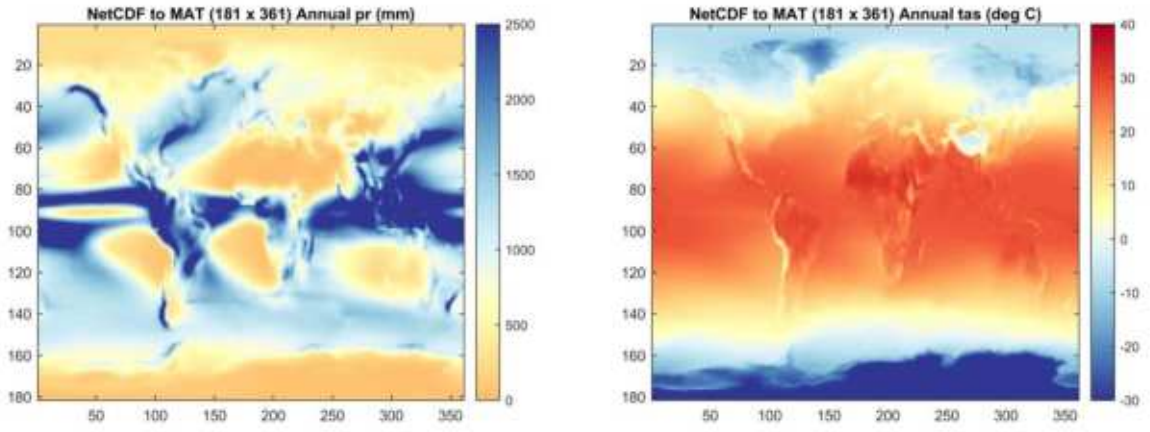

[1] The raw data from the World Bank has a spatial resolution of 181 latitude x 361 longitude. Based on communication with the Climate Change Knowledge Portal team, we removed the 361st longitude column

Panel B. Result of Step 3

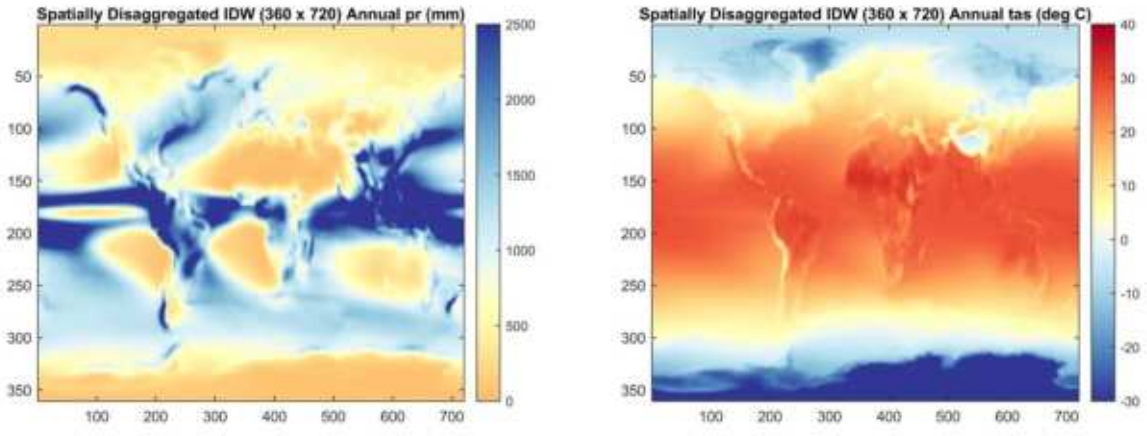

Panel C. Result of Step 5

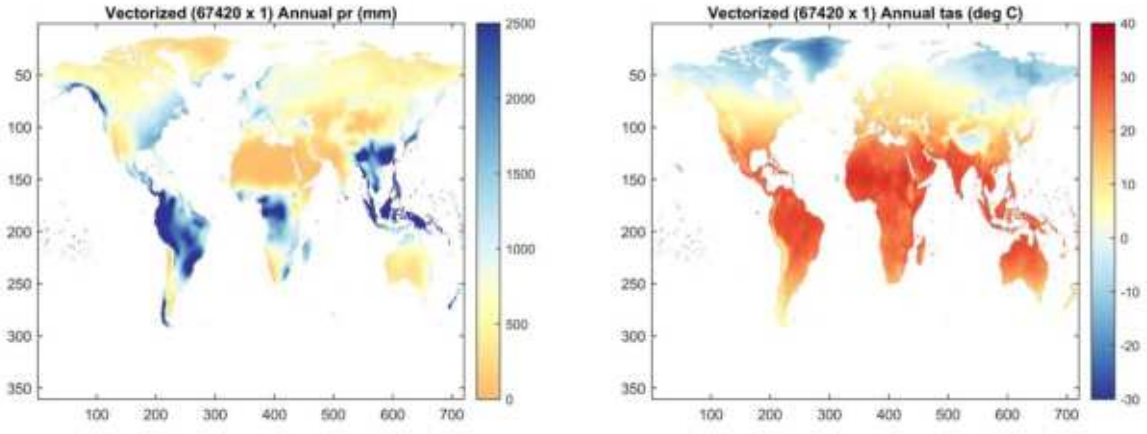

A4. SELECTION OF CLIMATE SCENARIOS

For this study, we analyzed the available set of GCM/SSP permutations previously shown in Table A1 to obtain a subset of scenarios that represent an appropriate range of possible future climate conditions. In particular, we consider two different sets of climate futures: **one to assess the impact of uncertain global mitigation efforts** and **one to assess local climate risks and overall model uncertainty**.[2] While scenarios that capture model uncertainty are relevant for any impact channel, certain inputs may be limited to SSP aggregates only. In those cases, the analysis relies on scenarios of global mitigation efforts alone.

The first set of scenarios (i.e., scenarios selected to allow for comparisons across emissions trajectories - referred as mitigation scenarios) are selected in accordance with World Bank guidance which recommends selecting an optimistic and a pessimistic scenario of GHG

[2] Climate model uncertainty: Diverse GCMs have been developed drawing on the best available science. These continue to evolve, and while sophisticated, they remain imperfect tools. Each model is unique and generates slightly different projections, even when run using identical greenhouse gas emissions scenarios.

concentrations that are driven by global GHG emissions trajectories and mitigation policies.[3] For these, we use the SSP3-7.0 ensemble mean as a pessimistic case and the SSP1-1.9 ensemble mean as an optimistic case. SSP1-1.9 represents reductions in GHG emissions in line with 1.5°C warming by 2100. SSP3-7.0 is a scenario in which warming reaches 4°C by 2100, due to lax climate policies or a reduction in ecosystems and oceans' ability to capture carbon.

For the second set of scenarios (i.e., scenarios selected to assess overall model uncertainty), we select a subset of extreme GCM runs that represent a "dry and hot" and a "wet and warm" future for the country under analysis, for the study period between 2020 and 2050. This process is made up of the following steps:

1. Calculate country-scale changes in mean annual temperature and mean total precipitation between 2031 and 2050 versus the historical baseline of 1995 to 2020.
2. Consider GCMs within the SSP2 and SSP3 ensembles (about 50 total), as potential candidates for extreme conditions. This eliminates from consideration the aggressive mitigation pathway (SSP1) and the aggressive emissions pathway (SSP5).
3. Select three hot/dry scenarios around the 10th percentile of change in mean precipitation (i.e., dry) and 90th percentile change in mean temperature (i.e., hot), across all GCMs (within SSP2-4.5 and 3-7.0). Compute a 4th scenario as the mean across the 3 selected GCM/SSP runs.
4. Select three wet/warm scenarios around the 90th percentile of change in mean precipitation (i.e., wet) and 10th percentile change in mean temperature (i.e., warm), as above, and a 4th scenario as the mean.

Figure A81 shows a visual representation of these steps for an illustrative country.

[3] Feb 3, 2022 World Bank Guidance on "Global scenarios for CCDR analyses"

FIGURE A81. CLIMATE SCENARIO SELECTION PROCESS

Panel A. Result of Step 1

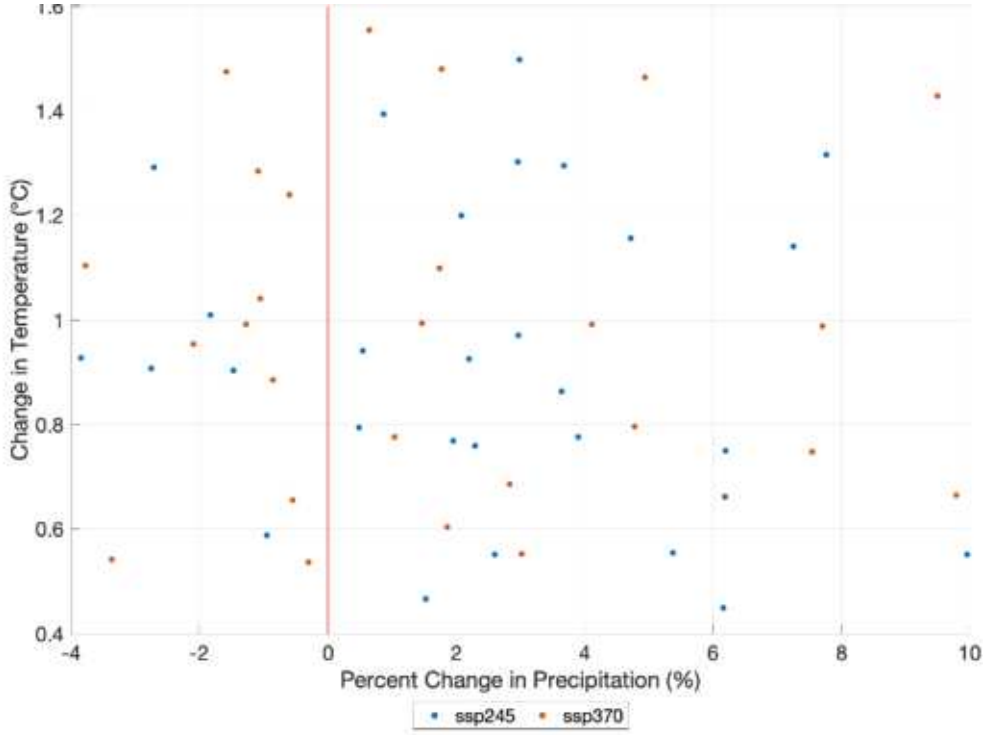

Panel B. Result of Step 3 and 4

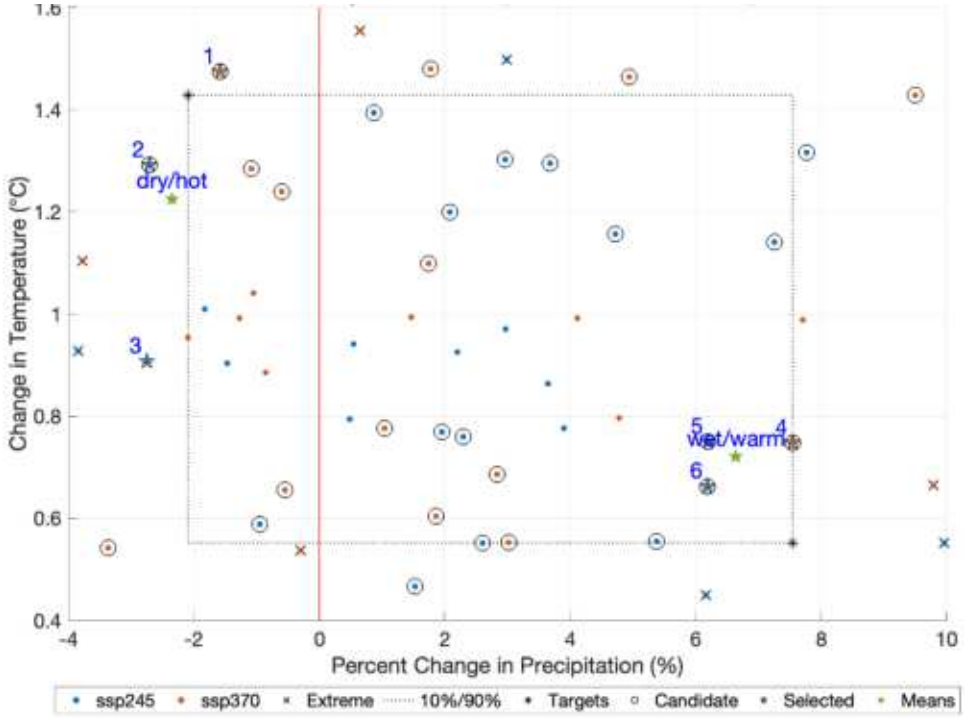

A5. DAILY INTERPOLATION OF MONTHLY DATA

Climate data from the Climate Change Knowledge Portal is available at a monthly timestep. However, many of the biophysical models used in this study rely on daily temperatures and precipitation. For the selected climate projections as well as historical baseline, we interpolate the already downscaled and bias-corrected monthly data to a daily timestep using a historical hindcast from 1948 to 2008 at a 05 x 0.5 degree gridded resolution from the Terrestrial Hydrology Research Group from Princeton University (Li, Sheffield, and Wood 2010). The process considers the following steps:

1. For each 0.5 x 0.5 grid cell, we group the daily hindcast by month, for each of the twelve months.
2. Then, we sort each month's data into quantiles based on the corresponding month's total precipitation or average temperature.
3. For each month in the monthly data from the Climate Change Knowledge Portal, we find the quantile that month falls into and randomly select a daily value to use based on that month's daily variability.

A6. RESULTS OF THE CLIMATE SCENARIO SELECTION PROCESS

Figure A82 shows the results of the climate scenario selection process. The scatterplot shows the distribution of SSP/GCM combinations based on changes in temperature and precipitation, highlighting those that were selected (including the ensemble mean scenarios for reference).

FIGURE A82. GCM SELECTION RESULTS FOR DRY/HOT AND WET/WARM FUTURES

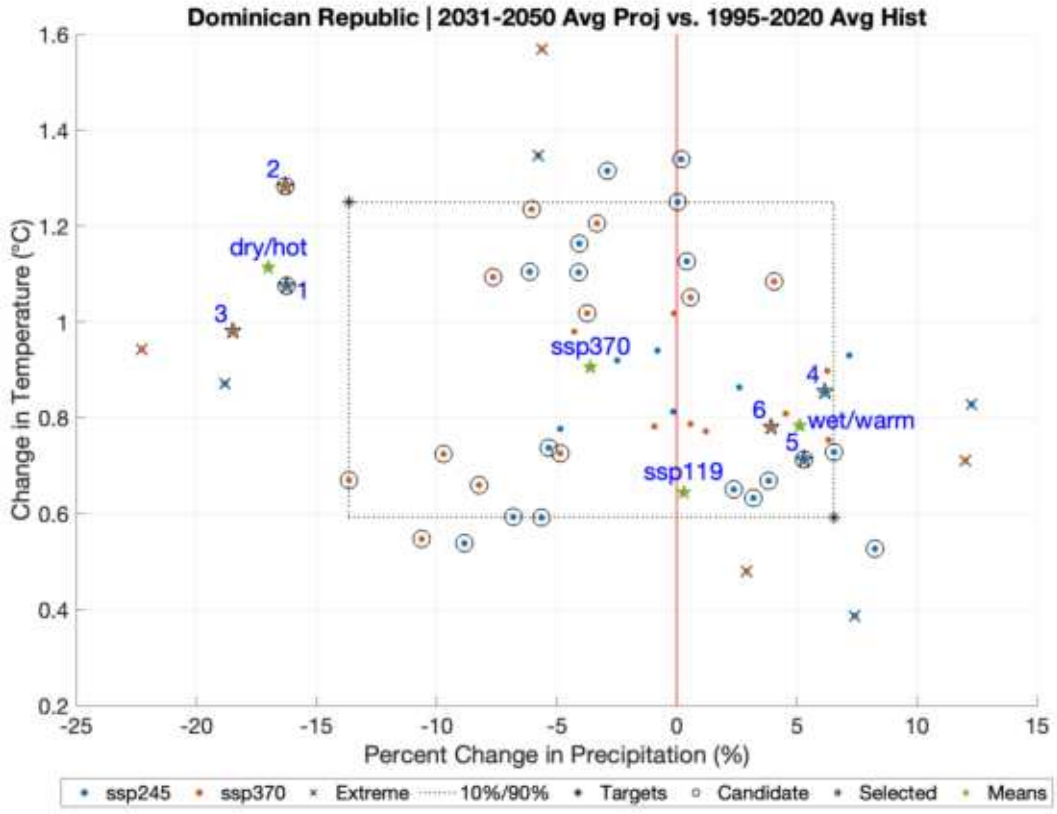

TYPE	#	SSP	GCM
Dry / hot future	1	SSP2-4.5	TAIESM1
	2	SSP3-7.0	KACE-1-0-G
	3	SSP2-7.0	IPSL-CM6A-IR
Wet / warm future	4	SSP2-4.5	CMCC-CM2-SR5
	5	SSP2-4.5	NORESM2-LM
	6	SSP3-7.0	CMCC-CM2-SR5

Trajectories of changes in temperature and precipitation for the selected scenarios are presented in Figure A83 for the mean scenarios (i.e., ensemble means and dry/hot and wet/warm means). Figure A84 presents the trajectory of specific SSP/GCM combinations. Finally, maps that show spatial changes in temperature and precipitation are presented in Figure A85.

FIGURE A83. MEAN TEMPERATURE (°C) AND PRECIPITATION (%) CHANGE TRAJECTORIES

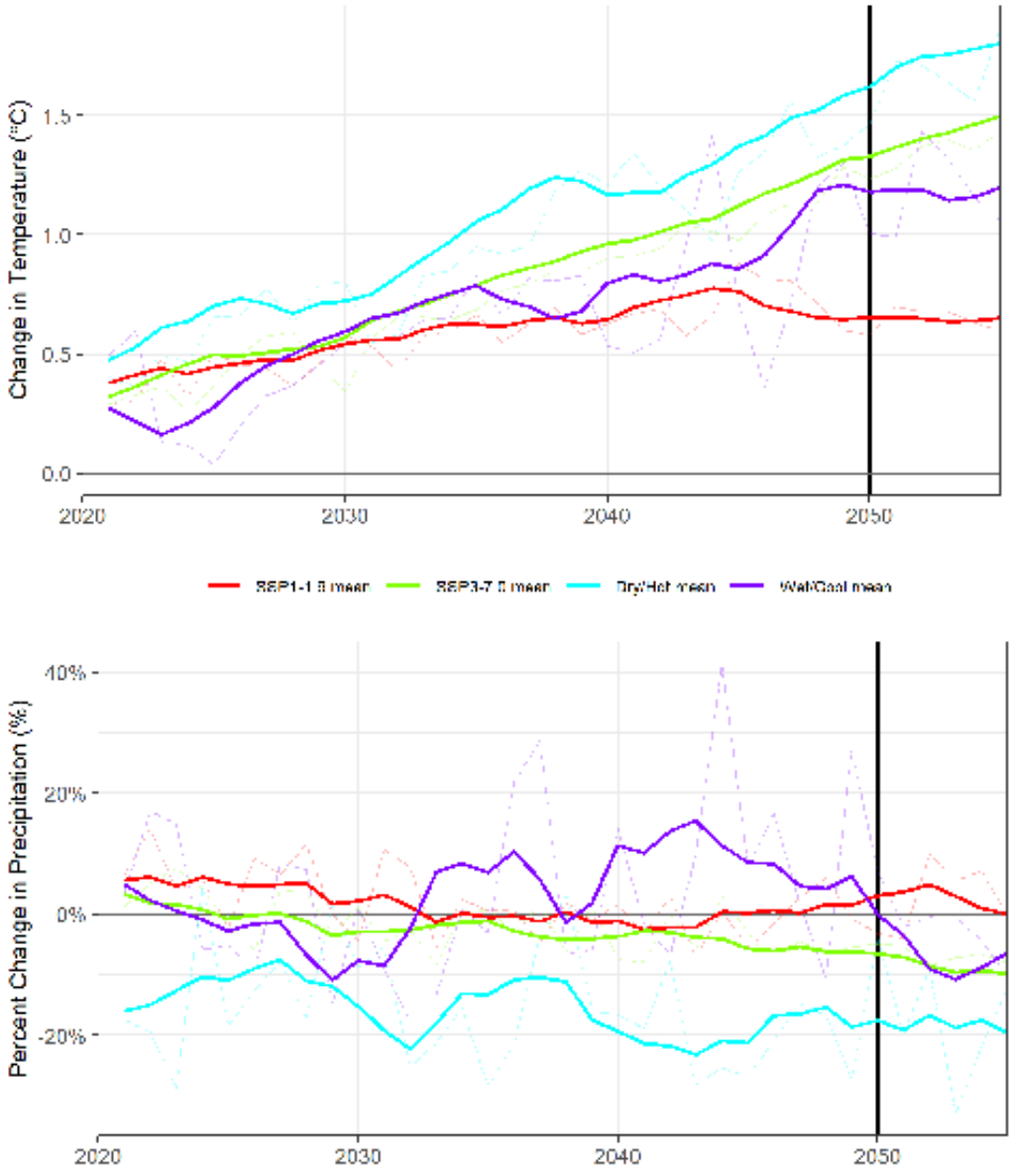

FIGURE A84. GCM TEMPERATURE (°C) AND PRECIPITATION (%) CHANGE TRAJECTORIES

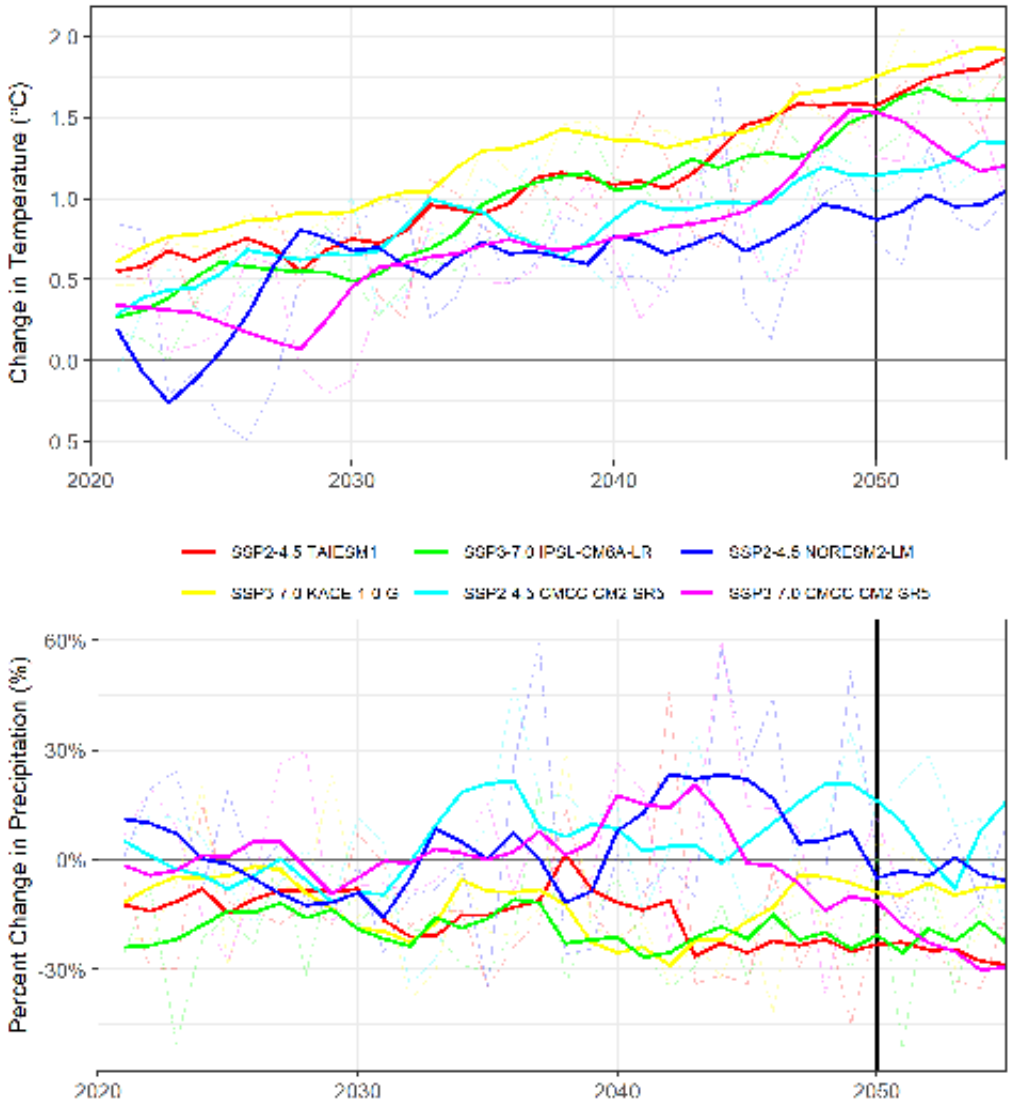

FIGURE A85. GCM TEMPERATURE (°C) AND PRECIPITATION (%) CHANGE BY 0.5 DEGREE GRID CELL, 2031-2050 VS 1995-2020

Panel A: Temperature

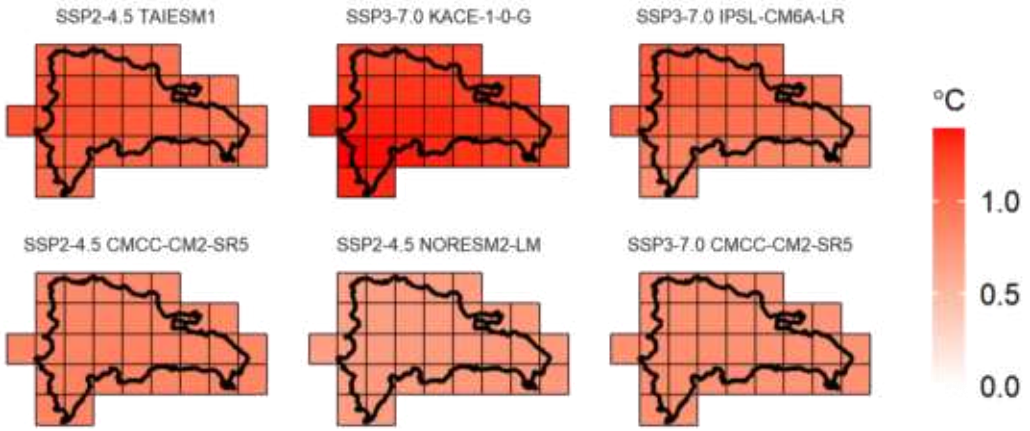

Panel B: Precipitation

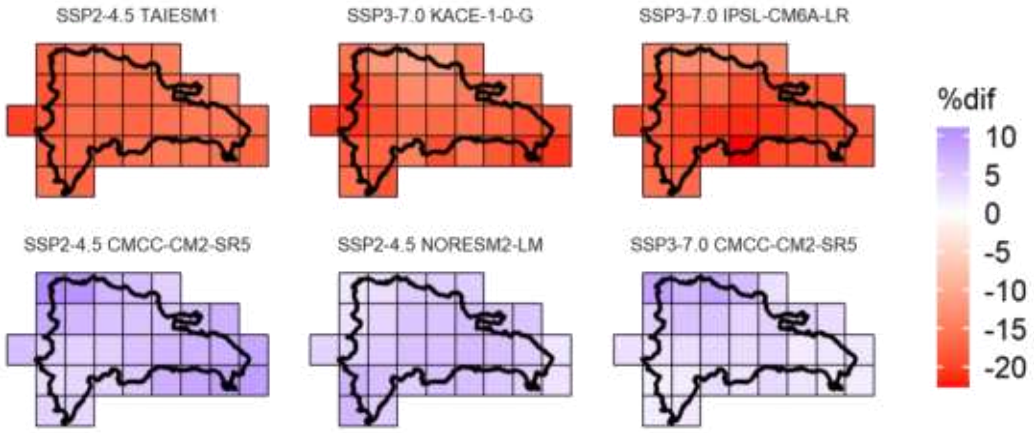

Cervigni, Raffaello, Rikard Liden, James E. Neumann, and Kenneth M. Strzepek. 2015. "Enhancing the Climate Resilience of Africa's Infrastructure: The Power and Water Sectors." Africa Development Forum. Washington, DC: World Bank. doi: 10.1596/978-1-4648-0466-3.

Harris, Ian, Timothy J. Osborn, Phil Jones, and David Lister. 2020. "Version 4 of the CRU TS Monthly High-Resolution Gridded Multivariate Climate Dataset." Scientific Data 7 (1): 109. https://doi.org/10.1038/s41597-020-0453-3.

Li, Haibin, Justin Sheffield, and Eric F. Wood. 2010. "Bias Correction of Monthly Precipitation and Temperature Fields from Intergovernmental Panel on Climate Change AR4 Models Using Equidistant Quantile Matching." Journal of Geophysical Research: Atmospheres 115 (D10). https://doi.org/10.1029/2009JD012882.

World Bank. 2021. "Climate Change Knowledge Portal." 2021. https://climateknowledgeportal.worldbank.org/.

APPENDIX B: IMPACT CHANNEL METHODS

B.1 INTRODUCTION

Climate change impacts on the country's economy are modeled through impact channels. The impact channels considered in this study are summarized in Chapter 2 of the main report. For each channel, shocks to macroeconomic inputs are generated for future climate projections under multiple scenarios - these are presented in Chapter 3 of the main report. Chapter 4 of the main report briefly describes how each impact channel was modeled and presents results for each channel. This appendix presents further technical detail on the analytical approach used to model each channel, including a description of the limitations of the methodology. Appendix C presents an overview of the specific data sources used to evaluate each impact channel.

B.2 HUMAN CAPITAL

Climate change may reduce human capital through increases in extreme temperatures that result in excess mortality and reduced labor capacity, as well as by facilitating the spread of infectious diseases as larger areas experience favorable climatic conditions, which in turn cause excess mortality and increased disease incidence on the population. We estimate these effects through the following channels:

- **Labor heat stress:** which models changes in the ability of labor to perform work as workday temperatures increase in the future.
- **Human health:** which models changes in the incidence and mortality of vector-borne (malaria and dengue), water-borne (i.e., cholera, dysentery, etc.), and heat-related diseases as local temperatures and precipitation levels and patterns change in the future.

In addition, both the coverage and the quality of basic services can play a significant role in the overall prevalence of certain diseases in the population. While these changes respond to policy decisions rather than to changes in climate, their effect is intertwined with human health effects and can either mitigate the effects of climate change or generate additional co-benefits. We consider the following channels to model these effects:

- **Water, sanitation, and hygiene (WASH):** which models the effects of improved WASH coverage on the incidence of diarrheal diseases.

Labor supply model

All the channels mentioned above impact labor. Heat stress reduces the productivity of labor by reducing the effective number of hours a person can perform work, while human health and the associated policy channels impact total labor supply by way of changes in death and incidence of diseases. In order to calculate these effects, we model the total labor hours in the country, which we then shock from each effect.

First, we obtain annual population estimates for both history and projected future by sex and age, considering population ages 15 to 64 as the working age population (OECD 2023). When available, we use both historical and projected future labor force statistics. If such statistics are not available, we apply available labor participation rates by sex to estimates of the working age population to compute the total labor force. The labor force is multiplied by available data on mean weekly hours worked for both males and females to produce the total annual hours of labor supply.

B.2.1 LABOR HEAT STRESS

Temperature directly affects the productivity of labor, where the effect intensifies for labor types that are outdoors and are conducting more intense physical work. Labor productivity impacts follow the methodology applied by the International Labor Organization (ILO 2019), which has been applied globally and used in other similar studies, such as in Kjellstrom et al. (2018). The approach is based on workday wet bulb globe temperatures as an indicator of heat stress, which refers to the exposure of individuals to extreme heat or hot environments that lead to the body's inability to regulate internal temperature (CDC 2020). A measure of heat stress is used to quantify the percentage of a typical working hour that a person can work. The analysis is done at a 0.5 x 0.5 degree spatial resolution for the relevant sectors of the economy, resulting in annual shocks to labor productivity for every scenario being evaluated.

Methodology

Workers are exposed to different temperatures during typical workday hours. The functional relationship between work ability and heat stress is quantified using wet bulb globe temperatures (measured in Celsius degrees). Wet bulb temperature is a measure of air temperature in relation to moisture content, while dry bulb temperature is a measure of ambient temperature. The globe temperature is a measure of the thermal radiation that would be absorbed by someone's skin. We utilize the Australian Bureau of Meteorology equation used by Kjellstrom et al. (2008) to calculate wet bulb globe temperatures based on daily workday temperatures and monthly mean relative humidity levels.[4] To approximate workday temperatures from daily minimum and maximum temperatures, we use the "4+4+4" method used by the (ILO 2019). This method assumes that in a typical 12-hour daylight day, 4 hours per day are close to minimum daily temperatures, 4 are close to the maximum, and 4 are close to the midpoint between the two. As done by the ILO, we assume these temperatures apply to indoor workers as air temperature is measured in shade. For outdoor labor, it is assumed that the wet bulb globe temperatures are +2°C higher at full sun exposure.

Labor productivity effects are then estimated based on the percentage of hours that an acclimatized worker can be engaged in work based on their level of heat stress. Occupations with lower physical activity can tolerate higher levels of heat stress. Labor productivity loss curves from wet bulb globe temperatures for three levels of physical activity (measured in Watts), presented in Figure B86, are derived from the ISO 7243:1989 standard (ISO 1989) and Kjellstrom et al. (2018) and validated through additional epidemiological studies, as presented in ILO (2019b). Generally, 200 Watts represents clerical or light physical work, 300 Watts

[4] ABoM: http://www.bom.gov.au/info/thermal_stress/#approximation

moderate physical work in industry, and 400 Watts heavy physical work in agriculture or construction. Work intensities are then matched to labor hours by sector and occupation, from available reported data. We apply available assumptions on outdoor exposure by occupation to data on employment by sector in order to split the share of hours worked indoors versus outdoors. Then, we estimate the impacts of heat stress on labor productivity for each category of workers (by sector and occupation), and for both indoor and outdoor workers.

FIGURE B86. WORK CAPACITY AS A PERCENTAGE FROM WET BULB GLOBE TEMPERATURES

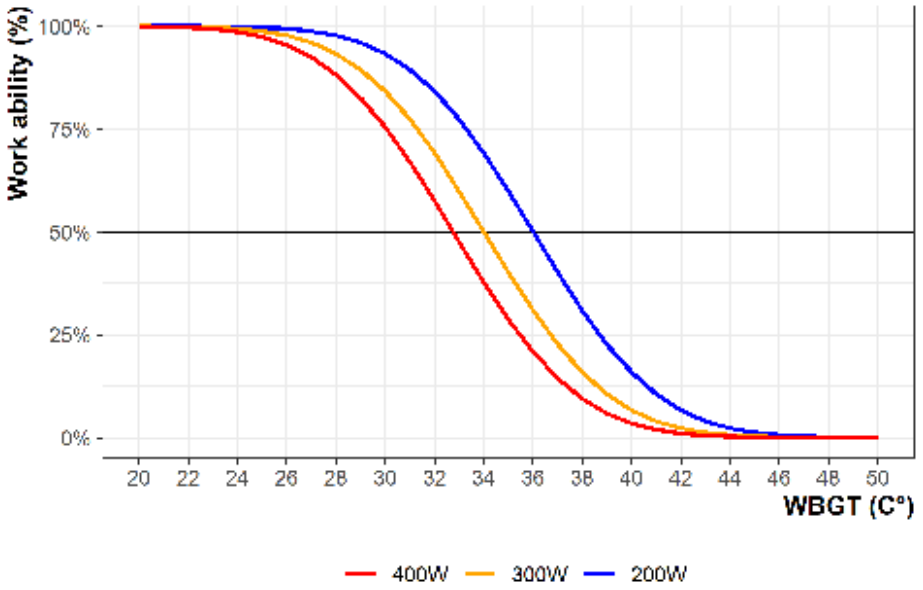

Source: IEc analysis

For indoor workers, we exclude the share of those who worked in spaces with air conditioning and assume they do not experience any heat stress. Adoption of air conditioning within a country (by 0.5 degree grids) is estimated using regional percent coverage of curves from Davis et al. (2021), based on mean household income levels and cooling degree days by grid cell.[5] Generally, regions with higher mean household incomes and/or cooling-degree days have a higher air conditioning adoption rate. Mean household incomes by country are obtained from United Nations and World Bank data (World Bank, n.d.; United Nations 2022). When available, data on mean percent adoption of air conditioning at a national scale is used to calibrate the estimates obtained from Davis et al.

For the final step, monthly labor productivity impacts by 0.5 degree grid cell are aggregated nationally by macroeconomic sectors (agriculture, industry, and services) and on an annual scale for all the completed time series. For agriculture, grid cell level impacts are aggregated using the share of cropland as a proxy of the spatial distribution of agricultural workers, using data from the Copernicus Fractional Land Cover dataset (Buchhorn et al. 2020). For industry, we assume a distribution of workers using gridded gross domestic product data from Wang and Sun (2022).

[5] Cooling degree days are based on the assumption that when the outside temperature is 65°F, people do not need cooling to be comfortable. Cooling degree days are the difference between the daily mean temperature minus 65°F. https://www.weather.gov/key/climate_heat_cool

For services, we aggregate using gridded population data from WorldPop of the University of Southampton (Bondarenko et al. 2020b; 2020a).

Limitations

- Work intensities and the outdoor exposure of each occupation is matched to labor statistics based on the best available information.
- All occupations are assumed to be performed evenly throughout the day and year. No seasonality of occupations is considered.
- Wet bulb globe temperatures are approximated using monthly mean relative humidity, which is kept constant for future years. While there are more sophisticated methods to estimate wet bulb globe temperatures that utilize wind speeds and solar radiation, such data are not available for this study.
- Data regarding adoption of air conditioning is sparse. We utilize regional curves for household coverage as a proxy for workplace coverage.

B.2.2 HUMAN HEALTH

Climate change may impact the total labor supply through increased incidence of and death rate from various diseases, which results in time away from work due to absenteeism as well as from an increased number of deaths. Climate change could result in increased health effects of vector-borne diseases such as malaria and dengue, waterborne infectious diseases that cause acute diarrhea, and heat-related diseases (WHO 2014; Romanello et al. 2021). The approach utilizes different biophysical and statistical relationships between climate variables and the incidence of or transmissibility for each disease.

Changes in incidence and death rates are calculated to model the number of hours of labor supply lost. On the one hand, excess deaths relative to the baseline will reduce the total labor (see equation A below). This effect is calculated independently for every year and does not consider population fertility and death rate dynamics. On the other hand, absenteeism from work due to people falling sick will further reduce the total available labor. This effect is divided in two, following the methodology applied by John et al. (2021). First, there is a direct effect from working age population getting sick and not able to work, and second, an indirect effect from children getting sick and needing parental care for the duration of the disease. Total hours of labor lost for each disease are then calculated for the country for both historical periods as well as future projections, for each disease and effect. Lastly, a percent shock to available labor supply relative to the baseline conditions is then calculated for the country total.

A. Labor hours lost due to death (hours/year):
   - $LS_d = D \times p_{15-64} \times l_{15-64} \times h_w$

B. Labor hours lost due to absenteeism for the disease (hours/year):
   - $LS_{c,direct} = C \times p_{15-64} \times l_{15-64} \times r$
   - $LS_{c,parental} = C \times p_{0-15} \times l_{15-64} \times r$

- D = deaths = *f*(climate)
- C = cases = prevalence x total population = *f*(climate)
- p_{15-64}= 15-64 fraction on total population (%)
- p_{0-15}= 0-15 fraction on total population (%)
- l_{15-64}= labour participation 15-64 (%)
- r = average recovery time = week/year (*f*(disease)) x h/week
- h_w = average hours worked per year per person

Methodology - Vector-Borne Diseases

Vector-borne diseases are illnesses that are transmitted to humans through the bites of infected arthropods, typically mosquitoes. Malaria and dengue are two major vector-borne diseases that cause of public health concerns around the globe. The modeling approach is based on the modeling of the conditions for stable transmission of the disease (i.e., suitable areas), based on the methodology applied by Ebi et al. (2005). The analysis is done for both malaria and dengue, typical mosquito-borne diseases whose spread depends on the right environmental conditions occurring for the mosquitoes to live, breed and increase in number, at a 0.5 degree resolution. These conditions are approximated from three climate variables: mean monthly temperatures, cumulative annual precipitation, and minimum annual winter temperature. Those variables are normalized using fuzzy functions following Craig et al. (1999), determining a suitability index ranging 0 to 1.

Fuzzy functions based on the equation below are applied to each climate variable. The S and U factors are the upper and bottom thresholds of the climate variables respectively, x is the observed climate variable, y is the resulting fuzzy variable (the fuzzy variable being y for the decreasing curve, (1-y) for the increasing curve):

$$1\text{-}y = \cos^2\left[\frac{x-U}{S-U} \times \frac{\pi}{2}\right]$$

When the fuzzy variable is 0 (i.e., non-suitable), transmission is very unstable, with the disease either absent or with rare epidemics; when the fuzzy variable is 1 (i.e., suitable), disease transmission is most likely stable; values between zero and one (0.1–0.9) represent a gradient from unstable to increasingly stable transmission. We select the minimum value between temperature and precipitation's fuzzy variables. Then, the mean value of each year is compared to the minimum winter temperature fuzzy variable.

For malaria, the thresholds are U=0, S=80 for precipitation; U=18, S=22 for the mean monthly temperature increasing part of the curve, S=32, U=40 for the decreasing part of the curve; and U=4, S=6 for annual winter temperature (i.e., minimum value of coldest month) (Ebi et al. 2005). Figure B87 illustrates the shape of the fuzzy functions for malaria. The same general equations are applied for dengue transmissibility. The corresponding threshold values are U=450, S=800 for precipitation; U=15, S=20 for the mean temperature (increasing), S=25, U=30 (decreasing); and U=-1, S=3 for winter temperature (Caminade et al. 2012). Figure B88 illustrates the shape of the fuzzy functions for dengue.

FIGURE B87. FUZZY FUNCTIONS FOR MALARIA

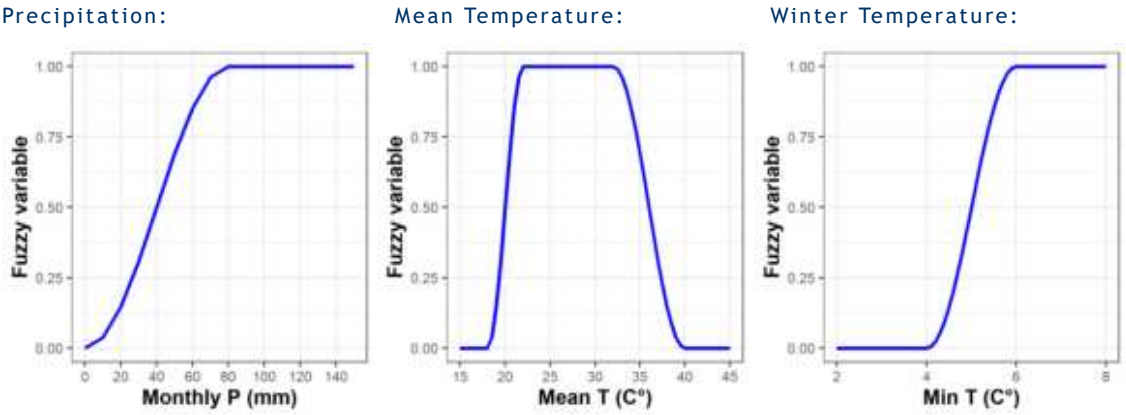

FIGURE B88. FUZZY FUNCTIONS FOR DENGUE

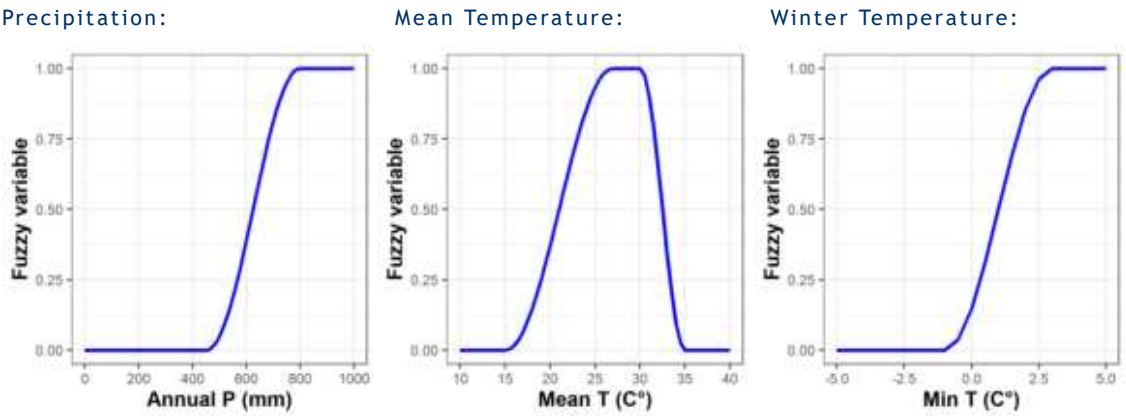

Annual fuzzy variables are then used to calculate the exposed population by grid cell, as a probability of the occurrence of the disease in the area (LeSueur et al. 1998). Consequent deaths and cases due to the disease are then normalized and calibrated using reported deaths and prevalence rates from official sources. While malaria generally exhibits a stable transmission rate over time (with increasing or decreasing rates), dengue is more episodic and prone to random outbreaks that are difficult to attribute to clear factors (Chen et al. 2015). For this analysis, we do not model outbreaks or other epidemiological dynamics, and calculate changes in death and incidence rates for both diseases relative to the average reported rates of the latest five years, or the best available data.

Methodology - Heat-related Illness

Heat is a risk factor that can lead to a group of conditions that occur when the temperature of the human body is exposed to high temperature and humidity. Heat-related illnesses can include severe conditions such as exhaustion or stroke (CDC 2020). Heat effects on mortality and morbidity are modeled based on the *2021 Report of the Lancet Countdown on Health and Climate Change* (Romanello et al. 2021). The methodology is based on calculating excess mortality from daily maximum temperatures, following the study by Honda et al. (2014). The temperature–mortality relationship is assumed to be V-shaped (see Figure 17), and the

temperature value at which mortality is lowest is defined as the optimum temperature (OT). For temperatures above the optimum threshold for a given location, excess heat-mortality burden is defined daily as a fraction of the average total non-injury-related deaths occurring that day.

FIGURE B89. V-SHAPED FUNCTION OF EXCESS MORTALITY DUE TO HIGH TEMPERATURES

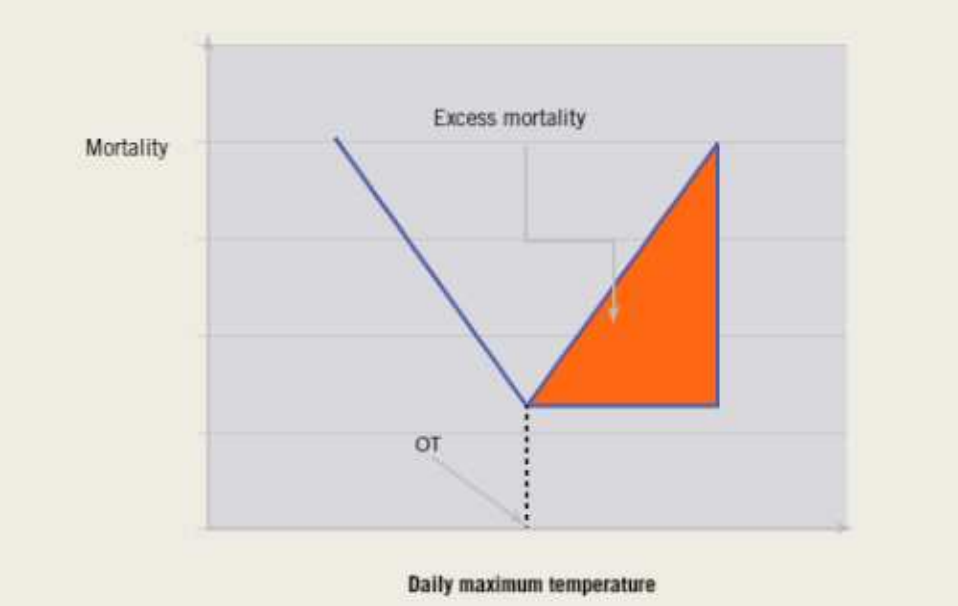

Source: WHO 2014

An equivalent approach to vector diseases is applied to compute heat-related morbidity and is quantified by the following equation:

$$E = y_0 \times Pop \times AF$$

- E = heat-related excess mortality/morbidity in one day
- y_0 = non-injury mortality rate on that day (yearly rate divided by 365)
- AF = attributable fraction on that day, calculated as

$$AF = (RR - 1) \,/\, RR = 1 - e^{-\beta(t - OT)}$$

- t = daily maximum temperature
- β = exposure-response factor (Honda et al. 2014)
- OT = optimum temperature (Honda et al. 2014)

Excess mortality is calculated for each grid cell and calibrated to nationally reported statistics of non-injury heat-related mortality.

Methodology - Waterborne Diseases

Waterborne diseases are illnesses caused by contact with water that is contaminated with infectious microorganisms that cause diarrhea, vomiting, and fever. Waterborne pathogens can spread through drinking water, irrigation waters, or recreational water bodies. Climate change is likely to increase the spread of waterborne pathogens such as cholera, typhoid, dysentery, or

leptospirosis, resulting in increased mortality and morbidity from diarrheal diseases (Levy et al. 2018; Nichols et al. 2018). Our analysis is based on the modeling approach applied in WHO (2014). While most studies highlight a positive association between the incidence of diarrhea and temperature, results of the association between mean monthly rainfall and E. Coli diarrheal cases are more varied, and the effect is much smaller (Philipsborn et al. 2016). For this reason, the WHO model applies gridded estimates only of average annual temperature anomalies to a statistical temperature–mortality risk relationship.

The approach considers combining total estimated diarrheal deaths and cases in the future without climate change, and estimating the climate change-attributable percent change. The following general equation is applied at a yearly time-step at a 0.5 degree grid cell resolution:

$$n = N \frac{e^{\beta \Delta T} - 1}{e^{\beta \Delta T}}$$

- n = number of climate change-attributable average annual diarrhea deaths or cases
- N = total number of average annual diarrheal deaths or cases in a future without climate change, obtained as the product between population and a baseline rate from available official statistics
- ΔT = yearly temperature anomaly
- β = log-linear increase in diarrheal deaths per degree of temperature increase with
    - $\beta = \log(1 + \alpha)$, where α is the linear increase in diarrheal deaths per degree of temperature increase. We assume α as a mid-estimate from WHO (2014).

The annual number of diarrheal cases and deaths is then calculated as n+N for each grid cell and then aggregated at the country level. Figure B90 illustrates the percent change in the incidence of cases and deaths from temperature changes.

FIGURE B90. CHANGE IN WATER-BORNE DISEASE INCIDENCE FROM CHANGES IN TEMPERATURE

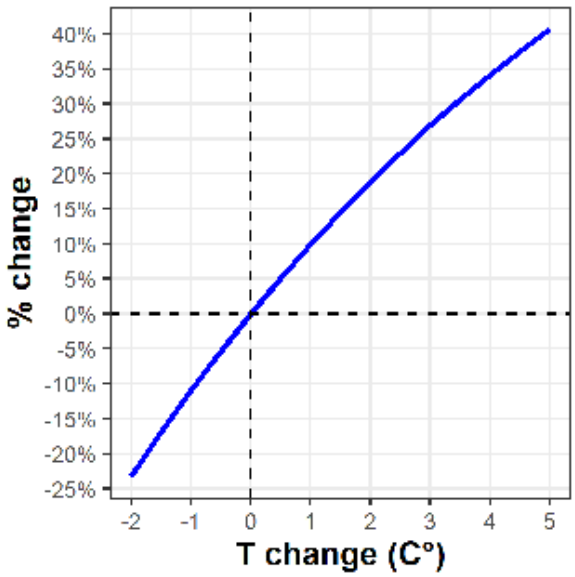

Limitations

- We considered those diseases that are more widely cited and modeled in the literature. However, this is not an exhaustive list of all the health effects than can be caused by climate change. Other direct and indirect causes of illness that can be linked to climate variables, such as schistosomiasis, outdoor air pollution, occupational hazards, or malnutrition are not considered in this analysis.
- We utilize mean baseline mortality and incidence rates to measure the mean effects of climate change. Outbreaks and more complex epidemiological dynamics are not modeled.
- Population dynamics over time that account for factors such as births, deaths, or aging of the population and result in later effects in labor supply are not considered in this study.

B.2.3 WATER, SANITATION, AND HYGIENE

The human health effects of climate change documented earlier in this section focus on assessing potential impacts on labor supply due to increase mortality, including the spread of water-borne diarrheal diseases. Yet, development policy initiatives in WASH can indirectly influence the severity of potential climate change impacts on human capital, as the quality of infrastructure can help to reduce diarrhea cases and related mortality (World Bank 2018).

This impact channel evaluates the benefits of enhanced investments in WASH, by comparing a baseline scenario where current trends of coverage and quality of infrastructure continue over time, relative to a scenario where additional investments in WASH reduce the incidence of water-borne diseases. These investments are presented as part of the policy scenarios discussed in Chapter 3 of the main report. The approach follows the methodology applied by Wolf et al. (2019), which is based on a statistical relationship between a fecal contamination composite index (FAECI) and the relative risk of diarrheal diseases.

Methodology

A population-attributable fraction of the total diarrheal deaths and cases is computed to assess the part of those deaths and cases caused by inadequate WASH. This is based on available official statistics on WASH coverage. The relative risk associated with such WASH access is computed and the change in relative risk due to different policy scenarios is reflected through changes in the population-attributable fraction. The relative risk assessment is estimated through the FAECI (Wolf et al. 2019), which utilizes a rubric to assign a 0, 1, or 2 value to eight indicators related to water, sanitation and hygiene access (see Figure 22). The FAECI corresponds to the sum of these indicators, ranging from 0 to 16. Figure B92 presents the relationship between the FAECI and corresponding diarrhea relative risk.

FIGURE B91. FECAL CONTAMINATION COMPOSITE INDEX INDICATORS

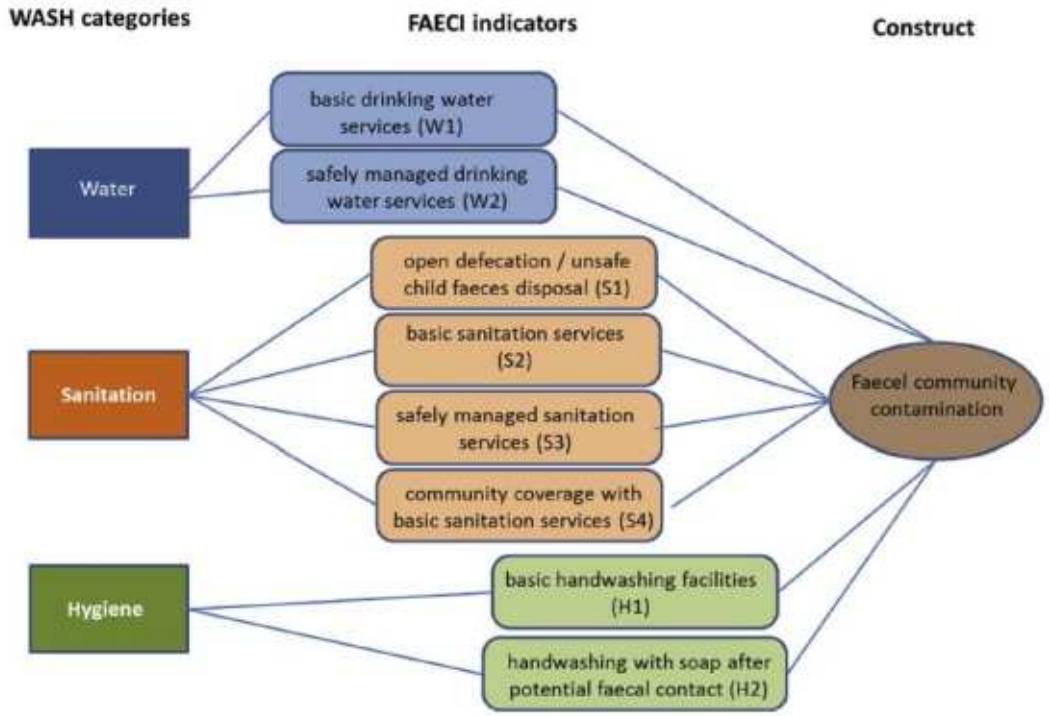

Fig. 2. WASH indicators for assessing faecal environmental contamination.

Source: Wolf et al. 2019

FIGURE B92. DIARRHEAL DISEASE RELATIVE RISK

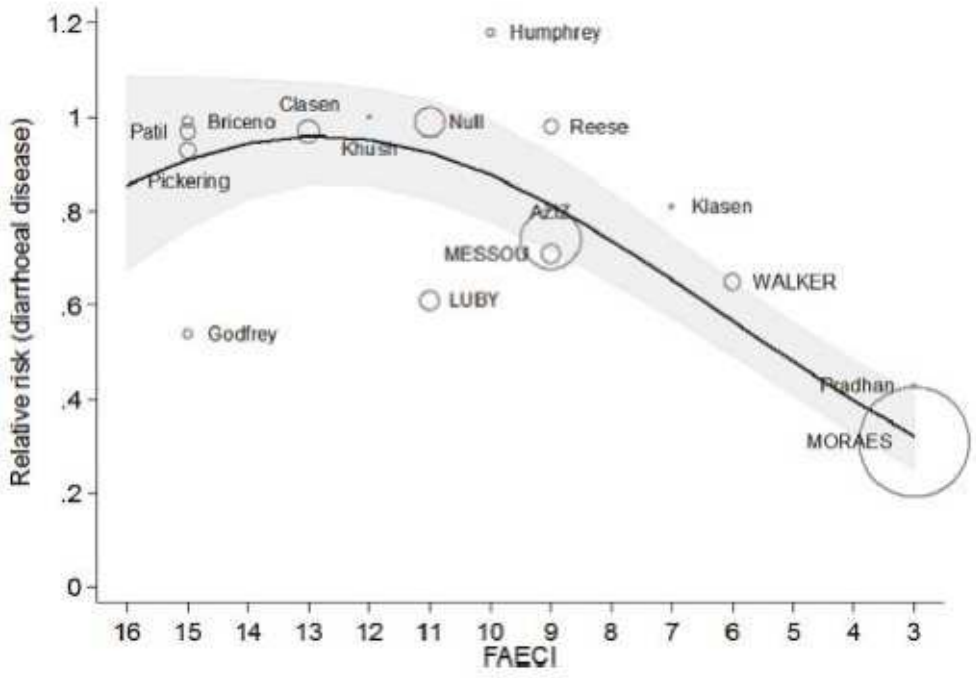

Source: Wolf et al. 2019

Resulting relative risks are calibrated for the country using reported data on mortality and morbidity linked to inadequate WASH infrastructure. Then, a percentage change in diarrheal mortality and morbidity from improvements in WASH infrastructure relative to base conditions scenarios is computed for each scenario at a country scale.

Limitations

- We utilize mean baseline mortality and incidence rates to measure the mean effects of climate change. Outbreaks and more complex epidemiological dynamics are not modeled.
- Population dynamics over time that account for factors such as births, deaths, or aging of the population and result in later effects in labor supply are not considered in this study. In particular, child stunting impacts from inadequate WASH and associated population effects (e.g., the later effect on labor supply of changing death rates in children) are not considered.

B.3 WATER AND AGRICULTURE

Overall, natural resources are expected to experience a variety of impacts from climate change. Changes in precipitation patterns can result in reduced water resources for rainfed agriculture, hydropower generation, and other uses, as well as impacting erosion levels that can result in additional downstream effects. Temperature increases are likely to reduce the suitability and productivity of crops and can have additional impacts on overall water resources availability. We estimate these effects through the following channels:

- **Water supply:** which models changes in the availability of water resources for particular, water-dependent sectors of the economy.
- **Crop production:** which models changes in crop productivity as a function of the availability of rainfall and irrigation resources, as well as heat stress effects from increasing temperatures.
- **Erosion:** which models changes in soil conditions and topsoil erosion from altered precipitation, which in turn results in changes in crop productivity.
- **Hydropower:** which models changes in hydropower generation due to changes in river runoff from altered precipitation regimes.

Water system model

Figure B93 summarizes the modeling approach of the water system in the country. The analysis starts with climate data on temperature, precipitation, and potential evapotranspiration, which is converted into water supply as river runoff through the rainfall-runoff model CLIRUN. In addition, crop irrigation needs, which are influenced by the projected availability of rainfall, are modeled using the FAO66 approach (see Crop Production channel section) as one key input of water demand. Other drivers of water demand are included within the WEAP modeling step.

FIGURE B93. WATER RESOURCES MODELING APPROACH

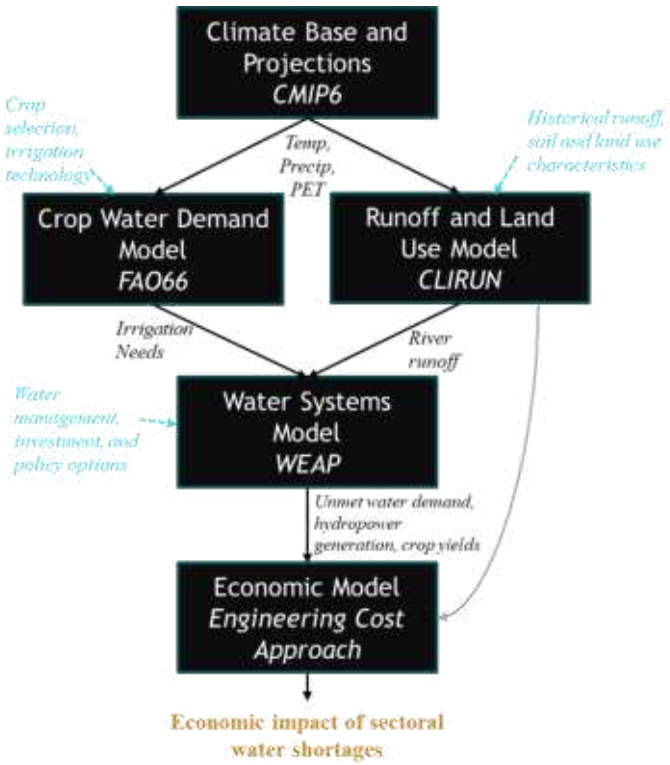

The Water Evaluation And Planning (WEAP) tool, developed by the Stockholm Environment Institute's United States Center, is used to evaluate climate change impacts on water availability. The WEAP model is used to simulate the allocation, use, and management of water resources within a catchment and is used to analysis the impacts of management options on the balance between supply and demand for water resources (Yates et al. 2005).[6] It uses water balance principles to simulate sectoral water demand such as water supply for municipal, industrial and irrigated agriculture uses, as well as hydropower generation, and environmental flows. Figure B94 presents a visual illustration of the modeling of a catchment in WEAP, where black boundaries represent catchments, light blue lines rivers, red circles demand sites, and green arrows transmission links.

[6] https://www.weap21.org/index.asp?action=200

FIGURE B94. ILLUSTRATION OF A CATCHMENT MODELED IN WEAP

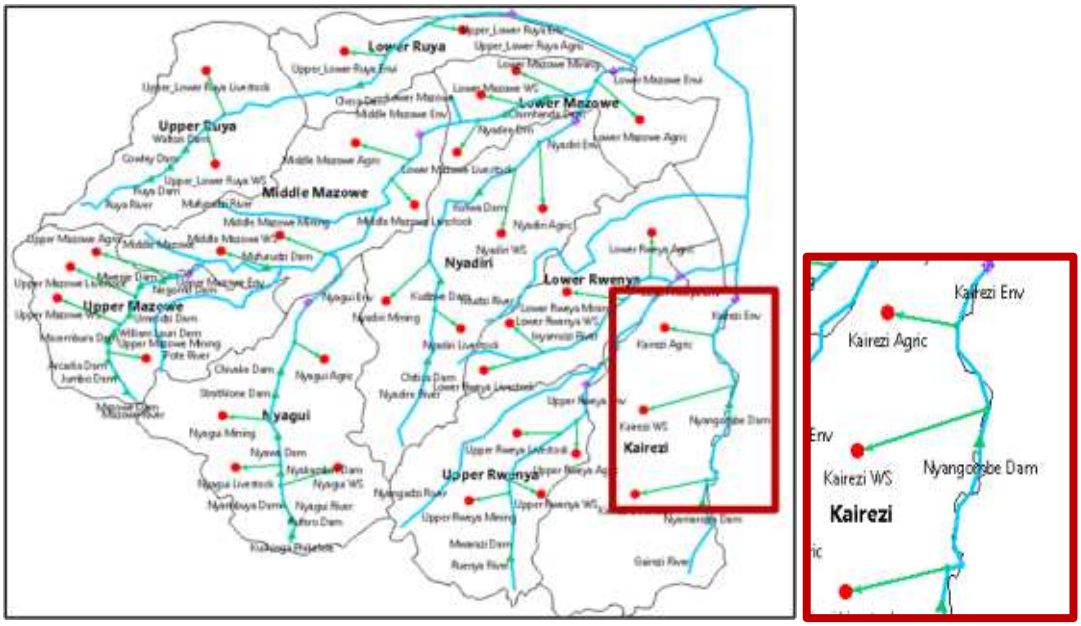

Generally, the analysis requires first setting up the spatial boundaries of the study, the components of the water system, and the configuration of the problem. This means, first, delineating the basins of the country in alignment with the level of detail required for the analysis and the available data, and second, assessing the sectoral water demands (municipal, industrial, agricultural) together with the reservoirs and hydropower facilities for each basin. Given the temporal frame, the system is calibrated using observed data on water resources, supply, and demand. The model can then incorporate alternative climate scenarios as well as changes in relevant infrastructure and water-related policies to simulate the consequences on future supply and demand. For each scenario, WEAP generates a time series of surface water availability (runoff), reservoir storage, hydropower, and major water demands in the country in order to allow investigation of intersectoral competition between demands. A hierarchical structure of water demands is used, which includes agriculture, urban and rural domestic sectors, industrial demands, and hydropower. The demand analysis is carried out by disaggregating these different sectors, utilizing economic, demographic, and water-use patterns that influence demand, which can vary by scenario. The climate and policy scenarios are characterized by unique inflows and growing irrigation demand, hydropower, and reservoir storage. The data structure and level of detail in the model are customized to meet the requirements of the study and the availability of data to set up and calibrate the model.

We use the best available data from local or global sources to estimate water withdrawals for domestic, industry, hydropower, and irrigation uses. Existing modeling studies conducted in the country are used to calibrate the analysis, including shapefiles of nationally recognized river basins. For river runoff data, calibration is conducted using at least 10 years of monthly historical data from gauges in each basin. The model is then used to simulate future withdrawals, considering investments in hydropower and irrigation, when relevant. WEAP maximizes meeting the requirements for demand sites, reservoir filling, user-specified instream flows, and

hydropower subject to priorities in consumption, supply preferences, overall balance, and other constraints. In general, the outputs produced by the model include unmet water demand by sector/user (irrigation, municipal, industrial), hydropower generation, and environmental flows.

B.3.1 WATER SUPPLY

Insufficient water supply can affect manufacturing and other water-dependent industries in a country, as well as domestic use by the general population. We use a water systems model (described above) to evaluate shortfalls to municipal and industrial demand, given competing uses, climate change effects, and available storage infrastructure.

This channel assesses the macroeconomic shock from water availability either as (a) the impact of shortages or (b) the cost of a replacement water supply (e.g., desalinization), for the climate and policy scenarios being considered. Policy scenarios may consider improved infrastructure as well as changes in water demands across all sectors. Annual shortages or replacement costs will be compared against baseline conditions to quantify the macroeconomic shocks.

Methodology

The analytical approach for this channel follows the description of the water systems model presented above. In general, the analysis considers four steps.

1. First, a basin delineation process, which considers determining a reasonable number of basins in the country to be assessed based on the level of detail required for the analysis as well as of the available data. The delineation should follow officially recognized basins, previous studies, or globally modeled basins, such as the ones from HydroATLAS, at the most suitable resolution. Basins of particular interest (e.g., large demands or the presence of an important reservoir) may be drawn separately to ensure important features are captured in the modeling.
2. Second, gathering data on reservoirs and hydropower facilities, including point location, storage volumes, turbine capacity, generation capacity, electricity production, and other available technical characteristics of reservoirs. When available, local sources are preferred to international sources. If data is unavailable, values are estimated through regional or international standards.
3. Third, demands assessment. Industrial, municipal, and irrigation demands are gathered or estimated from local databases at the highest possible resolution, and then allocated to each basin. This may include reported statics, recent master plans, or similar studies where available and projected demands are based on historical population growth factors. When only national or regional values are available, we downscale demands based on statistics such as gridded population distribution or the location of relevant water-consuming industries (see illustration in Figure B95). Irrigation demands are assessed using crop water requirements (see irrigation section within the Crop Production channel).
4. Finally, the WEAP model is built for the country. Each basin is designated a main river, one or multiple nodes for sectoral demands (i.e., irrigation, municipal, and industrial), transmission links from the main river to each node, return flows, sectoral withdrawal

priorities, reservoirs, and hydropower facilities. The model is then calibrated using the available historical observations of runoff, demands, storage, and generation.

FIGURE B95. DEMAND DOWNSCALING PROCESS ILLUSTRATION

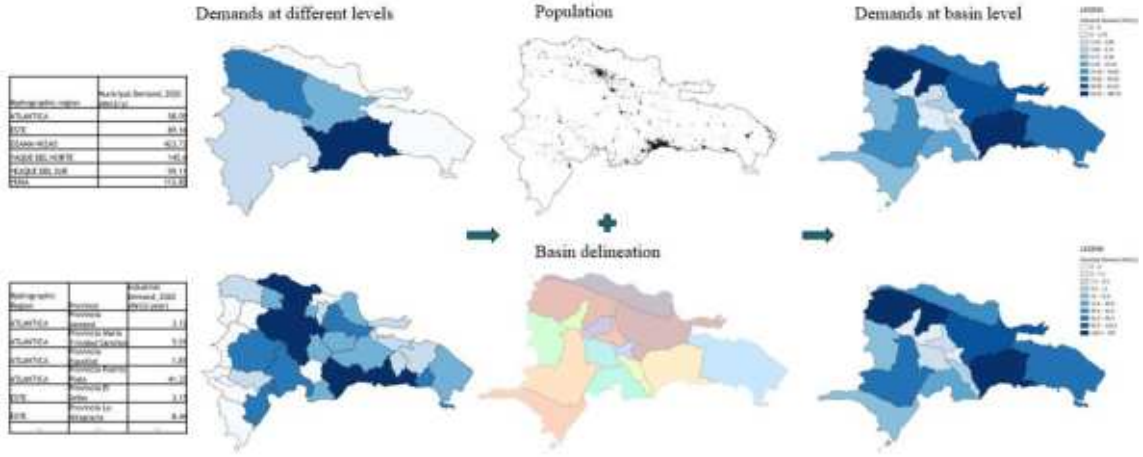

Once the calibration is completed, the model is run for a range of climatic and policy scenarios of interest. The availability of water resources for municipal and industrial users will be converted into unmet demands, which in turn, will be broken down by the relevant sectors of the economy (e.g., manufacturing) and population (urban, rural), as possible. Unmet demands are driven primarily, by a combination of factors including changes in resources resulting from climate change, changes in demands for other water-intensive sectors (i.e., irrigation and hydropower) due to capital or technological changes, environmental flow requirements, and the priority of uses in the country.

Limitations

- The shortage of data on groundwater availability and withdrawals is an important source of uncertainty in the analysis, and deserves further attention as part of any efforts to pursue new surface water-based irrigation investments.
- Assessment of the implications of deteriorating water quality and increasingly saline soils on water demands in future years is not included. The decrease in quality could likely either further reduce water reuse or cause productivity impacts.
- Actual water allocation to users is complex and water system models simplify these into priorities or decision rules, particularly when available water is scarce.
- Actual water levels in reservoirs that generate hydropower may differ from reality.

B.3.2 CROP PRODUCTION

Under climate change, rainfed crop yields will be affected by changes in rainfall patterns, increasing evaporative demands, and extreme heat as temperatures rise. The analysis is conducted for selected crops at a 0.5 x 0.5 degree spatial resolution.

The approach relies on the Food and Agriculture Organization's Irrigation and Drainage Paper 66, *Crop Yield Response to Water* (Steduto et al. 2012), in which rainfed crop yields are estimated by applying crop-specific water sensitivity coefficients to the ratio of effective precipitation to potential crop evapotranspiration. This approach is the basis for the Food and Agriculture Organization's monthly crop model CropWat, which is the predecessor to their daily biophysical crop model, AquaCrop.[7]

The water availability approach is then supplemented with impacts to crop yields from extreme heat during reproductive stages of development, when crops are more sensitive, causing a reduction in seed numbers (Prasad et al. 2015; Roberts 1988). Heat stress impacts are modeled daily following AquaCrop's approach (Salman et al. 2021), which considers a negative relationship between supra-optimal temperatures during the flowering stage of crop development.

Methodology

First, representative crops are selected for the country. In general, crops are selected so as to represent at least 80 percent of the total production revenues as well as harvested area in the country. Additional crops of national relevance may also be added to the list. For each country, crop calendars are obtained from the Food and Agriculture Organization (FAO 2022) and supplemented with local sources when available. Crop calendars (i.e., the time of the year when crops are sown, grown, and harvested) are allocated to 0.5 degree grid cells based on the production zones in the Food and Agriculture Organization's calendar, which is based on administrative districts and/or agro-climatic regions. We gathered harvested area, production, yield, and revenue statistics from available local or global sources. We also gathered irrigation statistics from the best available sources, distinguishing rainfed from irrigated production.

Potential evapotranspiration (ET_0) is used as a reference to estimate crop water requirements by adjusting it based on the crop and growth stage. For each crop, water demand is calculated by multiplying monthly potential evapotranspiration (ET_0) by monthly crop water demand coefficients (K_c), which produce annual crop evapotranspiration requirements (ET_c). Monthly potential evapotranspiration was calculated using the modified Hargreaves method (Droogers and Allen 2001), which requires data on extraterrestrial radiation, monthly precipitation, and minimum and maximum temperatures. Crop water demand coefficients for each month of the growing season were obtained from the Food and Agriculture Organization's Irrigation and Drainage Papers 33 and 56 (Allen et al. 1998; Doorenbos and Kassam 1979). Rainfed crop water supply is effective precipitation (P_e), which is monthly precipitation adjusted for drainage qualities of the soil and then capped at ET_c levels. P_e is calculated from monthly precipitation data following the methodology from the Food and Agriculture Organization's *Irrigation Water Management Training Manuel no. 3* (Brouwer and Heibloem 1986). Next, we calculate the annual ratio of effective precipitation (P_e) and crop water need (ET_c) by grid cell for each crop and then multiply these results by the corresponding annual yield response coefficient (K_y), as presented in the equation below, following the approach from the Food and Agriculture Organization's Irrigation and Drainage Paper 66 (Steduto et al. 2012). Maximum crop

[7] https://www.fao.org/aquacrop/overview/whatisaquacrop/en/

evaporation assumes no water constraints, whereas actual evapotranspiration is reduced based on available rainfall, which allows for the calculation of actual yields (Y_a), as a deficit from non-water-constrained yields (Y_x). For K_y values below one, crop yields fall below the water deficit, whereas for K_y values greater than one, yield losses are relatively greater than the water deficit.

$$\left(1 - \frac{Y_a}{Y_x}\right) = K_y\left(1 - \frac{P_e}{ET_c}\right)$$

Figure B96 illustrates the relationship between mean monthly precipitation and resulting annual yield response following the approach described above, for 6 different levels of mean monthly potential evapotranspiration (PET). For a given potential evapotranspiration level, higher precipitation volumes result in higher yield responses. When potential evapotranspiration is low, less precipitation is required to reach the maximum yield response (i.e., 1)

FIGURE B96. RELATIONSHIP BETWEEN PRECIPITATION AND CROP YIELD RESPONSE

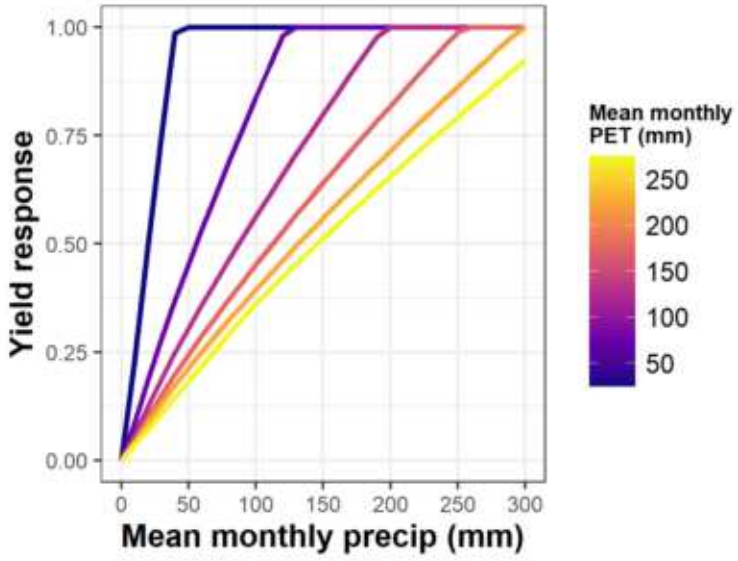

For irrigated crops, the analysis is completed by crop at the water system model's resolution. The agricultural demand modeling uses the following inputs: shapefiles of the irrigated areas in the country or the total irrigated hectares of each basin, historical withdrawals, crop irrigation water use, different irrigation technology mix and system-wide irrigation efficiency. Specific data on irrigation technologies or devices (e.g., sprinkler, drip, or flooding irrigation) are considered when possible. Water requirements by crop are determined following the same approach from the Food and Agriculture Organization's papers 56 and 66 as for rainfed crops (described above), obtaining per-hectare estimates of millimeters of water required. Irrigation water requirements correspond then to the balance of water required to meet crop demands after accounting for effective precipitation supply (P_e) and considering crop water needs (ET_c), monthly crop coefficients (K_c), and growing calendar. Irrigation water requirements are then translated to water withdrawals by river basin based on total hectares of irrigated cropland and basin-level irrigation efficiencies. To evaluate the impacts of climate change on irrigated crops,

the resulting unmet water demands at a basin scale from the water system model are used to quantify reductions in crop yields, as done for rainfed crops.

Next, a yield impact from temperature (K_s) is calculated based on daily maximum temperatures, determined by crop-specific optimum temperatures and tolerance thresholds. The modeling starts by gathering optimum and maximum tolerance temperatures by crop from the Food and Agriculture Organization's Crop Ecological Requirements (ECOCROP) database (2015), which will determine at which temperature a crop will start experiencing damage until it suffers full loss. Crops are typically more vulnerable to heat during reproductive stages than vegetative stages. We consider the months during the flowering stage of crop development to determine the maximum temperature a crop is exposed to. These months are identified following the methods outlined in the Food and Agriculture Organization's Irrigation and Drainage Papers 33 and 56 (Allen et al. 1998; Doorenbos and Kassam 1979). Temperature yield responses (K_s) are estimated based on a logistic relationship between temperature and maximum attainable yields, as indicated in the equation below and illustrated in Figure B96 for an illustrative threshold of 35°. T_{opt} is the optimum temperature above which crop yields start decreasing; T is the maximum daily temperature, and B and v are factors that are calibrated for each crop based on its tolerance thresholds. Results range from 1 to 0, where 1 represents no stress and zero represents total crop failure.

$$K_s = 1 - \frac{1}{(1 + e^{-B(T-Topt)})^{1/v}}$$

FIGURE B97. ILLUSTRATIVE RELATIONSHIP BETWEEN TEMPERATURE AND YIELD RESPONSE

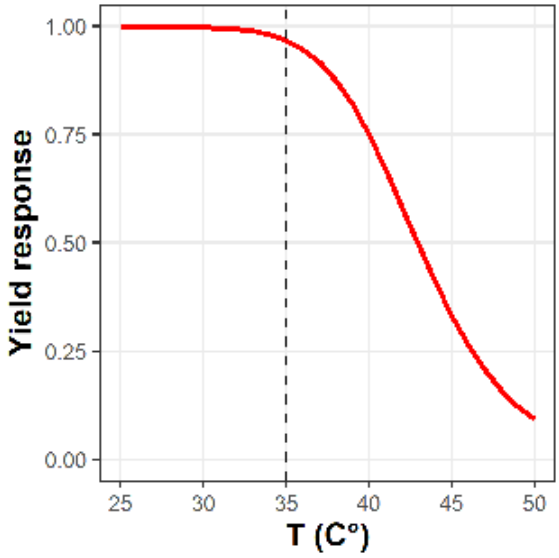

Temperature effects are typically experienced after consecutive days of exposure. For each day during the flowering period, we consider the lowest effect between the daily effect on t, t-1, and t-2 from the equation above. Major food crops, such as wheat, sorghum, maize, and oil crops start experiencing the effects of heat after three consecutive days of exposure (Wahid et al. 2007; Nuttall et al. 2018; Hatfield and Prueger 2015; Gourdji et al. 2013). We utilize the highest 3-day effect across the entire flowering period as the annual temperature effect on yields for all crops.

Temperature impacts the potential yield of crops during the flowering stage, while precipitation impacts the resulting production, therefore producing multiplicative effects. Hence, water availability and temperature shocks are then combined into a single shock by crop. Grid cell level shocks are aggregated nationally based on the spatial distribution of crop production from available sources. Crop-specific shocks are also aggregated into a total production shock using crop revenues as weights.

Limitations

- We consider a subset of all crops grown in the country, which necessarily excludes some crops.
- Additional effects from agricultural practices, soil characteristics and conditions, fertilizer use, and other climate variables (e.g., wind speed or radiation) are not considered in the model.
- Both water and temperature coefficients are taken from existing literature for representative varieties of each crop. Whether local varieties have different levels of tolerance is not considered in this study.
- We consider heat exposure for crops during the hottest 3-day period during the flowering stage, which is the time at which crops are most sensitive to heat. However, shorter episodes of extreme heat as well as longer periods of consistently high temperatures can result in additional yield losses or potential crop failure. In addition, crop biomass could suffer from heat exposure in other stages of development, however, these effects are not considered.
- The start date and length of the crop's growing seasons are assumed to be static over time. However, farmers may adjust growing patterns based on short-term weather forecasts.
- An assessment of the implications of deteriorating water quality and increasingly saline soils on water demands in future years is not included. The decrease in water quality could likely either further reduce water reuse practices or cause productivity impacts.
- Reservoir volumes are assumed to remain constant at reported levels, with limited effects from sedimentation considered. This assumption may overestimate water storage availability over the next 40 years.

B.3.3 EROSION

Soil erosion is a major concern in many countries. Erosion can be detrimental to landscapes, impacting plant and animal life, reducing the efficacy of reservoir storage and hydropower production through sedimentation, and causing declines in agricultural production by removing valuable nutrients from the topsoil, which may be made worse if climate change intensifies future rainfall intensity. In addition, Nambajimana et al. (2020) find a correlation between higher poverty levels and estimated erosion rates.

To determine erosion rates, we use the Revised Universal Soil Loss Equation (RUSLE) developed by the United States Department of Agriculture (Wischmeier and Smith 1978) and

revised by Renard et al. (1997). This equation is the most widely used approach to estimate erosion and soil loss rates and has been used in Rwanda (Nambajimana et al. 2020), Uganda (Karamage et al. 2017), and many other nations worldwide (Panagos et al. 2017). For information on the uncertainties of the Revised Universal Soil Loss Equation approach, see Alewell et al. (2019) and Benavidez et al. (2018). Soil erosion estimates are converted into crop yield losses following an approach developed by the Food and Agriculture Organization (Kassam et al. 1991).

Methodology

The Revised Universal Soil Loss Equation calculation requires five key inputs, which are shown below. A is the soil loss and R is rainfall-runoff erosivity (i.e., the potential of rainfall to cause erosion by generating runoff). K and LS are static climate and land factors, while C and P are activity and farm-level management factors. The following outlines the data sources and approaches used to determine each of these parameters.

$$A = R * K * LS * C * P$$

Estimating the revised rainfall-runoff erosivity (R) requires highly temporally detailed (30 min) rainfall records for a variety of storm events. However, many methods have been developed to approximate R. Two datasets are used to determine the rainfall-runoff erosivity: we use a historical dataset of R factors from Panagos et al. (2017), and adjust for future climate scenarios using Lo et al. (1985).

The soil erodibility factor (K) correlates with soil properties (i.e., fraction of sand, silt, clay, and organic carbon). The K-factor was estimated using the relationship between soil properties and K developed by Williams (1995).

The slope and slope length (LS) factor is a product of slope length (L-factor) and slope steepness (S-factor). The L-factor was computed following the method proposed by Desmet and Govers (1996) while the algorithm recommended by McCool et al. (1989) was used to calculate the S-factor.

The C-factor determines the impact of land cover and management practices on the magnitude of soil erosion. The equation proposed by Durigon et al. (2014) is used here to approximate the C-factor. This requires land cover data, which was sourced from the biweekly mean MODIS (or Moderate Resolution Imaging Spectroradiometer) normalized difference vegetation index (NDVI) provided by the National Aeronautics and Space Administration (NASA 2022).

Lastly, support practices (P) reflect erosion-reducing practices employed by farmers and vary by conservation support practices such as contouring, strip-cropping, and terracing. Although all three of these practices can be implemented, a generic P-factor is used that was recommended by Wischmeier and Smith (1978), which varies with slope.

Generally, areas that are impermeable (e.g., rocky surfaces or waterbodies) and areas with mean slopes that exceed 20 percent are excluded from the analysis because erosion on these surfaces tends to be low or highly uncertain with the Revised Universal Soil Loss Equation approach.

As noted, soil loss can reduce the nutrients available to crops, if not replenished by fertilizers, by eroding the topsoil. Although topsoil is generated naturally, natural generation is slow, usually

less than 1 mm/year, or roughly 12t/ha, depending on soil density (Hammer 1981; Hudson 1981). To approximate the impact this has on the major crops, we use a method developed by the Food and Agriculture Organization (Kassam et al. 1991). The approach is based on a tolerable loss rate over time and varies by levels of inputs (high, intermediate, and low) as well as the susceptibility of soils to productivity loss. We use global raster data of fertilizer use (nitrogen and phosphorus) from the Global Agricultural Inputs dataset to determine the level of input in a country (Potter et al. 2010).

Limitations

- While this approach is appropriate for a nation-level assessment, the methods rely on satellite-derived datasets. For farm-level analysis, more detailed data on farm practices, soils, rainfall erodibility, slope, and other locally derived information will provide a more accurate estimate of farm-level erosion.
- Although outputs from state-of-the-art global climate models are used in this analysis, these models are not able to accurately estimate changes in extreme events such as heavy rainfall that can cause significant soil loss in a short period of time. The Revised Universal Soil Loss Equation approximates soil loss on short time scales (half-hour), but changes in precipitation on these time scales are beyond the scope of global climate models.
- Erosion causes the depth of the soil layer to deplete over time. The depth to bedrock or other semi-impervious ground content (such as heavy clay) may significantly reduce the rooting depth that crops can achieve during the growing season. Shallower rooting depths reduce the soil water available to crops, which then reduces crop yields and eventually renders crop fields unusable. This effect was not evaluated in this study.
- Production decreases in response to topsoil loss from this approach are not crop-specific.

B.3.4 HYDROPOWER

Climate change may impact hydropower generation directly through a reduction in river runoff and reservoir levels, and indirectly through changes in the water demands for competing uses (e.g., irrigation). These nexus effects are modeled through the water systems model presented above. To estimate the effect of climate change on hydropower production, the following reservoir balance approach is applied to each catchment:

$$Storage_m = Inflows_m - Release_m - Spill_m + Storage_{m-1} - Evap_m$$

where storage is the volume of water in the reservoir each month, inflows are upstream runoff, releases are allowed to flow out of storage to meet demands, and spill is any excess outflow over and above releases that is needed to keep the reservoir volume below its maximum.

This channel evaluates changes in hydroelectric energy under the selected climate scenarios, as well as relevant policy and infrastructure interventions being explored (e.g., new reservoirs and powerplants). Monthly hydropower generation (in GWh) is produced as model output and an

evaluation of climate change impacts is carried out by comparing the baseline production across the different scenarios.

Methodology

Hydropower generation is a function of flow through the turbines and potentiometric water head each month. To convert reservoir storage to hydropower generation (including for run-of-river facilities) requires a volume-elevation curve to relate volume to head, as well as turbine elevations, maximum turbine flows, turbine efficiencies, minimum turbine flows, and capacity factors. We gathered these data from local sources where possible, and where no local data was available, we made assumptions based on similar facilities elsewhere. If missing, turbine flow capacity was extrapolated using the hydropower production equation:

$$P = Q * h * \eta * g * \rho$$

where P represents power capacity in megawatts (MW), Q the flow rate or turbine flow (m3/s), h the net head or usable fall height (m), η the turbine efficiency (assumed to be 0.9), g the acceleration from gravity (9.81 m/s²), and ρ the water density (~ 1000 kg/m3).

Modeled runoff data for each scenario serve as input into the reservoir balancing model. Potential evapotranspiration is one of the key inputs to runoff models, and represents the amount of water lost through evaporation and transpiration, assuming that sufficient water is available over the period in question. Monthly potential evapotranspiration was calculated using the modified Hargreaves method (Droogers and Allen 2001), which relies on precipitation, temperature, and average daily temperature range data, along with the latitude of the basin centroid, which is used to estimate solar radiation.

Data on reservoir storage, demand, and outflows were gathered from local sources, where available. In cases where these data were not readily available, international datasets on reservoir storage were used in combination with documented techniques to approximate both agricultural and non-agricultural water demands (e.g., irrigated areas/crops combined with climate information for irrigation, gridded population for domestic and industrial use). This same approach was also used for other key assumptions, which include: turbine flow and position, volume-elevation curves, generation assumptions for plant capacity factors (representing the percentage of each month that the plant is running), generation efficiency (i.e., the overall operation effectiveness in converting the energy of the falling water into electricity), energy demands, and value of electricity. Generally, the values were extrapolated from other reservoirs or hydropower facilities with available data, assuming a similar behavior.

An example of a reservoir-hydropower scheme is presented in Figure B_. The figure shows two reservoirs (green triangles). If the reservoir is dedicated to hydropower production, the node will utilize the assumptions on physical characteristics (e.g., storage capacity, initial storage, volume-elevation curve, etc.) and hydropower-specific characteristics (e.g., turbine flow capacity, tailwater elevation, plant factor, efficiency, etc.) to calculate the total generation over a period of time.

FIGURE B63. ILLUSTRATION OF RESERVOIR SCHEMATIC IN WEAP

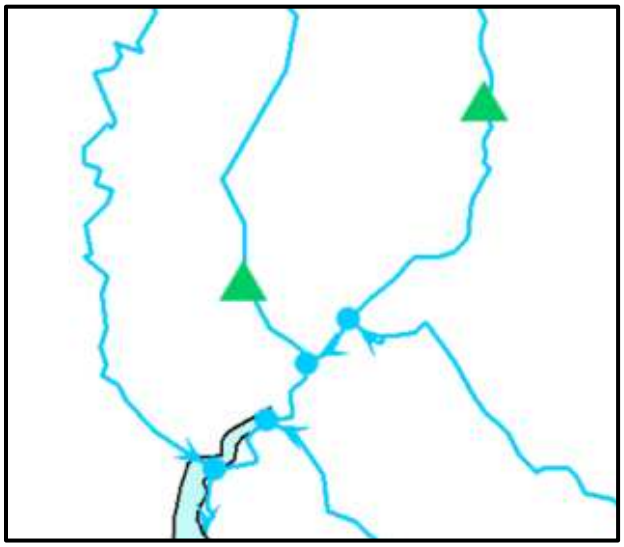

Limitations

- The delineation and resolution of basins are based on the best available river runoff data. Such planning scale data can be too coarse to catch the full range of complexities in sub-catchments as well as in national water systems.
- Actual water allocation to users is complex and water system models simplify these into priorities or decision rules, particularly when available water is scarce. Actual water levels in reservoirs that generate hydropower may differ from reality.
- The monthly time step assumes water can be allocated efficiently within a month and does not account for fluctuations in reservoir levels from either inflow or hydropower generation during peak demand hours or days (e.g., weekend vs weekday). Monthly water system models tend to miss smaller time-scale unmet demands that can particularly impact domestic or industrial water users.

B.4 INFRASTRUCTURE AND SERVICES

Climate change is likely to impact infrastructure, and the services provided by it, by increasing the frequency and magnitude of extreme events that result in damages to assets, as well as by increasing deterioration caused by heat and precipitation levels. We model these effects through the following channels:

- **Inland flooding:** which models damages to capital across the country from changes in the magnitude and frequency of riverine (fluvial) flooding events.
- **Sea-level rise and storm surge:** which shocks coastal capital from increases in mean sea-level as well as changes in the frequency and magnitude of storm surge events.

- **Tropical cyclones:** which models damages to capital across the country from changes in the recurrence and magnitude of tropical cyclones.
- **Tourism:** which considers a shock to tourism revenues due to damages and disruptions to tourism infrastructure from extreme events, as well as from changes in overall climatic conditions.

Infrastructure and capital stock model

Various biophysical models will be used to estimate the hazard and the damages on each individual infrastructure channel. The exposure and vulnerability of assets are determined by three key variables: the geospatial location, the type or sector of the asset, and the total value of the asset. We developed a common asset location and value layer that served as the basis for the calculation of damages and impacts. Asset values are determined at a national scale based on data or estimates of total capital value from gross domestic product. Total capital stock value is estimated by dividing gross domestic product data by the capital-output ratio of the country or region (i.e., the ratio of the total economic output generated for each unit of invested capital). Capital-output ratios are used as an indicator of the efficiency of an economy, with lower values indicating high productivity and lower capital requirements to achieve additional growth. If local information is not available, national capital stocks and output-ratios are obtained from the International Monetary Fund's Investment and Capital Stock Dataset (IMF 2021). Then, sectoral as well as spatial breakdowns are modeled using the best available information from local sources, which typically is available by province, district, or similar administrative boundaries.

In cases where these data are unavailable, we estimate the spatial distribution using proxy high-resolution data such as land use land cover data from the Copernicus Fractional Land Cover dataset (Buchhorn et al. 2020), gridded population data from WorldPop of the University of Southampton (Bondarenko et al. 2020b; 2020a), gridded gross domestic product data from Wang and Sun (2022), value of crop production from the Food and Agriculture Organization's Global Agro-Ecological Zones project (GAEZv4) (Fischer et al. 2021), and shapefiles of specific infrastructure types (e.g., residential, industry, transport) from the Humanitarian OpenStreetMap Team geospatial data (HOTOSM 2020).

B.4.1 INLAND FLOODING

Flooding events disrupt daily life and cause damage to infrastructure and physical capital. Climate change may exacerbate flooding by increasing the frequency, intensity and duration of storm events. This analysis relies on projected changes in the return interval of peak precipitation events from the World Bank's Climate Knowledge Portal. Flood hazard maps are developed to determine areas with a certain probability of flooding for a given baseline and climate change projected return period. The outputs of flood hazard mapping include the extent and depth of flood inundation, which are then used to estimate damages to infrastructure.

The analysis is done for the available eras, recurrence intervals, climate scenarios in the Climate Change Knowledge Portal for changes in the annual exceedance probability of the largest 1-day precipitation relative to history, at a spatial resolution determined by the available hydrology and asset distribution data. An era refers to a period of time with distinct characteristics or patterns, for example, a decade or a 30-year period. The eras considered are 2010-2039 (centered in

2025), 2035-2064 (center 2050), and 2060-2089 (center 2075). The modeling considers a combination of the probability of occurrence of 5, 10, 20, 25, 50 and 100-year return period events. The resulting outputs are aggregated to a national scale, and correspond to the expected share of assets damaged relative to a historic baseline (1995 to 2020).

Methodology

The first step in the process is to model runoff from historical daily precipitation data for a range of return periods using the TR-20 approach, which relies on curve numbers to estimate the amount of runoff. Curve numbers are an empirical parameter developed by the United States Department of Agriculture (USDA) Soil Conservation Service that represent the ability of the surface to absorb rainfall before rainfall occurs, depending on the land use, soil type, and moisture conditions. For this process, curve numbers are determined for each catchment, then, estimating runoff as the excess between rainfall and soil infiltration. Figure B98 illustrates the relationship between precipitation (P) and runoff (Q) for different curve numbers. Next, peak flows in cubic meters per second (m3/s) are estimated for each catchment and used to generate a hydrograph. Projected future runoff is calculated by applying the change in the annual exceedance probability for each scenario from the Climate Change Knowledge Portal to historical precipitation, and recalculating runoff.

FIGURE B98. CURVE NUMBER MODEL

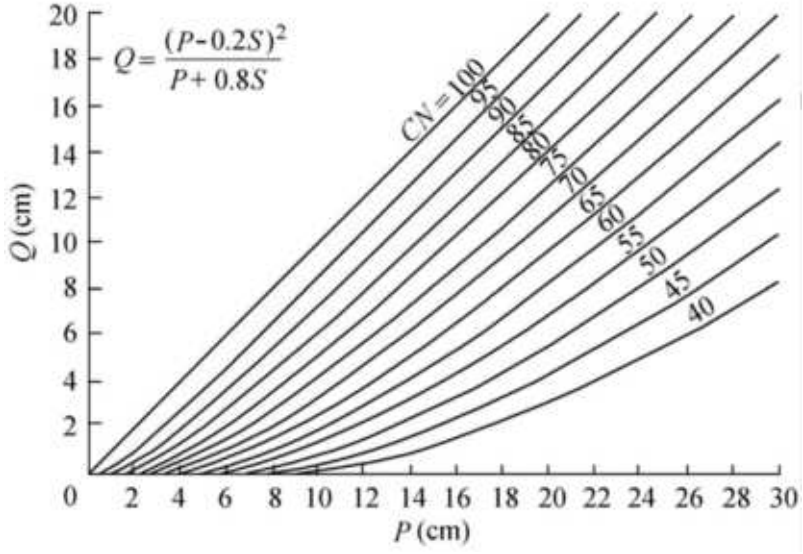

For the next step in this process, we utilize the HydroRivers geospatial dataset (Lehner and Grill 2013), which contains a vectorized river network for the globe, to estimate floodplain boundaries as buffers around river centerlines. We model river flows from the modeled runoff data using the Muskingum-Cunge method of flood routing (Ponce 2014), which considers routing parameters based on hydraulics to simulate accumulating flows as water moves from upstream to downstream over time. Brunner and Gorbrecht (1991) present an application of this method. Figure B99 presents a schematic of this process. The HydroBasin data is used to develop a stream network from the pour point at the ocean all the way upstream, which could extend

beyond the country borders. Peak discharge time increases and peak flows decrease as flow is routed downstream (see the right diagram for nodes 45, 48, and 49).

FIGURE B99. ROUTING OF HYDROGRAPHS SCHEMATIC

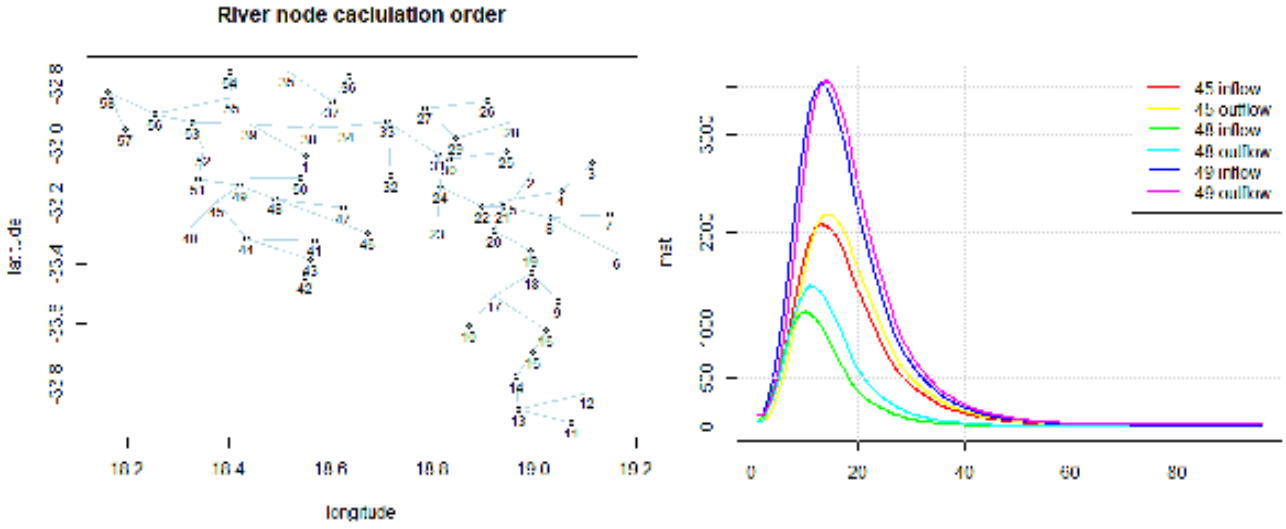

Next, we identify those floodplain areas within which assets are subject to damage. We calculate a bankfull river width (i.e., the surface width at a bankfull river stage) for each river link using the equation developed by Allen et al. (1994). For calculating bankfull widths, we consider the streamflows that are exceeded by 10 percent of the observed records (i.e., q10 flows). Then, we calibrate floodplain extent based on floodplain-to-width of stream ratios developed by Bhowmik (1984), which take into account stream order. The stream order value indicates the river ordering from sink to source, with downstream rivers having lower floodplain-to-width ratios. For each climate scenario, flood widths are next converted into flood depths within the identified floodplain. Depths are calculated for each stream reach using a triangular arithmetic approach based on widths obtained from the routing model, a rectangular cross-section, and Manning's equation which relates flow rate, velocity, and depth of water in a river as shown below:

$$Q = \left(\frac{1}{n}\right) * A * R^{\frac{2}{3}} * \sqrt{S}$$

Where Q represents the flow rate (m^3/s), n the Manning's roughness coefficient (dimensionless), A a cross-sectional area of flow (m^2), R the hydraulic radius (m), and S the channel slope (m/m).

Flood hazard maps are finally produced for the various scenarios and used as the basis for quantifying capital losses. Depths for each section of the floodplain are then combined with depth-damage functions to estimate the total share of infrastructure that is damaged in a particular flood event. Damage functions describe the relationship between the level of asset damage and the flooding depth. The maximum flood damage to an object can be computed as a certain damage factor multiplied by the total dollar value of the object. Global flood depth-damage functions are available by region and state defined for water depths between 0 and 6 meters (Huizinga et al. 2017). Figure B100 shows an illustration of available depth-damage functions from Huizinga et al. for agricultural, commercial, and residential capital, for three different regions of the world. We calibrate these depth-damage functions by assuming that, for

each catchment, infrastructure is built to withstand the historical 10-year event, hence experiencing no damage at the corresponding flood depths.

FIGURE B100. DEPTH-DAMAGE FUNCTIONS

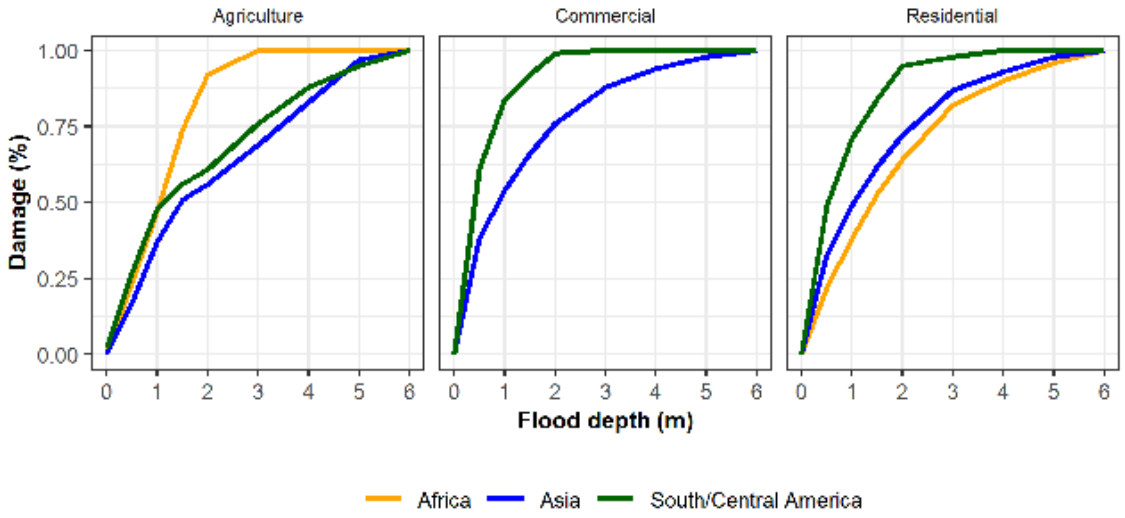

Lastly, we estimate the resulting damage from rainfall events of the return periods available in the climate data (i.e., 5, 10, 20, 25, 50, and 100-year events) for every catchment by overlaying capital value data by the percent damage from the damage function according to the estimated flood depth. The overlap between the floodplain and capital represents the total exposed assets, while the multiplication of its values and the percent loss from the damage function returns the absolute loss. Total expected damage (i.e., the damage times the probability) is also quantified by summing the total area under the damage-exceedance probability curves presented above and multiplying by the total exposed assets within each basin. Final results are aggregated nationally, weighted by the share of assets within each basin, representing the total damages to the country.

Limitations

- The analysis considers the flooding impacts from single-day extreme rain events within the region. Flooding may be caused by longer periods of continuous rain. These effects are not considered in this study.
- Detailed modeling and high-resolution terrain data would be required to estimate more accurate depths at a given location.
- We are not able to calibrate and verify the model output fully, in some cases, due to a lack of available records collected during major flood events. Project-scale analysis and modeling should be used to evaluate and verify these results when available.
- More complex numerical hydrologic models are available but require extensive input and field measurements to ensure accuracy.
- Asset values are proxied using the best available information on localized gross domestic product and capital-output ratios, and damages are quantified using generic

depth-damage curves. Localized damages to a particular building may differ from these estimates depending on actual infrastructure conditions, flood depth and infiltration, or location of critical inventory such as mechanical and electrical equipment.

- Capital value is estimated using high-level (e.g., for a whole country or sector) capital-output ratios, which assume the same levels of productivity and conditions of capital. Local values may differ from this estimate due to differences in the type of the physicality of capital (i.e., different types of infrastructure), age, depreciation levels, sectors, and overall conditions and context.

B.4.2 TROPICAL CYCLONES

Tropical cyclones and hurricanes can have substantial economic consequences. We model the impacts of cyclones using an approach previously applied to the island of Mauritius, in which a large number of synthetic hurricane tracks are generated. We collaborated with WindRiskTech, led by Massachusetts Institute of Technology Professor Emeritus Kerry Emanuel, who pioneered this technique, with detailed methods provided in Emanuel et al. (2006) and Emanuel et al. (2008). For each of these tracks, we then run a deterministic, coupled numerical model to simulate the storm intensity. Incremental damages to capital value relative to the baseline period are then estimated. Shocks are calculated for specific infrastructure types based on available data on the value and location of assets for a set of eras and Shared Socioeconomic Pathway ensembles available from the WindRiskTech data. These include track ensembles for eight climate models (CESM2, CNRM6, ECEARTH6, IPSL6, MIROC6, MPI6, MRI6, and UKMO6), four time periods including a historical or "hindcast" ensemble and three future ensembles (1995-2015, 2021-2040, 2041-2060, and 2081-2100), and two SSPs (SSP2-4.5 and SSP3-7.0).

Methodology

Cyclone event generation begins by randomly seeding a given ocean basin with weak tropical cyclone-like disturbances, and using our intensity model to determine which one of these develops to tropical storm strength or greater. Tracks can be generated globally, or for a specified ocean basin, and filters can be applied to the track generator to select tracks coming within a specified distance of a point or region of interest (for example, a city or county) or passing through any of a set of user-specified line segments. In filtering the tracks, a record is kept of the number of discarded tracks and this is used to calculate the overall frequency of storms that pass the filter. Once the cyclone tracks have been generated, a coupled hurricane intensity model is then run along each of the selected tracks to produce a history of storm maximum wind speed. This model uses monthly climatological atmospheric and upper ocean thermodynamic information but is also affected by ambient environmental wind shear that varies randomly in time. Figure 66 shows an ensemble of 800 tracks and the max wind speed (in knots) at each point along its path, for the 2041-2060 era and SSP3-70. This includes tropical cyclones from all of the eight climate models.

FIGURE B101. ENSEMBLE OF TROPICAL CYCLONE TRACKS AND MAX WIND SPEEDS (KNOTS)

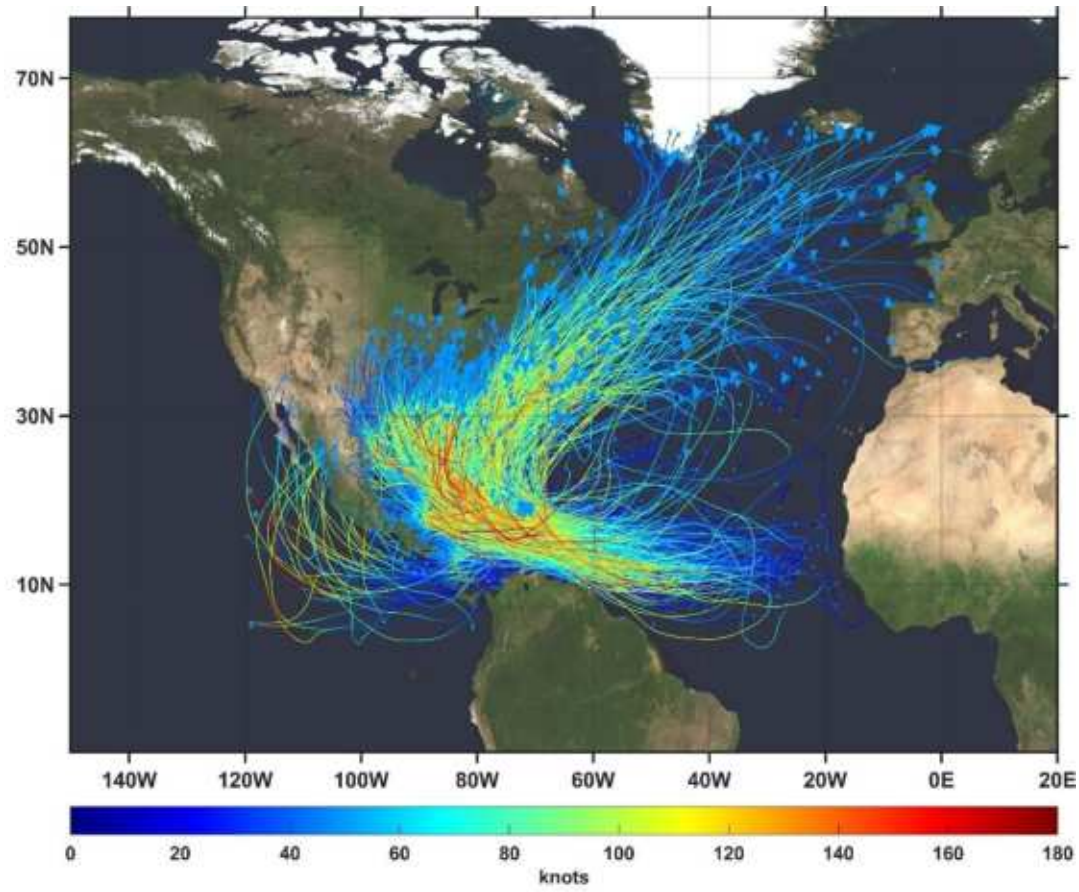

The coupled deterministic model produces a maximum wind speed and a radius of maximum winds, but the detailed aspects of the radial storm structure are not used, owing to the coarse spatial resolution of the model. Instead, as a post-processing step, we use idealized radial wind profiles, fitted to the numerical output, to estimate maximum winds at fixed points in space away from the storm center. For each point of interest, the intensity model is run many times to produce desired statistics such as wind speed exceedance probabilities for that point. Both the synthetic track generation method and the deterministic model are fast enough that it is practical to estimate exceedance probabilities to a comfortable level of statistical significance. Changes in exceedance probabilities are then translated into increases in tropical storm damages, which are utilized as shocks to the macroeconomic model.

Wind speed damage is estimated for a series of grids across the country using the peak wind speed for that grid for each tropical cyclone. These peak wind speeds are translated to damage using an established wind-to-damage relationship first introduced in Emanuel et al. (2012), where 50 knots is the peak wind speed at which damage begins. Peak wind speeds below this threshold result in zero damage for that event. This wind-to-damage relationship is summarized below.

The fraction of the property value lost (f) is estimated as

$$f = \frac{v^3}{1 + v^3}$$

where *v* is a function of peak wind speed, *V,* when *V* is greater than 50 knots.

$$v = \frac{[V - 50]}{60\ knots}$$

This relationship produces an S-curve shape as shown in Figure B102.

FIGURE B102. RELATIONSHIP OF PEAK WIND SPEED TO PROPERTY DAMAGE (EMANUAL 2012)

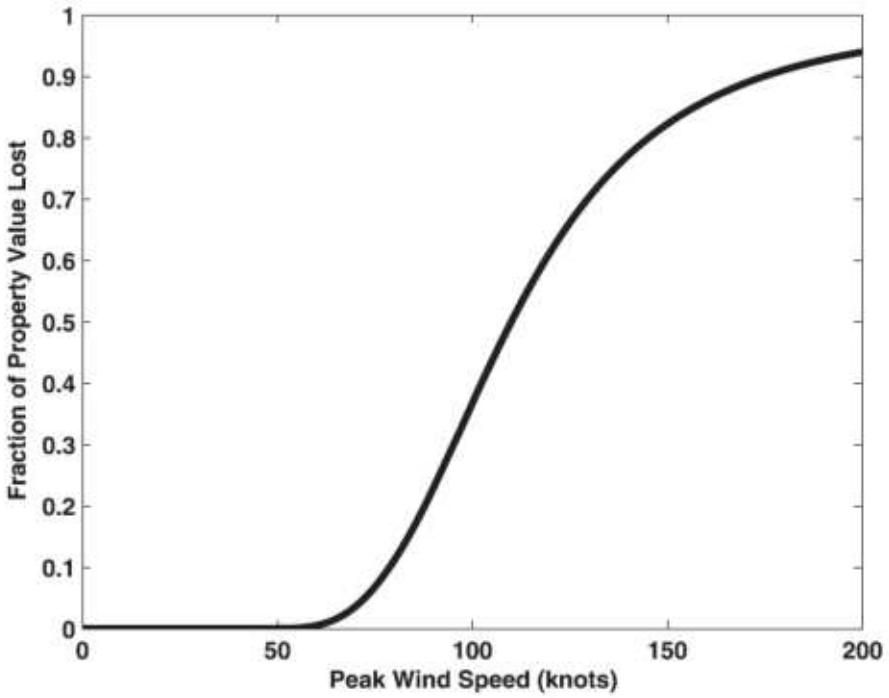

Relative capital value at each grid is estimated similarly to other impact channels, where a gridded layer of GDP is overlaid on a land cover map to determine the relative value of built-up areas and buildings within each evaluation grid.

Limitations

- Tropical cyclones are highly uncertain and while this approach makes use of the most advanced numerical representation of downscaled, global climate model-specific, tropical cyclone tracks and characteristics, the results are still uncertain and offer a wide range of possibilities for the future.
- Wind and precipitation damage assessments are also highly uncertain and depend on decisions made in the construction process as well as a natural degradation of structural integrity over time.
- Actual damage and impacts of tropical cyclones will change depending on the time between events. For example, a second hurricane in the same month will impact how evacuations occur and how buildings with existing damage will be impacted in the second event. We do not take these effects into consideration.

- Capital value is estimated using high-level (e.g., for a whole country or sector) capital-output ratios, which assume the same levels of productivity and conditions of capital. Local values may differ from this estimate due to differences in the type on the physicality of capital (i.e., different types of infrastructure), age, depreciation levels, sectors, and overall conditions and context.

B.4.3 SEA-LEVEL RISE AND STORM SURGE

Rising mean sea levels and temporary flooding from storm surge events threaten coastal infrastructure and land. This analysis uses a GIS to estimate the share of assets (i.e., capital and land) inundated under various sea-level rise scenarios. Note that this analysis does not conduct a detailed geospatial analysis of coastal infrastructure and erosion impacts. The analysis is conducted at 30m by 30m spatial resolution and uses sea-level rise projections from the Coupled Model Intercomparison Project 6, available via the National Aeronautics and Space Administration's Sea Level Projection Tool (Gerner et al. 2021). While the ensembles used to assess this impact channel match the climate scenarios utilized in other channels, outputs for individual global climate models are not available. For that reason, we model the 50th and 80th percentile of the available Shared Socioeconomic Pathways (including SSP1-1.9, SSP1-2.6, SSP2-4.5, SSP3-7.0, SSP5-8.5) to consider more extreme projections within the ensemble statistics. These sea level projections are available in 10-year increments from 2020 to 2100 but interpolated to develop sea level changes for each year, the time step of this analysis.

Methodology

The analysis starts by obtaining elevation data for coastal regions of the country from the ASTER Global Digital Elevation Model (NASA, METI 2019). This dataset has a 1m vertical resolution and is considered an accurate elevation model. In order to capture increases in sea level lower than 1m, we interpolate the DEM to approximately a 1cm vertical resolution.

The mean sea level is indicated in the DEM by a value of zero. From there, the total water level, from where built infrastructure and urbanization typically starts, is constructed by incorporating tides, storm surges, and wave runup. We calculate tide and surge based on the mean maximum daily tide height from historical tide gauge records for at least 15 years, gathered from the University of Hawaii's Sea Level Center (Caldwell et al. 2015). Figure B103 shows the mean daily extreme water levels i.e., the water level above the mean higher high water (MHHW) height of each tidal day observed for an illustrative station. We consider an additional 30 cm (1 ft) as a standard buffer to account for wave runup and high tide events.

FIGURE B103. MEAN DAILY WATER LEVEL EXTREMES (LEVEL ABOVE MEAN HIGH-WATER

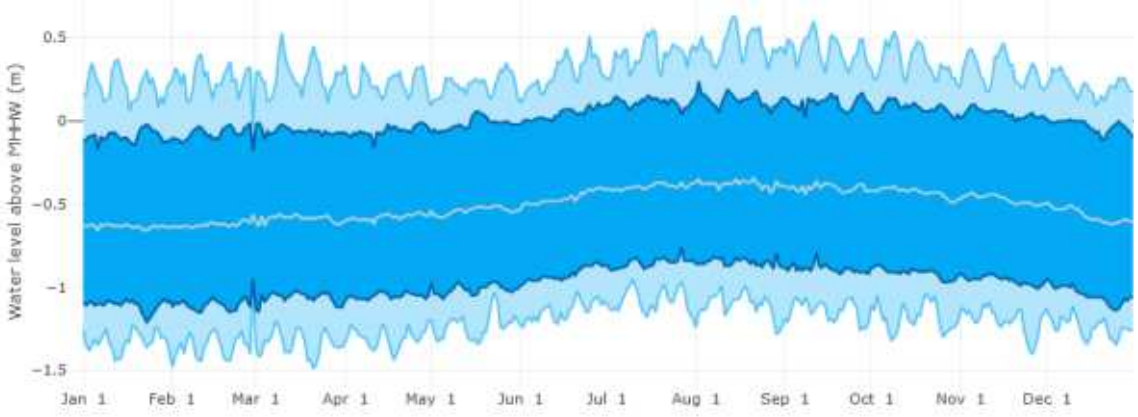

Coastal flood inundation extent and depth are approximated using a simplified bathtub approach, which does not take into account wave heights, hydraulic connectivity, or dynamic flow patterns, and is commonly used in areas without detailed topography and historical records of flood extents. This approach overlays sea level heights onto the topography by comparing the elevation of the sea or surge height to the elevation of the land and calculating the area inundated (i.e., with land elevations below the sea elevation or surge height inundated). To estimate the value inundated, we first establish a buffer along the coast where we assume there is no valuable infrastructure that is also vulnerable to flood damage. This buffer is established at elevations between mean sea level and the high tide mark of the 2-year return period event. After this no-value buffer, the relative infrastructure value at each elevation contour is determined using the area inundated overlayed onto a gridded GDP dataset that is used to estimate the relative value of capital loss. Finally, we intersect the inundated areas resulting from discrete sea level rise increments with the asset classes of interest to estimate the share that gets inundated. We then apply the sea level rise projections, interpolating the percent damages for each particular sea-level rise increment.

Storm surge impacts follow a similar approach as the impacts from sea level rise. The main difference is the use of a historical storm surge height above mean tidal levels to estimate the flood extent and depth of a storm surge event. Here we either rely either on literature sources that have already determined the storm surge heights above mean tidal levels for specified return period events (e.g., the 100-year or 1 percent annual storm event) or we use a global reanalysis dataset of relative storm surge heights estimated at discrete points along the coastline (Muis et al. 2016). Just as in the sea level inundation estimate described above, we adjust the storm surge flood height with rising sea levels and estimate the extent and depth of the flood using a bathtub approach.

In contrast to the impacts of permanent inundation (i.e., from sea level rise), storm surge impacts are both temporary and repairable, even though the cost for repair can be substantial and potentially unaffordable for property owners. In this way, it is akin to inland flooding and we apply the same depth-damage functions from Huizinga et al. (2017) to estimate the repair costs of impacts on capital stock in the macroeconomic model. Without adaptation efforts, we assume the costs accrue as the annual expected damage from storm surge increases with sea level rise.

There are many adaptation options available to protect properties from storm surges, ranging from engineered hard structures like sea walls and higher building elevation, to nature-based solutions that can slow down wave velocities. Also, since the near-coast areas become more vulnerable to periodic flooding from storm surges as sea levels rise, some property-owners may choose to permanently abandon their properties or decision-makers may organize a larger-scale managed retreat.

Limitations

- The bathtub approach is a simplified model of coastal flood inundation and does not capture a hydrologic connection to the ocean. We control for this to some extent by limiting the evaluation to a coastal zone where we expect inundation to occur. The numerical models that outperform a simpler bathtub approach in storm surge flood extent and depth are complex and require extensive, detailed input and field measurements to achieve reasonable accuracy.
- The timing and extent that the mean sea level rises over the next century are uncertain because of the many global factors that contribute to the rising sea, including dynamic ice sheet melting, changes in the gravitational pull, earth crust rebounding, local vertical land movement, among many others. We handle this by evaluating a range of scenarios of sea level rise developed with state-of-the-art tools and probability estimates, with these estimates updated regularly as the science behind them continues to develop.
- Adaptation response decisions in the coastal zone are complex, particularly at the local level. Other adaptation considerations not captured in this study could include local zoning bylaws, future land use plans, the presence of development-supporting infrastructure, or proximity to sites with high cultural value.
- The analysis does not consider the effects of climate on storm surge activity. Estimating changes in rare coastal storm events usually requires complex numerical models of both the ocean and the atmosphere.
- Capital value is estimated using high-level (e.g., for a whole country or sector) capital-output ratios, which assume the same levels of productivity and conditions of capital. Local values may differ from this estimate due to differences in the type on the physicality of capital (i.e., different types of infrastructure), age, depreciation levels, sectors, and overall conditions and context.

B.4.4 TOURISM

Climate change may affect tourism through changes in the suitability or attractiveness of a particular location for travelers, hence shifting travel patterns across the globe. While cooler countries may benefit from additional tourist arrivals, warmer countries may see a decline. The analysis relies on estimates of total tourism revenues generated from domestic and international as well as from business and leisure travelers. We assume that only leisure travelers are exposed to climate change and that business travel is independent of climatic conditions, hence the attractiveness of a location only affects revenues from leisure travel.

Methodology

We utilize local data on the total number of travelers and revenue per traveler when available. In cases where this data is unavailable or incomplete, we utilize data from the World Travel & Tourism Council Country Profiles (WTTC 2022) and the United Nations World Tourism Organization (UNWTO 2021) to estimate the size and breakdown of tourism revenues. Then, we distribute revenues from international leisure travelers to 0.5 x 0.5 degree grid cells in the country using the location of points of interest from the Humanitarian OpenStreetMap Team geospatial data (HOTOSM 2020), as well as available literature that accounts for high-revenue touristic sites that may be overlooked in the OpenStreetMap data (e.g., the point location of a major attraction may represent a higher volume of revenues than a relatively smaller site).

Impacts on leisure revenues due to changes in average climatic conditions are estimated following the approach developed by Hamilton, Maddison, and Tol (2005), which was also applied by Roson and Sartori (2016). Hamilton et al. identified the following functional relationship between mean annual temperature (T) and total visitor arrivals (A) and departures (D):

$$A = K_A \times e^{(\beta_1 \times T + \beta_2 \times T^2)}$$

$$D = K_D \times e^{(\gamma_1 \times T + \gamma_2 \times T^2)}$$

The K coefficients represent region-specific constants for all other factors beyond temperature, while β and γ are fixed constants that determine the relationship between T and arrivals and departures respectively. Figure B104 shows the shape of this coefficient. As seen in the figure, arrivals peak around 14° and decline as temperature increases, which indicates that international travelers prefer more pleasant (i.e., less hot) destinations. Departures reach a minimum at 19° and increase with higher temperatures following the same logic as international travelers.

FIGURE B104. FUNCTIONAL RELATIONSHIP BETWEEN TEMPERATURE AND ARRIVALS AND DEPARTURES

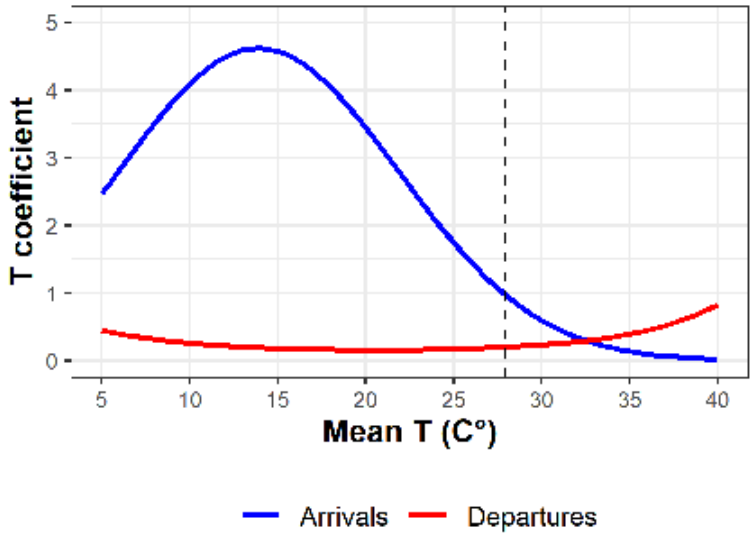

We consider the percent change in total arrivals as a proxy for the percent change in revenues from international leisure travelers. If available, we utilize seasonal or monthly visitation statistics to weigh monthly temperature and estimate a relevant mean annual temperate (i.e., a

temperature value that weighs higher in the months with higher demand) to quantify the change in arrivals. For changes in domestic leisure travelers, we consider the percent change in total departures, which results in a decrease in revenues from an increase in departures (i.e., as a region gets hotter, residents will prefer more pleasant locations elsewhere). This approach assumes that the mean revenues generated per traveler remain constant as temperatures change. A final tourism shock is calculated by aggregating the effect on international and domestic leisure revenues, assuming the fraction of revenues from business travel does not change.

Limitations

- There are additional biophysical effects derived directly or indirectly from climate change that may impact tourism at a local scale, such as algal blooms on bathing waters, vector or infectious disease outbreaks, increased erosion on sandy beaches, or losses in flora and fauna of interest. These effects are not considered in this study.
- While the analysis considers the effect on revenues from domestic and international tourism, changes in travel patterns within the country, for both domestic and international, travelers are not modeled.

Alewell, Christine, Pasquale Borrelli, Katrin Meusburger, and Panos Panagos. 2019. "Using the USLE: Chances, Challenges and Limitations of Soil Erosion Modelling." *International Soil and Water Conservation Research* 7 (3): 203–25. https://doi.org/10.1016/j.iswcr.2019.05.004.

Allen, Peter M., Jeffrey C. Arnold, and Bruce W. Byars. 1994. "Downstream Channel Geometry for Use in Planning-Level Models." *Journal of the American Water Resources Association* 30 (4): 663–71. https://doi.org/10.1111/j.1752-1688.1994.tb03321.x.

Allen, Richard G., Luis S. Pereira, Dirk Raes, and Martin Smith. 1998. "Crop Evapotranspiration - Guidelines for Computing Crop Water Requirements." FAO Irrigation and Drainage Paper 56. Rome: FAO - Food and Agriculture Organization of the United Nations. https://www.fao.org/3/X0490E/x0490e00.htm#Contents.

Benavidez, Rubianca, Bethanna Jackson, Deborah Maxwell, and Kevin Norton. 2018. "A Review of the (Revised) Universal Soil Loss Equation ((R)USLE): With a View to Increasing Its Global Applicability and Improving Soil Loss Estimates." *Hydrology and Earth System Sciences* 22 (11): 6059–86. https://doi.org/10.5194/hess-22-6059-2018.

Bhowmik, Nani G. 1984. "Hydraulic Geometry of Floodplains." *Journal of Hydrology* 68: 369–401. https://doi.org/10.1016/0022-1694(84)90221-X.

Bondarenko, Maksym, David Kerr, Alessandro Sorichetta, and Andrew Tatem. 2020a. "Census/Projection-Disaggregated Gridded Population Datasets, Adjusted to Match the Corresponding UNPD 2020 Estimates, for 183 Countries in 2020 Using Built-Settlement Growth Model (BSGM) Outputs." University of Southampton. https://doi.org/10.5258/SOTON/WP00685.

———. 2020b. "Census/Projection-Disaggregated Gridded Population Datasets for 51 Countries across Sub-Saharan Africa in 2020 Using Building Footprints." University of Southampton. https://doi.org/10.5258/SOTON/WP00683.

Brouwer, C., and M. Heibloem. 1986. "Irrigation Water Needs." *Irrigation Water Management* Training Manual 3. https://www.fao.org/3/s2022e/s2022e00.htm#Contents.

Brunner, Gary W., and Jurgen Gorbrecht. 1991. "A Muskingum-Cunge Channel Flow Routing Method for Drainage Networks." Davis, CA: U.S. Army Corps of Engineers.

Buchhorn, Marcel, B. Smets, L. Bertels, M. Lesiv, N-E. Tsendbazar, D. Masiliunas, L. Linlin, M. Herold, and S. Fritz. 2020. "Copernicus Global Land Service: Land Cover 100m: Globe (Version V3.0.1)." [Data set]. 10.5281/zenodo.3939050.

Caldwell, P. C., M. A. Merrifield, and P. R. Thompson. 2015. "Sea Level Measured by Tide Gauges from Global Oceans — the Joint Archive for Sea Level Holdings (NCEI Accession 0019568)." Version 5.5. NOAA National Centers for Environmental Information. doi:10.7289/V5V40S7W.

Caminade, Cyril, Jolyon M. Medlock, Els Ducheyne, K. Marie McIntyre, Steve Leach, Matthew Baylis, and Andrew P. Morse. 2012. "Suitability of European Climate for the Asian Tiger Mosquito Aedes Albopictus: Recent Trends and Future Scenarios." *Journal of The Royal Society Interface* 9 (75): 2708–17. https://doi.org/10.1098/rsif.2012.0138.

CDC. 2020. "Heat Stress." Centers for Disease Control and Prevention. 2020. https://www.cdc.gov/niosh/topics/heatstress/default.html.

Chen, Yirong, Alex R. Cook, and Alisa X.L. Lim. 2015. "Randomness of Dengue Outbreaks on the Equator." *Emerging Infectious Diseases* 21 (9): 1651–53. https://doi.org/10.3201/eid2109.141030.

Craig, M. H., R. W. Snow, and D. le Sueur. 1999. "A Climate-Based Distribution Model of Malaria Transmission in Sub-Saharan Africa." *Parasitology Today* 15 (3): 105–11. https://doi.org/10.1016/S0169-4758(99)01396-4.

Davis, Lucas, Paul Gertler, Stephen Jarvis, and Catherine Wolfram. 2021. "Air Conditioning and Global Inequality." *Global Environmental Change* 69 (July): 102299. https://doi.org/10.1016/j.gloenvcha.2021.102299.

Desmet, P. J. J., and G. Govers. 1996. "A GIS Procedure for Automatically Calculating the USLE LS Factor on Topographically Complex Landscape Units." *Journal of Soil and Water Conservation* 51 (5): 427–34. https://go.gale.com/ps/i.do?p=AONE&sw=w&issn=00224561&v=2.1&it=r&id=GALE%7CA18832564&sid=googleScholar&linkaccess=abs.

Doorenbos, J., and A. H. Kassam. 1979. "Yield Response to Water." FAO Irrigation and Drainage Paper 33. Rome: FAO - Food and Agriculture Organization of the United Nations.

Droogers, Peter, and Richard G Allen. 2001. "Estimating Reference Evapotranspiration Under Inaccurate Data Conditions." *Irrigation and Drainage Systems* 16: 33–45.

Durigon, V.L., D.F. Carvalho, M.A.H. Antunes, P.T.S. Oliveira, and M.M. Fernandes. 2014. "NDVI Time Series for Monitoring RUSLE Cover Management Factor in a Tropical Watershed." *International Journal of Remote Sensing* 35 (2): 441–53. https://doi.org/10.1080/01431161.2013.871081.

Ebi, Kristie L., Jessica Hartman, Nathan Chan, John Mcconnell, Michael Schlesinger, and John Weyant. 2005. "Climate Suitability for Stable Malaria Transmission in Zimbabwe Under Different Climate Change Scenarios." *Climatic Change* 73 (3): 375–93. https://doi.org/10.1007/s10584-005-6875-2.

Emanuel, Kerry, Fabian Fondriest, and James Kossin. 2012. "Potential Economic Value of Seasonal Hurricane Forecasts." *Weather, Climate and Society 4.2*, April, 110–17. https://dspace.mit.edu/handle/1721.1/75075.

Emanuel, Kerry, Sai Ravela, Emmanuel Vivant, and Camille Risi. 2006. "A Statistical Deterministic Approach to Hurricane Risk Assessment." *Bulletin of the American Meteorological Society* 87 (3): 299–314. https://doi.org/10.1175/BAMS-87-3-299.

Emanuel, Kerry, Ragoth Sundararajan, and John Williams. 2008. "Hurricanes and Global Warming: Results from Downscaling IPCC AR4 Simulations." *Bulletin of the American Meteorological Society* 89 (3): 347–68. https://doi.org/10.1175/BAMS-89-3-347.

FAO. 2015. "Crop Ecological Requirements Database (ECOCROP)." Food and Agriculture Organization of the United Nations. 2015. https://www.fao.org/land-water/land/land-governance/land-resources-planning-toolbox/category/details/en/c/1027491/.

———. 2022. "Crop Calendar: Information Tool for Crop Production." Food and Agriculture Organization of the United Nations. 2022. https://cropcalendar.apps.fao.org/#/home.

Fischer, Günther, Freddy Nachtergaele, Harrij van Velthuizen, Federica Chiozza, Gianluca Franceschini, Matieu Henry, Douglas Muchoney, and Sylvia Tramberend. 2021. "Global Agro-Ecological Zone v4 – Model Documentation." Rome: FAO - Food and Agriculture Organization of the United Nations. https://doi.org/10.4060/cb4744en.

Gerner, G. G., T. Hermans, R. E. Kopp, A. B. A. Slangen, T. L. Edwards, A. Levermann, S. Nowikci, et al. 2021. "IPCC AR6 Sea-Level Rise Projections." Version 20210809. PO.DAAC, CA, USA. https://podaac.jpl.nasa.gov/announcements/2021-08-09-Sea-level-projections-from-the-IPCC-6th-Assessment-Report.

Gourdji, Sharon M, Adam M Sibley, and David B Lobell. 2013. "Global Crop Exposure to Critical High Temperatures in the Reproductive Period: Historical Trends and Future Projections." *Environmental Research Letters* 8 (2): 024041. https://doi.org/10.1088/1748-9326/8/2/024041.

Hamilton, Jacqueline M., David J. Maddison, and Richard S.J. Tol. 2005. "Climate Change and International Tourism: A Simulation Study." *Global Environmental Change* 15 (3): 253–66. https://doi.org/10.1016/j.gloenvcha.2004.12.009.

Hammer, W. I. 1981. "Soil Conservation Consultant Report." Technical Note No.7. Bogor, Indonesia: Centre for Soil Research.

Hatfield, Jerry L., and John H. Prueger. 2015. "Temperature Extremes: Effect on Plant Growth and Development." *Weather and Climate Extremes* 10 (December): 4–10. https://doi.org/10.1016/j.wace.2015.08.001.

Honda, Yasushi, Masahide Kondo, Glenn McGregor, Ho Kim, Yue-Leon Guo, Yasuaki Hijioka, Minoru Yoshikawa, et al. 2014. "Heat-Related Mortality Risk Model for Climate Change Impact Projection." *Environmental Health and Preventive Medicine* 19 (1): 56–63. https://doi.org/10.1007/s12199-013-0354-6.

HOTOSM. 2020. "HOTOSM Points of Interest (OpenStreetMap Export)." Humanitarian OpenStreetMap Team (HOT); Humanitarian Data Exchange (HDX). https://data.humdata.org/organization/hot.

Hudson, Norman. 1981. *Soil Conservation*. London: Batsford.

Huizinga, Jan, Hans de Moel, and Wojciech Szewczyk. 2017. "Global Flood Depth-Damage Functions: Methodology and the Database with Guidelines." EUR 28552. European Commission, Joint Research Centre. https://data.europa.eu/doi/10.2760/16510.

ILO. 2019. “Working on a Warmer Planet: The Impact of Heat Stress on Labour Productivity and Decent Work.” Geneva: International Labour Office.

IMF. 2021. “Investment and Capital Stock Dataset (ICSD).” International Monetary Fund. 2021. https://data.imf.org/?sk=1CE8A55F-CFA7-4BC0-BCE2-256EE65AC0E4.

ISO. 1989. “Hot Environments—Estimation of the Heat Stress on Working Man, Based on the WBGT-Index (Wet Bulb Globe Temperature).” ISO Standard 7243. Geneva: International Standards Organization.

John, Denny, M. S. Narassima, Jaideep Menon, Jammy Guru Rajesh, and Amitava Banerjee. 2021. “Estimation of the Economic Burden of COVID-19 Using Disability-Adjusted Life Years (DALYs) and Productivity Losses in Kerala, India: A Model-Based Analysis.” *BMJ Open* 11 (8): e049619. https://doi.org/10.1136/bmjopen-2021-049619.

Karamage, Fidele, Chi Zhang, Tong Liu, Andrew Maganda, and Alain Isabwe. 2017. “Soil Erosion Risk Assessment in Uganda.” *Forests* 8 (2): 52. https://doi.org/10.3390/f8020052.

Kassam, A. H., H. T. van Velthuizen, P. H. Sloane, G. W Fischer, and M. M. Shah. 1991. “Agro-Ecological Land Resources Assessment for Agricultural Development Planning: A Case Study of Kenya.” Resources Data Base and Land Productivity. Rome: Food and Agriculture Organization of the United Nations (FAO) and International Institute for Applied Systems Analysis (IIASA).

Kjellstrom, Tord, Chris Freyberg, Bruno Lemke, Matthias Otto, and David Briggs. 2018. “Estimating Population Heat Exposure and Impacts on Working People in Conjunction with Climate Change.” *International Journal of Biometeorology* 62 (3): 291–306. https://doi.org/10.1007/s00484-017-1407-0.

Kjellstrom, Tord, R. Sari Kovats, Simon J. Lloyd, Tom Holt, and Richard S. J. Tol. 2008. “The Direct Impact of Climate Change on Regional Labour Productivity.” *ESRI* Working Paper No. 260.

Lehner, Bernhard, and Günther Grill. 2013. “Global River Hydrography and Network Routing: Baseline Data and New Approaches to Study the World’s Large River Systems.” *Hydrological Processes* 27 (15): 2171–86.

LeSueur, D., M. Craig, C. Fraser, B. Sharp, and C. Martin. 1998. “Towards an Atlas of Malaria Risk in Africa: First Technical Report of the MARA/ARMA Collaboration.” Durban: Mapping Malaria Risk in Africa / Atlas du Risque de a Malaria en Afrique. http://hdl.handle.net/10625/31644.

Levy, Karen, Shanon M. Smith, and Elizabeth J. Carlton. 2018. “Climate Change Impacts on Waterborne Diseases: Moving Toward Designing Interventions.” *Current Environmental Health Reports* 5 (2): 272–82. https://doi.org/10.1007/s40572-018-0199-7.

Lo, A., S. El-Swaify, E. Dangler, and L. Shinshiro. 1985. “Effectiveness of EI30 as an Erosivity Index in Hawaii.” In *Soil Erosion and Conservation*, by S. El-Swaify, W. Moldenhauer, and A. Lo, 384–92. Ankeny, IA: Soil Conservation Society of America.

https://www.semanticscholar.org/paper/Effectiveness-of-EI30-as-an-erosivity-index-in-Lo-El%E2%80%90Swaify/2d4b1c8511e49c9d24c831cba7636db50b9a2a67.

McCool, D. K., G. R. Foster, C. K. Mutchler, and L. D. Meyer. 1989. "Revised Slope Length Factor the Universal Soil Loss Equation." *Transactions of the American Society of Agricultural Engineers* 32: 1571–76. https://doi.org/doi: 10.13031/2013.31192.

Muis, Sanne, Martin Verlaan, Hessel C. Winsemius, Jeroen C. J. H. Aerts, and Philip J. Ward. 2016. "A Global Reanalysis of Storm Surges and Extreme Sea Levels." *Nature Communications* 7 (1): 11969. https://doi.org/10.1038/ncomms11969.

Nambajimana, Jean de Dieu, Xiubin He, Ji Zhou, Meta Francis Justine, Jinlin Li, Dil Khurram, Richard Mind'je, and Gratien Nsabimana. 2020. "Land Use Change Impacts on Water Erosion in Rwanda." *Sustainability* 12 (1): 50. https://doi.org/10.3390/su12010050.

NASA. 2022. "MOD13Q1—MODIS/Terra Vegetation Indices 16-Day L3 Global 250m SIN Grid." NASA Goddard Space Flight Center. 2022. https://ladsweb.modaps.eosdis.nasa.gov/.

NASA, METI, AIST, Japan Spacesystems, and U.S./Japan ASTER Science Team. 2019. "ASTER Global Digital Elevation Model V003." NASA EOSDIS Land Processes DAAC. https://doi.org/10.5067/ASTER/ASTGTM.003.

Nichols, Gordon, Iain Lake, and Clare Heaviside. 2018. "Climate Change and Water-Related Infectious Diseases." *Atmosphere* 9 (10): 385. https://doi.org/10.3390/atmos9100385.

Nuttall, James G., Kirsten M. Barlow, Audrey J. Delahunty, Brendan P. Christy, and Garry J. O'Leary. 2018. "Acute High Temperature Response in Wheat." *Agronomy Journal* 110 (4): 1296–1308. https://doi.org/10.2134/agronj2017.07.0392.

OECD. 2023. "Working Age Population (Indicator)." Text. 2023. https://doi.org/10.1787/d339918b-en.

Panagos, Panos, Pasquale Borrelli, Katrin Meusburger, Bofu Yu, Andreas Klik, Kyoung Jae Lim, Jae E. Yang, et al. 2017. "Global Rainfall Erosivity Assessment Based on High-Temporal Resolution Rainfall Records." *Scientific Reports* 7 (1): 4175. https://doi.org/10.1038/s41598-017-04282-8.

Philipsborn, Rebecca, Sharia M. Ahmed, Berry J. Brosi, and Karen Levy. 2016. "Climatic Drivers of Diarrheagenic Escherichia Coli Incidence: A Systematic Review and Meta-Analysis." *The Journal of Infectious Diseases* 214 (1): 6–15. https://doi.org/10.1093/infdis/jiw081.

Ponce, Victor M. 2014. "The Muskingum-Cunge Method." In *Fundamentals of Open-Channel Hydraulic*. Online textbook.

Potter, Philip, Navin Ramankutty, Elena M. Bennett, and Simon D. Donner. 2010. "Characterizing the Spatial Patterns of Global Fertilizer Application and Manure Production." *Earth Interactions* 14 (2): 1–22. https://doi.org/10.1175/2009EI288.1.

Prasad, P. V. V., S. A. Staggenborg, and Z. Ristic. 2015. "Impacts of Drought and/or Heat Stress on Physiological, Developmental, Growth, and Yield Processes of Crop Plants." In

Advances in Agricultural Systems Modeling, edited by L.R. Ahuja, V.R. Reddy, S.A. Saseendran, and Qiang Yu, 301–55. Madison, WI, USA: American Society of Agronomy and Soil Science Society of America. https://doi.org/10.2134/advagricsystmodel1.c11.

Renard, K. G., G. R. Foster, G. Weesies, D. McCool, and D. Yoder. 1997. "Predicting Soil Erosion by Water: A Guide to Conservation Planning with the Revised Universal Soil Loss Equation (RUSLE)." Washington, DC: U.S. Dept. of Agriculture, Agricultural Research Service.

Roberts, E H. 1988. "Temperature and Seed Germination." *Symposia of the Society for Experimental Biology* 42 (January): 109–32.

Romanello, Marina, Alice McGushin, Claudia Di Napoli, Paul Drummond, Nick Hughes, Louis Jamart, Harry Kennard, et al. 2021. "The 2021 Report of the Lancet Countdown on Health and Climate Change: Code Red for a Healthy Future." *The Lancet* 398 (10311): 1619–62. https://doi.org/10.1016/S0140-6736(21)01787-6.

Roson, Roberto, and Martina Sartori. 2016. "Estimation of Climate Change Damage Functions for 140 Regions in the GTAP 9 Database." *Journal of Global Economic Analysis* 1 (2): 38.

Salman, M., M. García-Vila, E. Fereres, D. Raes, and P. Steduto. 2021. "The AquaCrop Model – Enhancing Crop Water Productivity : Ten Years of Development, Dissemination and Implementation 2009–2019." FAO Water Report No. 47. Rome, Italy: FAO. https://doi.org/10.4060/cb7392en.

Steduto, Pasquale, Theodore C. Hsiao, Elias Fereres, and Dirk Raes. 2012. "Crop Yield Response to Water." FAO Irrigation and Drainage Paper 66. Rome: FAO. https://www.fao.org/3/i2800e/i2800e00.htm.

Strzepek, Kenneth, Alyssa McCluskey, Brent Boehlert, Michael Jacobsen, and Charles Fant. 2011. "Climate Variability and Change: A Basin Scale Indicator Approach to Understanding the Risk to Water Resources Development and Management." Washington, DC: World Bank. http://hdl.handle.net/10986/17250.

United Nations. 2022. "Database on Household Size and Composition 2022." Department of Economic and Social Affairs. https://www.un.org/development/desa/pd/data/household-size-and-composition.

UNWTO. 2021. "Tourism Data Dashboard." UN World Tourism Organization. 2021. https://www.unwto.org/unwto-tourism-dashboard.

Wahid, A, S Gelani, M Ashraf, and M Foolad. 2007. "Heat Tolerance in Plants: An Overview." *Environmental and Experimental Botany* 61 (3): 199–223. https://doi.org/10.1016/j.envexpbot.2007.05.011.

Wang, Tingting, and Fubao Sun. 2022. "Global Gridded GDP Data Set Consistent with the Shared Socioeconomic Pathways." *Scientific Data* 9 (1): 221. https://doi.org/10.1038/s41597-022-01300-x.

WHO. 2014. “Quantitative Risk Assessment of the Effects of Climate Change on Selected Causes of Death, 2030s and 2050s.” World Health Organization. https://apps.who.int/iris/handle/10665/134014.

Williams, J. R. 1995. “The EPIC Model.” In *Computer Models of Watershed Hydrology*, by V. P. Singh, 909–1000. Highlands Ranch, CO: Water Resources Publications.

Wischmeier, Walter H., and Dwight David Smith. 1978. “Predicting Rainfall Erosion Losses:A Guide to Conservation Planning.” Washington, DC: U.S. Department of Agriculture. https://naldc.nal.usda.gov/catalog/CAT79706928.

Wolf, Jennyfer, Richard Johnston, Paul R. Hunter, Bruce Gordon, Kate Medlicott, and Annette Prüss-Ustün. 2019. “A Faecal Contamination Index for Interpreting Heterogeneous Diarrhoea Impacts of Water, Sanitation and Hygiene Interventions and Overall, Regional and Country Estimates of Community Sanitation Coverage with a Focus on Low- and Middle-Income Countries.” *International Journal of Hygiene and Environmental Health* 222 (2): 270–82. https://doi.org/10.1016/j.ijheh.2018.11.005.

World Bank. 2018. “When Water Becomes a Hazard: A Diagnostic Report on The State of Water Supply, Sanitation, and Poverty in Pakistan and Its Impact on Child Stunting.” Washington, DC: World Bank. https://openknowledge.worldbank.org/handle/10986/30799.

———. n.d. “Households and NPISHs Final Consumption Expenditure.” International Comparison Program, World Bank | World Development Indicators database, World Bank | Eurostat-OECD PPP Programme. https://data.worldbank.org/indicator/NE.CON.PRVT.PP.KD.

WTTC. 2022. “Economic Impact Reports.” World Travel & Tourism Council. 2022. https://wttc.org/research/economic-impact.

Yates, David, Jack Sieber, David Purkey, and Annette Huber-Lee. 2005. “WEAP21—A Demand-, Priority-, and Preference-Driven Water Planning Model.” *Water International* 30 (4): 487–500. https://doi.org/10.1080/02508060508691893.

APPENDIX C: DATA SOURCES

C.1. LABOR HEAT STRESS

DATA	SOURCE
LABOR SUPPLY	
Working age population (ages 15-64)	Oficina Nacional de Estadistica, Estimaciones y proyecciones de la población 2000-2030 (2015). United Nations Population Prospects, 1995-2050, medium variant estimate.
Labor force (total employment and by sector and occupation)	International Labor Organization Labor Force Statistics, 2016-2020 (International Labor Organization 2023)
Weekly hours worked	International Labor Organization Labor Force Statistics, 2016-2020 (International Labor Organization 2023)
EXPOSURE AND AIR CONDITIONING	
Outdoor exposure by occupation	Occupational requirements survey (Bureau of Labor Statistics 2022)
AC household adoption	Encuesta de Hogar de Propósitos Múltiples 2021
Household size	United Nations Household Size and Composition, 2022 (United Nations 2022a)
Household income	World Bank World Development Indicators, Purchasing Power Parity constant 2017 international $ (World Bank, n.d.)
Electricity rates	Cable.co.uk. 2021. "The Price of Electricity per KWh in 230 Countries." 2021. https://www.cable.co.uk/energy/worldwide-pricing/#resources.
Air conditioner prices	Lutz, Amanda. 2023. "How Much Does a New Air Conditioner Cost? (2023 Guide)." *Architectural Digest* (blog). 2023. https://www.architecturaldigest.com/reviews/hvac/air-conditioner-cost.
LABOR FORCE SPATIAL ALLOCATION	
Population distribution	WorldPop United Nations adjusted population counts, 100m resolution (Tatem 2017)
GDP distribution	Global gridded GDP data set consistent with the shared socioeconomic pathways (Wang and Sun 2022)

Cropland distribution	Copernicus Fractional Land Cover dataset (Buchhorn et al. 2020)

C.2. HUMAN HEALTH

DATA	SOURCE
LABOR SUPPLY & POPULATION	
Working age population (ages 15-64)	Oficina Nacional de Estadistica, Estimaciones y proyecciones de la población 2000-2030 (2015). United Nations Population Prospects, 1995-2050, medium variant estimate
Labor force (total employment and by sector and occupation)	International Labor Organization Labor Force Statistics, 2016-2020 (International Labor Organization 2023)
Weekly hours worked	International Labor Organization Labor Force Statistics, 2016-2020 (International Labor Organization 2023)
HISTORICAL ILLNESS INCIDENCE	
Baseline disease incidence and mortality	Global Burden of Disease Database (Institute for Health Metrics and Evaluation 2019)

C.3. WATER, SANITATION, AND HYGIENE

DATA	SOURCE
LABOR SUPPLY & POPULATION	
Working age population (ages 15-64)	Oficina Nacional de Estadistica, Estimaciones y proyecciones de la población 2000-2030 (2015). United Nations Population Prospects, 1995-2050, medium variant estimate.
Labor force (total employment and by sector and occupation)	International Labor Organization Labor Force Statistics, 2016-2020 (International Labor Organization 2023)
Weekly hours worked	International Labor Organization Labor Force Statistics, 2016-2020 (International Labor Organization 2023)
HISTORICAL ILLNESS INCIDENCE AND WASH COVERAGE	
Baseline disease incidence and mortality	Global Burden of Disease Database (Institute for Health Metrics and Evaluation 2019)
Baseline WASH coverage	Joint Monitoring Programme for Water Supply, Sanitation and Hygiene, 2021

C.4. WATER SUPPLY

DATA	SOURCE
CATCHMENTS AND GEOSPATIAL DATA	
Basin delineation	Received from client

Spatial distribution of irrigated areas (shapefile)	Instituto Nacional de Recursos Hidráulicos (INDRHI)
Reservoirs´ location (shapefile)	Instituto Nacional de Recursos Hidráulicos (INDRHI)
HISTORICAL FLOWS, WITHDRAWALS, AND DEMAND	
Average country consumption in l/ab/day (household, industrial)	Instituto Nacional de Aguas Potables y Alcantarillados (*INAPA)*, 2015. Apéndice II
List of industrial sites with daily water use in m3 both from groundwater and surface water	Instituto Nacional de Aguas Potables y Alcantarillados (*INAPA)*, 2015. Apéndice II
Municipal, industrial and irrigation water demands	Plan Hidrológico Nacional República Dominicana. Instituto Nacional de Recursos Hidráulicos (INDRHI, 2012).
Wastewater production by region (as flow in l/s)	Instituto Nacional de Aguas Potables y Alcantarillados (*INAPA)*, 2015. Apéndice II
Historical runoff	Global Runoff Data Centre I GRDC (Bundesanstalt für Gewässerkunde)
Irrigation efficiency	Plan Hidrológico Nacional República Dominicana. Instituto Nacional de Recursos Hidráulicos (INDRHI, 2012).
Environmental flows	Plan Hidrológico Nacional República Dominicana. Instituto Nacional de Recursos Hidráulicos (INDRHI, 2012).
STORAGE INFRASTRUCTURE	
Max turbine flow	EMPRESA DE GENERACIÓN HIDROELÉCTRICA DOMINICANA (EGEHID). MEMORIA INSTITUCIONAL 2017-2020
Reservoirs 'volume and height	Presas en Operación por Regiones Hidrográficas en República Dominicana. INDRHI - Departamento de Presas, 2010
Capacity factor (number of hours in operation) and energy production (GWh)	EMPRESA DE GENERACIÓN HIDROELÉCTRICA DOMINICANA (EGEHID). Estadísticas Institucionales, 2022.
Information about dams' use	INVENTARIO NACIONAL DE CANALES DE LOS DISTRITOS DE RIEGO. INDRHI, 2006.

C.5. CROP PRODUCTION

DATA	SOURCE
CATCHMENTS AND GEOSPATIAL DATA	
Basin delineation	Received from client

Spatial distribution of irrigated areas (shapefile)	Instituto Nacional de Recursos Hidráulicos (INDRHI)
Spatial distribution of crop production	IFPRI. 2019. "Global Spatially-Disaggregated Crop Production Statistics Data for 2010 Version 2.0." International Food Policy Research Institute, Harvard Dataverse, V4. https://doi.org/10.7910/DVN/FSSKBW.
CROP STATISTICS	
Crop harvested area and production	FAOSTAT – Crops and Livestock Products (FAO 2021)
Crop revenues	FAOSTAT – Value of Agricultural Production (FAO 2021)
Irrigation water demands	Plan Hidrológico Nacional República Dominicana. Instituto Nacional de Recursos Hidráulicos (INDRHI, 2012).
Irrigated crop area	Food and Agriculture Organization, AQUASTAT, Perfil de Pais – Republica Dominicana, 2015 IFPRI. 2019. "Global Spatially-Disaggregated Crop Production Statistics Data for 2010 Version 2.0." International Food Policy Research Institute, Harvard Dataverse, V4.
CROP CALENDARS, COEFFICIENTS, AND THRESHOLDS	
Crop calendars	FAO. 2022. "Crop Calendar: Information Tool for Crop Production." Food and Agriculture Organization of the United Nations. 2022. https://cropcalendar.apps.fao.org/#/home.
Crop coefficients	Allen, Richard G., Luis S. Pereira, Dirk Raes, and Martin Smith. 1998. "Crop Evapotranspiration - Guidelines for Computing Crop Water Requirements." FAO Irrigation and Drainage Paper 56. Rome: FAO - Food and Agriculture Organization of the United Nations. https://www.fao.org/3/X0490E/x0490e00.htm#Contents.
Crop yield response to water coefficients	Steduto, Pasquale, Theodore C. Hsiao, Elias Fereres, and Dirk Raes. 2012. "Crop Yield Response to Water." FAO Irrigation and Drainage Paper 66. Rome: FAO. https://www.fao.org/3/i2800e/i2800e00.htm.
Temperature thresholds	FAO. 2015. "Crop Ecological Requirements Database (ECOCROP)." Food and Agriculture Organization of the United Nations. 2015. https://www.fao.org/land-water/land/land-governance/land-resources-planning-toolbox/category/details/en/c/1027491/.

C.6. EROSION

DATA	SOURCE
LAND USE LAND COVER	

Land cover	NASA Goddard Space Flight Center. MOD13Q1—MODIS/Terra Vegetation Indices 16-Day L3 Global 250m SIN Grid. Available online: https://ladsweb.modaps.eosdis.nasa.gov/ (accessed on January 2022).
SOIL CHARACTERISTICS AND MANAGEMENT	
Physical properties of soil	Poggio, L., de Sousa, L. M., Batjes, N. H., Heuvelink, G. B. M., Kempen, B., Ribeiro, E., and Rossiter, D.: SoilGrids 2.0: producing soil information for the globe with quantified spatial uncertainty, SOIL, 7, 217–240, https://doi.org/10.5194/soil-7-217-2021, 2021.
Slope and slope length	Amatulli, G., Domisch, S., Tuanmu, M.-N., Parmentier, B., Ranipeta, A., Malczyk, J., and Jetz, W. (2018) A suite of global, cross-scale topographic variables for environmental and biodiversity modeling. Scientific Data volume 5, Article number: 180040. DOI: doi:10.1038/sdata.2018.40.
Historical rainfall-erosivity	Panagos, P.; Borrelli, P.; Meusburger, K.; Yu, B.; Klik, A.; Jae Lim, K.; Yang, J.E.; Ni, J.; Miao, C.; Chattopadhyay, N.; et al. Global rainfall erosivity assessment based on high-temporal resolution rainfall records. Sci. Rep. 2017, 7, 4175.
HISTORICAL CROP AREA, PRODUCTION, AND REVENUE STATISTICS	
Crop area, production, and revenues	International Food Policy Research Institute, 2020, "Spatially-Disaggregated Crop Production Statistics Data in Africa South of the Sahara for 2017", https://doi.org/10.7910/DVN/FSSKBW, Harvard Dataverse, V2

C.7. INLAND FLOODING

DATA	SOURCE
HYDROLOGY AND TOPOGRAPHY	
Flood curve numbers	Wischmeier, Walter H., and Dwight David Smith. 1978. Predicting Rainfall Erosion Losses: A Guide to Conservation Planning. Washington, DC: U.S. Department of Agriculture.
Annual exceedance probability of flooding events	World Bank's Climate Knowledge Portal (CCKP)
Land cover and soil infiltration	Buchhorn, Marcel, B. Smets, L. Bertels, M. Lesiv, N. E. Tsendbazar, D. Masiliunas, L. Linlin, M. Herold, and S. Fritz. 2020. "Copernicus Global Land Service: Land Cover 100m: Globe (Version V3.0.1)."

River network	Lehner, Bernhard, and Günther Grill. 2013. "Global River Hydrography and Network Routing: Baseline Data and New Approaches to Study the World's Large River Systems." *Hydrological Processes* 27 (15): 2171–86.
Hydrological basins	Linke, Simon, Bernhard Lehner, Camille Ouellet Dallaire, Joseph Ariwi, Günther Grill, Mira Anand, Penny Beames, et al. 2019. "Global Hydro-Environmental Sub-Basin and River Reach Characteristics at High Spatial Resolution." *Scientific Data* 6 (1): 283. https://doi.org/10.1038/s41597-019-0300-6.
RESOURCES AT RISK	
Capital stock and capital-output ratio	IMF. 2021. "Investment and Capital Stock Dataset (ICSD)." International Monetary Fund. 2021. https://data.imf.org/?sk=1CE8A55F-CFA7-4BC0-BCE2-256EE65AC0E4.
Capital spatial distribution	Wang, Tingting, and Fubao Sun. 2022. "Global Gridded GDP Data Set Consistent with the Shared Socioeconomic Pathways." *Scientific Data* 9 (1): 221. https://doi.org/10.1038/s41597-022-01300-x.
Flood damage curves	Huizinga, Jan, Hans de Moel, and Wojciech Szewczyk. 2017. "Global Flood Depth-Damage Functions: Methodology and the Database with Guidelines." EUR 28552. European Commission, Joint Research Centre. https://data.europa.eu/doi/10.2760/16510.

C.8. TROPICAL CYCLONES

DATA	SOURCE
STORM TRACKS	
Tropical cyclone tracks for hindcasts and projections	Purchased from WindRiskTech via Kerry Emanuel. For model details and further references, see the following paper: Emanuel, K. Atlantic tropical cyclones downscaled from climate reanalyses show increasing activity over past 150 years. Nat Commun 12, 7027 (2021). https://doi.org/10.1038/s41467-021-27364-8
CAPITAL VALUE AND LOCATION	
Gridded GDP	Wang, T. and Sun, F.: Spatially explicit global gross domestic product (GDP) data set consistent with the Shared Socioeconomic Pathways, Earth Syst. Sci. Data Discuss. [preprint], https://doi.org/10.5194/essd-2021-10, 2021.
Land cover	Buchhorn, Marcel, B. Smets, L. Bertels, M. Lesiv, N. E. Tsendbazar, D. Masiliunas, L. Linlin, M. Herold, and S. Fritz. 2020. "Copernicus Global Land Service: Land Cover 100m: Globe (Version V3.0.1)."

DAMAGE FUNCTIONS	
Damage function	Emanuel, Kerry, Fabian Fondriest, James Kossin (2012) Potential Economic Value of Seasonal Hurricane Forecasts. Vol 4, pgs. 110-117, DOI: 10.1175/WCAS-D-11-00017.1

C.9. SEA-LEVEL RISE AND STORM SURGE

DATA	SOURCE
HYDROLOGY, TIDE GAUGES, AND TOPOGRAPHY	
Sea level rise projections	Garner, G. G., T. Hermans, R. E. Kopp, A. B. A. Slangen, T. L. Edwards, A. Levermann, S. Nowikci, M. D. Palmer, C. Smith, B. Fox-Kemper, H. T. Hewitt, C. Xiao, G. Aðalgeirsdóttir, S. S. Drijfhout, T. L. Edwards, N. R. Golledge, M. Hemer, R. E. Kopp, G. Krinner, A. Mix, D. Notz, S. Nowicki, I. S. Nurhati, L. Ruiz, J-B. Sallée, Y. Yu, L. Hua, T. Palmer, B. Pearson, 2021. IPCC AR6 Sea-Level Rise Projections. Version 20210809. PO.DAAC, CA, USA. Dataset accessed [YYYY-MM-DD] at https://podaac.jpl.nasa.gov/announcements/2021-08-09-Sea-level-projections-from-the-IPCC-6th-Assessment-Report.
Historical mean tidal levels	Carrère et al. FES 2012: A new global tidal model taking advantage of nearly 20 years of altimetry. in Proceedings of 20YPRA symposium 3–8 (2012).
Surge and extreme sea level exceedance curves	Muis et al. (2016) A global reanalysis of storm surges and extreme sea levels. Nature Communications. doi: 10.1038/NCOMMS11969
Topography	Earth Resources Observation And Science (EROS) Center. (2017). Shuttle Radar Topography Mission (SRTM) 1 Arc-Second Global [Data set]. U.S. Geological Survey. https://doi.org/10.5066/F7PR7TFT
CAPITAL VALUE AND LOCATION	
Gridded GDP	Wang, T. and Sun, F.: Spatially explicit global gross domestic product (GDP) data set consistent with the Shared Socioeconomic Pathways, Earth Syst. Sci. Data Discuss. [preprint], https://doi.org/10.5194/essd-2021-10, 2021.
Land cover	Buchhorn, Marcel, B. Smets, L. Bertels, M. Lesiv, N. E. Tsendbazar, D. Masiliunas, L. Linlin, M. Herold, and S. Fritz. 2020. “Copernicus Global Land Service: Land Cover 100m: Globe (Version V3.0.1).”
DAMAGE FUNCTIONS	

Damage functions by building type	Huizinga, Jan, Hans de Moel, and Wojciech Szewczyk. 2017. Global Flood Depth-Damage Functions: Methodology and the Database with Guidelines. EUR 28552. European Commission, Joint Research Centre.

C.10. TOURISM

DATA	SOURCE
TOURISM AND TRAVEL DATA	
Monthly arrivals of passengers by residence and airport used, 2019	Central Bank of the Dominican Republic, Department of National Accounts and Economic Statistics, 2019
Monthly departures of passengers by residence and airport used, 2019	Central Bank of the Dominican Republic, Department of National Accounts and Economic Statistics, 2019
Tourism revenues	World Travel & Tourism Council, Dominican Republic Annual Research, 2022
Punta Cana revenues	Hedrick-Wong, Y.; Choong, D. MasterCard 2015 Global Destination Cities Index. Tracking Global Growth: 2009-2015; Mastercard: New York, NY, USA, 2016.
POINTS OF INTEREST AND LOCATION	
Tourism Points of Interest Database	OpenStreetMap 2023, 2015

ADDENDUM TO ANNEX 2: DOCUMENTATION OF INVESTMENT COST ESTIMATES FROM IEC WORK

Estimations of costs and benefits of mitigation and adaptation activities are based on inputs from sector teams and existing World Bank work on decarbonization in the Dominican Republic, including those of IEc presented above. Below are data sources for each component of the analysis, broken out into mitigation and adaptation actions.

Mitigation

For energy and transport, the approach taken was to take investment costs provided by the sector teams, and use inputs provided from sector teams on avoided fuel use, and improved productivity to estimate benefits and co-benefits of the investments. Energy inputs came from Electricity Planning Model model, transport results were estimated from modelling completed by the transport team, and coefficients on the benefits from avoided fuel use and air pollution mortality results were taken from the Carbon Pricing Assessment Tool. For land use, prior work on decarbonization had developed Marginal Cost Curves for land use and AFOLU investments and the initial investment costs were also provided as a time series. These were used to estimate annual investment needs as well as the economic benefits of the interventions.

	Costs Quantified	Benefits Quantified in Monetary Terms
Power	Capital Investment + grid integration	CO2 Avoided Fuel consumption Air pollution mortality avoided
Transport	Public investments – BEV, HEV, Modal shift	CO2 avoided Avoided Fuel consumption Air pollution mortality avoided Traffic accidents avoided Road damage avoided
AFOLU	REDD+ Implementation and transaction costs	Opportunity costs of land use in terms of revenue

Adaptation

For SLR, Cyclones, Inland, and Coastal Flooding, costs are taken from modelling by IEC as a fraction of capital stock and converted to 2022 USD. Benefits are expressed as avoided capital damages also from inputs provided by IEC. For Heat Stress, water infrastructure, and crop production, investments include both capex and opex in USD

dollar values provided by IEc. Benefits are expressed in the units provided by IEc as well: %loss productivity, % yield loss, % unmet demand.

	Costs Quantified	Benefits Quantified in Monetary Terms
SLR/Storm Surge	Capital costs	Avoided damages
Cyclones	Capital costs	Avoided damages
Heat Stress	capital + operations costs	Labor productivity loss averted
Crops	capital + operations costs	Crop yield loss averted
Water M&I	capital + operations costs	Reduction in unmet demand